Characterisation of the Properties and Performance of Nanofluid Coolants with Analysis of Their Feasibility for Datacentre Cooling

By

Fahad Saleh Alkasmoul

Submitted in accordance with the requirements for the degree of
Doctor of Philosophy

The University of Leeds
School of Mechanical Engineering

August 2015

The candidate confirms that the work submitted is his own and that appropriate credit has been given where reference has been made to the work of others.

ACKNOWLEDGEMENTS

I am deeply indebted to my supervisors Dr. Mark Wilson and Prof. Harvey Thompson for their guidance, help and continuous support during the course of this study.

I would also like to acknowledge King Abdlulaziz City for Science and Technology (KACST) in general and the National Centre for Nanotechnology Research in particular and King Saud University (Mechanical Engineering Department).Special acknowledgment goes to Eng. Abdulaziz Al-jaiwi (National Centre for Nanotechnology Research at KACST) who offered unlimited help and support.

Finally, I am most thankful to my mother and father, wife, daughter, sisters and all my family members for their help, support, encouragement and patience during the years of my study.

ABSTRACT

It is a generally accepted belief that the use of nanofluids enhances heat transfer rates in comparison with a traditional fluid and can be considered to be one of the most important energy conservation measures in many industrial applications. Despite increased interest, detailed and systematic studies of nanofluids' flow and thermal characteristics are limited and their effect on heat transfer is often misunderstood. The concentration of a nanofluid is often chosen independently of the application conditions, nanofluid type or cost and other economic parameters such as the cost of energy and lifetime of the application. This thesis has three main objectives; the first is the measurement of the thermal properties of nanofluids and the proposal of a correlation model for nanofluid viscosity. The results of these measurements show that the nanofluid viscosity depends on the type of nanoparticles and their concentration and the fluid temperature. It is shown that the viscosity increases with increasing nanoparticle concentration and decreases with increasing temperatures over the nanoparticle concentration and temperature ranges investigated.

The second objective is concerned with the measurement and evaluation of heat transfer performance and pressure drop of various nanofluids via an experiment using forced convection heat transfer within the turbulent regime. In general, it is shown that the heat transfer coefficient of nanofluids decreases with increasing nanoparticle concentration at a specific flow rate and the base fluid gives higher heat transfer with respect to the nanofluids. In the other hand, Assessing the thermal performance of nanofluids by considering the Nusselt number and its variation with Reynolds number is misleading because both Nusselt number and Reynolds number depend on the nanofluid properties (i.e. thermal conductivity, density and viscosity that are function of the volume fraction). This can lead to a false impression that some nanofluids produce an improvement in heat transfer performance. Moreover, using nanofluid will require additional pumping power to achieve the corresponding base fluid's Reynolds number. Finally, existing single-phase liquid correlations of the heat transfer coefficient and pressure drop are compared and show good agreement in predicting nanofluid behaviour.

The third objective aims to determine recommended nanoparticle concentrations of a typical nanofluid used within immersion cooling of a data centre server; this is based on two different designs for immersion cooling by Iceotope at varying Reynolds numbers. This is determined by calculating the heat transfer and pressure drop through the server for various values of the volume fraction of nanoparticles by using a model created within the finite element solver, COMSOL. The server's total power consumption as a function of its CPU temperature and cooling system, including the increased pumping power required for varying nanofluid concentrations, are predicted and used in a proposed novel methodology to evaluate potential economic trade-offs in utilising nanofluids within an immersed liquid cooled data centre. This methodology is used to calculate the minimum total costs and economically optimum volume fraction of a nanofluid with this type of data centre. The results show that Al_2O_3-water nanofluids showed the highest thermal performance with respect to other nanofluids because Al_2O_3 has the highest thermal conductivity, however Al_2O_3-water nanofluids are the most viscous giving it the highest pressure drop and consequently the highest pumping costs.

Under the economic factors used, it is found that the most cost effective fluid for both the server with cooled plate having two parallel tubes and the server with cooled plate having serpentine tube configuration is the base fluid (water).

TABLE OF CONTENTS

LIST OF TABLES

LIST OF FIGURES

NOMENCLATURE

A	The inside surface area of the test section tube (m^2)
B	The base error
C_e	The current yearly total cost of energy (£/year)
C_{enr}	The present value of the cost of energy consumption over the lifetime of using nanofluid in the system (£)
C_p	Specific heat (J/kg.K)
c_{nf}	The cost of nanofluid per unit of mass (£/kg)
c_{bf}	The cost of base fluid per unit of mass (£/kg)
c_{tot}	The total cost (£)
D	The diameter of the test section tube (m)
D_B	Brownian diffusion coefficient (m^2/s)
D_{in}	The test section tube diameter inside (m)
D_{out}	The test section tube diameter outside (m)
D_T	Thermal diffusion coefficient (m^2/s)
d_p	particle diameter (nm)
E_c	vapour-compression cooling the electric energy consumption (W)
E_p	pump electric energy consumption (W)

E_s	CPU electric energy consumption (W)
E_{tot}	Total electric energy consumption, $E_{tot} = E_c + E_p + E_s$ (W)
F	Body force of gravity
f	The friction factor; mass fraction
g	Gravity acceleration
h	Convection coefficient.
I	pass test section electricity current
k	Thermal conductivity (W/m.K); turbulent kinetic energy
k_{tube}	Thermal conductivity of test section tube
L	The length of test section tube (m); and characteristic length
$\dot{m}$	The mass flow rate (kg/m^3)
m	An expected lifetime of using nanofluid (years),
p_c	The average coefficient of performance of the refrigeration system (COP)
P_p	The pump efficiency
n	number of thermocouples
Nu	Nusselt number

P	Pressure (Pa)
Pr	Prandtl number
PWF	The present worth factor
Q	Flow rate (m^3/s); energy source (W)
Q_g	The total heat gain from server per year (W)
q	Heat flux
R	The random error
Ra	Rayleigh number
Re	Reynolds number
r_i	inflation rate in energy cost
r_d	interest rate
T	Temperature (°C)
T_c	Cooling inlet fluid temperature (°C)
T_h	Heated temperature wall (°C)
$\boldsymbol{T_{s,in}}$	The inside surface test section temperature (°C)
$\boldsymbol{T_{b,m}}$	Average bulk temperature along the test section (°C)

$T_{b,in}$	Inlet bulk temperature of the test section fluid (°C)
$T_{b,out}$	Outlet bulk temperature of the test section fluid (°C)
$T_{s,out}$	Outside surface test section temperature (°C)
t	Time.
V	The test section tube volume (m^3), average fluid velocity (m/s), voltage difference (V) and dimensionless velocity in the y-direction
v	velocity component in the y-direction
U	dimensionless velocity the x-direction
u	velocity component in the x-direction (m/s), uncertainty
X	dimensionless x-coordinate
x	Coordinate distance
Y	dimensionless y-coordinate
y	Coordinate distance

Greek letters

α	Thermal diffusivity.
ϕ	Volume fraction of nanofluids
ϕ_{opt}	The optimum volume fraction
ε	turbulent dissipation rate,

β	Thermal expansion coefficient (1/K); the ratio between the nanolayer thickness surrounding the nanoparticle and the nanoparticle radius
ν	kinematic viscosity
θ	dimensionless Temperature
τ	dimensionless time
$\tau_{turbulent}$	tensor known as the specific Reynolds stress tensor
κ_b	Boltzmann constant =1.3807×10^{-23} J/K
ρ	Density (kg/m^3)
μ	Dynamic viscosity
μ_T	turbulent viscosity

Subscripts

av	average
bf	base fluid
nf	nanofluid
p	nanoparticle

CHAPTER 1: INTRODUCTION

1.1: The Problem Considered

Information and Communication Technology (ICT) has become an important source of data and information in our society. As a result, business, education, transportation, and the economy sectors now depend on it [1]. Consequently, data centres have become a crucial part of ICT storage, management, processing and exchange of data and information [2]. A data centre consists of four main types of equipment under one roof. These are power equipment such as power distribution units and batteries, cooling equipment such as chillers and computer room air-conditioning (CRAC) units, IT equipment such as servers and network, and miscellaneous component loads such as lighting and fire protection systems [3]; see Figure 1.1. In order to quantify and compare data centres efficiency, the Power Usage Effectiveness (PUE) is commonly used which is calculated by the ratio of the total power consumed by a data centre to the power used solely by the IT equipment:

$$\text{PUE}=\frac{\text{Total equipment power}}{\text{IT equipment power}}$$

In general, the most energy efficient data centre has a PUE close to unity.

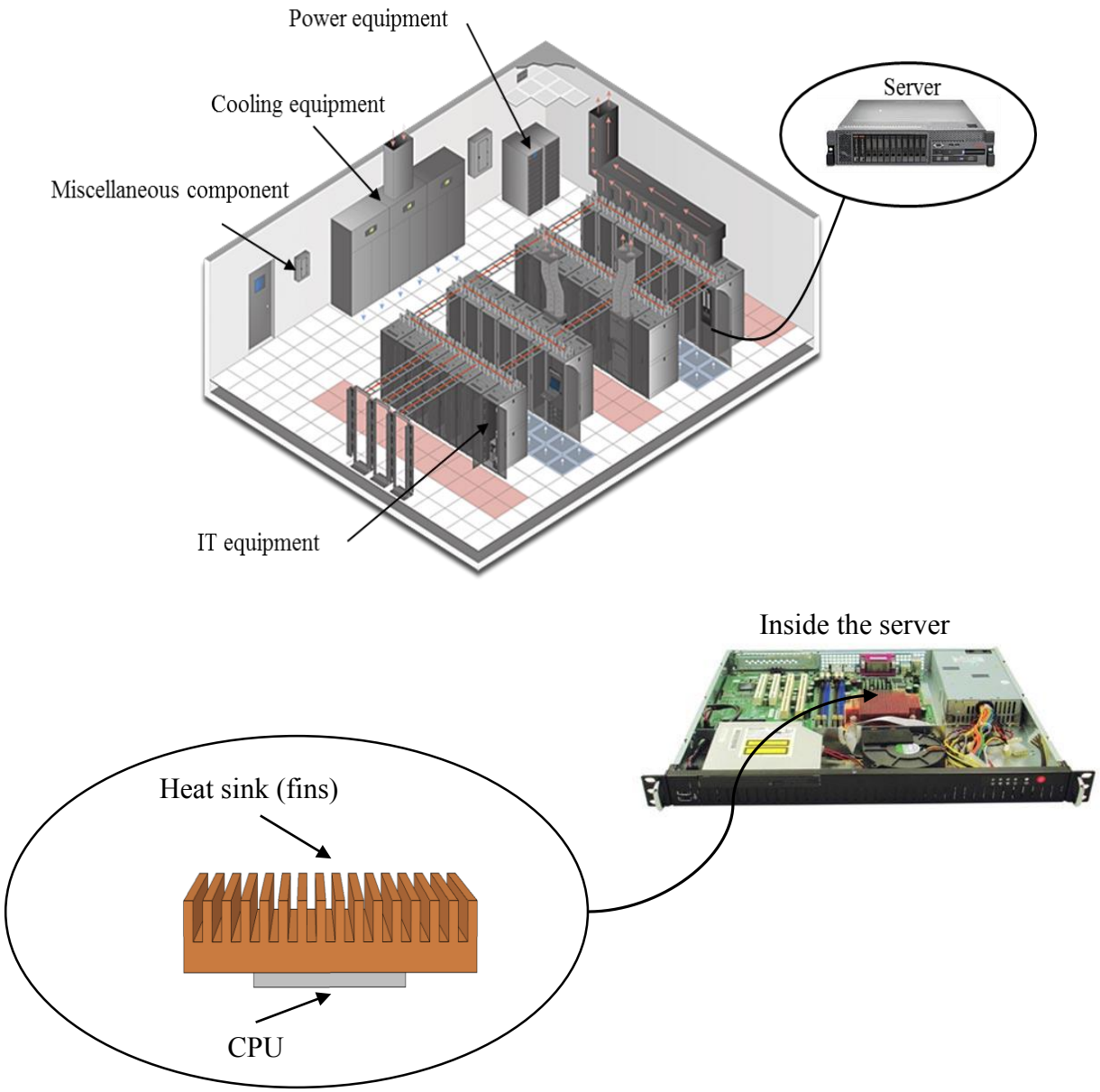

Figure 1.1: Typical data centre infrastructure (http://www.tripplite.com/lp/direct /rackcooling) and server (http://www.esis.com.au/index.php)

These data centres consume significant power, for example, Koomey [4] estimated that Google had 900,000 servers which used 1.9 billion kWh of electricity in 2010. More than three-quarters of the electric energy consumption of a typical data centre is used by IT and cooling equipment (Figure 1.2); and about half of this is used by the cooling system [3, 5]. This is a consequence of the heat load that is generated due to the densities of servers. Data centres demand a large amount of electrical energy which is estimated to be more than 40 times a traditional office building consumption [2]. There is a noticeable increase in data centres throughout the world and with energy costs increasing, there is a drive to find means of significantly reducing the energy consumption of data centres. A major part of the energy consumed by the cooling system in the data centre is due to the high heat flux loads generated by the servers Central Processing Unit (CPU), which is considered to be the dominant component of the total heat generation within the server. Additionally the CPU consumes more power with increasing temperature [6-8]. Therefore, reducing these loads and finding new ways of cooling the servers efficiently to decrease the CPU's operating temperature has the dual effect of protecting them and increasing the performance and so becomes one of the top priorities for energy conservation measures in data centres [7]. The cooling of a data centre can be based on either an air cooling system or a liquid cooling system. Air-cooling is the most common, however using liquid cooling can be superior since liquids have higher heat capacity to remove more heat and also help eliminate hotspots (undesirable environmental temperature of data centre) which is common when air cooling is used. There are several liquid cooling techniques such as bringing the cooled liquid close to the rack or into the rack and using air cooling through the interior of the server or immersing the entire server into a dielectric liquid eliminating the need for air altogether; these techniques will be explained in detail later in section 1.2.4.

Liquids play a vital role in heat transfer for heating or cooling in many applications such as industrial processes, chemical processes, air conditioning systems, microelectronics, etc. However, these liquids have limitations for heat transmission, because fluids such as water have a poor thermal conductivity compared to some solids.

One technique with the potential to enhance the heat transfer of these liquids is by adding solid nanoparticles [9]. The concept of adding nanoparticles to liquids (Nanofluid) is to increase their thermal conductivity and hence increase their heat transfer. Since the CPU power consumption depends upon its temperature, using nanofluid as liquid coolant in cooling system in data centre should offer a clear advantage.

The term ‘nanofluid’ was introduced by Choi in 1995 to describe a base fluid including suspensions of nanoparticles (metallic or non-metallic) with average size less than 100 nanometres [10]. The aim of adding nanoparticles to a base fluid is, therefore, to enhance the thermal performance of the base fluid by increasing the thermal conductivity, because the thermal conductivity of a solid is higher than the base fluid. For example, the thermal conductivity of copper (400 W/m.K) is 700 times greater than the thermal conductivity of water (0.613 W/m.K) [11]. Therefore, the thermal conductivity of the nanofluid should possess a relatively high value compared to the base fluid. The aim of using a nanofluid in an application is to increase the heat transfer performance and energy efficiency. Whilst investigation into nanofluids has been increasing, researchers are still debating the thermal performance enhancements due to nanofluid use [12]. The studies on nanofluids have shown that the nanofluid performance is a factor of its particles characteristics, such as the particle size, shape and concentration. In addition, nanofluids characteristics also depend on other factors such as the type of the host liquid and temperature. Despite the increase of investigations into nanofluids, there is a general lack of detail and agreement so far, although some researchers have shown close agreement amongst their experimental results.

The use of nanofluids is considered as one of the effective means of increasing heat transfer performance in some applications in recent years [10, 13-17]. Adding nanoparticles to the base fluid increases the thermal conductivity and viscosity of a nanofluid, therefore, nanofluids have different thermo-physical properties compared with base fluids [18, 19]. There are many types of nanofluids available, these differ with regard to the base fluid, nanoparticle type, concentration and particle size. As is the case in most practical applications, nanofluids have different thermal characteristics such as the heat transfer coefficient, and dynamic flow characteristics such as pressure drop when

compared to the base fluid. Thus, testing thermal performance of nanofluid under dynamic conditions is essential to understand how a nanofluid behaves. The accurate estimation of the convective heat transfer coefficient requires scientific investigation in order to properly use a nanofluid in a given application.

While nanofluids may offer benefits in terms of heat transfer performance, their use comes at a cost in terms of additional pumping power required to overcome increased pressure drops. Therefore, nanofluid use in a practical application must be subject to an economic analysis to evaluate this trade-off.

This thesis explores the development and application of nanofluids for the enhancement of electronic cooling systems. A full list of objectives is given at the end of this chapter.

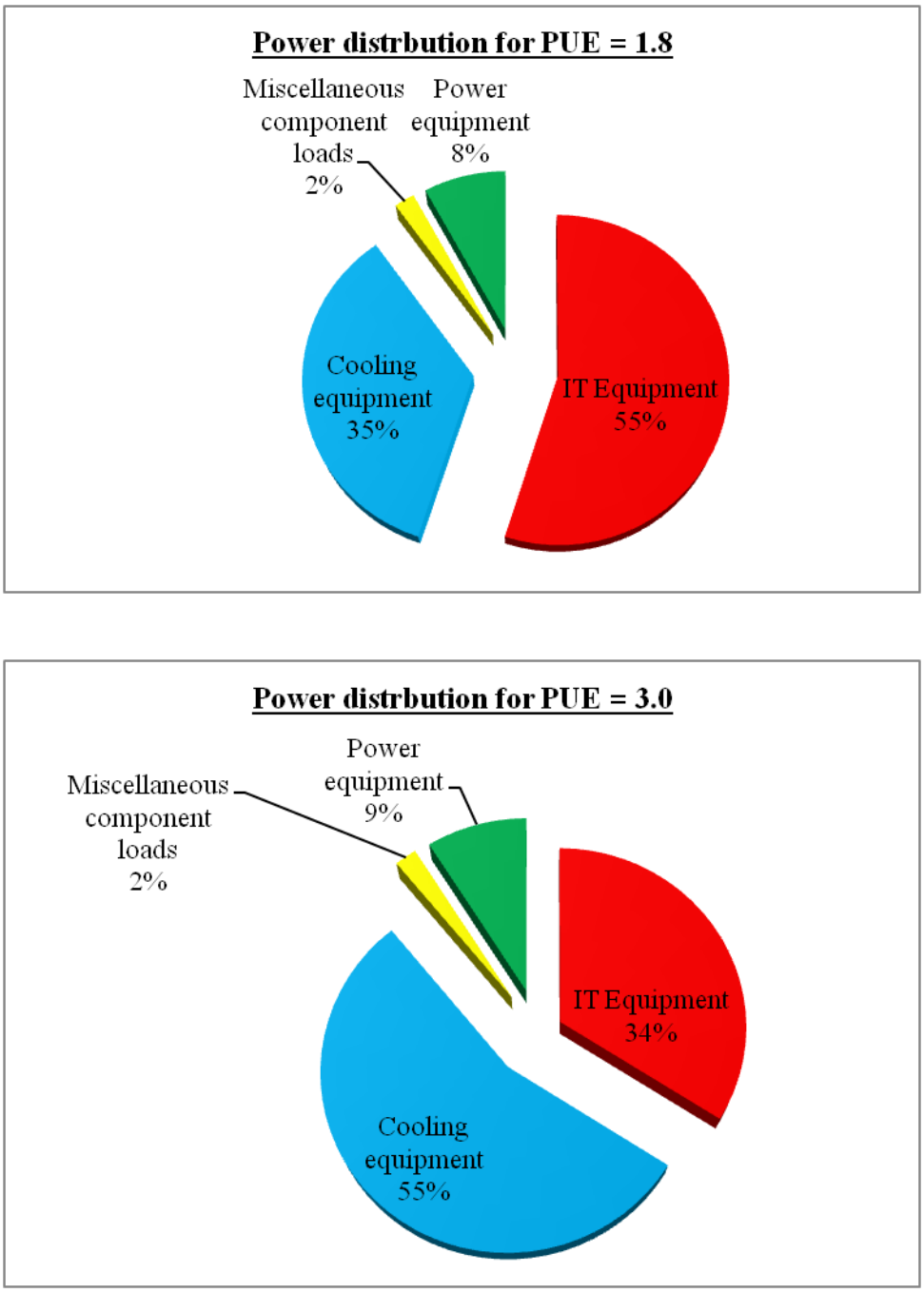

Figure 1.2: Energy consumption in typical data centres[3]

1.2: Literature Review

This section reviews some relevant and representative studies conducted with regards to measurement of nanofluid transport properties as well as studies regarding their heat transfer characteristics and previous economic analyses for assessing the benefits of nanofluids in practical applications. Finally, data centre cooling techniques are investigated to explore a potential application of nanofluids.

1.2.1: Experimental studies on the viscosity of nanofluids

With regards to the measurement of thermal and physical properties of nanofluids, there are, so far, no definitive sources and some published papers only focus on nanofluid thermal conductivity [18, 20-22]. However, there is a definite need to measure and test nanofluid properties, specifically the viscosity and thermal conductivity. In addition, the literature is lacking studies on the effects of particle volume concentration, particle material (i.e. types of nanoparticle), particle size, particle shape, particle aggregation, base fluid mediums, temperature, additives (materials that are added to the fluid to keep the nanoparticles in suspension), and acidity, on thermal conductivity and viscosity. Also, further research is needed regarding the other properties of nanofluids (e.g. the specific heat capacity).

A systematic and detailed review of nanofluid viscosity is direly needed similar to the work compiled by workers Buongiorno et al. [12] for nanofluid thermal conductivity. Their report uses comparable samples but different experimental approaches from 34 different organisations and was submitted to the International Nanofluid Property Benchmark Exercise (INPBE). A detailed comparison of the data was performed and showed no anomalous increases in thermal conductivity. The paper concludes that the enhancement of thermal conductivity is entirely a function of increasing nanoparticles concentration and nanoparticles aspect ratio, with minor differences reported due to the differing measurement techniques.

There are some theoretical models, which exist within the literature to estimate the viscosity of nanofluids under a number of assumptions, such as the nanoparticles being

spherical. The most common theoretical nanofluid viscosity models are the Einstein model, the Brinkman model, and Batchelor's model [18]; these models estimate the nanofluid viscosity as a function of the base fluid viscosity and nanoparticle concentration:

Einstein model: $\frac{\mu_{nf}}{\mu_{bf}} = (1 + 2.5\phi)$ for low concentration ($\phi \leq 0.02$ vol%) (1.1)

Brinkman model: $\frac{\mu_{nf}}{\mu_{bf}} = \frac{1}{(1-\phi)^{2.5}}$ for volume fractions up to ($\phi \leq 4$ vol%) (1.2)

Batchelor model: $\frac{\mu_{nf}}{\mu_{bf}} = 1 + 2.5\phi + 6.5\phi^2$ (1.3)

where μ_{bf} is the base fluid viscosity and ϕ is the volume fraction of nanoparticles.

Figure 1.3 shows all the theoretical models' trends; later these trends are compared to experimental data performed by the author and found to underestimate the nanofluid viscosity.

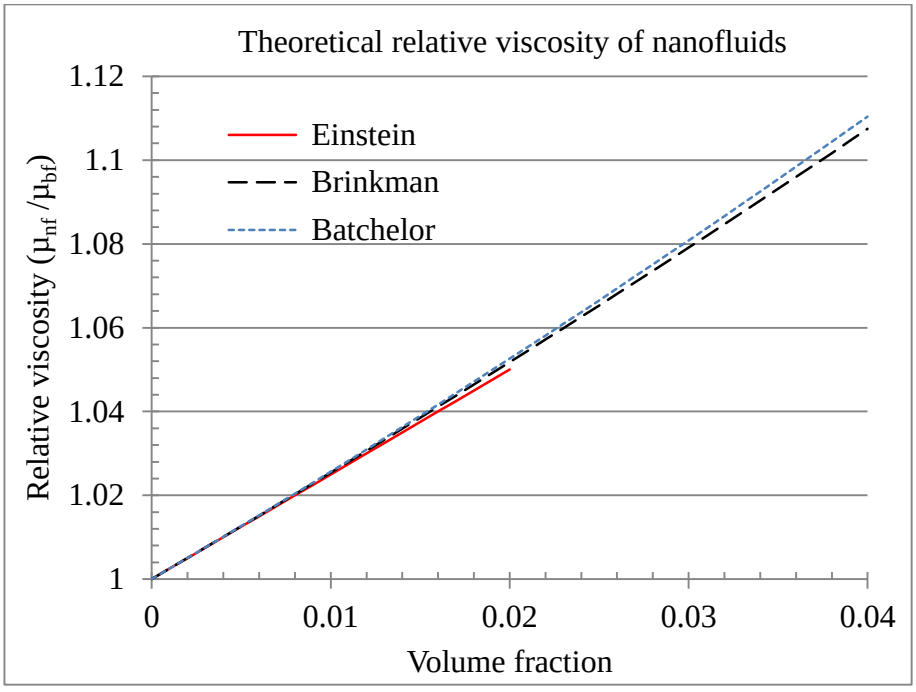

Figure 1.3: Theoretical correlations of nanofluid relative viscosity

The following is a review of previous empirical studies of nanofluid viscosities. Pak and Cho [23] used a Brookfield rotating viscometer to measure the viscosity of Al_2O_3-water and TiO_2-water nanofluids with nanoparticle size 13 and 27 nm respectively. They found that the viscosity of the nanofluids was significantly greater than that of the base fluid (water) and the relative viscosity of the Al_2O_3-water nanofluid was greater than that of TiO_2-water nanofluids of comparable concentration. For example, at a 10% volume fraction the viscosities were 3% and 200% compared to water for TiO_2-water and Al_2O_3-water respectively. Duangthongsuk and Wongwises [20] used a rotational rheometer to measure the dynamic viscosity of TiO_2-water nanofluid with average particle size 21 nm. The tests were conducted within a mean temperature range of 15 to 35 ^oC with volume fractions varying from 0.2 vol.% to 2.0 vol.%. Their results showed that the viscosity increases almost linearly with increasing nanoparticle load (volume fraction) whilst it decreases with rising temperatures and that the increase in viscosity compared to base fluid was about 4-15%. Comparison of their test measurements was also made with theoretical and measured values. They noted that a significant underestimate of the theoretical value was shown in general. In contrast, the comparison with previous experimental data showed a difference to their results by about 10 - 20%. The present author believes that the differences could be due to particle size, shape etc, as these were not detailed in the work and no reasons for the discrepancy was given within the study.

Chandrasekar et al. [24] measured the thermal conductivity and viscosity of Al_2O_3-water nanofluids with nanoparticle size 43 nm and concentrations 0.33 to 5.0 vol.% at room temperature. They noticed that both thermal conductivity and viscosity increased with increasing nanoparticle concentration and that the viscosity increase was significantly higher than the increases in thermal conductivity. It was also found that the relative viscosity increases nearly linearly up to 2% volume fraction and the nanofluid viscosity, at high concentrations (5.0 vol.%), was up to 2.36 times that of the base fluid. Williams et al. [25] and Heyhat et al. [26] measured the viscosity and thermal conductivity of Alumina (Al_2O_3-water) nanofluid for various nanoparticle volume fractions and different temperature ranges. Under their test conditions, their results indicate that the viscosity of the nanofluid increases significantly with increasing nanoparticle concentration and the relative viscosity is unaffected by temperature. The empirical

viscosity model for their results was created as a function of the base fluid viscosity and the nanoparticle loading as shown below:

Williams et al. [25] $$\mu_{nf} = \mu_{bf}(T)e^{\frac{4.91\phi}{(0.2092-\phi)}} \quad (1.4)$$

Heyhat et al. [26] $$\mu_{nf} = \mu_{bf}(T)e^{\frac{5.989\phi}{(0.278-\phi)}} \quad (1.5)$$

where μ_{bf} is base fluid viscosity as a function of temperature (T) and ϕ is the volume fraction; a comparison of these models is made in section 3.4.

The viscosity and thermal properties of alumina and silica water nanofluids at high temperature ranges up to 80 °C were investigated by Mondragon et al. [27]. They observed that the viscosity and thermal conductivity were highly affected by nanoparticle agglomeration (i.e. when individual nanoparticles aggregate together due to the surface energy between the nanoparticles); they both increased with increasing agglomeration. They also observed that the increase in viscosity is noticeably higher than that of thermal conductivity.

Fedele et al. [22] used a rotational rheometer to study the viscosity of a TiO_2-water nanofluid with 76 nm nanoparticle concentrations of 0.24 vol.% to 11.22 vol.% across a temperature range of 10 °C to 70 °C. Their results showed that under the study conditions, the nanofluid behaves as a Newtonian fluid and viscosity increases with increasing nanoparticle load and decreases with increasing temperature. They also mentioned that the relative viscosity increase was independent of temperature and the nanofluid viscosity increase was 20%, 60% and 215% compared to the base fluid, for volume fractions 2.54 vol.%, 5.54 vol.% and 11.22 vol.%, respectively. The Batchelor predictive model underestimated the viscosity values except at low concentrations where they gave a good agreement; however, there are significant discrepancies in their viscosity values when compared to measurements made in comparable studies. Again, the present author believes that the differences could be due to particle size, shape etc, as details of these were not given and no reasons for the discrepancy was suggested within the study. Turgut et al. [28] also measured the viscosity of a TiO_2-water nanofluid with (21 nm) nanoparticle

concentrations of 0.2 vol.% to 3.0 vol.% and temperature range of 13 °C to 55 °C using a vibro-viscometer. Their results indicate that the nanofluid viscosity increased with increasing nanoparticle loads and decreased with increasing temperatures. The nanofluid viscosity trend is similar to the base fluid with increasing temperature. Comparison with the Einstein theoretical model showed that the viscosity theoretical model could not be used to predict the viscosity value at high nanoparticle concentrations.

Nguyen et al. [29] used a piston-type calibrated viscometer to measure the viscosity values of some nanofluids, two Al_2O_3-water nanofluids and one CuO-water nanofluid, with different particle sizes of 36 nm, 47 nm and 29 nm respectively. The measurements were conducted at a temperature range of 22 to 75 ^oC and varying volume fraction concentrations within the range 1.0 vol.% to 9.4 vol.%. The results show that the measured viscosity value depends on the type of nanoparticle, particle size, particle concentration and temperature. Their results also indicate that higher temperature leads to lower dynamic viscosity values and that higher nanoparticle loads and sizes generally result in higher dynamic viscosities. Pastoriza et al. [30] reported that nanofluids with small nanoparticles had higher viscosity when compared to similar volume fraction, when they tested two CuO-water nanofluids, with average nanoparticle size 30 nm and 11 nm. This result seems to be inconsistent with Nguyen et al's study.

Duan et al. [31] investigated the viscosity and rheological behaviour of an Al_2O_3-water nanofluid with volume fractions 1-5 vol.% and an average nanoparticle size 25 nm using a controlled rate rheometer. The tests were conducted after two weeks of preparation without and with re-ultrasonication. Their results indicated that the nanofluid without re-ultrasonication behaved as a non-Newtonian fluid; however, it became Newtonian after re-ultrasonication. It was found that the ratio of the viscosities of the nanofluid and the base fluid without re-ultrasonication was higher than with re-ultrasonication; it was 43 and 1.9 times the base fluid at high concentrations (5.0 vol.%) respectively and the relative viscosity was higher than the relative viscosity predicted by Einstein model. It was suggested that particle agglomeration was the main reason for the nanofluid’s behaviour and the cause of the significant difference between the experimental results and those of the theoretical viscosity models.

Interestingly, studies of very low volume concentrations for Al_2O_3-water nanofluid (0.01 - 0.3 vol.%) [21], TiO_2-water nanofluid (0.02 - 0.2 vol.%) [32] and CuO-water nanofluid (>0.016 vol.%) [33] have shown that the theoretical viscosity model by Einstein model could not estimate the viscosity of nanofluids.

An attempt was made by Sundar et al. [18] and Mahbubul et al. [34] to review all available experimental and theoretical literature for nanofluid properties with a specific focus on viscosity. They found that the following factors have a significant effect on nanofluid viscosity: nanoparticle concentration, nanoparticle size, nanoparticle shape, base fluid type and nanofluid temperature. It is noted that these correlations estimate the dynamic viscosity of a nanofluid to increase with increasing volume fraction concentration and decrease with temperature. They also noted that there was no consistency in the reported rheological behaviour of nanofluids or in viscosity trends across various types of nanofluids. Khanafer and Vafai [35] developed a correlation for an Al_2O_3-water nanofluid's dynamic viscosity with respect to volume fraction, nanoparticle size and temperature. This correlation summarised the previous experimental studies in the literature for volume fractions from 1% to 9%, temperatures from 20 to 70 °C and nanoparticle diameters between 13 nm and 131 nm. From this correlation, Mena et al. [36] extrapolated a correlation to predict the low temperature and low volume concentration behaviours of Al_2O_3-water nanofluids. Based on various researchers' experimental data for nanofluid viscosity, Corcione [37] developed an empirical correlation to predict dynamic viscosity. This correlation is given for nanofluids with volume fractions between 0.01 and 7.1 vol.%, nanoparticles with diameters between 25 and 200 nm, and temperatures in the range 20 to 50 °C. Recognising the discrepancy between the empirical and theoretical nanofluid viscosity models, Nwosu et al. [38] analysed them and suggested a technique which uses an algorithm to select a viscosity nanofluid model. This technique is based on user defined parameters such temperature, volume fraction, type of nanoparticle material and particle radius.

1.2.2: Heat transfer characteristic analyses of nanofluids

Previous studies concerning the evaluation of a nanofluid's heat transfer performance within a system or application may be classified into two main areas experimental analysis and numerical analysis.

- **Experimental studies**

The experimental studies may also be divided into two subcategories: whole system energy analyses or studies on convective heat transfer within tubes and pipes. The main advantage of the whole system analyses, which are less common, is the ability to evaluate the heat transfer enhancement of the whole system as a single part by measuring the thermal performance and the energy consumption of the whole system. However, this comes at the disadvantage of having to incorporate many factors and severely increases the complexity of such studies.

Roberts and Walker [39] investigated the heat transfer performance of a commercial electronic liquid cooling system for computational processing units using Al_2O_3 nanofluids with different concentrations up to 1.5 vol.%. They observed that the heat transfer coefficient was enhanced using nanofluids by 18% compared to the base fluid (deionized water). Rafati et al. [40] used three different nanofluids Al_2O_3, TiO_2 and SiO_2 in a mixture of deionized water and ethylene glycol for cooling a computer processor. Their results indicated that using nanofluids enhances the heat transfer by decreasing the operating temperature of the processor when compared to the base fluid and Al_2O_3 nanofluid gave the best cooling at volume fraction 1% by reducing the operating temperature from 49 to 44 °C.

Minsheng et al. [41] measured and compared the thermal conductivity of different nanofluids and investigated the effect of multi-walled carbon nanotube (MWNT)/water as a nanofluid on the performance of a 10-TR water chiller (air conditioner). Their results showed better thermal performance when using the nanofluid, which increased the cooling capacity by 4.2% at the standard rating conditions. Shengshan Bi et al. [42] investigated the thermal performance of domestic refrigerators by using TiO_2-R600a

nanorefigerants and pure R600a as a working fluids and found that TiO_2-R600a nanorefrigerant worked safely and normally. The energy consumption of the refrigerator decreased by 5.94% and 9.60% by adding 0.1 g/L and 0.5 g/L of TiO_2-R600a respectively.

Peyghambarzadeh et al. [43] used a nanofluid in an automobile radiator for enhancing the convection heat transfer by adding nanoparticles of Al_2O_3 into water at five different concentrations from 0.1 to 1.0 vol. % and at different operating inlet temperature (37-49 ^oC). Their results indicate that the Nusselt number was increased by up to 45% compared to the base fluid and this was strongly dependent on the particle concentration and the flow conditions, it was weakly dependent on the temperature. This enhancement of Nusselt number is attributed to the particle movement. Peyghambarzadeh et al. [44] also considered a water/ethylene glycol/Al_2O_3 nanofluid for the same application which gave a good agreement with the previous study: the Nusselt number was enhanced by up to 40% for both nanofluids and strongly depended on the particle concentration and the flow conditions, and was also weakly dependent on the temperature.

Naraki et al. also experimently investigated the overall themal performance of a car radiator using CuO-water nanofluids [45]. Data is given for CuO-water nanofluids with concentration range from 0.0 to 4.0 vol.% and under laminar flow behaviour. Their results showed that the heat transfer coefficient increased with increasing nanofluid concentrations and the enhancement was up to 8% at volume fraction 4.0 vol.%. This is significantly lower than Peyghambarzadeh et al. [43], and may suggest that Al_2O_3 nanofluids offer superior heat transfer because the Al_2O_3 nanoparticle has higher thermal conductivity when compared to CuO nanoparticle.

Teng et al. applied a Al_2O_3-water nanofluid in an air-cooled exchanger under laminar flow [46]. Their results indicated that, in general, the heat exchanger capacity was higher than with water for all concentrations and under their experimental conditions; they achieve 93% and 5.6% enhancement in the heat exchange capacity and pressure drop, respectively. Several researchers investigated using nanofluids in a flat plate solar collector [47-50]. They found the efficiency of the solar collectors increased by using nanofluids.

Experiments that deal with specific components, and not the system as a whole, have their own merits. The heat and flow characteristics of the fluid can be calculated accurately and in isolation of other effects. The outcome of these procedures can also contribute to or correlate with a numerical analysis. Previous studies concerning the evaluation of a nanofluid's convective heat transfer performance used forced convection, either experimentally or numerically for laminar and turbulent regimes. Experimental studies are reviewed first followed by numerical studies later in this section.

Williams et al. [25] experimentally investigated the heat transfer coefficient and pressure drop behaviour of fully developed turbulent flow (the same technique used in the present study). The tests were conducted for alumina (Al_2O_3)-water and zirconia (ZrO_2)-water nanofluids. Under the test conditions, their results indicate that using conventional correlations (Dittus–Boelter correlation) and models can predict the heat transfer coefficient and pressure drop of nanofluids. They also noted that the enhancement of heat transfer for the specified nanofluids was not abnormal under the test conditions. Heyhat et al. [26] also measured the heat transfer coefficient and pressure drop of Al_2O_3-water nanofluids at constant surface temperatures using a fully developed turbulent flow. They showed that the heat transfer coefficient and pressure drop of nanofluids could be estimated by applying conventional correlations and models. They argued that increasing the volume fraction of a nanofluid increases the heat transfer coefficient whilst there is minimal effect on the heat enhancement with increasing Reynolds number at a fixed nanoparticle concentration. Fotukian and Esfahany [51] also used γAl_2O_3-water nanofluid with volume concentration $\phi < 0.2\%$ within a turbulent flow regime to measure the convective heat transfer and pressure drop experimentally. Their results showed that using nanofluids noticeably increased the heat transfer performance. They also found that at Re = 10,000 with a volume fraction of 0.054%, the heat transfer was increased by 48% when compared to pure water and that traditional correlations of the heat transfer coefficient underestimated their results. The results indicated that pressure loss increases with increasing nanoparticles concentration.

Heat transfer and flow behaviour of Al_2O_3-water nanofluids were investigated experimentally by Sahin et al. [52]. The tests were conducted by varying the Reynolds

number from 4000 to 20,000 with volume fractions of 0.5, 1.0, 2.0 and 4.0 vol.%. They noted that heat transfer and pressure drop increase with increasing nanoparticle concentration with a notable exception that nanoparticle concentrations lower than 2.0 vol.% gave a higher heat transfer. It is found that at Re = 8000 and 0.5 vol.% the heat transfer enhancement is the highest and a correlation for convective heat transfer was developed.

Xuan and Li [53] used turbulent forced convection to investigate the heat transfer coefficient of Cu-water nanofluids flowing within a uniformly heated tube. They noticed that the heat transfer coefficient of the nanofluid increased significantly with increasing nanoparticle loads (volume fractions). Using a constant Reynolds number, the heat transfer coefficient of the nanofluids increased from 6% to 39% upon increasing nanoparticle loads from 0.5 vol.% to 2.0 vol.%. It was also noticed that, at the same Reynolds number, no significant pressure drop increase was found for any nanofluid concentrations. Interestingly, the experimental results showed that, at the same velocity, the nanofluid heat transfer coefficient increased with increasing nanoparticle concentrations. Furthermore, the existing conventional correlation (Dittus-Boelter correlation) poorly predicted the heat transfer coefficient. In contrast, the theoretical prediction of pressure drop shows better agreement when predicting the nanofluid pressure drop.

Pak and Cho [23] experimentally investigated the heat transfer performance of γ-Al_2O_3 (13 nm) and TiO_2 (27 nm) water based nanofluids under turbulent flow within a uniformly heated tube. Their results show that the Nusselt number of a nanofluid increases with increasing nanoparticle load and Reynolds number. However, they also noted that at a constant average velocity, the convective heat transfer coefficient of the nanofluid was 12% lower than that of pure water. The effect of nanoparticle diameter on heat transfer and pressure drop was studied by Arani and Amani [54]. The tests were conducted within the turbulent regime of TiO_2-water nanofluids with varying diameters (10, 20, 30 and 50nm) and Reynolds numbers. Their results showed that decreasing nanoparticle diameter had a minimal effect on heat transfer enhancement whilst the pressure drop increased noticeably with increasing Reynolds number and with decreasing nanoparticle diameter.

It was found that the nanoparticles with diameter 20nm gave the highest thermal performance factor under test conditions.

The turbulent heat transfer coefficient and pressure drop of TiO_2-water nanofluids with volume fractions of less than 0.25% in a circular tube and fully developed turbulent flow were investigated by Sajadi and Kazemi [55]. Their results were consistent with the previous study in that the heat transfer coefficient increased by about 22% and the pressure drop went up by 25% when compared to pure water. Also the comparison of the experimental data was in disagreement with the published correlation of Nusselt number such as Pak and Cho [23] and Xuan and Li [53] with the average discrepancy being about 30% too low.

He et al. investigated the heat transfer and flow characteristics of TiO_2-water nanofluid in a vertical pipe for laminar and turbulent flows [56, 57]. Their results showed that an increase in nanoparticle concentration enhanced the convective heat transfer coefficient at a given Reynolds number and particle size whereas the pressure drop of the nanofluid remained similar to the base fluid. Kayhani et al. [58] investigated the effect of particle volume fraction concentrations of TiO_2 nanoparticles (average size 15nm) in distilled water on heat transfer convective performance and pressure drop within the turbulent flow regime in a horizontal tube with constant heat flux boundary condition. They found that adding nanoparticles increases the heat transfer coefficient and pressure drop; however, the increase was not considered significant compared to the base fluid at a given Reynolds number. Sajadi and Kazemi [59] studied the heat transfer performance and pressure drop under turbulent flow of low concentration (less than 0.25 vol. %) TiO_2 nanoparticles in water. They found that there is a noticeable enhancement in heat transfer when adding nanoparticles. However, this enhancement was not affected by increasing nanoparticle concentration whilst the pressure drop increased with increasing nanoparticle concentrations. Also they found that increasing the Reynolds number decreased the ratio of heat transfer coefficient of the nanofluid with respect to the base fluid.

Convective heat transfer performance and pressure loss of CuO-water nanofluids ($\geq 0.3\%$) under turbulent flow in a tube was investigated by Fotukian and Esfahany [60]. The study's results tended to overestimate values up to 15% of the published values.

The heat transfer coefficient of γ–Al_2O_3–water nanofluid in a single tube (1.02 mm diameter) under constant heat flux and laminar flow were examined by Lai et al. [61] and Wen and Ding [62]. Their results show that the convective heat transfer coefficient increases with increasing nanoparticle concentration and volumetric flow rate. The effect of sonication on TiO_2–water nanofluid performance in a convective heat transfer loop under laminar flow with constant heat flux was studied by Rayatzadeh et al. [63]. Their results illustrated that using continuous sonication during the test enhanced the heat transfer performance of the nanofluid, especially at high concentration of nanoparticles. The convective heat transfer and pressure drop characteristics for Al_2O_3–water and ZrO_2–water nanofluids within a laminar flow regime are investigated experimentally by Rea et al. [64]. It is found that the heat transfer coefficient increased by 27% for 6 vol.% Al_2O_3–water nanofluids and by and 3% for 3.5 vol.% ZrO_2–water nanofluids compared to their base fluid; and that the pressure drop for both nanofluids was significantly higher than that of the base fluid. The prediction of traditional correlations of single-phase liquid showed good agreement with their results. The effect of particle size in Al_2O_3–water nanofluids on convective heat transfer characteristics in laminar developing regions in a tube was investigated by Anoop et al. [65]. The experiment was carried out with constant heat flux and two average sizes of nanoparticle (45 nm and 150 nm). The results indicated that both nanofluids with different particle sizes enhanced convective heat transfer considerably. Also, the nanofluid with average diameter 45 nm showed a higher heat transfer coefficient than the one with 150 nm; for example, at concentration 4 wt.% the enhancement in heat transfer coefficient with respect to base fluid was 25% and 11% for the nanofluid with 45 nm and 150 nm respectively. The result also showed a higher heat transfer characteristic with increase in nanoparticle concentration.

Heris et al. [66] experimentally investigated the heat transfer coefficient of CuO-water and Al_2O_3–water nanofluids in a circular tube at constant wall temperature under laminar flow. They found that nanofluids enhanced the convective heat transfer and that

the Al_2O_3–water nanofluid was superior to the CuO-water nanofluid. The heat transfer coefficient of nanofluid gives a higher value with respect to the correlation of single-phase liquid. On the other hand, convective heat transfer of tube with square cross section was investigated under constant heat flux and laminar flow using Al_2O_3–water nanofluid by Heris et al. [67]. The results indicated that using nanofluids enhanced the heat transfer rate compared to the base fluid through the square tube and the predicted traditional correlation of single-phase liquid for laminar flow (by Sieder–Tate correlation) gave lower value to the experiment results. The present author believes that the enhancement of convictive heat transfer is due to not only the thermal conductivity increase but also Brownian motion, particle migration and dispersion.

To conclude the experimental studies, various experimental forced convection heat transfer studies were reviewed comprehensively by Gupta et al. [68]. They found that in general, using nanofluids enhanced the convective heat transfer coefficient with respect to the base fluid and this enhancement increased with increasing nanoparticle concentration and Reynolds number. Lack of agreement is likely due to no standardised testing method and poor research into or characterisation of agglomeration. Further research needs to show when agglomeration takes place.

- **Numerical studies**

Computational Fluid Dynamics (CFD) is also used to analyse thermal and flow characteristics of nanofluids. There are several commercial CFD programmes like Fluent and COMSOL available. These convert the governing fluid equations to algebraic equations using control volume, finite difference or finite element methods, allowing the governing equations to be solved numerically. The results of this are pressure, temperature and velocity distributions which can be used to calculate heat transfer and flow characteristics, etc... The studies on nanofluid were considered to dealing with nanofluid as a single phase (by considering the fluid phase and nanoparticles to be in thermal equilibrium with the same velocity) and a two-phase model (considering the fluid and nanoparticles to have different velocities). This section describes a selection of numerical studies on nanofluids.

A number of researchers have previously numerically studied forced convection of a nanofluid. Demir et al. [69] used CFD (Fluent) to investigate the flow and thermal performance in a horizontal tube by using TiO_2-water and Al_2O_3-water nanofluids with different volume fractions. Their results showed that the nanofluids significantly enhanced the heat transfer and this enhancement increased with increasing particle concentration, but also increased the pressure drop. The heat transfer in a horizontal circular tube with Al_2O_3-water nanofluids was also studied numerically using a two-phase Eulerian model considering the fluid and nanoparticles to have different velocities by Lotfi et al. [70]. They also compared their results from a single-phase model and a two-phase mixture model to published experiment results; the mixture model predicted the Nusselt number of the experimental results much better than the other two models.

Santra et al. [71] used the finite difference method to analyse two-dimensional steady-state heat transfer in a rectangular duct with two walls at a constant temperature using a copper-water nanofluid. Their study considered the effect of assuming the nanofluid to be Newtonian and non-Newtonian, using Reynolds numbers of 5 to 1500 and volume fractions of 0.0 to 5.0 vol.%. The results show that the heat transfer coefficient of the nanofluid is higher than for the base fluid and increases with increasing Reynolds

number and volume fraction for both cases. Raisi et al. [72] also studied the heat transfer of microchannel which was heated partially from the top and bottom walls using water and copper-water nanofluids as a coolant by applying a control volume method. The effect of varying Reynolds number from10 to 500 and volume fractions of 0.0 to 5.0 vol.% with slip and no slip boundary conditions on heat transfer was investigated. It was observed that there is a high heat transfer rate at high Reynolds numbers, which increases with increasing volume fractions. At low Reynolds numbers, the effects of volume fraction and slip boundary condition are negligible. However, the slip velocity increased the heat transfer rate significantly at higher Reynolds numbers.

The heat transfer coefficient of a straight tube was numerically investigated under the laminar flow regime using Fluent by He et al. [73]. The results indicated that the effect of thermal conductivity was dominant on convective heat transfer and the effect of Brownian force and thermophoretic force was negligible. Fard et al. [74] calculated the heat transfer coefficient of different nanofluids using single-phase and two-phase models under laminar flow and constant wall temperature conditions within a circular tube. Their results showed that both models gave a good agreement with the empirical results, but the two-phase model was more accurate. They predicted that using nanofluids enhanced the heat transfer coefficient, which increased with increasing nanofluid concentrations and Peclet numbers. Moraveji and Esmaeili [75] also numerically studied single-phase and two-phase models to predict the heat transfer performance of water-Al_2O_3 nanofluids in a circular tube under constant heat flux and laminar flow conditions. Their results indicated that single phase and two-phase models showed good agreement with each other and with the literature.

1.2.3: Nanofluids economic analysis

Using nanofluids in practical applications is subject to an economic analysis evaluation; since nanofluids increase both the heat transfer and the pressure drop they may only provide an economic benefit in certain applications where pumping costs are low or high density cooling is required. Besides this the high cost of nanofluids increases capital costs and is considered one of the key obstacles in employing nanofluids in some applications [40, 68, 76].

There are few studies applying economic analysis to nanofluids. Faizal et al [77] analysed the solar collector economically using various nanofluids to achieve the same output temperature. The results showed that reduction in solar collector area compared to conventional one was estimated to be 25.6%, 21.6%, 22.1% and 21.5% for CuO, SiO_2, TiO_2 and Al_2O_3 nanofluids respectively. This could therefore reduce the weight and cost to manufacture the collector. The solar collector payback period was estimated to be 2.4 and 2.5 years using nanofluids and traditional fluids, respectively. Otanicar and Golden [76] also investigated the economic impact of using nanofluids in a solar collector. Their results showed that the nanofluid improved the solar collector efficiency and they found the conventional solar collector gave a slightly shorter payback period with respect to using nanofluid; they attribute this to the cost of nanofluids.

1.2.4: Data centre cooling

A major part of the energy consumed in a data centre is due to the cooling system needed to manage the heat generated from the servers processors and memory [78]. Therefore, reducing these loads and finding a new way to efficiently cool the servers both protects their components and increases the performance and reliability; this is one of the most important energy conservation measures in a data centre [3]. The use of nanofluids as liquid cooling in data centre cooling system will serve this very objective [40].

There are several techniques for cooling the electronic systems within data centres such as forced air cooling, liquid cooling and direct contact cooling (immersion cooling) [3, 78-81]. Air cooling methods are the most common means of cooling a data centre [3], see Figure 1.4. The computer room air conditioning (CRAC) units supply the cool air through an under floor plenum to the front of the rack which passes through the servers to cool them, then the hot air flows back to the CRAC units which cools the air and re-circulates back to the under floor plenum. This method needs to maintain a relative humidity within the recommended operating envelope to avoid condensation which can cause corrosion issues or too dry an air which causes electrostatic discharge risk [82, 83]. Liquid cooling methods bring the cooled water to the rack or into the server as a heat exchanger on the front or rear of the rack or alternatively to heat sinks on the top of the chips, see Figure 1.5 and Figure 1.6 respectively. The back or front door cooling method uses cool air as in Figure 1.5, which is passed through servers to remove the heat and passes it through the heat exchanger to dissipate the gained heat by fans; then the cool air circulates again. Whereas Figure 1.6 shows a system bringing the cool water into the server through the cooled plate over the chip to remove the heat directly. There is, however, the risk of water leaks from liquid cooling methods which may damage electronic components of the server and result in data loss [84, 85]. Therefore, using a dielectric liquid coolant, such as mineral oil or fluorocarbons (i.e. perfluorocarbons types and hydrofluoroethers (HFE)) which are among the most commonly used in direct cooling systems [86, 87], is desirable to protect the server electronic components.

The direct contact liquid cooling technology is used in two ways; the servers can be submerged in either an open or a closed bath of dielectric liquid as shown in Figure

1.7 and Figure 1.8, respectively. In the open bath system the cooled dielectric liquid is pumped to the bath to remove the heat from the server component and then pumped back to the heat exchanger to dissipate the heat. Whereas, in the closed bath, the dielectric liquid removes the heat from the chip by boiling and then condenses to liquid again at the cooling coils; the difference between the opened and the closed bath cooling system is that the latter does not need a pump to circulate the dielectric liquid. The other technique of immersion methods is offered by a manufacturer of liquid cooling equipment, Iceotope [3], see Figure 1.9. The server is sealed as a bath and filled with a dielectric liquid (HFE) to immerse the server motherboard to remove the generated heat of the electric components by applying heat exchanger on the wall of server bath. The heat exchanger coolant (water) is circulated to cool.

In this study, an analysis of the thermal performance and the flow characteristic on a data centre server based on the server of Iceotope model using nanofluids as a coolant is carried out.

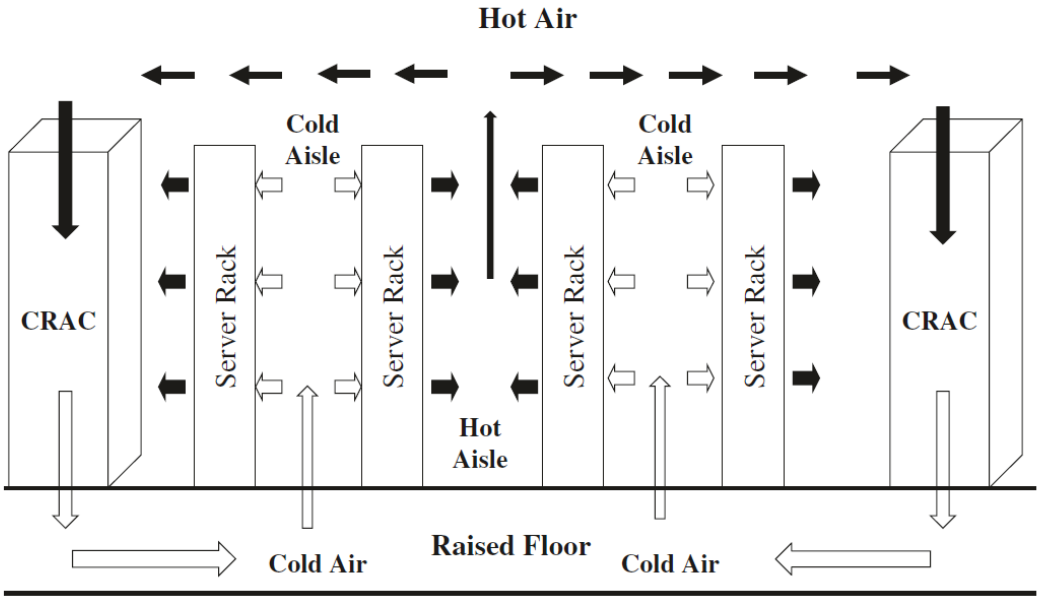

Figure 1.4: A diagram of air cooling data centre [3]

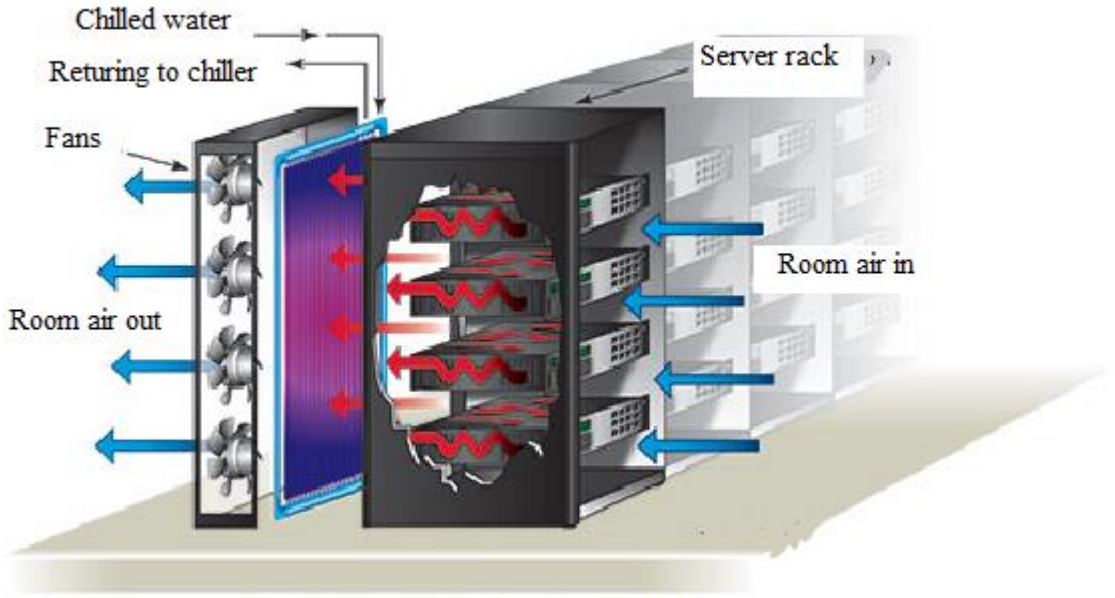

Figure 1.5: Rear door rack liquid cooling system
(http://www.icsdatacentrecooling.co.uk/server-rack-cooling-systems/)

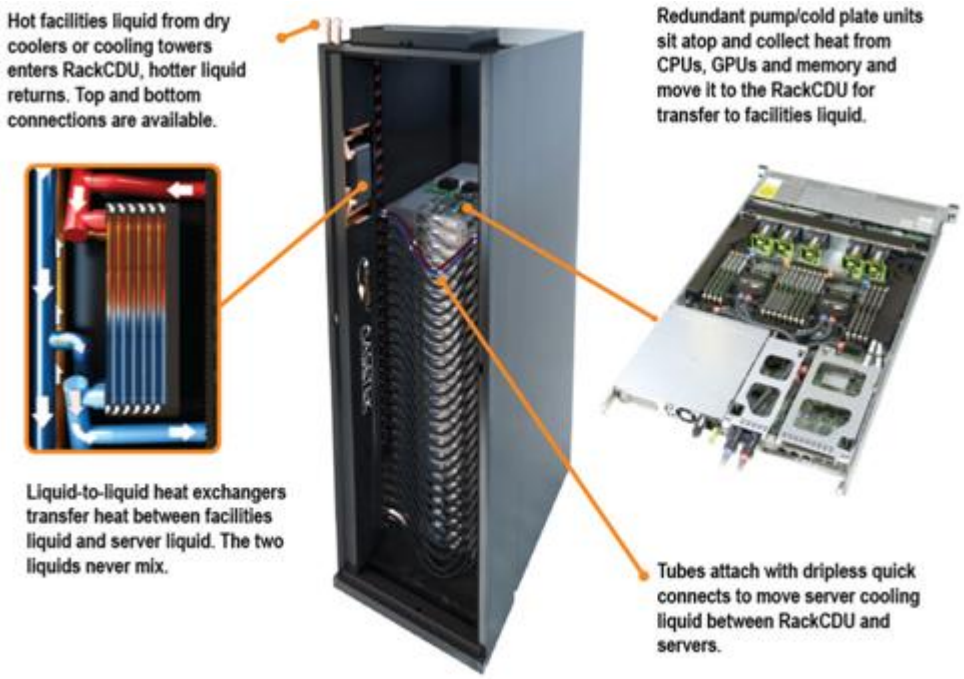

Figure 1.6: The picture shows server cooling by liquid cooling system [88]

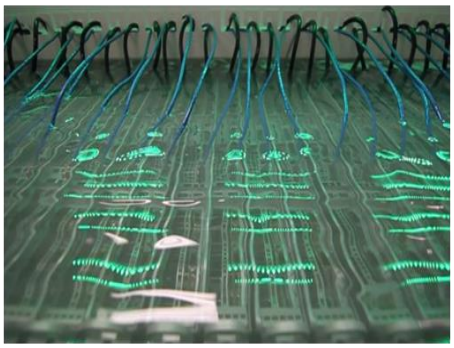

Figure 1.7: Open bath immersion cooled cooling system(http://www.grcooling.com/gallery/)

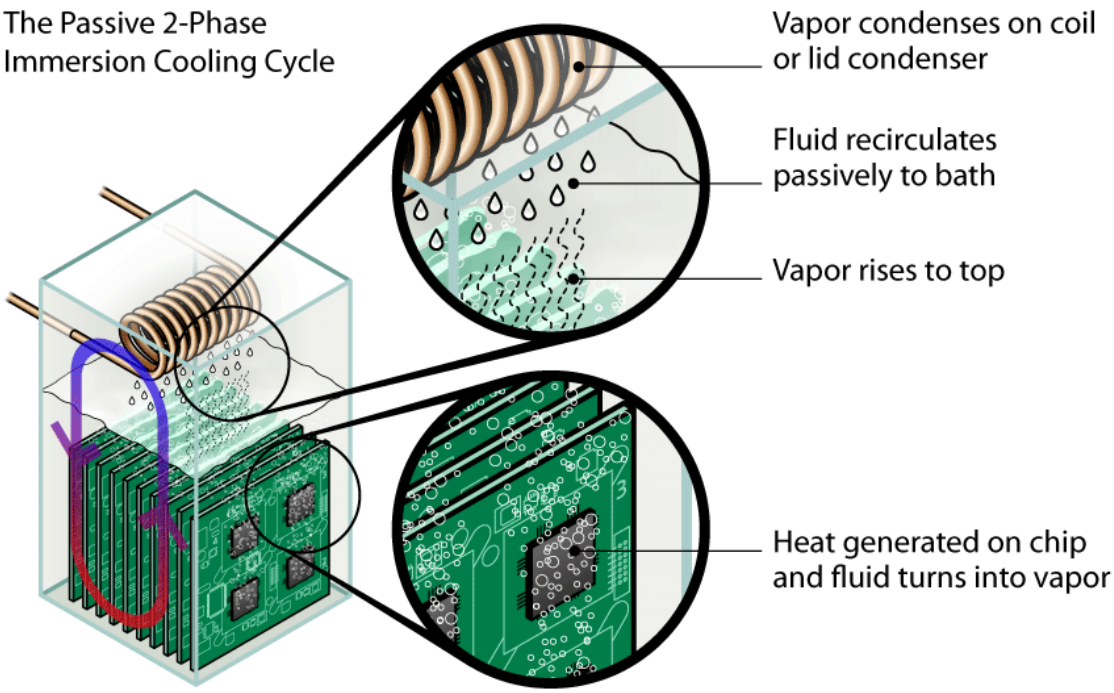

Figure 1.8: close path two-phase immersion cooled cooling system (http://www.allied-control.com/immersion-cooling)

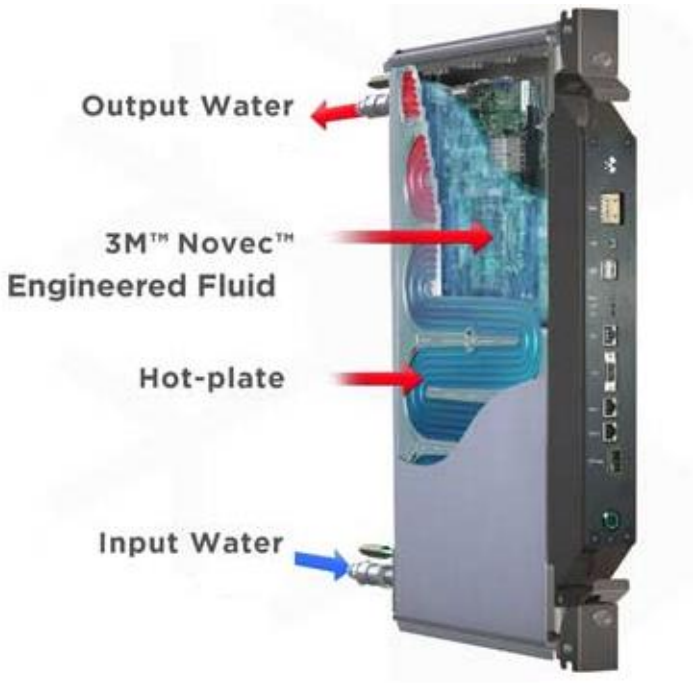

Figure 1.9: A diagram of the direct contact liquid cooling of Iceotope liquid cooling system [89].

1.3: Summary of Literature Review

In general, there is a need to standardise the experimental procedure for the measurement of properties such as the thermal conductivity (as Buongiorno et al. [12]) and viscosity of nanofluids since there is no consistent method in the literature for determining and calculating these values. In addition, there is a need to make comparisons with published values and to establish methods of calculating values as dynamic viscosity for a specific type of nanofluid as a function of the nanoparticle type, nanoparticle size, volume concentration and temperatures as well as corrections for the stability of the nanofluids as it ages. In addition, the viscosity of nanofluids, which are used to evaluate the thermal performance and the pump power, needs to be considered in detail.

Determination of the thermal characteristics of many different specific components of a system as well as the system as a whole, using refined thermal properties of nanofluids and accurate representations of the heat transfer characteristics, is needed since there are differing opinions on the true benefits and costs of employing nanofluids to enhance heat transfer. Using nanofluids has the potential to improve heat transfer but there are still difficulties in determining the true benefits and costs of using nanofluids and significant disagreements between experimental and theoretical studies. There is also controversy on whether to deal with a nanofluid as a homogeneous liquid or a two-phase material. A great deal of investigation is still required in order to calculate the optimum concentration of nanofluids recommended for a specific application to work normally, safely and efficiently by calculation of the thermal performance and the energy consumption of the system as well as its pressure drop.

The thermal performance and the energy transfers within a system depend upon the type of the nanoparticles and their concentration within the base fluid, and the system itself. An economic analysis is required along with the heat transfer calculations in order to determine the optimum nanofluid to use in a system since nanofluids have high costs.

There are different cooling techniques to reduce the temperature of a data centre as well as the temperature of the electronic components of a server; nanofluids are seen as a promising cooling technique.

1.4: Practical Relevance

The viscosity of various nanofluids measured in the present study is used in the experimental and computational thermal analyses, also carried out in this thesis. These properties could also be of use to other investigators, especially since there is a general shortage of detailed and reliable measurements of nanofluid viscosity. The present experimental activity also includes measurements of the viscosity of nanofluids at different temperatures and nanoparticle concentrations. Such information is useful since the nanofluids are usually subjected to large temperature fluctuations in practical applications, and dynamic viscosity can vary appreciably with nanoparticle concentration and temperature.

The thermal performance (heat transfer coefficient) and flow characteristics (pressure drop) of nanofluids measured in specific components are important. Comparisons with data in the literature are carried out and also dealing with nanofluid as a single phase or two phases flow is of vital importance, since there is a controversy of nanofluid behaviour.

Another important issue that concerns the practical relevance of the present thesis is the determination of recommended nanofluid concentrations for typical data centre cooling systems. This issue is of vital importance with regard to energy conservation in data centres. The use of a nanofluid with an optimum volume fraction is a major step towards optimizing the total cost, which comprises the cost of energy consumption due to the electronic devices (servers in the data centre), cooling system and pump plus the cost of the nanofluids itself. The volume fraction calculated for typical nanofluids under the considered conditions should benefit the energy conservation in data centres.

1.5: Objectives

There are three main objectives in the present work. The first objective is measuring the thermophysical properties of nanofluids and proposing a correlation viscosity. The second objective is the measurement and calculation of the thermal and flow characteristics of various nanofluids. The third objective is simulating nanofluids within a data centre cooling liquid loop using different nanofluids and predicting the recommended volume fraction for these nanofluids by the application of an economic analysis. In general, all objectives can be summarised as follows:

1. Survey and collect samples of nanofluids produced by commercial companies and also try to produce nanofluids in our laboratory.

2. Measure the viscosity of the nanofluids as a function of temperature as well as nanoparticle volume fraction.

3. Suggest and propose a correlation for viscosity as a function of volume fraction and temperature. Then compare this with current theoretical and empirical correlations.

4. Build an experimental loop to evaluate heat transfer performance and pressure drop of commonly used nanofluids.

5. Measure thermal and flow characteristics of nanofluids by applying them in the test loop. A comparison with the conventional and existing correlation will be made in terms of heat transfer coefficient and pressure drop.

6. Survey and collect information of data centre cooling techniques and collect data regarding the thermal properties of server materials.

7. By utilising a model based on the finite-element method (COMSOL program), evaluate and compare the thermal performance and flow characteristics of a cooling nanofluid within a data centre server based on various nanoparticle volume fractions.

8. Evaluate the benefit of nanofluids within the cooled plate of immersed liquid cooling scenarios.

9. Determine the optimum nanoparticle concentration and recommended nanofluids for the application under work conditions and given types of nanofluids and nanoparticles concentration. These would be subject to certain (thermal performance) thermal conditions of the data centre and specific values of a number of economic parameters.

10. Investigate the effects of some parametric study on the optimum nanoparticles concentration such as changing the configuration of server and the effect of economic factors

CHAPTER 2: NANOFLUIDS PREPARATION AND CHARACTERISTICS

2.1: Introduction

There are many types of nanofluids available; these differ with the base liquid type such as water, ethylene glycol and oil. They also differ in regards to nanoparticle material, size, shape and concentration [90]. An important issue facing scientists in creating a nanofluid is dispersing the nanoparticles homogeneously within the base fluid and the stability of these over time. Another issue is reducing the agglomeration of nanoparticles to avoid sedimentation due to gravity [91].

There are two main techniques for dispersing nanoparticles into a base fluid when preparing a nanofluid: the single step technique and the two step technique. The single step technique involves simultaneously producing and dispersing nanoparticles into a base fluid at the same time. The two step method involves first producing the nanoparticles and then dispersing them into the base fluid, this needs high shear and ultrasound to aid dispersion of the nanoparticles into the fluid. This technique is mainly used to produce nanofluids with oxide nanoparticles and is preferred by researchers [11, 90-92] since it is easy to find the oxide nanoparticles and prepare nanofluids. However, the single step method is characterised by stability and less agglomeration of nanoparticles and also it is easier to control the size and the shape of the nanoparticles, but is more expensive.

The nanoparticles of the two step technique are produced by physical processing such as mechanical grinding and ball milling or can be synthesised by chemical processes such as Chemical Vapour Deposition (CVD) or chemical precipitation. The output of these processes is a powder with different size and shape and a variety of types such as carbon nanotubes, oxide ceramics, nitride ceramics, carbide ceramics, metals or composite materials [11, 90].

From the previous studies, the procedures of nanofluid preparation and evaluation can be summarized in the diagram shown in Figure 2.1. The abbreviations of TEM and SEM refer to Transmission Electron Microscopy and Scanning Electron Microscopy, respectively.

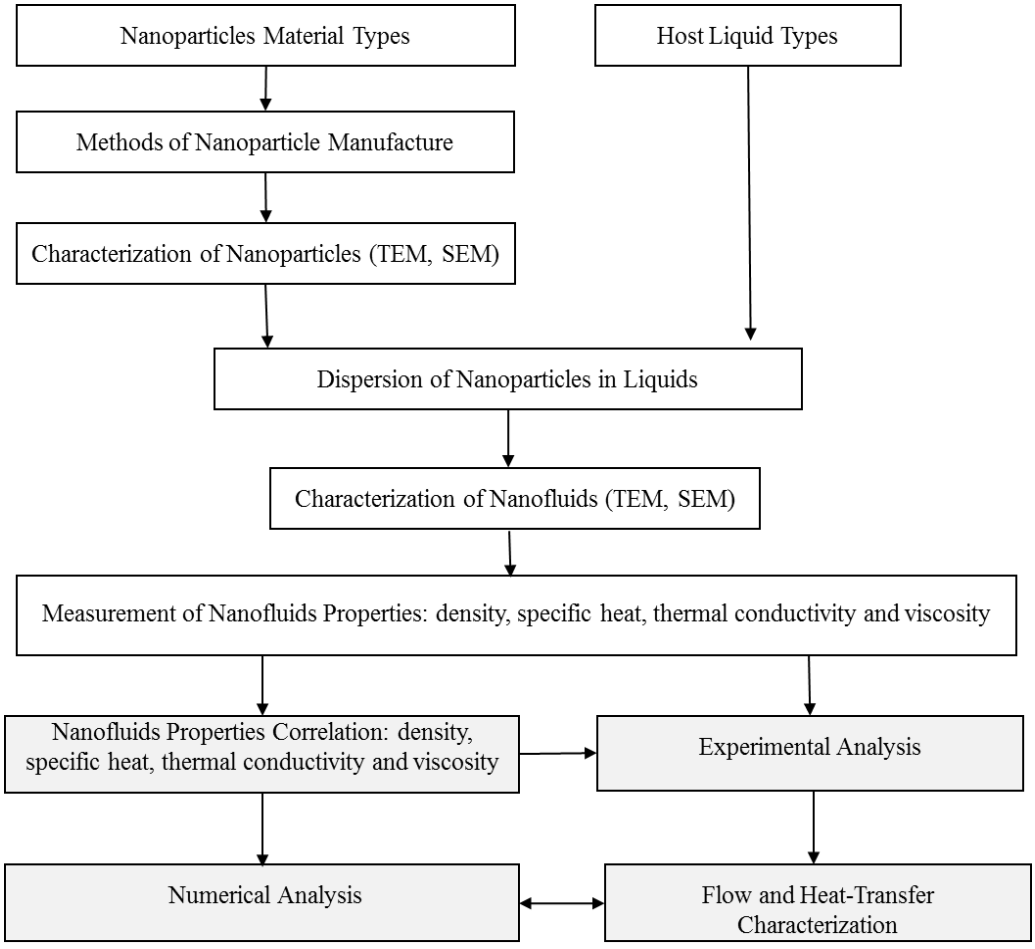

Figure 2.1: Diagram showing a preparation procedure of a nanofluid.

2.2: Nanofluids Preparation

In this study, aluminium oxide (Al_2O_3-water), titanium oxide (TiO_2-water) and copper oxide (CuO-water) nanofluids were chosen because they are the most commonly used, easiest to prepare and are commercially available as a nanofluid.

The alumina (Al_2O_3-water) nanofluids were prepared using the two step technique mentioned above. The nanoparticles were supplied by Sigma-Aldrich with an average size of 50 nm and added to distilled water using magnetic stirring and ultrasonic agitation to disperse the nanoparticles in the base fluid to get a nanofluid with mass fraction of 20 wt.%. While titanium oxide (TiO_2-water) and copper oxide (CuO-water) nanofluids were purchased premixed from Alfa Aesar as a colloidal dispersion nanofluid with mass fractions of 50 wt.% and 45 nm average nanoparticle size for TiO_2-water nanofluid and 35 wt.% with nanoparticle size 30 nm for the CuO-water nanofluid. These concentrations of the nanofluids were diluted into distilled water to get nanofluids with a variety of volume fractions, as explained in the next section. The dilution process was undertaken by stirring and shaking the mixture without any additional processes.

2.3: Dilution Processes

The nanofluids discussed above with mass fractions 20 wt.%, 50 wt.% and 35wt% were diluted into distilled water to get nanofluids with a variety of volume fraction concentrations i.e. 0.5, 0.9, 1.8, 2.7, 3.6, 4.7, 5.9 vol.% for Al_2O_3-water and 0.5, 1.5, 2.5, 3.5, 4.5 vol.%; and 0.4, 0.8, 1.2 and 1.6 vol.% for TiO_2-water and CuO-water nanofluids. It should be emphasised here that the dilution was calculated based on the properties of the base fluid and nanoparticles at room temperature (22 °C). Also because of the high cost of CuO-water nanofluid, only low concentration amounts were prepared.

The dilution process calculations are as follows.

The mass fraction, f and volume fraction, ϕ of the nanofluid are calculated from:

$$f = \frac{m_p}{m_t} \text{ and } \phi = \frac{V_p}{V_t}$$

where m_t and V_t are respectively the total mass and volume of the base fluid and nanoparticles together (i.e. the nanofluid), and m_p and V_p are respectively the mass and volume of the nanoparticles. Hence $m_t = m_{bf} + m_p$ and $V_t = V_{bf} + V_p$ where m_{bf} and V_{bf} are respectively the mass of volume of the base fluid. Naturally, the density of the base fluid is given by $\rho_{bf} = m_{bf} / V_{bf}$ and that of the particles is $\rho_p = m_p / V_p$.

The relationship between volume fraction and mass fraction is:

$$\phi = \frac{f\rho_{bf}}{\rho_p(1-f) + f\rho_{bf}} \tag{2.1}$$

and the nanofluid density is calculated by $\rho_{nf} = \rho_{bf}(1-\phi) + \rho_p\phi$.

It is assumed that the purchased nanofluid's advertised specific mass fraction $f(1)$ is precise and accurate, and further volume fractions used are diluted from this assumed value. From Eq. (2.1), the volume fraction of the nanofluid $\phi(1)$ can be *calculated*. In order to create a nanofluid sample of the required volume fraction $\phi(2)$, the stock nanofluid should be diluted with a volume $V_{bf}(\text{add})$ of distilled water. If the initial volume of nanofluid is $V_t(1)$, the volume of the nanoparticles within this volume is $V_p(1) = \phi(1)V_t(1)$. This particle volume remains the same after dilution, so it follows that $\phi(1)V_t(1) = \phi(2)V_t(2)$ where $V_t(2) = V_t(1) + V_{bf}(\text{add})$ is the nanofluid (i.e. total) volume after dilution. Rearranging this yields

$$V_{bf}(add) = \left(\frac{\phi(1) - \phi(2)}{\phi(2)}\right) V_t(1)$$

as the volume of distilled water required to achieve the desired nanoparticle concentration.

2.4: Nanoparticle Imaging

The morphology of the nanoparticles within the synthesized and purchased nanofluids was explored using Transmission Electron Microscopy (TEM) images (Jeol JEM-2100F model) to verify the nanoparticles' size and shape. The TEM images were produced by the author by taking two spots of a sample; two images can be seen in each of Figures 2.2 to 2.4 for the three different nanofluids. The images, Figure 2.2, Figure 2.3 and Figure 2.4 show that Al_2O_3 and TiO_2 nanoparticles are of non-spherical and irregular shape and variety of sizes; the average size of the particles is about 50 nm and 45 nm respectively. In contrast, CuO is almost spherical in shape with typical diameter of 30 nm, as stated by the manufacturer. The TEM was also used to determine the nanofluid agglomeration – as observed from Figure 2.2 - 2.4; the nanoparticles aggregate forming larger particles. However, the drawback of the TEM is that the sample of nanofluid should be dried out before insertion inside the device. This causes the nanoparticle agglomeration, and so the agglomeration observed in Figures 2.2 to 2.4, could be a result of the drying process rather than existing in the original sample.

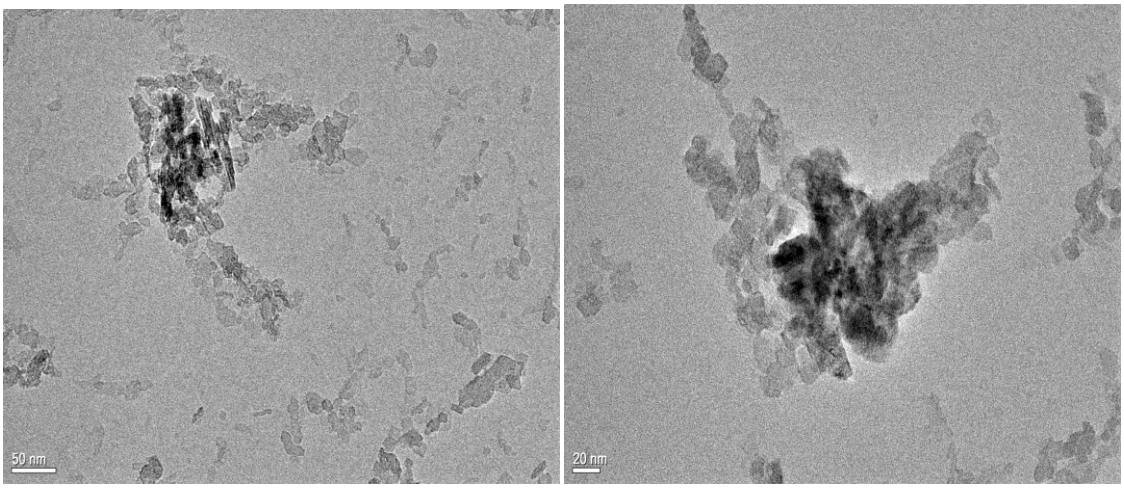

Figure 2.2: TEM images showing the shape and diameter of the Al_2O_3 nanoparticles.

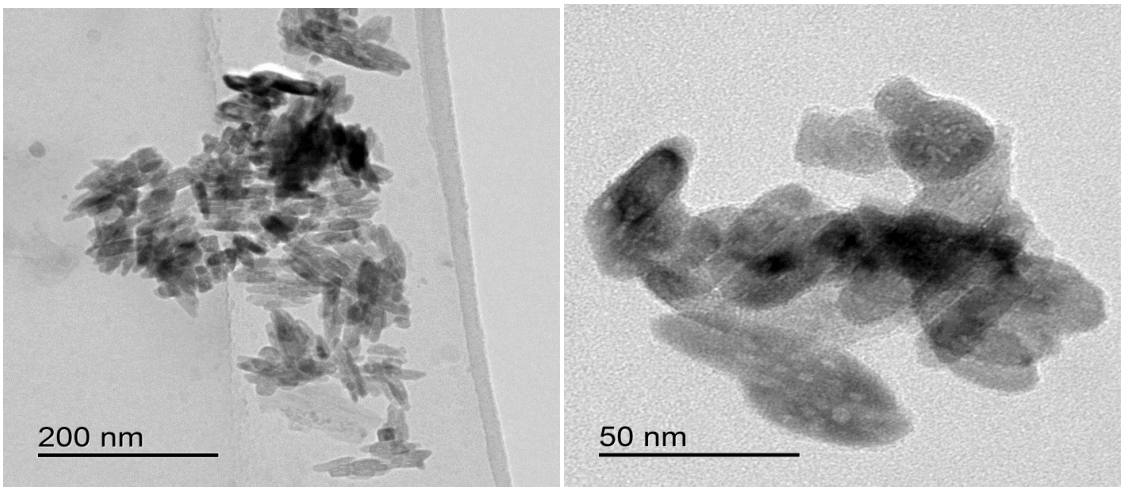

Figure 2.3: TEM images showing the shape and diameter of the TiO_2 nanoparticles

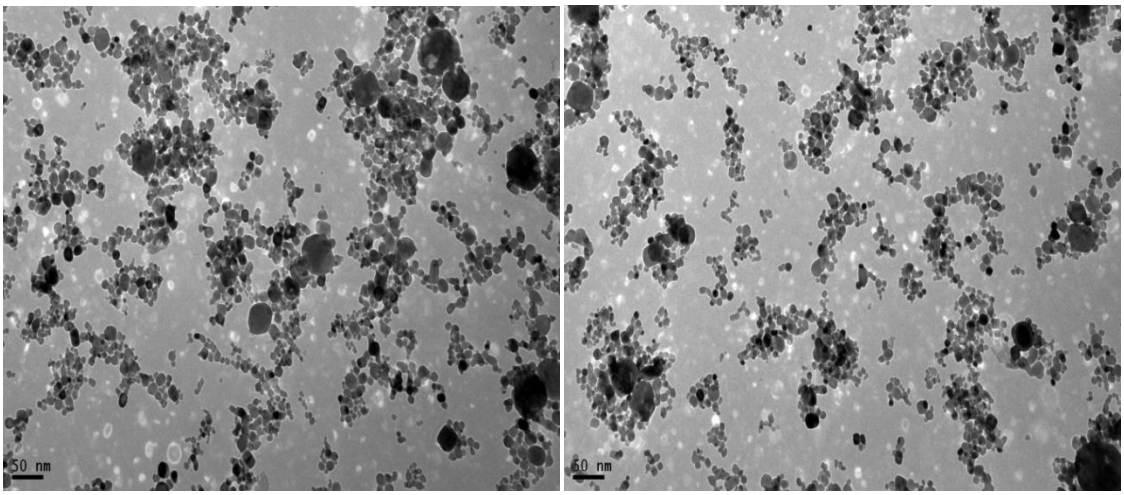

Figure 2.4: TEM images showing the shape and diameter of the CuO nanoparticles

2.5: Conclusion

Nanofluids are composed of a base fluid, such as water or ethylene glycol, and a nanoparticle, which enhances the thermal conductivity and heat transfer performance of the base fluid. There are two methods to produce a nanofluid namely the single step technique or the two step technique. The two step method is commonly used when producing a nanofluid which contains oxide metals. In this study the aluminium (Al_2O_3-water), titanium oxide (TiO_2-water) and copper oxide (CuO-water) nanofluids were chosen because they are most commonly used. In order to produce a variety of volume fractions of these nanofluids, a dilution process was followed. Transmission Electron Microscopy (TEM) was used to verify the nanoparticle morphology.

CHAPTER 3: MEASUREMENTS OF THE VISCOSITY OF NANOFLUIDS

3.1: Introduction

Estimation of the heat transfer coefficient and pressure drop of a nanofluid within an application depends strongly on the fluid's viscosity and thermal conductivity. Accurate CFD analyses of such systems require the thermo physical property values of the fluid as an input, therefore accurate and reliable representations of the nanofluid properties are essential. Within the literature, previous experiments carried out on nanofluid properties have specifically focussed on measuring the thermal conductivity of nanofluids and few experiments have examined the measurement of viscosity [18, 22, 24, 34, 35, 38]. Within these experiments, there is little or no consistency in the prediction of specific viscosities [18, 19].

The accuracy of these property values is sometimes questionable since complete and important information is often lacking. On many occasions, viscosity values are quoted for nanofluids without giving the type of nanofluid and temperature. Besides, the viscosity of many nanofluids is subject to nanoparticle stability effects, which also depend upon nanoparticle size and the nanofluid synthesis method. In general, the properties of nanofluids depend on the nanoparticle concentration, temperature, type, as well as particle size and structure or aggregation [63, 64, 66] which may significantly affect nanofluid viscosity. Therefore, it is very important to develop a database for nanofluid properties and especially commercially manufactured nanofluids.

The present study uses an accurate experimental technique for measuring the viscosity of some commonly used nanofluids. The effects of temperature and volume fraction variations on the viscosity are also examined and comparisons are made with previous experimental and theoretical studies.

3.2: Experimental Methods

3.2.1: General methods for measuring viscosity

There are many instruments available for measuring viscosity, which is defined as the continuous deformation (shear rate) of fluid under the action of a shear stress or more generally as the resistance of a liquid to flow [93]. These instruments are based on different principles and techniques. The techniques are broadly classified as, those which measure the resistance of liquid to flow using a stationary object such as a capillary viscometer, or those which measure viscosity using moving objects such as rotational viscometers [94]. In principle, Capillary viscometers calculate the flow rate of a liquid sample of known dimensions, where the flow from one side to the other is governed by a pre-determined pressure drop or gravity. For this type of viscometer, the testing time is a function of the sample's viscosity. Rotational viscometers, on the other hand, measure the torque required to rotate a spindle in a liquid. Therefore, rotational viscometers are distinguished or preferred mainly by their ease of use and the short time, typically in the region of a couple of minutes, required to obtain the desired results.

3.2.2: The Kinexus system

The Malvern Kinexus Pro rheometer, which utilises the rotational rheometer platform technique, was used in the present work to measure the viscosity of the nanofluids (see Figure 3.1). The following sections give a brief description of this technique and its theoretical background. More details and the technical use of various other options and extensions that the apparatus can support can be found in the user manual [95].

Figure 3.1: Diagram of the Malvern Kinexus Pro rheometer and a typical element and sample arrangement[95].

3.2.3: Description

The Malvern Kinexus Pro rheometer is designed to measure viscosity, based on the theory of controlled shear deformation of a sample by applying torque [94]. The test sample is placed on the lower geometry (circular plate) and the spindle cone, with diameter 40 mm and incline 4°, is positioned above the lower plate; the gap between them is 0.03 mm (see Figure 3.1).

The main advantages of the Kinexus rheometer are: accuracy (the manufacturer quotes a value of ± 1% but this is verified in the next section); that it gives a wide range of viscosity measurements; that it produces results in a relatively short time; and that it can use different spindle sizes to accommodate different sample types. It is however constrained to a sample size of about 5ml. The temperature of the sample can be controlled, since rheological properties are a strong function of temperature, within the range -40 to 200°C with resolution of 0.01°C. The sample is covered to protect it from environmental conditions and contamination.

3.2.4: Measurement procedure

The first part of the experiment involved measuring the dynamic viscosity of water at different temperatures to verify the accuracy of the Kinexus rheometer. The second part involved measuring the viscosity of all nanofluids, which had been previously prepared, at atmospheric pressure and different mean temperatures in the range 15 to 40 ^{o}C. Measurements were carried out for three specimens of each test sample of the nanofluids; the viscosity was measured for each specimen by applying shear rates from 200 to 1400 s^{-1} for the whole range of test temperatures, then mean values of viscosity were obtained by averaging.

The nanofluid rheological behaviour was checked just for the highest concentration of each nanofluid by applying variable shear rates from 100 to 1400 s^{-1} for the whole of the temperature range studied. Since the nanoparticles in nanofluids tend to settle over time, they were shaken using ultrasonic agitation prior to each measurement test. The results of the experiment will be discussed in the next section.

3.3: Experimental Verification Test

The accuracy of the Kinexus rheometer was checked by measuring the viscosity of distilled water at different temperatures from 15 to 40 °C and compared to data from the literature using equation (3.1)[54]. The results show that the dynamic viscosity values are within 5% of average values (see Figure 3.2 and Table 3.1).

$$\ln\left(\frac{\mu_{bf}(T)}{0.001792}\right) = -1.24 - 6.44\left(\frac{273.15}{T}\right) + 7.68\left(\frac{273.15}{T}\right)^2 \qquad (3.1)$$

where μ_{bf} is the base fluid viscosity in (Pa.s) and T is the temperature in (°C).

Table 3.1 summarizes the values of the measured viscosity of water under investigation conditions at atmospheric pressure. The measured viscosity values are presented based on average data ± a standard deviation and also the fitting value which comes from the relation between shear stress and shear rate; they show that the results are within 5% and 7% of average, respectively. This indicates that the measured dynamic viscosity in this study is accurate and precise.

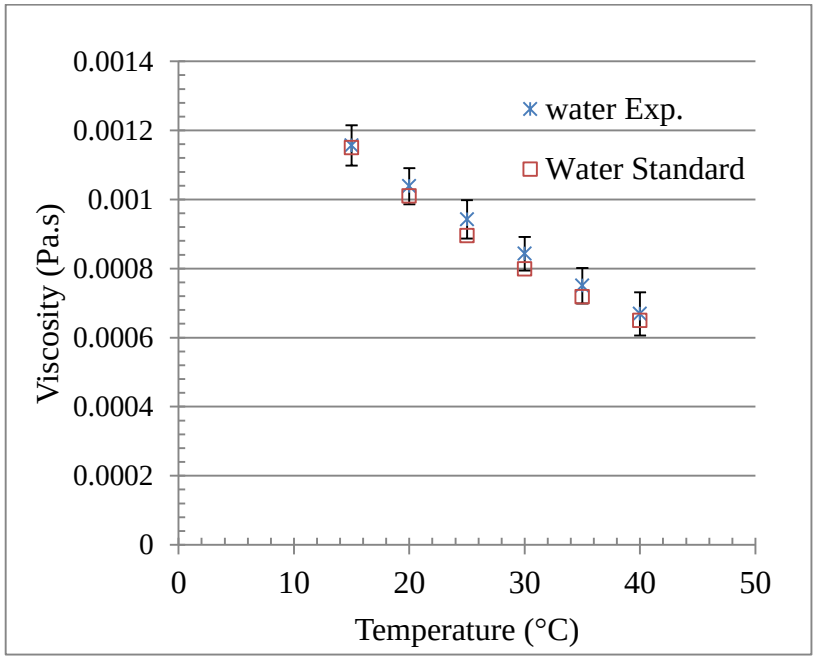

Figure 3.2: Average viscosity measurements for pure water with standard viscosity values; at atmospheric pressure and various temperatures

Table 3.1: Comparison of viscosity measurements for pure water with standard viscosity values; at atmospheric pressure and various temperatures

Temperature (°C)	Viscosity (fitting) (Pa.s)	Viscosity (averaging) (Pa.s)	Reference water viscosity (Pa.s)	Discrepancy (%)	Discrepancy (averaging) (%)
15	1.16×10^{-3}	$1.18\times10^{-3} \pm 5.8\times10^{-5}$	1.150×10^{-3}	0.55	2.73
20	1.04×10^{-3}	$1.06\times10^{-3} \pm 5.2\times10^{-5}$	1.0106×10^{-3}	2.76	4.60
25	9.42×10^{-4}	$9.60\times10^{-3} \pm 5.5\times10^{-5}$	8.9528×10^{-4}	5.25	7.22
30	8.43×10^{-4}	$8.60\times10^{-3} \pm 4.8\times10^{-5}$	7.9917×10^{-4}	5.49	7.61
35	7.50×10^{-4}	$7.69\times10^{-3} \pm 5.1\times10^{-5}$	7.1840×10^{-4}	4.45	7.09
40	6.69×10^{-4}	$6.93\times10^{-3} \pm 6.2\times10^{-5}$	6.5002×10^{-4}	2.88	6.62

3.4: Nanofluid Viscosity Results

After checking the accuracy of the apparatus, the nanofluids' rheological behaviour was tested and dynamic viscosity measured. Since nanofluids are synthesised from base fluids and nanoparticles, they must possess higher viscosity values relative to the base fluid due to their nanoparticle loads.

Figures 3.3 - 3.5 present the variation in shear stress against shear rate for the highest concentration nanofluids studied, in the temperature range 15 to 40 °C. The measurements indicate that, over the shear rate range considered, the shear stress increases with increasing shear rate. The relation between shear stress and shear rate becomes, in general, practically linear and converges to zero shear stress at zero shear rates. Under the conditions of the present study, all of the nanofluids studied behaved as a Newtonian fluid.

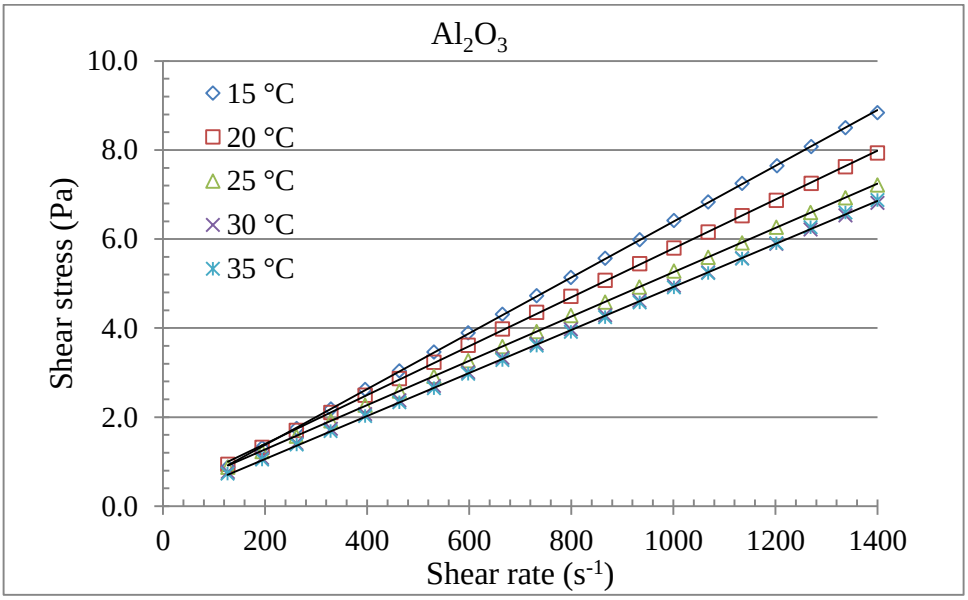

Figure 3.3: The variations of the shear stress with shear rate for the highest concentration (5.9 vol%) Al_2O_3-water nanofluid at different temperatures

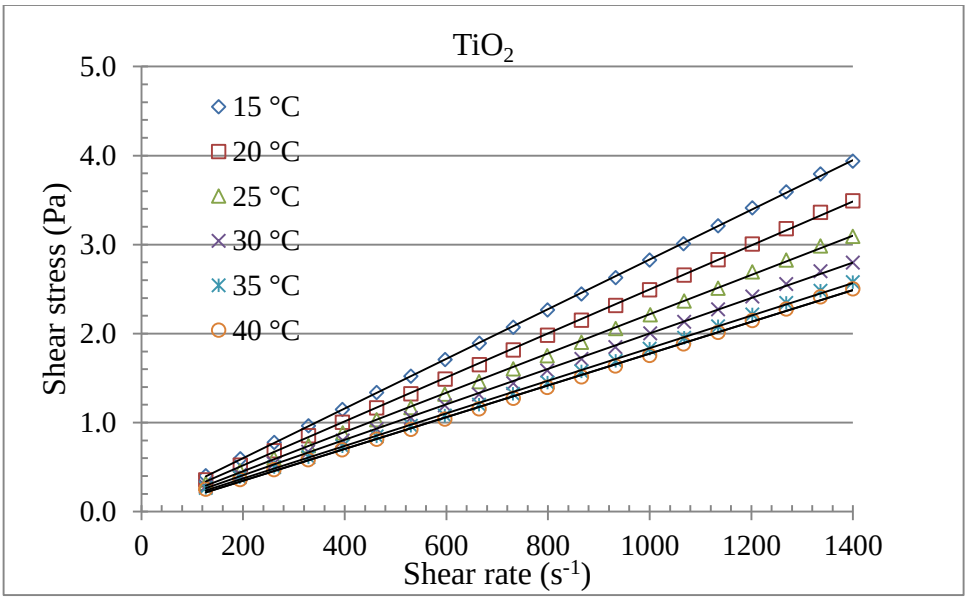

Figure 3.4: The variations of the shear stress with shear rate for the highest concentration (4.5 vol%) TiO_2-water nanofluid at different temperatures

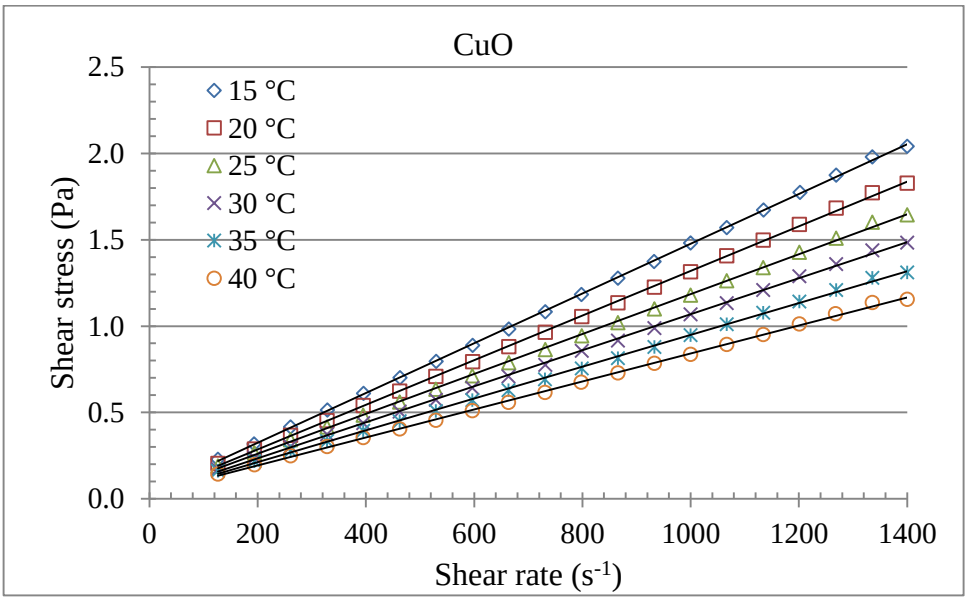

Figure 3.5: The variations of the shear stress with shear rate for the highest concentration (1.6 vol%) CuO-water nanofluid at different temperatures

The dynamic viscosity of nanofluids was measured for the same temperature range (15 to 40 °C) and various volume fractions at atmospheric pressure for all nanofluids. The measured nanofluids' viscosity results are presented as an average viscosity ± the standard deviation for Al_2O_3, TiO_2 and CuO water nanofluids; see Appendix A for the raw data. The results are summarized in Figure 3.6 to 3.8, which give the results for the whole temperature range and various volume fractions for each type of nanofluid. These results are also presented and discussed in a line chart in order to highlight and clarify the comparative differences. Figures 3.6 - 3.8 present the variations in viscosity with temperature and volume fraction concentration for all investigated nanofluids. For comparison, the corresponding curves of the base fluid (distilled water) are presented as dashed lines in the figures. The measurements indicate that, over the temperature and concentration ranges considered, the viscosity decreases with increasing temperature, while it increases with increasing nanoparticle concentration. It is apparent that increases in temperature have less of an impact on viscosity than increases in nanoparticle concentration.

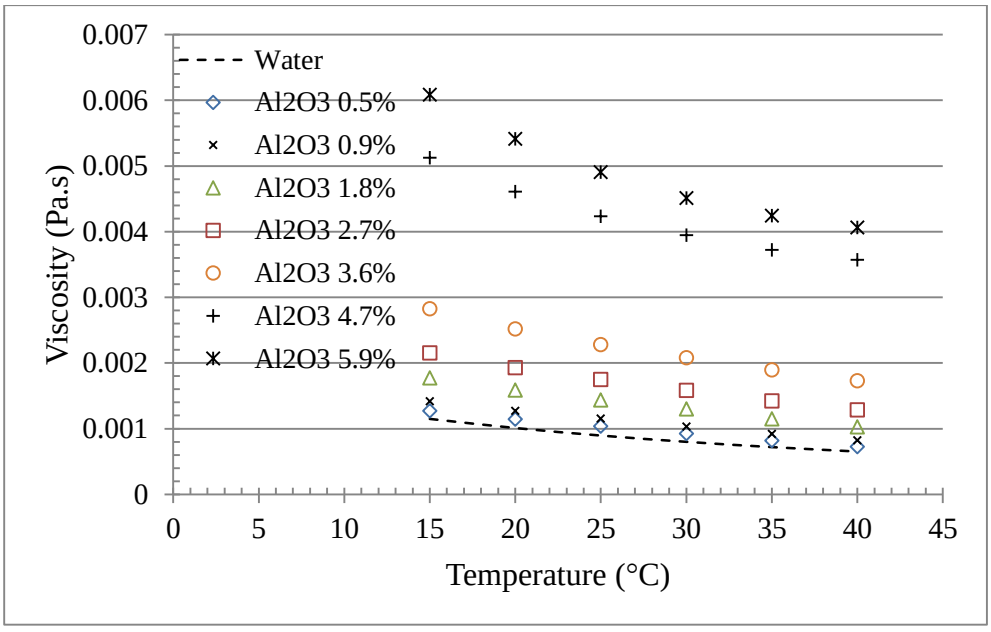

Figure 3.6: Dynamic viscosity measured for an Al_2O_3-water nanofluid at different temperatures and concentrations; numbers quoted with nanoparticle types refer to volume fraction concentrations.

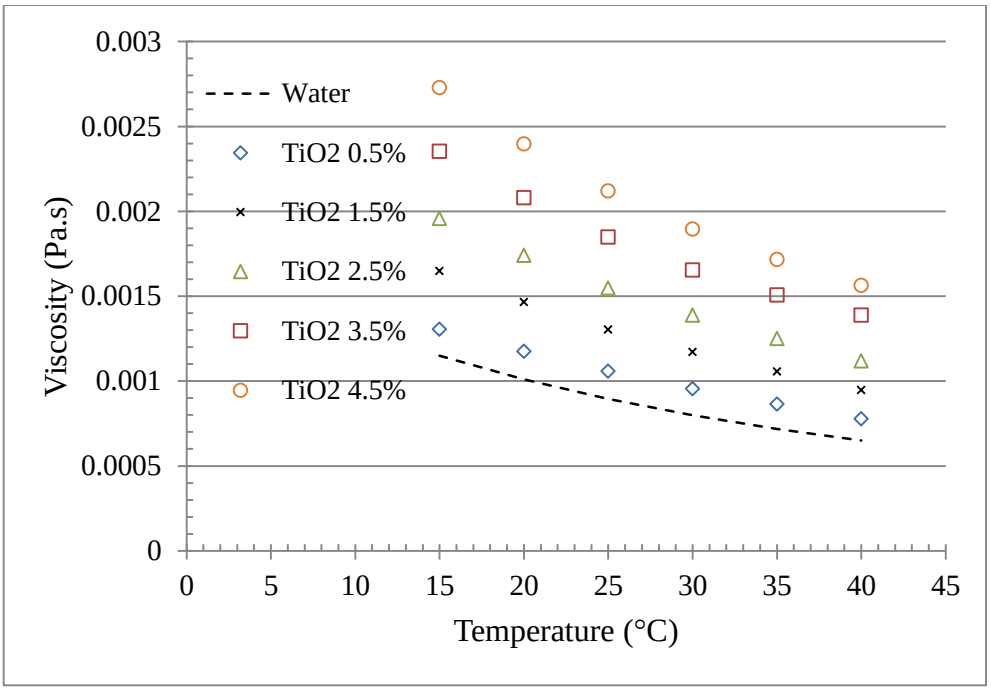

Figure 3.7: Dynamic viscosity measured for a TiO_2-water nanofluid at different temperatures and concentrations; numbers quoted with nanoparticle types refer to volume fraction concentrations.

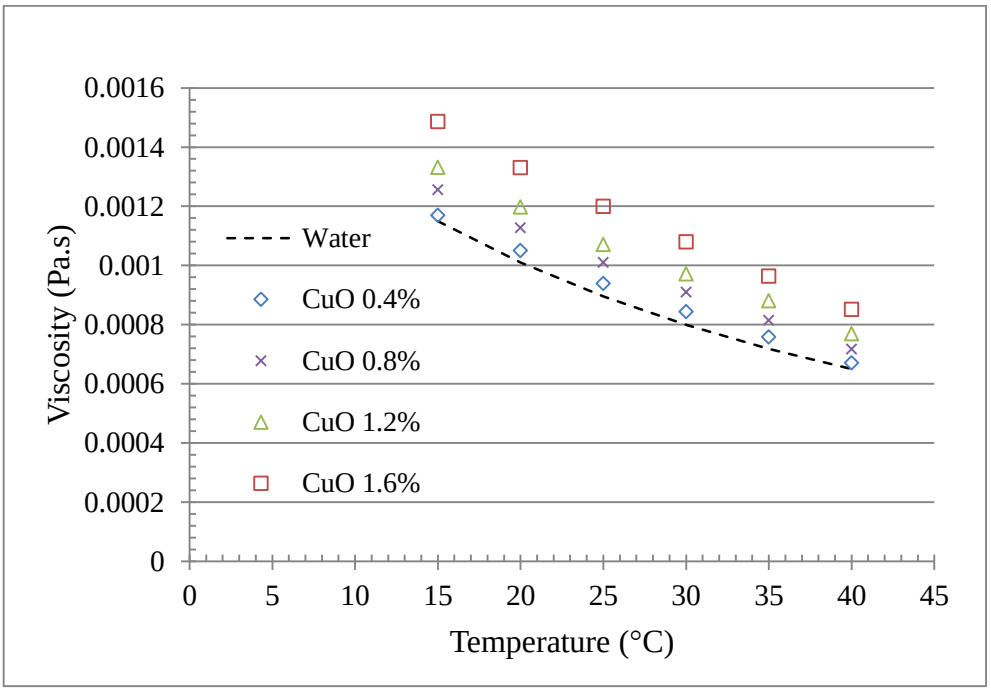

Figure 3.8: Dynamic viscosity measured for a CuO-water nanofluid at different temperatures and concentrations; numbers quoted with nanoparticle types refer to volume fraction concentrations.

The relative viscosity of the nanofluids (i.e. the ratio of nanofluid viscosity to base fluid viscosity) is plotted as a function of temperature in Figures 3.9 - 3.11 for Al_2O_3, TiO_2 and CuO nanofluids respectively. It is worth mentioning that the relative viscosity increases almost linearly (but very little) with temperature, except for the higher volume fractions of the nanofluid Al_2O_3 (i.e. 4.75% and 5.9%), where the relative viscosity increases more rapidly with increasing temperature. This has also been noted by other researchers [20, 29]. It should also be mentioned that even if a nanofluid has a constant relative viscosity, its actual viscosity is still depends on the base fluid viscosity and nanoparticle volume fraction.

Figures 3.12 - 3.14 show the effect of volume fraction on the relative viscosity at different temperatures. It can be seen that the relative viscosity increases with increasing nanoparticle concentration as expected. The relative viscosity of Al_2O_3-water nanofluid increases by 1.13, 1.27, 1.59, 1.94, 2.57, 4.89 and 5.65 times base fluid viscosity for 0.5 vol.%, 0.9 vol.%, 1.8 vol.%, 2.7 vol.%, 3.6 vol.%, 4.7 vol.% and 5.9 vol.% volume fractions respectively. While TiO_2 viscosity increases by 1.18 to 2.38 times, compared to base fluid for 0.5 to 4.5 vol.% volume fraction; and the viscosity of CuO-water was higher than the based fluid by 1.04 to 1.33 times; for volume fraction from 0.4 to 1.6 vol.%. It is noted that at low concentrations, the viscosity values of all nanofluid types are close, but at higher concentration there was a significant difference; for example the value for Al_2O_3-water is two times higher than that of TiO_2-water, at 4.6%. This indicates that the viscosity also depends significantly on the type of nanoparticles used. From the above, it is clear that nanofluid viscosity depends weakly on the temperature and strongly on the type of nanofluid nanoparticle and its concentration. Further study is needed to investigate nanofluid properties under comparable condition such as the same nanofluid type, nanoparticle size and concentration as well as a similar temperature range.

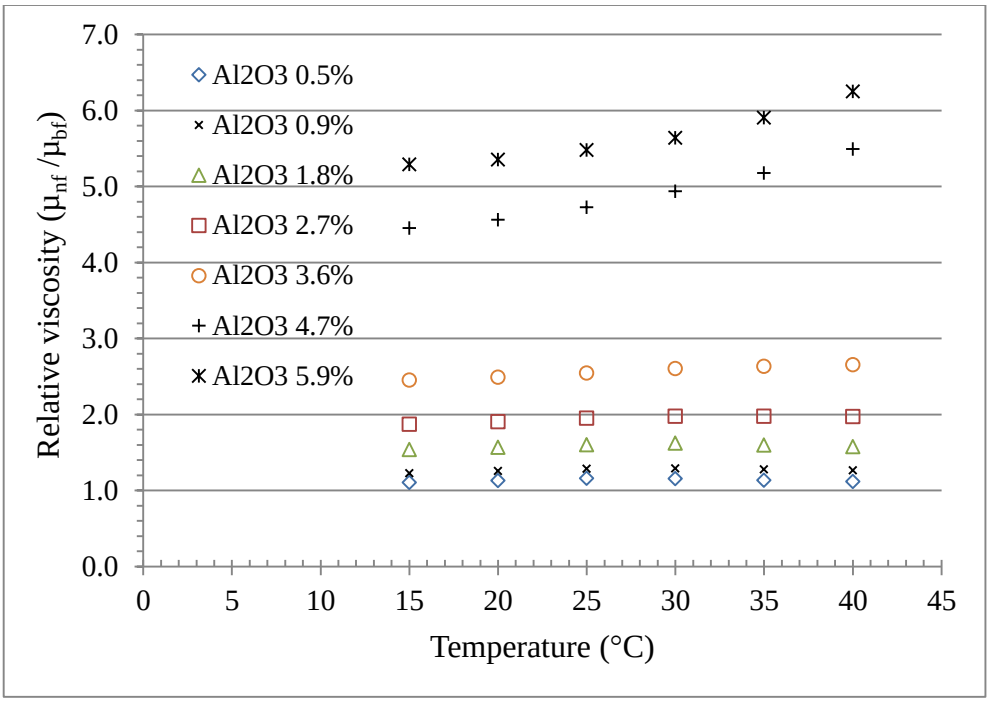

Figure 3.9: Relative viscosity measured for an Al_2O_3-water nanofluid at different temperatures; numbers quoted with nanoparticle types refer to volume fraction concentrations

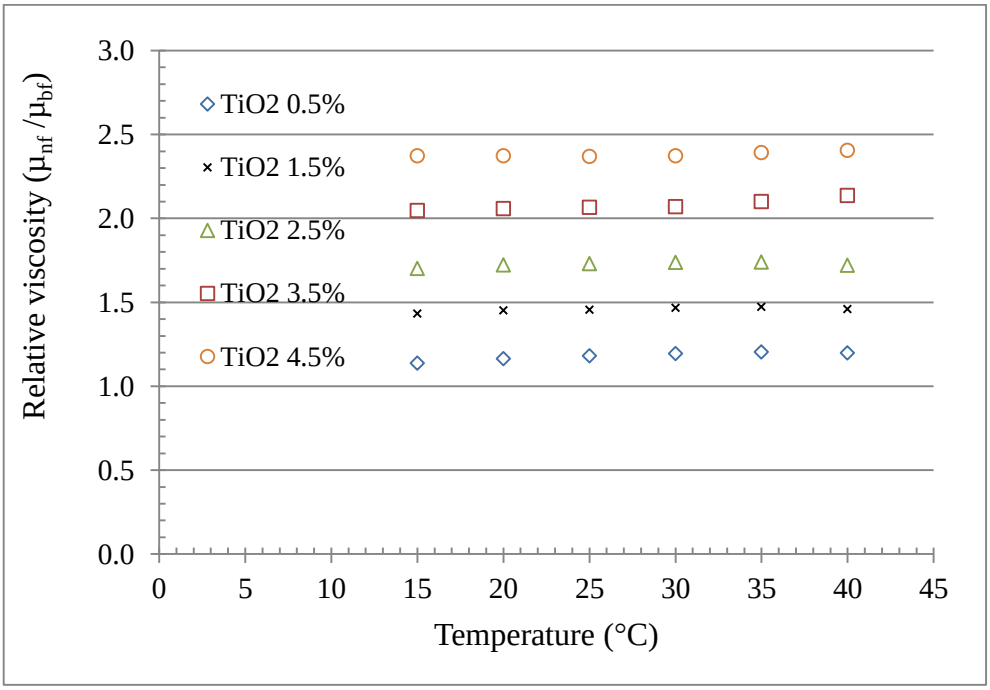

Figure 3.10: Relative viscosity measured for a TiO_2-water nanofluid at different temperatures; numbers quoted with nanoparticle types refer to volume fraction concentrations

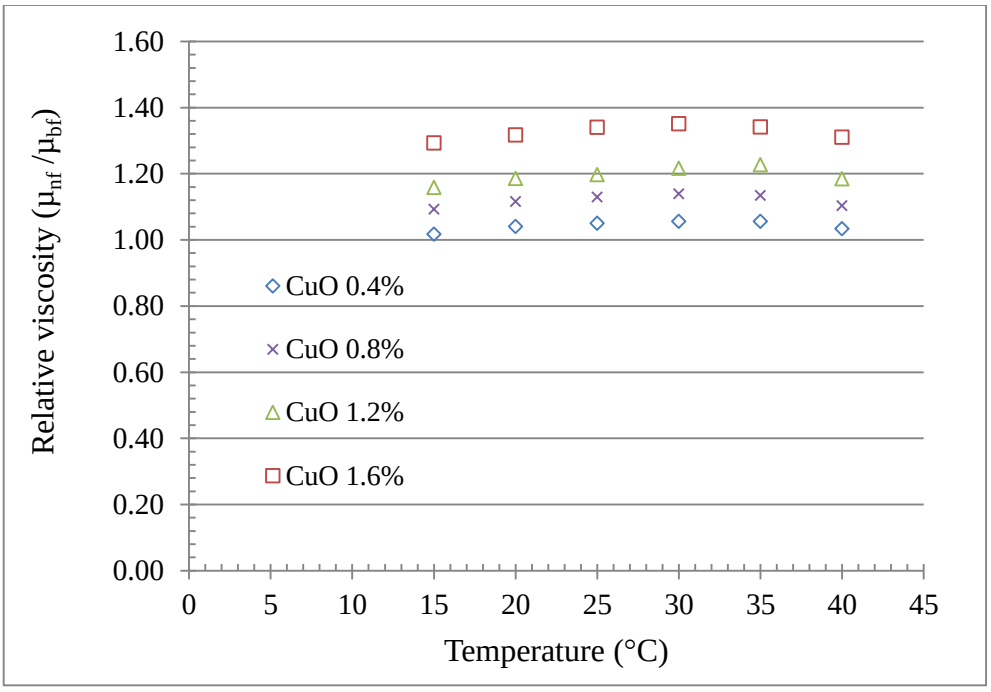

Figure 3.11: Relative viscosity measured for a CuO-water nanofluid at different temperatures; numbers quoted with nanoparticle types refer to volume fraction concentrations

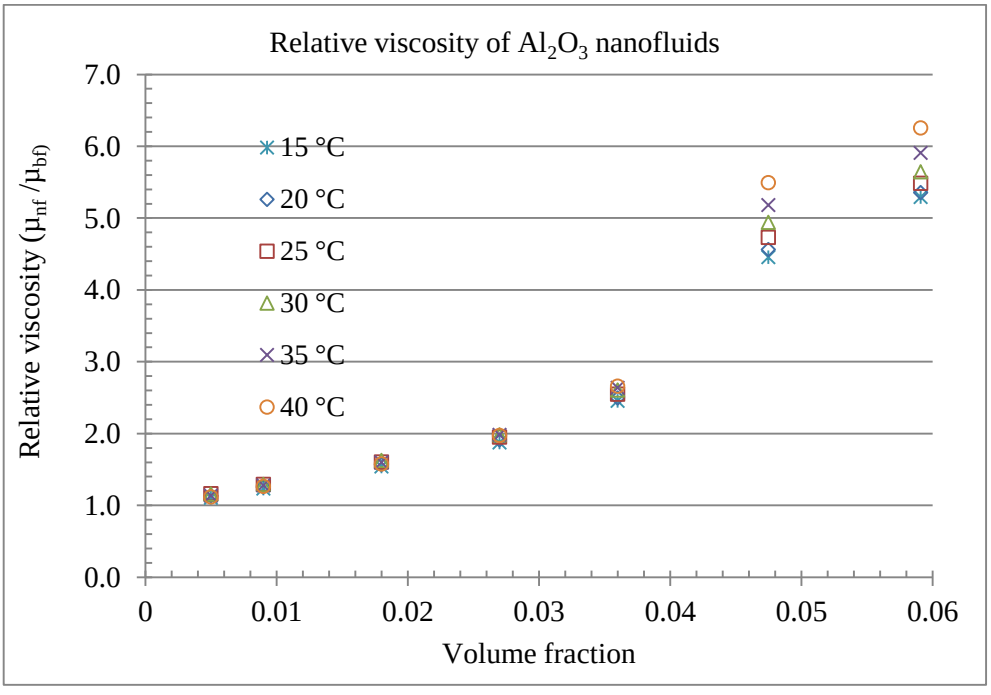

Figure 3.12: Relative viscosity measured for an Al_2O_3-water nanofluid at different volume fractions

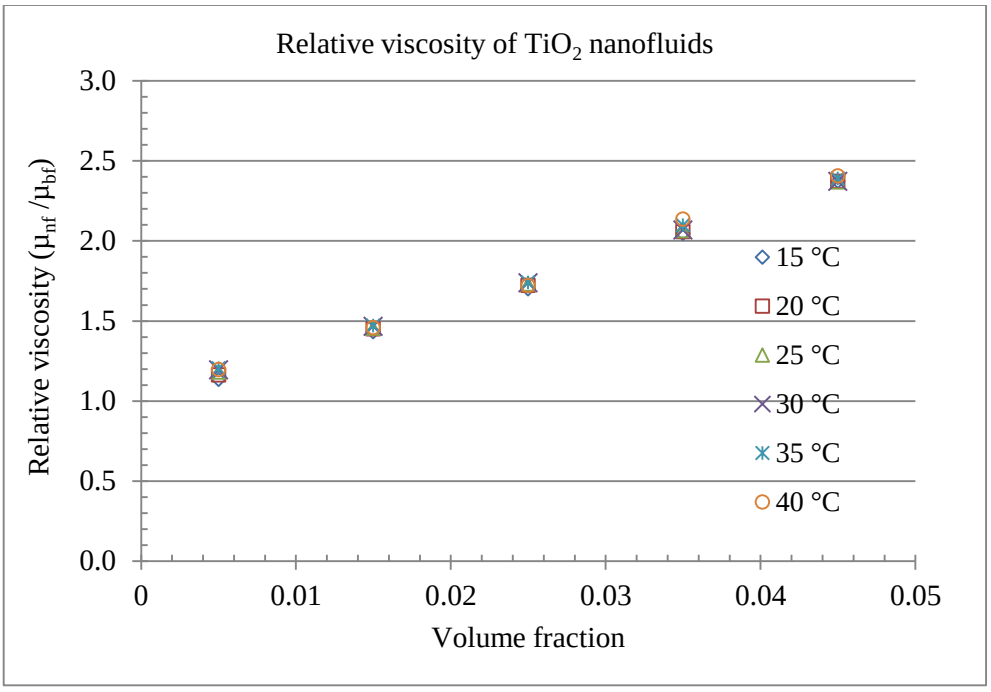

Figure 3.13: Relative viscosity measured for a TiO_2-water nanofluid at different volume fractions

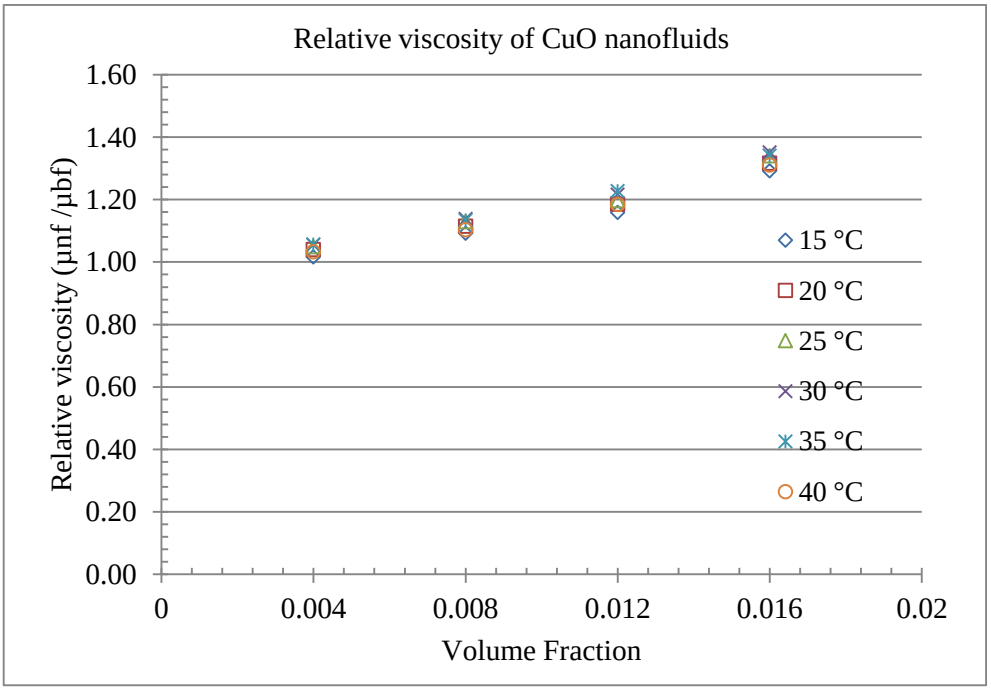

Figure 3.14: Relative viscosity measured for a CuO-water nanofluid at different volume fractions

3.5: New Correlations of Viscosity Data

Using the relative viscosity measurements determined in the previous section a linear relation between viscosity and temperature can be observed (see Figures 3.12 - 3.14). When plotted using Excel the equations can be determined by regression analysis. For the averaged data of Al_2O_3, TiO_2 and CuO water nanofluids the relative viscosities are given by equations (3.2), (3.3) and (3.4), respectively:

$$\frac{(\mu_{nf})_{Al_2O_3}}{\mu_{bf}(T)} = e^{\frac{6.599\phi}{0.288+\phi}} \approx 532.970\phi^2 + 22.923\phi + 1, \ \phi = 0 \text{ to } 4.0 \text{ vol.\% } R^2 = 0.9973 \quad (3.2)$$

$$\frac{(\mu_{nf})_{TiO_2}}{\mu_{bf}(T)} = 25.17\phi^2 + 29.562\phi + 1 \quad , \phi = 0 \text{ to } 4.5 \text{ vol.\% } \quad R^2 = 0.9977 \quad (3.3)$$

$$\frac{(\mu_{nf})_{CuO}}{\mu_{bf}(T)} = 776.28\phi^2 + 7.7392\phi + 1 \quad , \phi = 0 \text{ to } 2.0 \text{ vol.\% } \quad R^2 = 0.9963 \quad (3.4)$$

These equations are used for comparison later in this chapter as well as in the heat transfer performance and pressure drop calculations in subsequent chapters. It should be noted that because of the effect of temperature on the relative viscosity at higher volume fraction concentrations of Al_2O_3-water nanofluids (i.e. 4.75% and 5.9%), the developed equation is limited to volume fraction up to ϕ = 4.0 vol.%. It should also be mentioned that the equation of Al_2O_3-water nanofluids viscosity is similar to the equations of Williams et al. [25] and Heyhat et al. [26], but with different factors; this is further discussed in section 3.6.1.

Figure 3.15 shows the plot of the developed equations for all nanofluids. It can be seen that Al_2O_3 nanofluid gives the highest viscosity; however at volume fractions up to 1.5 vol.%, the Al_2O_3 nanofluid's viscosity is almost the same as the TiO_2 nanofluid's viscosity. On other hand, the CuO nanofluids show the lowest overall viscosities. It can be seen from Figure 3.15 that the nanofluid viscosity depends strongly on the nanoparticle material type and its concentration and temperature.

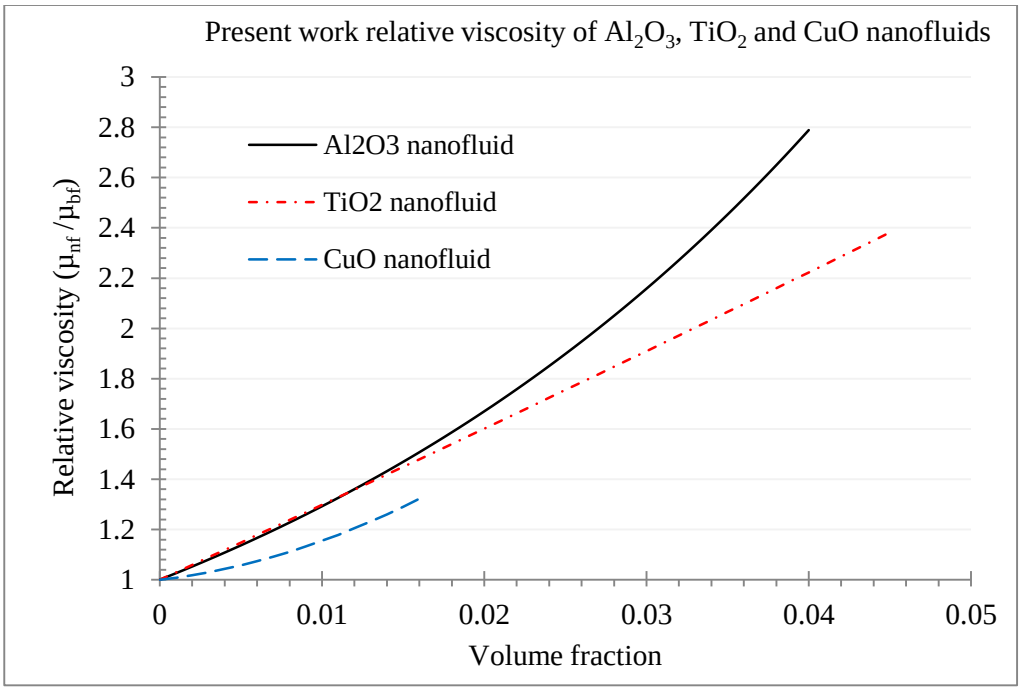

Figure 3.15: Relative viscosity measured for developed equations of Al_2O_3, TiO_2 and CuO nanofluids.

3.6: Comparison with Previous Work

Since there are few experimental results on the viscosity of nanofluids, it is worth comparing the results from the present work (captured in equations 3.2-3.4) with experimental and theoretical results in the literature, especially those using similar particle sizes to eliminate the effect of size on the results.

3.6.1: Experimental viscosity comparison

Williams et al. [25], Heyhat et al.[26]and Pak and Cho [23] measured the viscosity of Al_2O_3-water nanofluids with 46, 40 and 13 nm nanoparticle size respectively. Under their test conditions their results indicated that the viscosity of the nanofluid increased significantly with increasing nanoparticle concentration. In addition, the relative viscosity of the nanofluid with respect to the base fluid is independent of temperature. Therefore, the nanofluid viscosity models of Williams et al. and Heyhat et al. were created as a function of the base fluid viscosity and the nanoparticles load (see equations (1.4) and (1.5)). Figure 3.16 shows comparisons between the relative viscosity results of the present study for Al_2O_3-water nanofluids and those of Williams et al. [25], Heyhat et al. [26] and Pak and Cho [23]. It can be seen that there is a close agreement between the Williams et al. and Heyhat et al. results; the results of this study agree with Heyhat's model with a maximum difference of 4% for the considered concentrations. The Williams et al. model gives a much closer agreement (maximum difference of 2% for volume fractions up to 2.4 vol.%), however this deviates at higher concentrations and the discrepancy continues to rise with increasing volume fractions to reach about 14% at 4.0 vol.% loading. It is worth mentioning that the good agreement of the result is attributed to similar nanoparticles size and the differences could be attributed to the effects of agglomeration, nanofluid preparation, and the technique and apparatus used for viscosity measurement. On the other hand, the Pak and Cho result gives a significant difference, with their model overestimating the viscosity by an average error of about 15%. This discrepancy is most likely due to the smaller nanoparticle size (13 nm) of Pak and Cho study (this experiment used 50 nm) [23, 30].

The TiO_2-water nanofluids' relative viscosity results are compared to the experimental results of Fedele et al. with nanoparticle 76 nm [22] and Turgut et al. with nanoparticle 21 nm [28] in Figure 3.17. At low concentrations, up to a volume fraction of 1.8 vol.%, the measured relative viscosity for TiO_2-water nanofluid shows a reasonably close agreement with the values claimed by Turgut et al. with their results underestimated. However, above that volume fraction their results are overestimated. For example, the viscosity at 3 vol.% in the Turgut et al. study is nearly the same as the measured viscosity result at the volume fraction 4.2 vol.% in the present study. Fedele et al. observe a much larger difference where the predicted relative viscosity values are significantly underestimated when compared to the measured ones. This difference could be due to the difference in the nanoparticle size, which were 76 nm and 21 nm for Fedele et al and Turgut et al., respectively, whereas it was 50 nm in the present work.

Comparisons between the observed CuO-water nanofluids' relative viscosities with those of previous studies by Nguyen et al. [29] and Pastoriza et al. [30] with nanoparticles size 30 nm are summarized in Figure 3.18. At low volume fraction, all three studies give similar values: up to volume fraction 0.8% the results are all within 5% of each other. However, even from zero volume fraction, the divergence of the results with increasing volume fraction is clear, with both previous results yielding lower relative viscosity. This is somewhat surprising given that all three studies used a similar nanoparticle size. However, there are several other factors to consider – in particular the fact that a different preparation method was used previously, which may have resulted in a different nanoparticle shape, and also that surfactant was used to disperse the nanoparticles rather than the ultrasonic anti-agglomeration technique used in this study. A different measuring viscosity technique was also used in the previous work, though this should not produce such large discrepancies.

The differences seen between the present work and previous studies highlight the difficulties in developing universal relationships describing nanofluid properties.

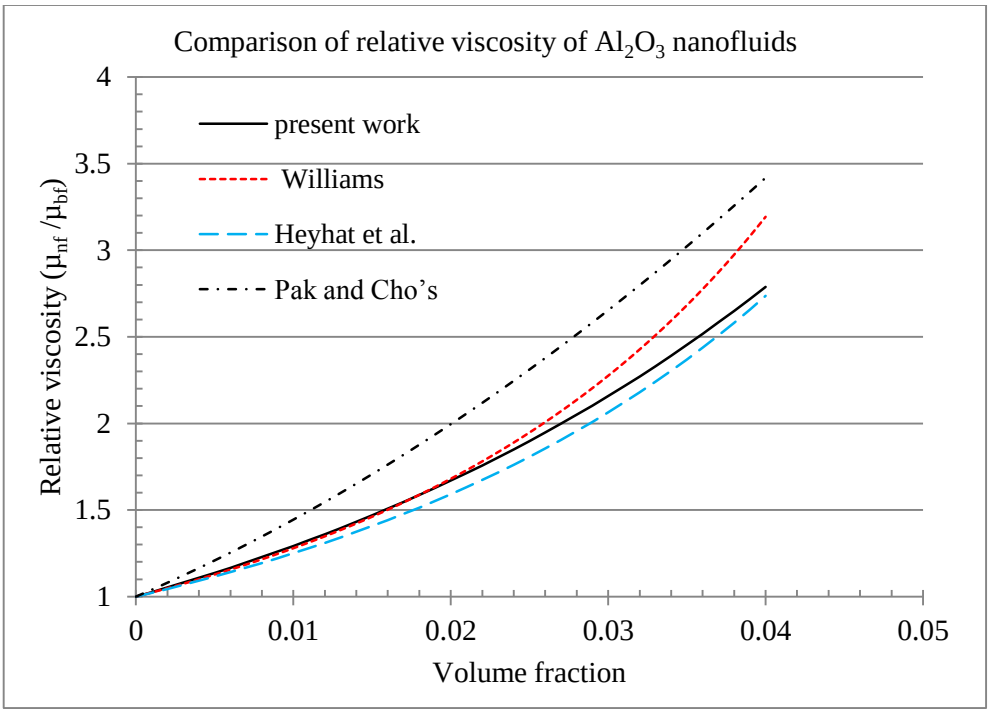

Figure 3.16: Comparison between the relative viscosity measured results with Williams et al. [25], Heyhat et al. [26] and Pak and Cho [23] results for an Al_2O_3-water nanofluids.

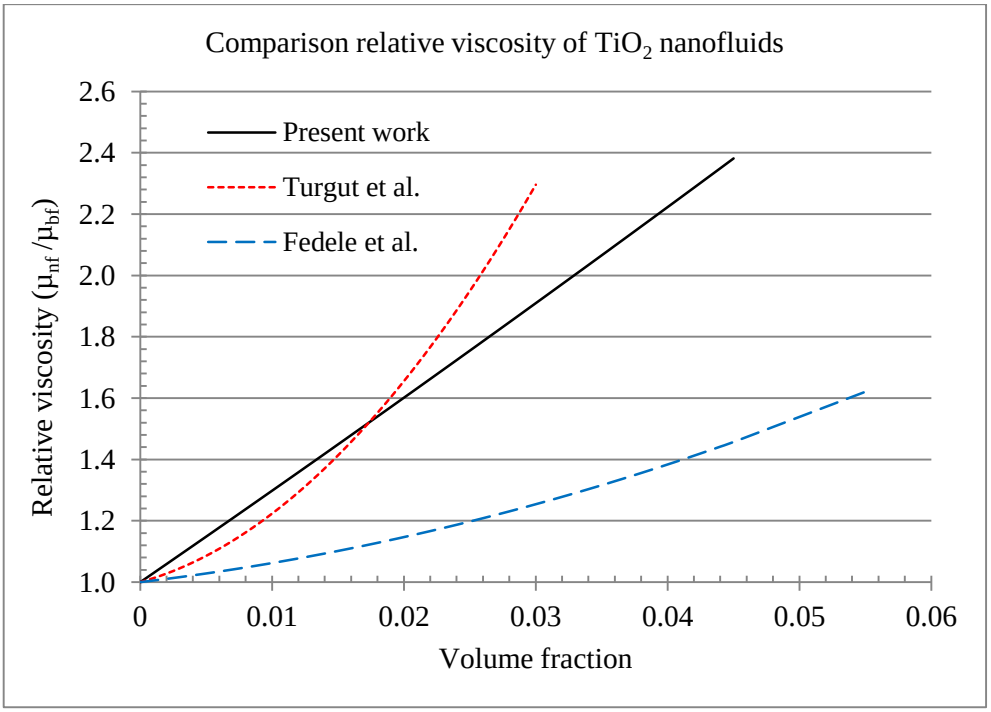

Figure 3.17: Comparison between the relative viscosity measured results and those of Fedele et al. [22] and Turgut et al. [28]Turgut et al. for the viscosity of a TiO_2-water nanofluids.

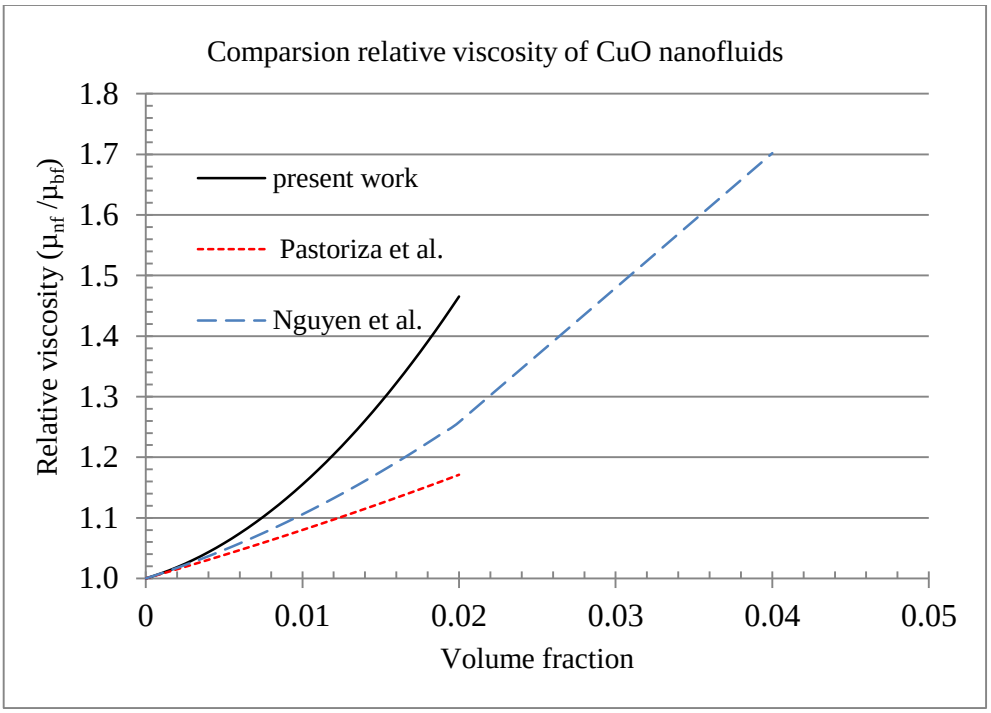

Figure 3.18: Comparison between the measured results and those of Nguyen et al. [29] and Pastoriza et al. [30] Pastoriza for the viscosity of a CuO-water nanofluid.

3.6.2: Theoretical correlation viscosity comparison

The viscosity is defined as a resistance of the fluid to flow; this effect is caused by interaction between the fluid and the surface and between the molecules of the fluid itself. For nanofluids, which have suspended nanoparticles, it is predicted that viscosity will be increased because of the interaction between the nanoparticles and molecules of the base fluid as well as between the nanoparticles themselves. The theoretical estimation of the viscosity of a nanofluid should take into consideration these influences. There are a number of formulae in the existing literature for the estimation of nanofluid viscosity, but each has its limitations. The most common nanofluid viscosity models in the literature are the Einstein model, the Brinkman model, and the Batchelor model [18]; they estimate nanofluid viscosity as a function of the base fluid, nanoparticle concentration, and temperature however each model is only valid for a limited range of volume fractions. Owing to the volume fractions used in this study the Brinkman model has been chosen for comparison (see Eqs. (1.1), (1.2) and (1.3)). Figure 3.19 shows a comparison of the experimental results to the Brinkman prediction of viscosity; it shows that Brinkman

model fails to estimate the viscosity of all types of nanofluids except that of the low concentration CuO-water nanofluids. It can also be seen that the model underestimates the measured viscosities significantly; this was also observed by other researchers [29, 31].

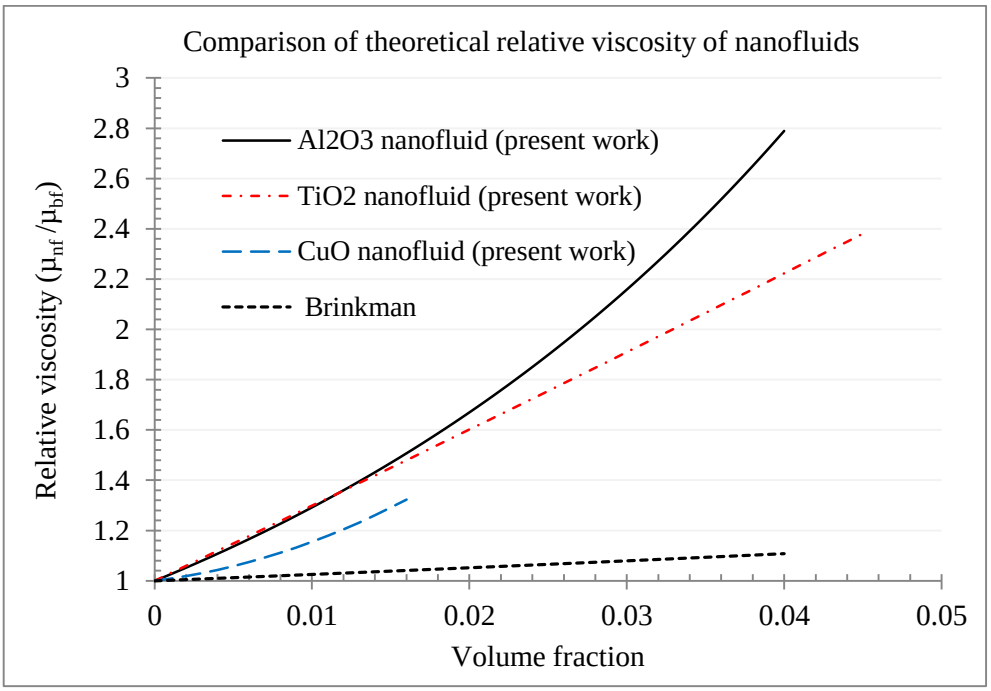

Figure 3.19: Comparison the measured relative viscosity results to Brinkman theoretical model for of all nanofluids.

3.7: Concluding Remarks

In this thesis, common nanofluids were prepared in various nanoparticle concentrations and the Kinexus rheometer technique was used to measure the dynamic viscosity of Al_2O_3, TiO_2 and CuO with varying volume fraction concentrations and temperature levels, which were representative of typical working temperatures for the fluids. A nanofluid viscosity–temperature relationship of all nanofluids was developed in equations (3.2), (3.3) and (3.4). These results were compared with other workers' experimental studies as well as existing theoretical models.

The results in general indicate that the viscosity of a nanofluid increases with increasing volume fraction whilst it decreases with increasing temperature. The measured values of dynamic viscosity for Al_2O_3 nanofluids were in close agreement with the Williams et al. and Heyhat et al. models. This is due to the similar nanoparticle sizes in the test and supported by the discrepancy shown by Pak and Cho's study, which used a much smaller nanoparticle size. However these studies recorded lower viscosities for TiO_2 and CuO nanofluids than measured values, this may be because their nanoparticle shape may have been different (though the size was similar) as they used a different preparation technique and added surfactant to the nanofluid instead of the ultrasound anti-agglomeration technique used in this study. They also used a different measuring technique. Based on comparison with the previous experimental studies, it is noted that the viscosity of the nanofluid with small nanoparticles size is higher than nanofluid with large nanoparticles see Figures 3.16 and 3.17. Finally, the theoretical correlation (Brinkman model) greatly underestimated the recorded experimental values. This result has been observed by other workers [29, 31], and this underestimation could be due to many factors not considered by the model such as agglomeration or the shape and type of nanoparticle; which the theoretical correlations assumed to be spherical. With regard to rheological behaviour, Newtonian behaviour was observed for these nanofluids under the test conditions.

CHAPTER 4: CONVECTIVE HEAT TRANSFER AND PRESSURE DROP CHARACTERISTICS OF NANOFLUIDS

4.1: Introduction

As mentioned before, the aim of this research is to evaluate the heat transfer performance and pressure drop characteristics of nanofluids under dynamic conditions, as is the case in most practical applications. Nanofluids may play an important role in affecting thermal characteristics such as the heat transfer coefficient as well as the dynamic flow characteristic, including the pressure drop. Thus testing the thermal performance of a nanofluid under dynamic conditions is essential to characterise its behaviour.

In this chapter an experimental study of turbulent forced convection heat transfer and pressure drop characteristics of common nanofluids with varying volume fraction concentrations through a uniformly heated horizontal circular tube are investigated, the nanoparticles under investigation are Aluminium oxide (Al_2O_3), Titanium dioxide (TiO_2) and Copper oxide (CuO) with a fluid base of distilled water.

4.2: Measurement Technique and Methodology

An experimental apparatus has been created and is described in detail in section 4.2.1, the nanofluids tested were prepared using the method described in chapter 2.

4.2.1: Heat transfer experiments

This study uses a forced convective heat transfer experimental technique to evaluate the heat transfer performance and pressure drop of nanofluids. The following sections briefly describe this technique and its theoretical background.

The convection loop setup is shown in Figure 4.1 and Figure 4.2. It can be seen that the loop consists of a two test sections, namely the heated test section and the isothermal test section. Both sections consist of a hollow circular tube of stainless steel (seamless stainless steel (SS) 316 / 316L based on ASTM standards and manufactured by SANDVIK Company under model number of 3R60) with outer and inner diameter and length of 0.5in (0.0127 m), 0.37in (0.0094 m) and 121.6in (3.040 m), respectively. In addition to the tubes, there is a pump to circulate the fluid through the loop, a heat exchanger to control the inlet test section temperature, an accumulator tank and various measurement devices connected to the loop. These measurement devices include; a flow meter (turbine flow meter (FTB-902, OMEGA), with accuracy 0.5% within flow range 0.75 to 5 GPM), differential pressure transducers (OMEGA PX293- 030D5V with operating range 0 to 207 kPa (0 to 30 psid) and accuracy within 0.5%,) and a gauge pressure transducer. A DC power supply (GENESYS 10 kW (20 V and 500 A), TDK-Lambda Americas Inc) was utilized to uniformly generate heat within the body of the heated test-section. The power supply was capable of displaying its power output with an accuracy of 0.5% of its rated (maximum designated) output. The current of the test was 333 A; hence, the accuracy will be ±1.7 A.

In order to circulate the fluid inside the loop, the pump (1 HP stainless steel STA-RITE pump) pulls fluid from the accumulator tank and pumps it into the heated test section, heated by the principle of Joule heating using the power supply. Before and after the test section the fluid bulk temperature and pressure drop were measured using the

submerged thermocouples and differential pressure transducer. Its outer surface temperature was also measured using 14 T-type thermocouples (T-type thermocouples (TJC36-CPSS-032U-12, OMEGA); accuracy of 0.5 ^{o}C or 0.4% from 0 – 350 °C) attached along the test sections top outer surface every 0.203 m. These procedures enabled detailed measurement of the temperature variation over the top surface of the heated test section. The fluid was cooled by passing it through the heat exchanger before entering the unheated test section. The temperature and pressure before and after the unheated test section are measured by submerged thermocouples and a differential pressure transducer. The fluid finally returns to the accumulator tank where the cycle is started again.

In order to control the flow rate of the loop, a by-pass valve to the accumulator tank was installed. All data is acquired and recorded using a National Instruments' data acquisition device and LabView software.

Figure 4.1: Picture of the forced convection loop.

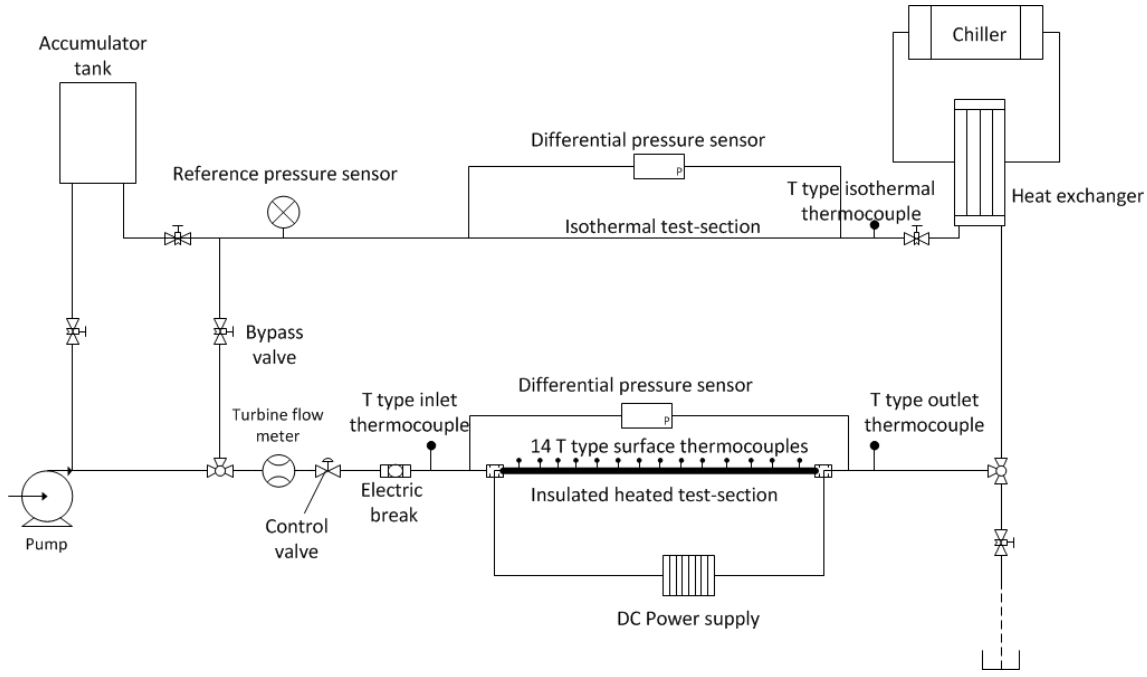

Figure 4.2: Schematic of the experimental loop setup

The goal of the experimental technique is to determine the Nusselt number or the convective heat transfer coefficient from the measurable quantities by applying the relevant equations.

The Nusselt number is defined as:

$$Nu = \frac{hD}{k} \tag{4.1}$$

Where h is heat transfer coefficient of fluid; D is the diameter of the test section and k is the thermal conductivity of fluid.

The heat transfer coefficient is the ratio of the heat input at the boundary to that transferred to the fluid when the fluid flows over a solid surface [96]. In order to calculate the heat transfer coefficient, the following equation is applied:

$$h = \frac{q}{A\Delta T}$$

Where q is the heat input at boundary, A is surface area and ΔT is the temperature difference between the boundary near the solid surface and the far field in the fluid. The interpretation of this ΔT varies but the common assumption is that the temperature near the surface is the same as the temperature of the surface and the temperature of the far field fluid is the average temperature between the inlet and outlet of the tube [96]. This assumption is used in this study as $\Delta T = T_{s,in} - T_{b,m}$ and then the heat transfer coefficient is :

$$h = \frac{q}{A(T_{s,in} - T_{b,m})} \tag{4.2}$$

where q is heat source or heat flux of the test section, A is inside surface area of the test section (calculated from $A = \pi D_{in} L$, where D_{in}(m) is the test section diameter and L(m) test section length), $T_{s,in}$ is the inside surface test section temperature and $T_{b,m}$ is the average bulk temperature along the test section (see eq.(4.4)).

The heat source of the test section, *q*, could be obtained directly from the current, *I*, and voltage difference, *V*, of the test section (both measured using a digital clamp meter); since *q=IV*. Assuming there is no heat lost from the heated test section i.e. that the test section has perfect thermal insulation, then the fluid heat gained is given by:

$$q = \dot{m} C_p (T_{b,out} - T_{b,in})$$

Where $\dot{m}$ is mass flow rate of fluid; calculated from $\dot{m} = \rho Q$ (kg/m^3) where ρ is fluid density, Q is flow rate (m^3/s) (is measured by flow meter), C_p is specific heat of the fluid and $T_{b,\,in}$ and $T_{b,\,out}$ are inlet and outlet bulk temperature of the test section fluid respectively (measured by the submerged thermocouples). This insulation assumption is challenged and verified later in Figure 4.5, which shows that the test section has an adequate thermal insulation.

The thermocouples give the temperature distribution over the outer surface of test section. From these temperatures, the inner surface temperature of the test section tube, $T_{s,\,in}$, is calculated from the analytical solution for a perfect insulation tube with uniform heat generation and known outer surface temperature [97]. That means that it is possible to calculate the inner surface temperature of the test section using:

$$T_{s,in} = T_{s,out} + \frac{q}{16 k_{tube} V}(D_{out}^2 - D_{in}^2) - \frac{q}{8 k_{tube} V} D_{out}^2 \ln \frac{D_{out}}{D_{in}} \qquad (4.3)$$

where $T_{s,out}$ is outside surface test section temperature (measured by thermocouples), D_{out} and D_{in} are the test section tube diameter outside and inside respectively, and k_{tube} is thermal conductivity of test section tube which is known as the tube was made of stainless steel [98], k_{tube}=$0.0127 T_{s,out} + 13.23188$ where $T_{s,out}$ is in $^{\circ}$C; since the tube thickness is very small (1.65mm). *V* is the volume of the test section tube and calculated as: $V = \frac{1}{4}\pi(D_{out}^2 - D_{in}^2)L$

It should be emphasized here that the thermo physical properties of the fluids (water and nanofluid) are taken at the average bulk temperature, $T_{b,m}$, [23, 25, 55], which are calculated from:

$$T_{b,m} = \frac{T_{b,in} + T_{b,out}}{2} \tag{4.4}$$

The local Nusselt number and local heat transfer coefficient can be determined by applying energy conservation from the equation 4.5:

$$T_{b,x} = T_{b,in} + \frac{q''(\pi D_{in} x)}{\dot{m} C_p} \tag{4.5}$$

In equation (4.5) the heat flux of the test section, q'', x is the distance from the inlet of the test section $(x = 0 \rightarrow L)$.

Alternatively the average Nusselt number and average heat transfer coefficient can be obtained by applying the local bulk temperature along the heated test section which could be determined by applying energy conservation from the equation below.

$$Nu_{ave} = \frac{h_{ave} D}{k} \quad \text{and} \quad h_{ave} = \frac{q}{A(T_{s,in,ave} - T_{b,m})}$$

Where $T_{s,in,ave}$ is the average inner surface temperature; was obtained from

$$T_{s,in,ave} = \frac{\sum_{n}^{14} T_{s,in,n}}{14}$$

4.2.2: Measurement procedure

Measurements were carried out for one specimen of each concentration for each nanofluid; this was repeated three times for each specimen and then averaged to give the mean value. The inlet bulk temperature of the test section was maintained at 20 ˚C, the

heat generated uniformly at about 5000W and the flow rate was varied from 0.75 to 2.0 GPM (gallon per minute) (i.e. 5×10^{-5} to 0.00013 m^3/s) for each sample. This process was initially run with water and then the nanofluids to provide a basis for comparison. The loop system was considered to be steady state under constant inlet temperature and constant heat flux. Therefore, all the outer surface temperatures and the bulk temperature profiles of the test section, which were measured by the thermocouples, should give a linear and parallel trend to each other with respect to time. This means that the difference between the test section surface-temperature and the bulk-temperature along the tube should be constant. After the tests reached steady state condition the temperature and pressure and flow rate data were recorded for three minutes duration at a rate of two data recordings per second; this was repeated three times for each sample and then averaged.

For ease of setup, the nanofluid with the highest nanoparticle concentration was examined first and then diluted according to the procedure detailed in chapter 2.

In order to compare the experimental results using the well-known correlation of Nusselt number or heat transfer coefficient for water and to measure the heat transfer coefficient and pressure drop of the nanofluids, the required properties used are detailed and explained in section 4.2.3.

4.2.3: Base fluid, Nanoparticles and Nanofluids properties

The thermal and physical properties of water and the nanoparticles were calculated from the existing literature and these properties are used to calculate and determine the nanofluids properties.

The properties of water were taken from Abbasian and Amani [54] with uncertainty of about 1.3%, as the below correlation Eqs. (4.6), (4.7), (4.8) and (4.9) for density, specific heat, thermal conductivity and viscosity, respectively:

Water density (kg/m^3):

$$\rho_{bf} = -764.475639 + 19.251515T - 0.07714568T^2 + 1.364893\times10^{-4}T^3 - 9.339158\times10^{-8}\ T^4 \quad (4.6)$$

Water specific heat (J/kg.K):

$$C_{p,bf} = 98531.690492 - 2894.853934T + 17.2363068T^2 - 0.05126994T^3 + 7.616133\times10^{-5}T^4 - 4.517821\times10^{-8}T^5 \quad (4.7)$$

Water thermal conductivity (W/m.K):

$$k_{bf} = -1.549404 + 0.01553952T - 3.65967\times10^{-5}\ T^2 + 2.9401\times10^{-8}T^3 \quad (4.8)$$

Water dynamic viscosity (Pa.s):

$$\ln\left(\frac{\mu_{bf}(T)}{0.001792}\right) = -1.24 - 6.44\left(\frac{273.15}{T}\right) + 7.68\left(\frac{273.15}{T}\right)^2 \quad (4.9)$$

Where ρ_{bf}, $C_{p,bf}$, k_{bf} and μ_{bf} are the base fluid (water) density, thermal conductivity, specific heat and dynamic viscosity; and T is the temperature in (K).

The properties of Al_2O_3, TiO_2 and CuO nanoparticles at room temperature were taken from the literature and are summarized in Table 4.1 below.

Table 4.1: Nanoparticles properties and its size used.

Nanoparticle type	Density (ρ_p) (kg/m^3)	Thermal conductivity (k_p) (W/m.K)	Specific heat capacity ($C_{p,p}$) (J/kg.K)	Nanoparticle size (nm)
Al_2O_3 [26]	3900	42.34	880	50
CuO [99]	6310	18	549	30
TiO_2 [55]	4170	11.8	711	45

Regarding the nanofluids thermophysical properties, the main nanofluid composite is a combination of the base fluid and nanoparticles. Therefore, the thermophysical properties may differ from the literature. Some experiments and correlations of previous studies are performed to estimate the nanofluid thermophysical properties. In this study, the nanofluids thermophysical properties calculated as below:

The nanofluid density and specific heat are taken from the equation of mixture theory and thermal equilibrium; as give a good agreement with experimental results [23, 26, 27, 35, 100].

Density of nanofluid (ρ_{nf}): $$\rho_{nf} = \rho_{bf}(1-\phi) + \rho_p\phi \tag{4.10}$$

Heat capacitance of nanofluid ($C_{p,nf}$): $$(\rho C_p)_{nf} = (\rho C_p)_{bf}(1-\phi) + \phi(\rho C_p)_p \tag{4.11}$$

Where ϕ is the volume fraction and; ρ_p and $C_{p,p}$ are density and specific heat of nanoparticle respectively.

The thermal conductivity of nanofluids k_{nf} can be represented by Yu and Choi's model [101] as: $$k_{nf} = k_{bf}\left(\frac{k_p + 2k_{bf} + 2(k_p - k_{bf})(1+\beta)^3\phi}{k_p + 2k_{bf} - 2(k_p - k_{bf})(1+\beta)^3\phi}\right) \tag{4.12}$$

Where k_{bf} and k_p are the thermal conductivity of the base fluid and nanoparticles respectively; β is the ratio between the nanolayer thickness, surrounding the nanoparticle and the nanoparticle radius and is taken to be 0.1. This equation was used due to the good agreement between experiments for different nanofluid types on thermal conductivity by multiple researchers [25-27, 102].

The viscosities of the previously prepared nanofluids are obtained from laboratory measurements detailed in Chapter 3. It is noted that the viscosity of the nanofluids vary according to the type of nanoparticles used and many other factors such as nanoparticles concentration, temperature, etc. The fit of the viscosity equation of Al_2O_3-water nanofluid, TiO_2-water nanofluid and CuO-water nanofluid are summarised in chapter 3 by Eq. (3.2), (3.3) and (3.4) respectively.

4.3: Experimental Verification

In the present section, the measurement of water convection characteristics and pressure loss are measured initially to validate the experimental setup (loop); as its properties and performance are well-known in the literature [54, 97].

4.3.1: Heat transfer verification test for water

The accuracy of the experimental results are validated by comparison with calculations made with conventional correlations carried out by Gnielinski's correlation [97]; because of the range of Reynolds number $3000 \leq \mathrm{Re} \leq 5\times10^6$ and Prandtl number $0.5 \leq \mathrm{Pr} \leq 2000$ as:

$$Nu = \frac{(f/8)(\mathrm{Re}-1000)\,\mathrm{Pr}}{1+12.7(f/8)^{1/2}(\mathrm{Pr}^{2/3}-1)}, \quad 0.5 \leq \mathrm{Pr} \leq 2000 \text{ and } 3000 \leq \mathrm{Re} \leq 5\times10^6 \qquad (4.13)$$

Where f is the friction factor; was obtain by Petukhov relation [97] as:

$$f = (0.790\ln \mathrm{Re} - 1.64)^{-2} \qquad \text{for } 3000 \leq \mathrm{Re} \leq 5\times10^6 \qquad (4.14)$$

Where Re is Reynolds number and Pr is Prandtl number and calculated from:

$$\mathrm{Re} = \frac{\rho V D}{\mu} \quad , \quad \mathrm{Pr} = \frac{C_p \mu}{k}$$

Where ρ, μ, k, C_p are density, dynamic viscosity, thermal conductivity and specific heat of fluid, V the average fluid velocity and D is the diameter of a tube.

The validation is carried out by using water with Reynolds numbers (Re) ranging from (8900 to 19500), as dictated by varying the flow rate.

Figure 4.3 and Figure 4.4 compare the measured local and average Nusselt number of water to the predicted Nusselt number by using Gnielinski's correlation. In order to compare, the error +/-5% and +/-10% of the measured result and the predicted results are presented as dotted lines in the figures. It can be seen that all the data of local and average Nusselt number falls within 10% and 5% of the predicted values respectively. Based on this close agreement the experiment loop is considered reliable and accurate to measure the turbulent heat transfer coefficient. All raw data for the test is detailed in Appendix B.

It should be noted that experimental uncertainty of the measured Nusselt numbers are estimated to be ±5% as shown in Appendix C.

With regard to the effect of heat loss, the local heat transfer coefficient of water was calculated by the fluid heat gain $q=\dot{m}C_p(T_{b,out}-T_{b,in})$ and compared to the theoretical maximum which considers no heat loss i.e. $q=IV$, as shown in Figure 4.5. It shows that the difference in local heat transfer coefficient is within about 5%. This indicates that the loop has very good insulation over the test section and therefore validates the use of Eq. (4.3) to calculate the inner surface temperature of the test section. In order to show more details of the test section surface temperature along the test section at the outside surface ($T_{s,out}$) are presented in Figure 4.6. These are given for water at different Reynolds numbers. It can be observed that temperature varies in a linearly along the test section indicating that the test has reached a steady state condition. It is also shown that the temperature increases linearly along the test section at constant heat flux, but it decreases as Reynolds number increases as expected.

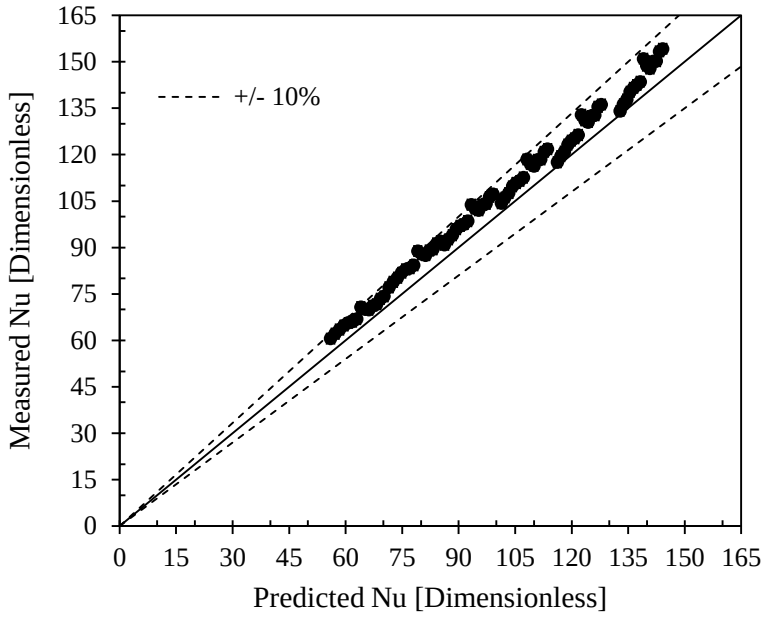

Figure 4.3: Comparison between the measured and the predicted (using Gnielinski's correlation) local Nusselt number for water-test

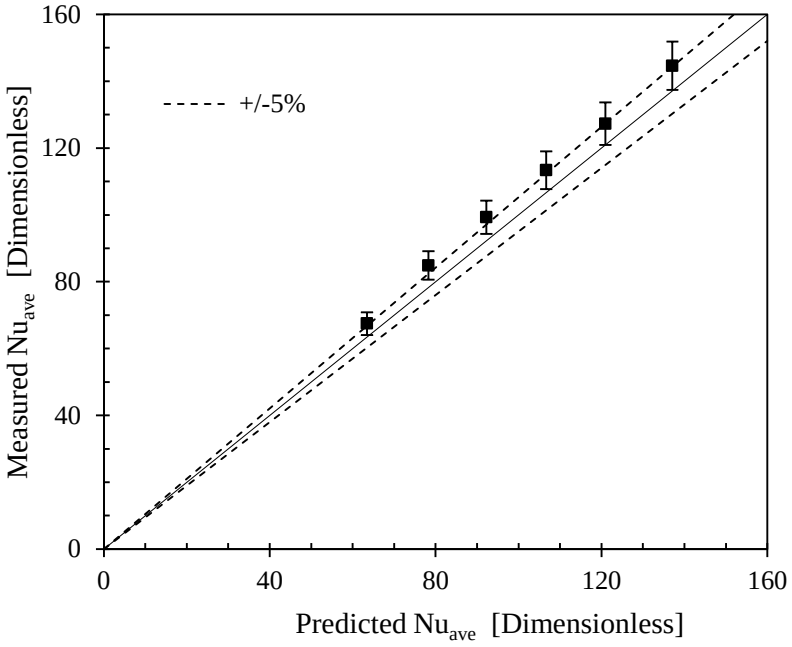

Figure 4.4: Comparison between the measured and the predicted (by Gnielinski's correlation) average Nusselt number for water-test

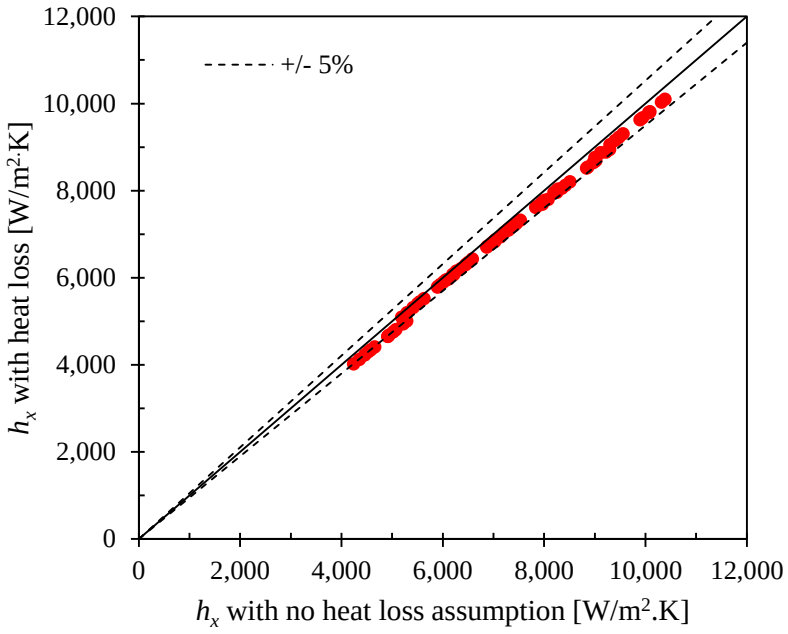

Figure 4.5: Comparison the actual local heat transfer coefficient with heat loss to the ones obtained by assuming no heat loss

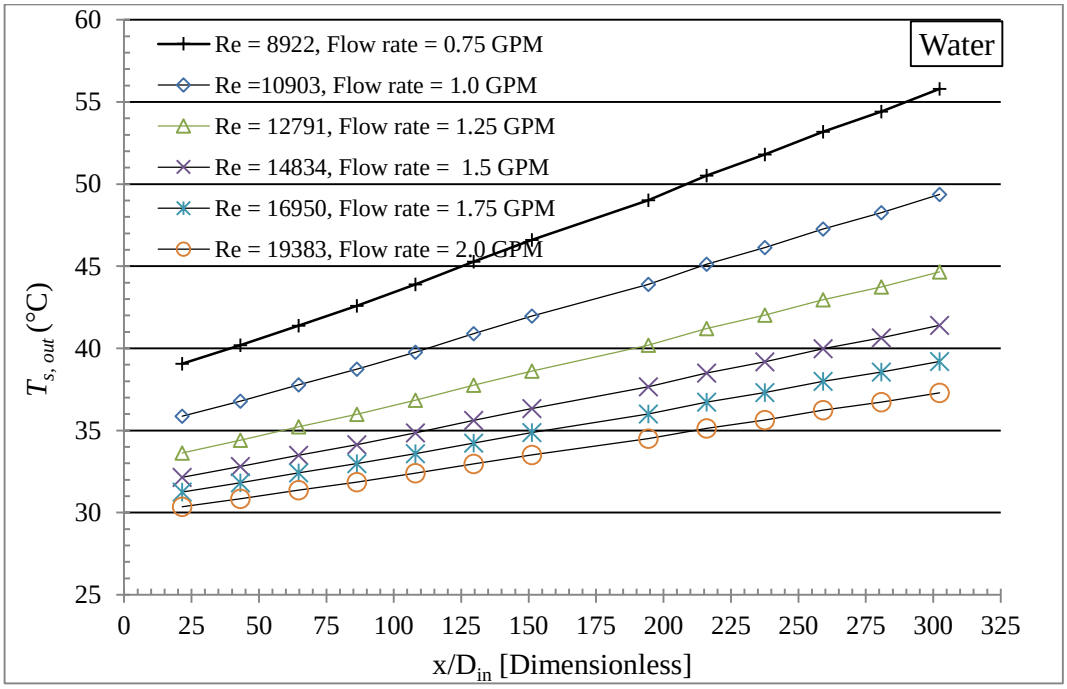

Figure 4.6: Temperature distribution along the test-section axis for water

4.3.2: Pressure drop verification test for water

When assessing the potential benefits of nanofluids, it is important to know the viscosity, which is a function of the fluids pressure drop. To investigate the pressure drop across the loop, first the measured pressure drop of water was compared with the existing correlation for a fully developed turbulent flow; where the surface of the tube is assumed to be smooth [97].

$$\Delta P = f \frac{L}{D_{in}} \left(\frac{\rho V^2}{2} \right) \tag{4.15}$$

Where L and D_{in} are the length and inner diameter of test section tube, respectively. The friction factor, f, can be calculated from Eq. (4.14) and V is the inlet velocity which measured from the flow rate.

The pressure drop measurement results for heated test section and isothermal test were in close agreement with the conventional semi-theoretical Eq. (4.15) as shown in Figure 4.7 with differences of less than 10%. It should be noted that the average experimental uncertainty of the measured pressure drop and friction factor are estimated to be ±7% and 8%, respectively, as shown in Appendix C.

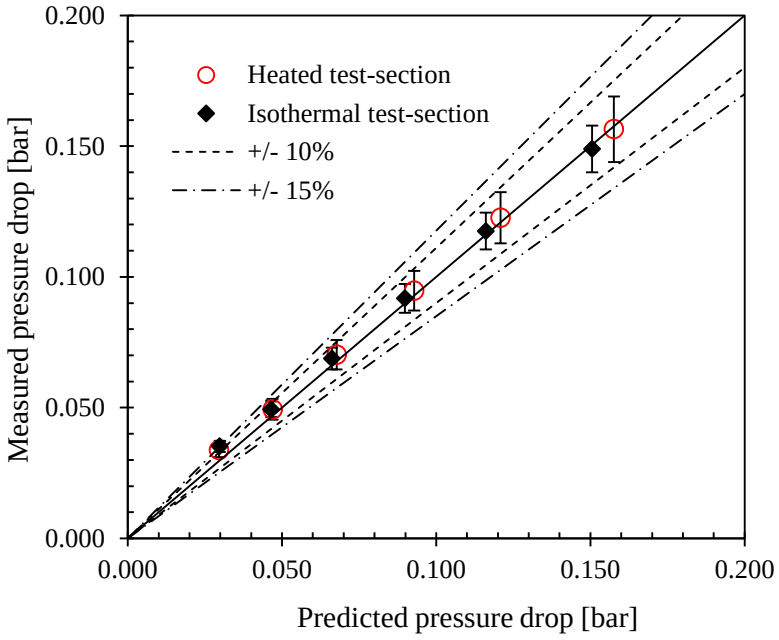

Figure 4.7: Water pressure drop comparison-test the heated and isothermal test sections.

From the above two tests (heat transfer and pressure drop), it can be concluded that the experimental set-up is reliable for further measurements of the heat transfer coefficient and the pressure drop of turbulent liquid flows. The next section describes and measures the nanofluid's convectional heat transfer and pressure drop.

4.4: Nanofluids Results and Discussion

This section presents the nanofluids convectional heat transfer performance and pressure drop as a function of the volume fraction concentration.

4.4.1: Convection Heat Transfer and Pressure Drop of Nanofluids

The convective heat transfer coefficient and pressure drop for all nanofluids were measured and compared to the base fluid (water). Also a comparison with the conventional correlations was performed to determine the viability of using existing correlations of single phase fluids to predict the heat transfer coefficient and pressure drop, since there is still controversy between researchers. A comparison to the existing correlations for nanofluids is also performed. All raw data for the following tests are given in Appendix B.

As mentioned above, the reliable experimental closed loop on forced convection for constant heat flux was used to measure the convective heat transfer coefficient and viscous pressure loss. Different nanofluid types (Al_2O_3-water nanofluid, TiO_2-water nanofluid and CuO-water nanofluid) were investigated with various nanoparticle concentrations.

In previous studies, a popular approach to assessing the thermal performance of nanofluids is by considering the Nusselt number and how this varies with Reynolds number. Adopting this approach, for now, using the data from the present study, leads to the plots in Figures 4.8 – 4.10 for the three types of nanofluid considered. In each plot, the performance of the water base fluid is given for comparison. For TiO_2 nanofluids, the nanoparticle loading has no distinguishable effect on the value or variation of the average Nusselt number with Reynolds number (see Figure 4.9). For CuO nanofluids (Figure

4.10), the nanoparticle loading has more influence, with lower concentrations giving slightly lower values of Nusselt number at given Reynolds number, but 1.2% and 1.6% concentrations giving slightly higher Nusselt number. In contrast, for the Al_2O_3 nanofluids the nanoparticle loading has a marked effect on the behaviour, with the average Nusselt number increasing with nanoparticle load for a given Reynolds number, as seen in Figure 4.8. For example, at a Reynolds number of about 8000 the Nusselt number increased by 7%, 10% 22%, 39%, and 54% for Al_2O_3-water nanofluids 0.5 vol.%, 0.9 vol.%, 1.8 vol.%, 2.7 vol.% and 3.6 vol.% respectively.

These plots give the impression that using Al_2O_3-water nanofluids would be beneficial – i.e. would lead to an enhanced heat transfer rate. However, these plots are misleading because both Nu and Re are themselves dependent on the nanoparticle loading, ϕ. The Nusselt number is scaled with thermal conductivity, which is a function of ϕ, while Re includes the density and viscosity and both these properties also depend on the nanoparticle concentration. Moreover, the viscosity of each nanofluid is higher than the base fluid, and increases with increasing nanoparticle concentration, so each nanofluid requires a higher pumping power in order to achieve the same corresponding Reynolds number as the base fluid.

To reveal the true effect of using nanofluids, the *actual* (dimensional) heat transfer coefficient should be considered, as a function of the (dimensional) flow rate. This leads to Figures 4.11 to 4.13., which give representative results of the variation of the average heat transfer coefficient with volumetric flow rate and different volume fraction concentrations of Al_2O_3-water nanofluid, TiO_2-water nanofluid and CuO-water nanofluid, respectively. This is in order to check the effect of the concentration of nanofluid on the convective heat transfer coefficient for a given type of nanofluid. In order to compare, the corresponding curves of base fluid (distilled water) are presented as solid lines in the figures.

It is now clear that the base fluid (i.e. water) actually outperforms *all* of the nanofluids considered – it has the highest heat transfer coefficient under the experiment conditions. In other words, nanofluids deteriorate the convective heat transfer rate and

this deterioration increases with increasing nanoparticle load. For example, the convective heat transfer coefficient decreases noticeably with Al_2O_3-water nanofluids concentrations of 0.5 - 5.9 vol.% by about 5 - 55%, respectively. Whereas, TiO_2-water nanofluids with volume fraction 0.5 vol.%, 1.5 vol.%, 2.5 vol.%, 3.5 vol.% and 4.5 vol.% give respective decreases in heat transfer coefficient of 11%, 24%, 34%, 43% and 50% compared to the base fluid. With regard to CuO-water nanofluid, at given volumetric flow rate, the base fluid has the highest heat transfer coefficient by an average of 8%. The performance of these nanofluids gives smaller thermal performance differences when compared to each other. Note that (as explained in chapter 2) only low concentrations of CuO-water nanofluid were prepared. Therefore, a comparison with other nanofluids at the higher concentrations cannot be undertaken.

This decrease in the heat transfer coefficient could be due to the increase of the boundary layer thickness because of increases in viscosity with increasing nanoparticles loads of nanofluid. This result was predicted by MacDevette at el. [96] using a theoretical model for nanofluid.

Note that the heat transfer performance of the nanofluids is actually even worse than indicated in Figures 4.11 to 4.13 when one considers the pressure drop in the system. As the nanoparticle concentration increases, the viscosity of the nanofluid increases, and therefore the pressure gradient required to achieve a certain flow rate also increases. Hence if the heat transfer coefficient at fixed pressure gradient were considered, the reduction in heat transfer coefficient with increasing nanoparticle concentration would be even greater. The influence of the pressure penalty on the overall value of using nanofluids is included in the economic model presented in Chapter 6.

It should be emphasized here that the Reynolds number at low flow rates i.e. less than 1.5 GPM and the highest volume fractions of Al_2O_3-water nanofluids i.e. 4.7 vol.% and 5.9 vol.% the flow was most likely laminar. In addition, the maximum flow rate of Al_2O_3-water nanofluid was 2.0 GPM at the maximum volume fraction; this is due to the higher viscosity, which increases with increasing nanoparticle loads. At the lowest flow rates, the highest concentrations of Al_2O_3-water nanofluid and TiO_2-water nanofluids

could not be measured because the measured test section surface temperatures reached the boiling temperature of water. More details for the surface of test section temperature will be given later (Appendix D)

It should be re-emphasized that some of the nanofluid properties are measured and some are calculated using initial values that are taken from the literature. The thermal conductivity of Al_2O_3 particle is higher than CuO particles and TiO_2 particles by 2.3 and 3.6 times, respectively. This explains that the Al_2O_3-water nanofluid has higher heat transfer performance than others.

In order to show more details of the test section surface temperature variations as affected by nanofluids concentration and flow rate, the temperature distribution for specific flow rate and nanofluid various volume fractions at the outside surface of the test section ($T_{s,out}$) are presented in Appendix D.

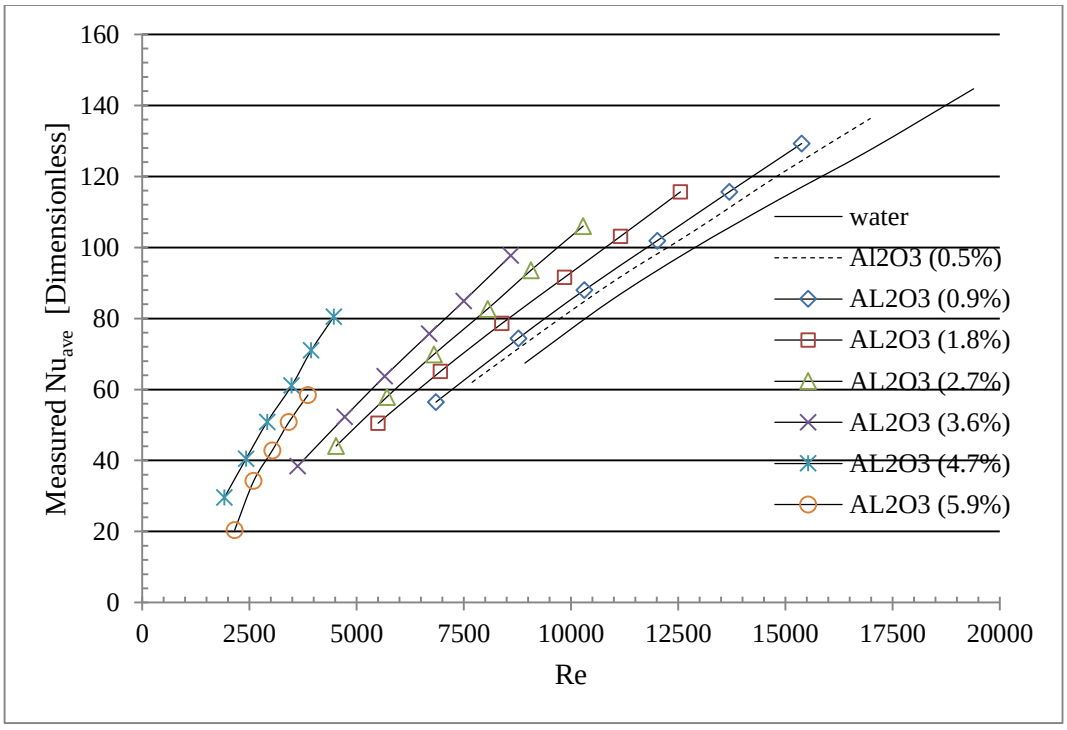

Figure 4.8: Average Nusselt numbers vs. Reynolds number of water and Al_2O_3-water nanofluid tests.

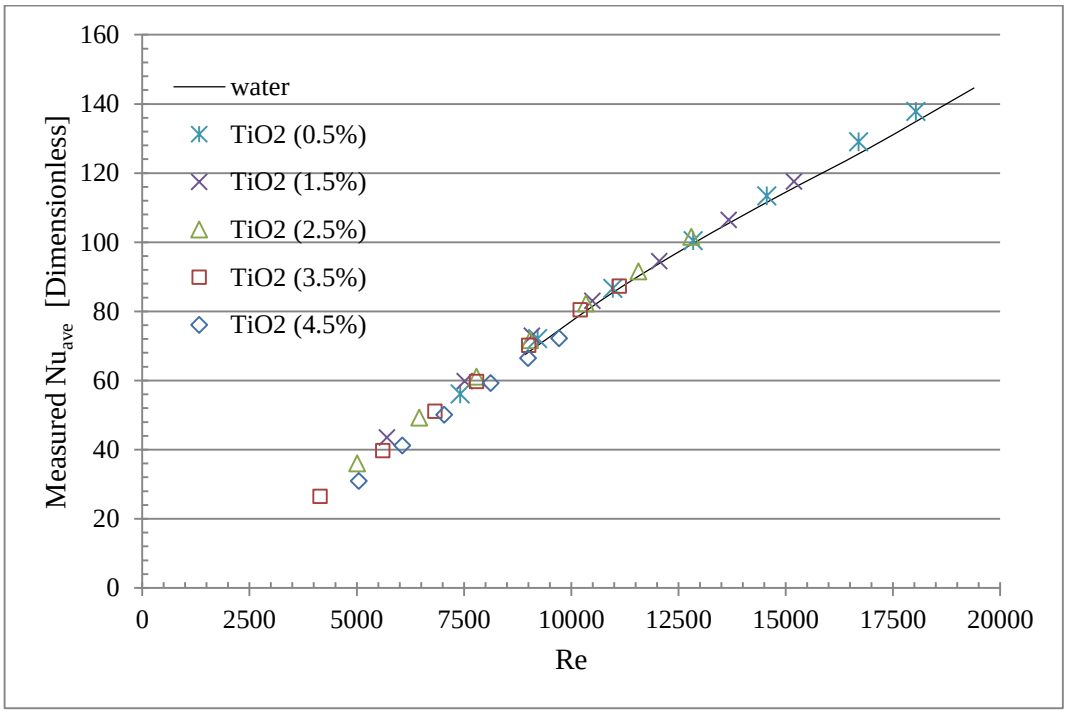

Figure 4.9: Average Nusselt numbers vs. Reynolds number of water and TiO_2-water nanofluids tests

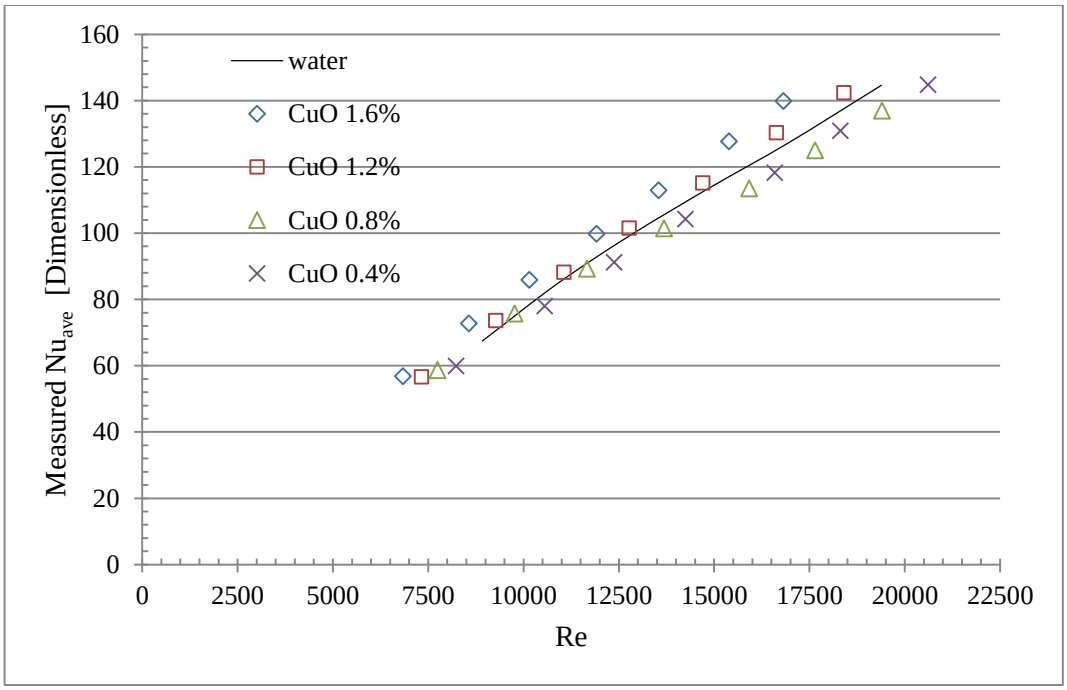

Figure 4.10: Average Nusselt numbers vs. Reynolds number of water and CuO-water nanofluids tests.

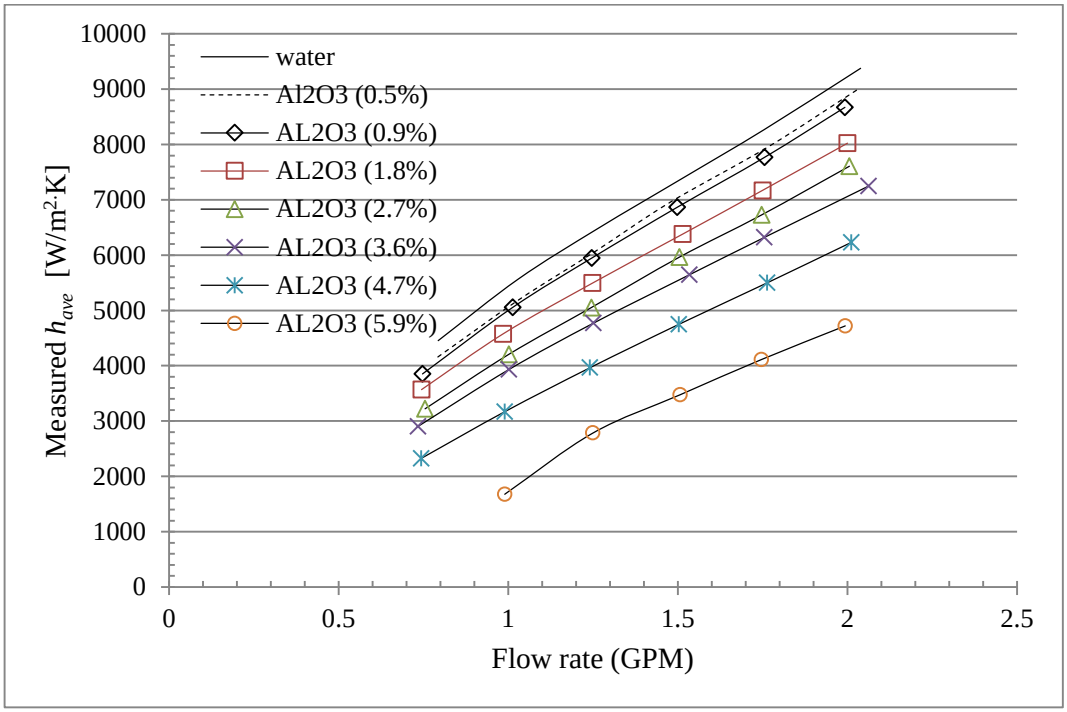

Figure 4.11: Average heat transfer coefficient vs. volumetric flow rate of water and Al_2O_3-water nanofluid tests

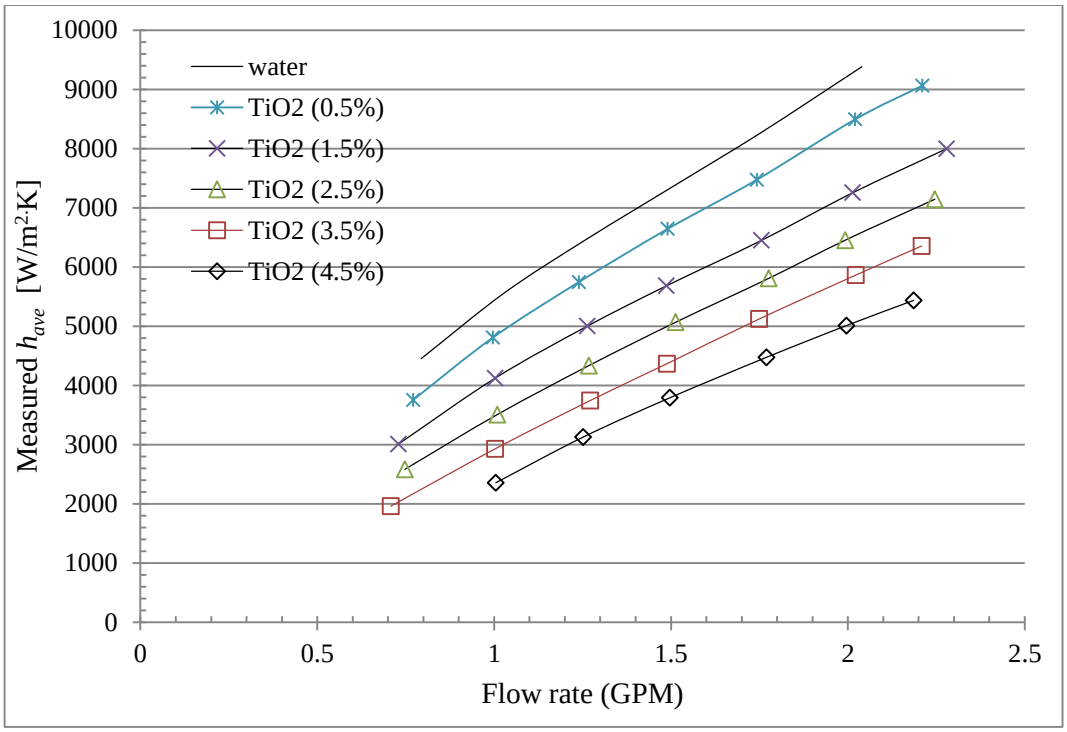

Figure 4.12: Average heat transfer coefficient vs. volumetric flow rate of water and TiO_2-water nanofluid tests

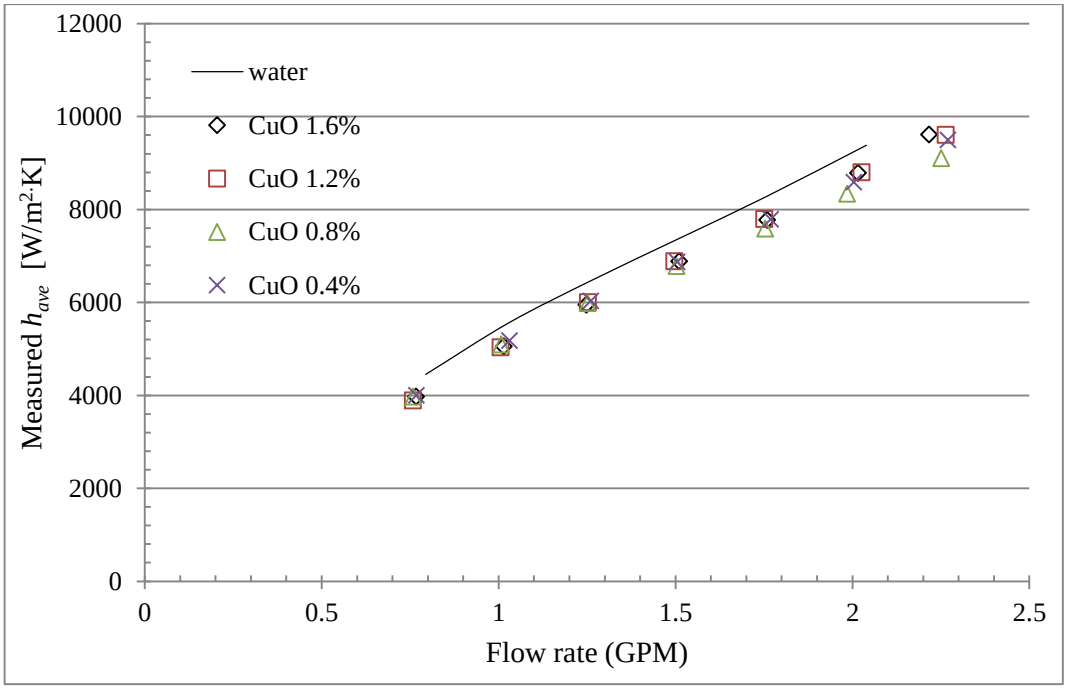

Figure 4.13: Average heat transfer coefficient vs. volumetric flow rate of water and CuO-water nanofluids tests

4.4.2: Comparison with existing Nusselt number correlations

The comparison of average Nusselt numbers nanofluids results to the predicted conventional correlation such as Gnielinski's correlation [97] was made as has been mentioned before to see the possibility of estimating Nusselt number. In order to compare, the error +/-10% and +/-20% of the measured result and the predicted results are presented as dot and central lines in the figures, respectively. It is found the measured Nusselt number values of Al_2O_3-water nanofluid and TiO_2-water nanofluid are shown in Figures 4.14 and 4.15, respectively. It is clearly seen that the results of the average Nusselt number are within a difference of about 20% when compared to Gnielinski's correlation. Whereas the average Nusselt numbers for CuO-water nanofluid agree well to within 10% with those predicted as shown in Figure 4.16. It is interesting to note that estimating Nusselt number using Gnielinski's correlation gives an overestimate for Al_2O_3-water nanofluid and a slight underestimate for TiO_2-water nanofluid. It is emphasized that the strategy adopted in the present study is to calculate the Reynolds number and Prandtl number the thermal and physical properties of the fluids (water and nanofluid) were obtained at the average bulk temperature, $T_{b,m}$. Such a difference could be due to the aggregation of nanoparticles, which affect the flow characteristics and measurement conditions. It should be noted that experimental uncertainty of the measured Nusselt numbers for Gnielinski's correlation and nanofluids are estimated to be ± 10% and 3-9%, respectively.

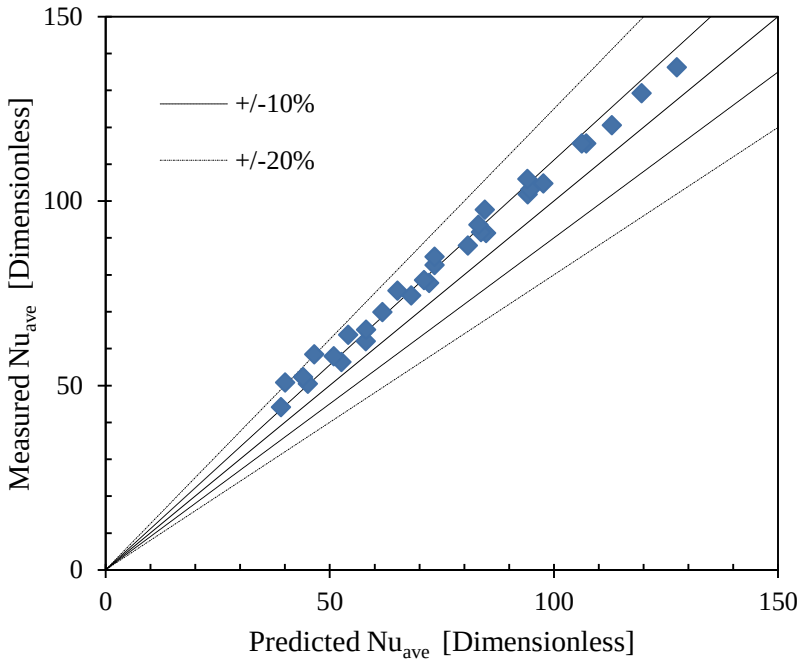

Figure 4.14: Comparison results of the measured and the predicted Gnielinski's correlation average Nusselt numbers for Al_2O_3-water nanofluids

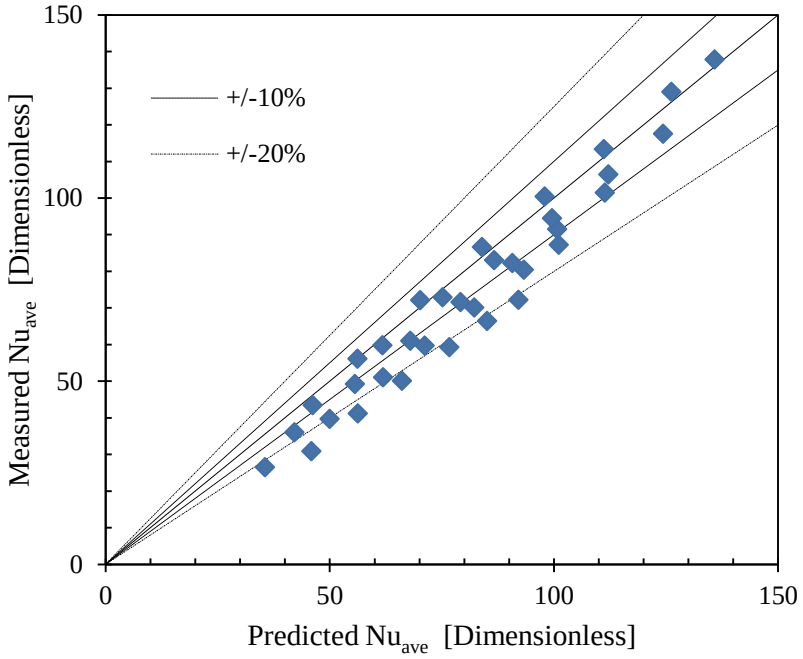

Figure 4.15: Comparison results of the measured and the predicted Gnielinski's correlation average Nusselt numbers for TiO_2-water nanofluids.

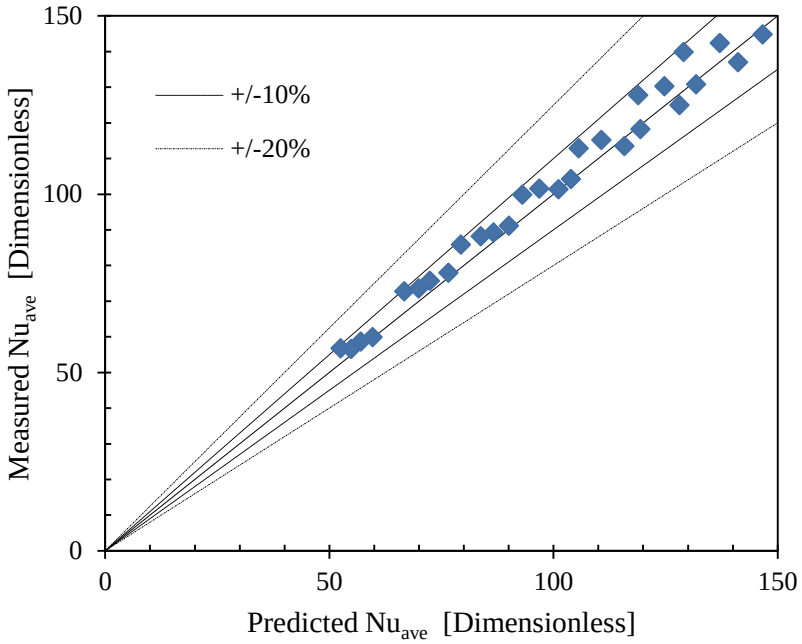

Figure 4.16: Comparison results of the measured and the predicted Gnielinski's correlation average Nusselt numbers for CuO-water nanofluids.

4.4.3: Comparison with existing nanofluid Nusselt number correlations

In this section, a comparison of the measured Nusselt numbers to existing experimental nanofluid correlations will be discussed. Pak and Cho [23], Sahin et al. [52] and Sajadi and Kazemi [55] have proposed Nusselt number correlation for predicting the heat transfer coefficient of nanofluids. There are limitations to using these correlations. Pak and Cho [23] established their correlation based on their experimental data on γ-Al_2O_3-water and TiO_2-water nanofluids with volume fraction (ϕ), Reynolds number (Re), and Prandtl number (Pr) ranging from 0 - 3 vol%, 10^4 to 10^5, and 6.54 to 12.33, respectively. Sahin et al. [52] constructed their correlation using experimental data on Al_2O_3-water nanofluids with limitations on Reynolds number, volume concentration, and Prandtl number range $4000 \leq \mathrm{Re} \leq 20000$, $0.005 \leq \phi \leq 0.04$ and $\mathrm{Pr} \approx 5–7$, respectively. Sajadi and Kazemi [55] derived the correlation based on their experimental data on TiO_2-water nanofluids with respect to volume fraction of $\phi \leq 0.25\%$ and a Reynolds number (Re) range between 5000 and 30000.

Their correlations are presented below:

Pak and Cho [23] correlation: $Nu_{Pak} = 0.021\,\mathrm{Re}^{0.8}\,\mathrm{Pr}^{0.5}$

Sajadi and Kazemi [55] correlation : $Nu_{Sajadi} = 0.067\,\mathrm{Re}^{0.71}\,\mathrm{Pr}^{0.35} + 0.0005\,\mathrm{Re}$

Sahin et al.[52]correlation: $Nu_{Sahin} = 0.106\,\mathrm{Re}^{0.588}(1.0 + \phi^{0.1096})\,\mathrm{Pr}^{0.258}$

It should be emphasized that the properties of the nanofluid are used to calculate Reynolds number (Re), and Prandtl number (Pr).

The Pak and Cho, Sahin et al. correlations are chosen to predict the present experimental results of Nusselt number for Al_2O_3-water nanofluids under their conditions in Figure 4.17. It is clearly seen that the Pak and Cho correlation predicts the Nusselt number within 5% of observed values. It should be noted that experimental uncertainty of the measured Nusselt numbers are estimated to be ±3 - 9%. On the other hand, Sahin et al's correlation gives a noticeable overestimation of the experimental results. This could be because of the Prandtl number (Pr) which the correlation was based on; the Prandtl

number (Pr) of this experiment is higher than that of the studies because the measured viscosity of Al_2O_3-water nanofluid result was higher. For example Prandtl number is Pr = 11 at volume fraction 3.6 vol.%.

Regarding TiO_2-water nanofluids Pak and Cho's correlation and Sajadi and Kazemi's correlation are used to predict the Nusselt number of the present experimental results in Figure 4.18. It can be seen that Pak and Cho's correlation overestimates the average Nusselt number by up to 20%. However, Sajadi and Kazemi's correlation gives a significant overestimation of the expemental data by over 40%. This is possible because they used Einstein's model to predict the viscosity of nanofluids for the correlation and, as mentioned in chapter 3, this theoretical viscosity model significantly underestimated the nanofluid viscosity. It should be emphasized here that the thermophysical properties of the nanofluids are taken at the average bulk temperature, $T_{b,m,}$ and used to calculate the dimensionless numbers, i.e. Reynolds number (Re) and Prandtl number (Pr).

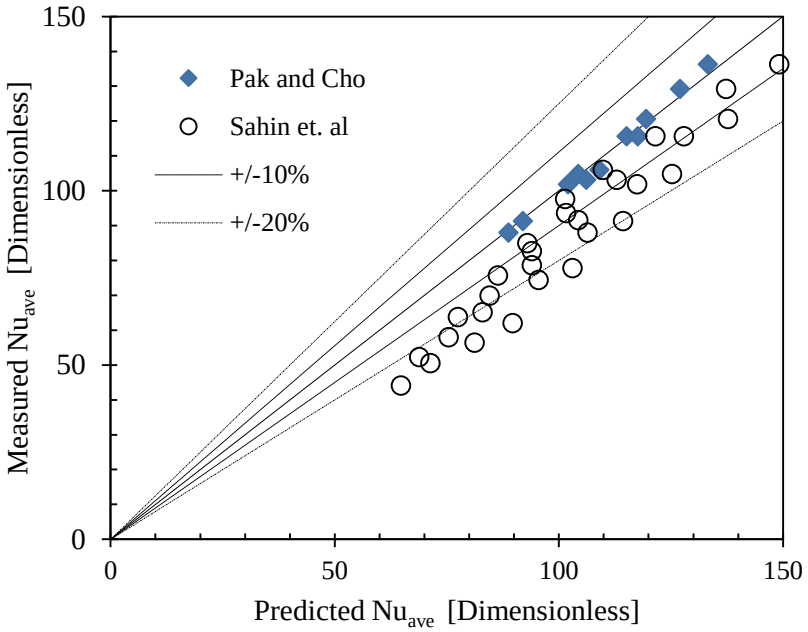

Figure 4.17: Comparison of various correlations in predicting the Nusselt numbers measured in the present study for Al_2O_3-water nanofluids.

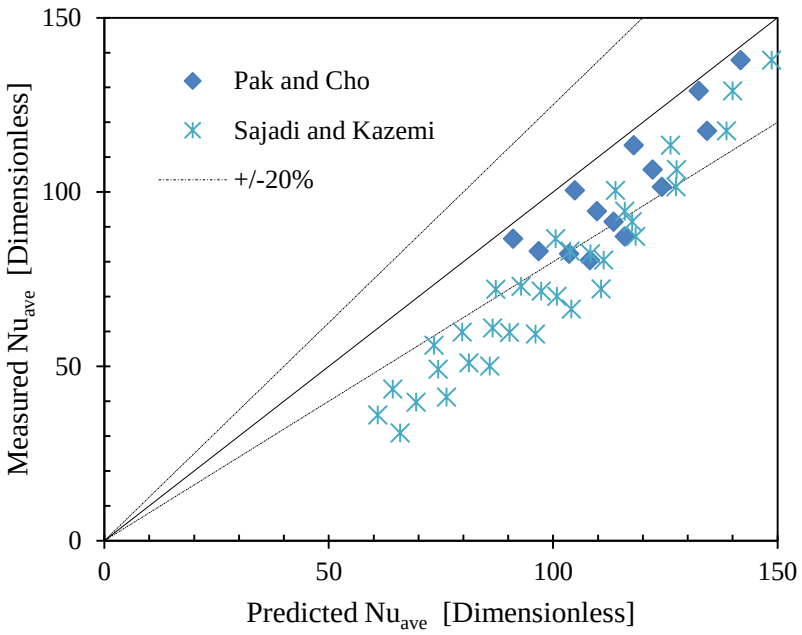

Figure 4.18: Comparison of various correlations in predicting the Nusselt numbers measured in the present study for TiO_2-water nanofluids.

4.4.4: Comparison of experimental pressure drop

Since nanofluids have an improved thermal performance at a specific Reynolds number when compared to the corresponding base fluid but an increased viscosity compared to their base fluid, as mentioned in chapter 3, a higher pumping power is required to maintain a specific Reynolds number. Therefore, the nanofluid pressure drop is vital for predicting the nanofluids performance in a practical situation.

In this section the viscous pressure loss of a nanofluid was tested and compared to the conventional semi-theoretical correlation Eq. (4.15) to determine the ability to predict a nanofluids pressure drop. This was compared with the base fluid (water) pressure drop to highlight the effect of increasing nanoparticles loads. The pressure drops of the test sections for nanofluids were measured, using differential pressure transducers.

Figures 4.19 - 4.21 present the variations in pressure drop with Reynolds number and volume fraction concentration of the test section for all investigated nanofluids (Al_2O_3-water nanofluid and TiO_2-water nanofluid and CuO-water nanofluid). The measurements indicate that over the Reynolds number and concentration ranges considered the pressure drop increases with both increasing Reynolds number and more significantly with increasing nanoparticle loads. For example, at a Reynolds number of about 8000, the pressure drop of Al_2O_3-water nanofluids with volume fraction 0.5 vol%, 0.9 vol.%, 1.8 vol.%, 2.7 vol.% and 3.6 vol.% is higher than the base fluid (water) by 1.6, 1.7, 2.5, 4.7 and 6.4 times, respectively. On the other hand, TiO_2 and CuO water nanofluids gives higher pressure drop compared to water by about 1.5 - 5.0 times and 1.2 - 1.8 times with respect to the volume fractions 0.5 - 4.5 vol.% and 0.4 - 1.6 vol.%, respectively. It is interesting to note that at similar concentrations of all the tested nanofluids the Al_2O_3-water nanofluid gave highest pressure drop.

Figures 4.22 – 4.24 show the corresponding pressure loss of the test section of all investigated nanofluids versus flow rate for various volume fractions. It is apparent that the measured pressure drop increases with increasing flow rates and more significantly

with increasing nanoparticle load. Therefore, it is unlikely these nanofluids can be utilised in practical heat transfer applications without modifying the flow rate

It can be seen from Figure 4.26 and Figure 4.27 that the conventional theoretical Eq. (4.15) can predict the pressure drop of TiO_2-water nanofluid and CuO-water nanofluid within 10% of the recorded values for all volume fractions under the test conditions. The same happens also to predict the pressure drop of Al_2O_3-water nanofluid for low volume concentration as presented Figure 4.25. The conventional correlation estimates the pressure drop to within 10% at lower concentrations but deviates with higher concentrations with a maximum error of approximately 20%. This could be due to the large temperature fluctuation along the test section that was observed, because at higher concentration, the flow becomes laminar or transitional, therefore the fully developed region is larger than that of turbulent flow; see Appendix D.

The highest value of the viscous pressure losses and friction factors are observed for the nanofluid with the highest nanoparticles load. This is mainly due to the fact that viscosity increases with nanoparticle load. It is interesting to mention that the friction factors of nanofluids with respect to base fluid follow their relative viscosity trend (see chapter 3, Figures 3.12 - 3.14); as shown in Figure 4.28,

It should be emphasized again that the thermophysical properties of the nanofluids are taken at the average bulk temperature, $T_{b,m}$, and used to calculate the dimensionless numbers, i.e. Reynolds number (Re), Prandtl number (Pr) and friction factors (f).

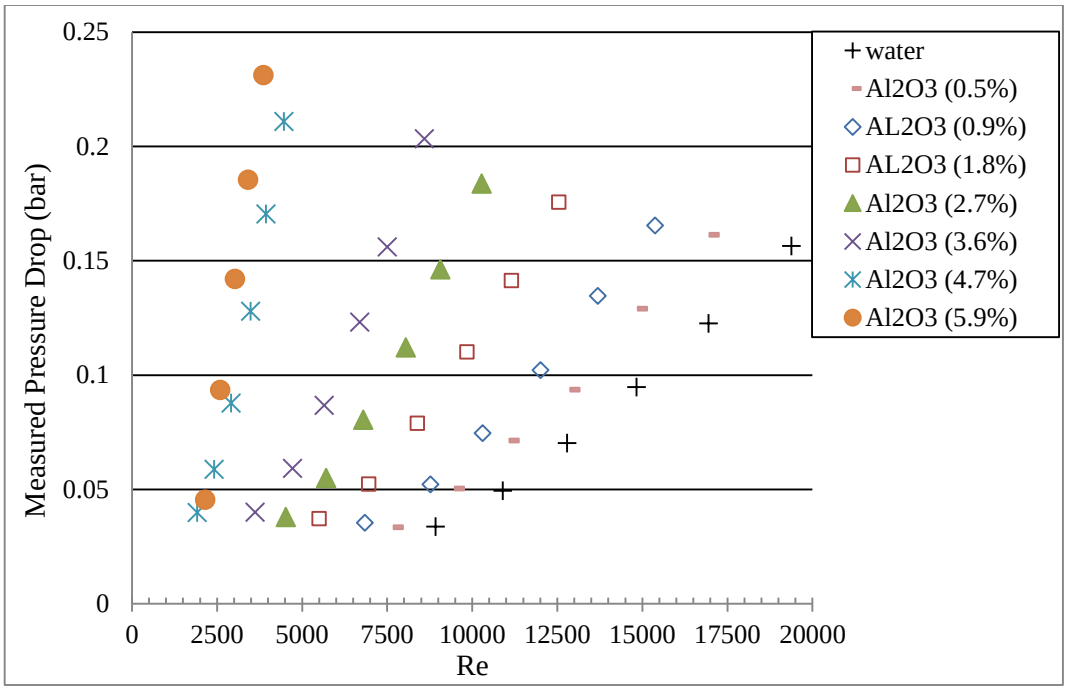

Figure 4.19: Pressure drop of Al_2O_3-water nanofluids versus Reynolds number

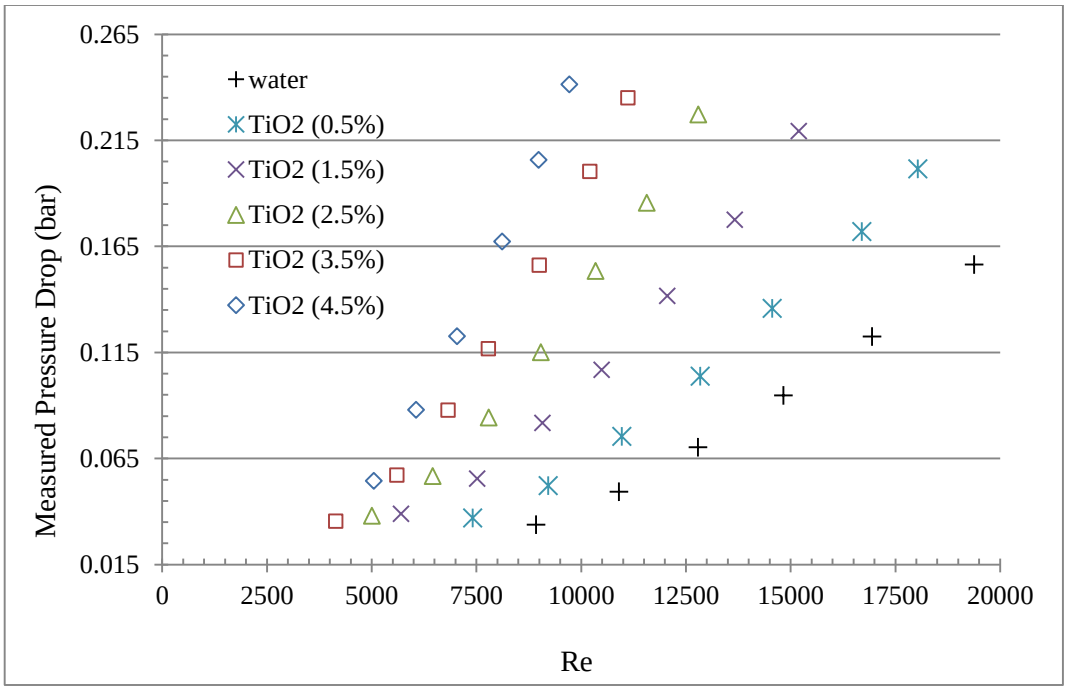

Figure 4.20: Pressure drop of TiO_2-water nanofluids versus Reynolds number

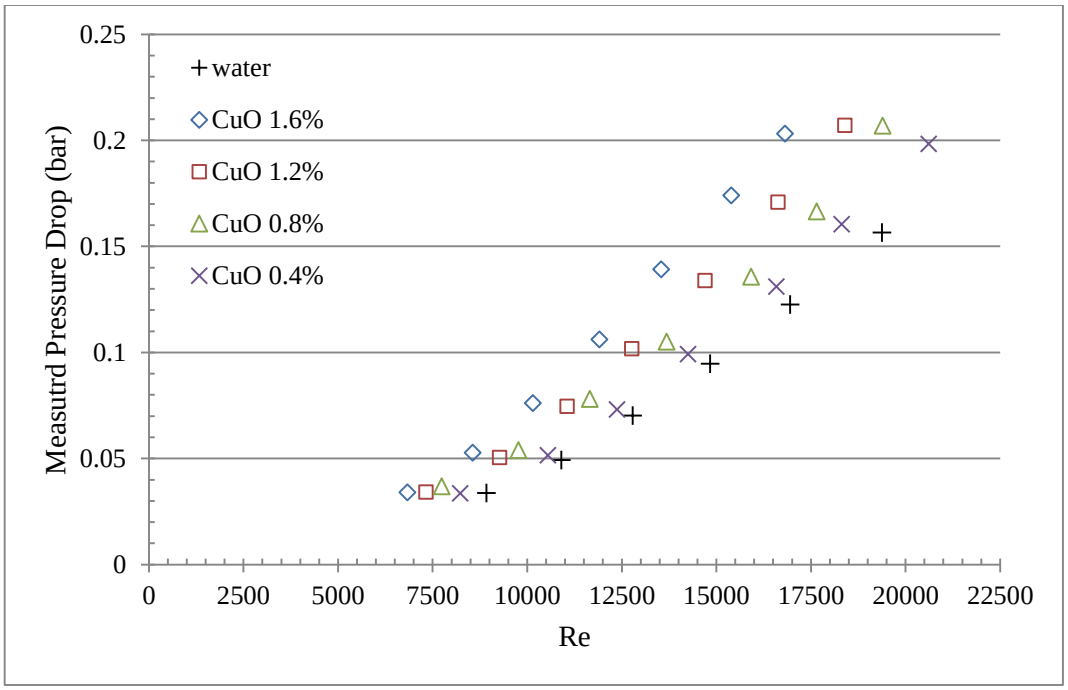

Figure 4.21: Pressure drop of CuO-water nanofluids versus Reynolds number

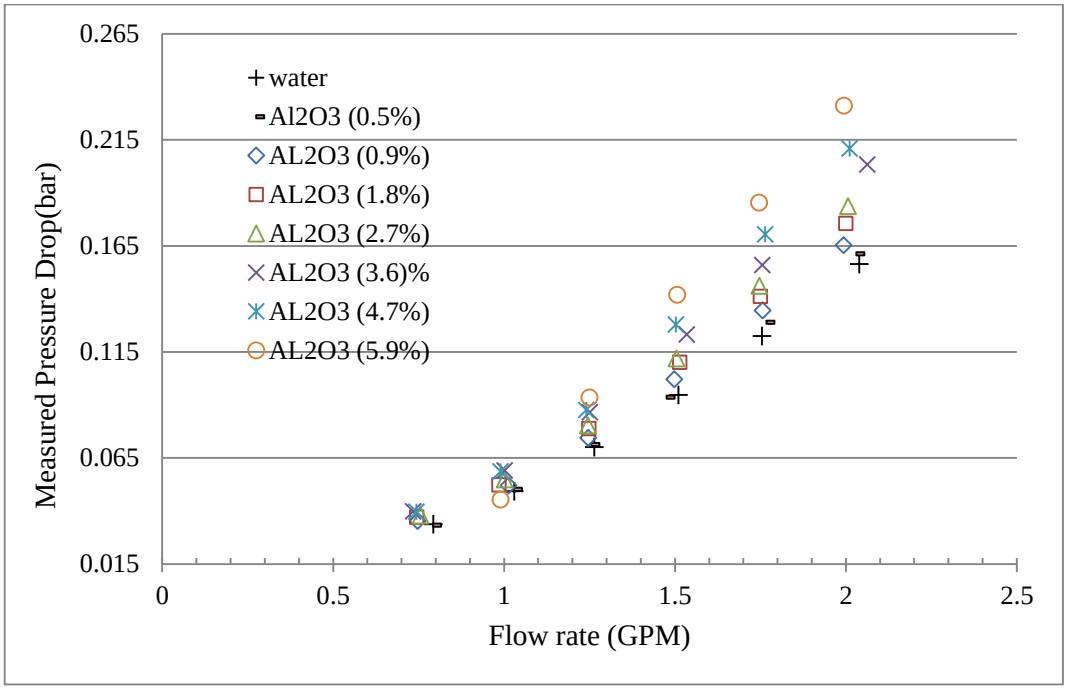

Figure 4.22: Pressure drop of Al_2O_3-water nanofluids versus flow rate

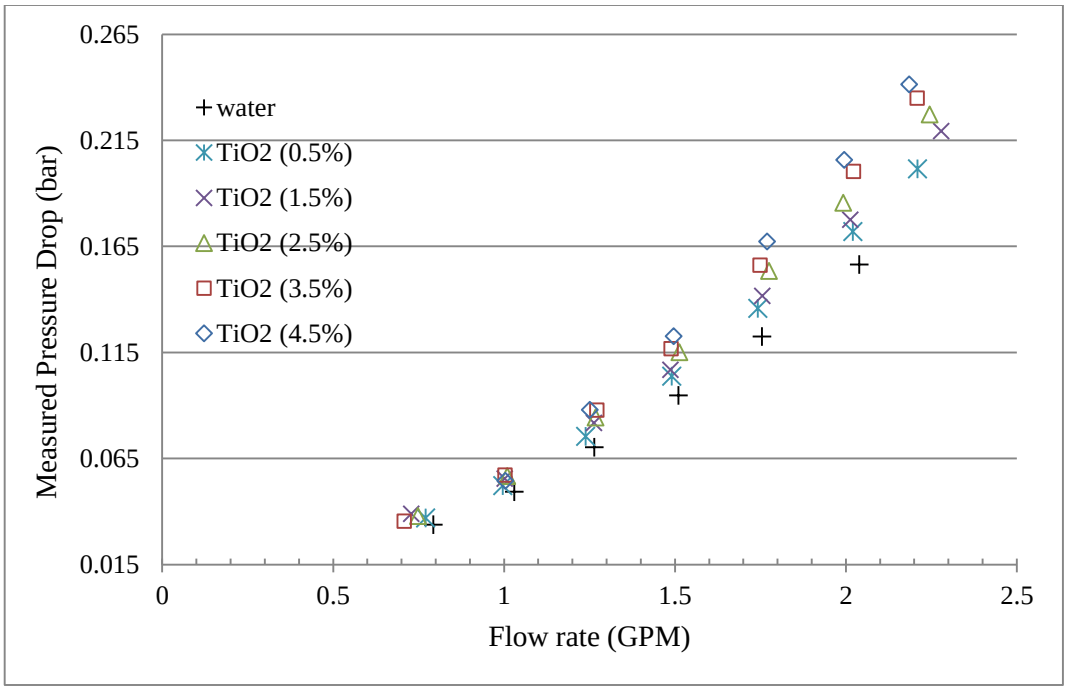

Figure 4.23: Pressure drop of TiO_2-water nanofluids versus flow rate

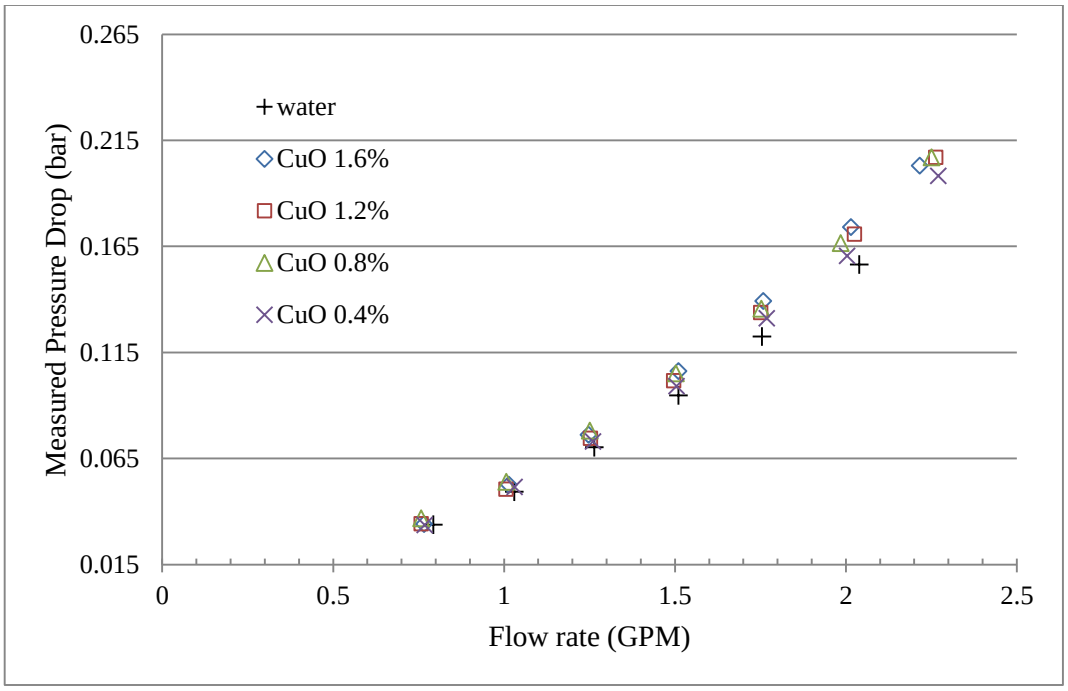

Figure 4.24: Pressure drop of CuO-water nanofluids versus flow rate

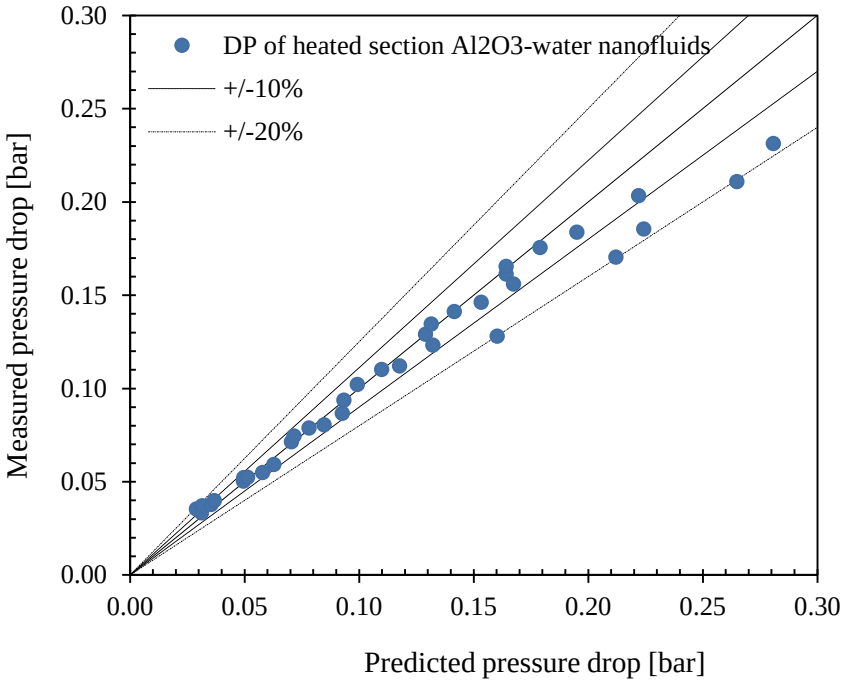

Figure 4.25: The measured pressure drop comparing to predicted pressure drop using Eq. (4.15) for Al_2O_3-water nanofluids.

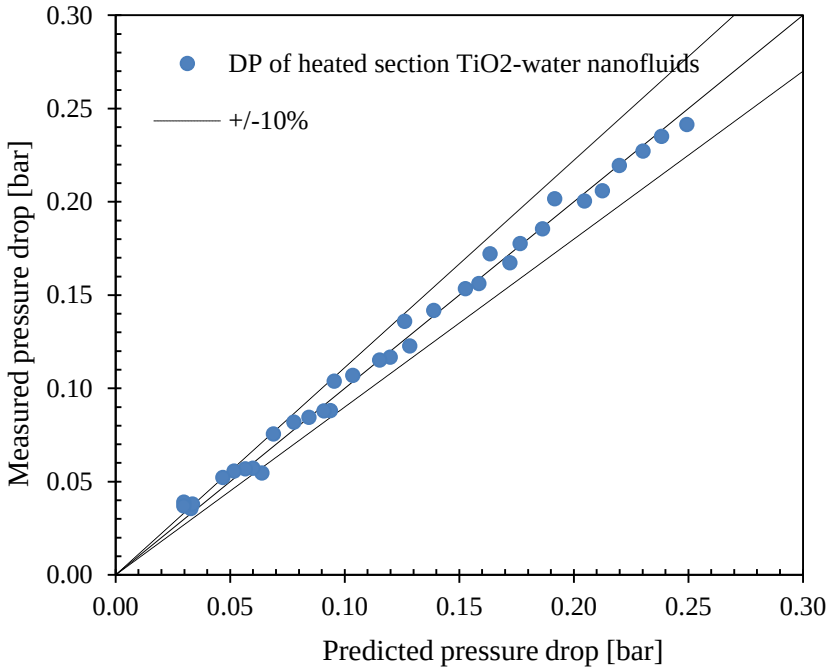

Figure 4.26: The measured pressure drop comparing to predicted pressure drop using Eq. (4.15) for TiO_2-water nanofluids.

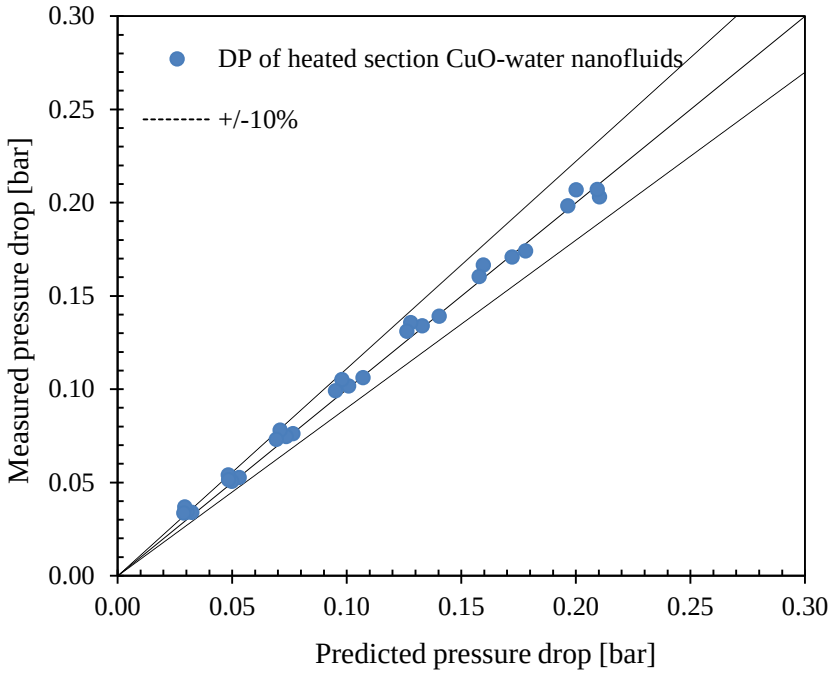

Figure 4.27: The measured pressure drop comparing to predicted pressure drop using Eq. (4.15) for CuO-water nanofluids.

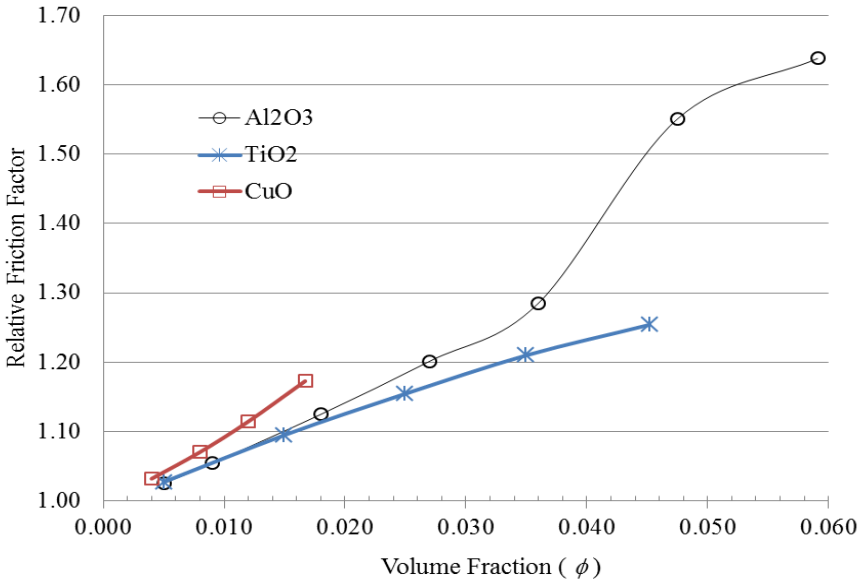

Figure 4.28: The Relative friction factor of nanofluids to the base fluid

4.5: Convection Heat Transfer and Pressure Drop of Dielectric Liquid (HFE)

In this section, an experimental study of turbulent forced convection heat transfer and pressure drop characteristics of dielectric liquid (hydrofluoroethers (HFE)) through a uniform heated horizontal circular tube are investigated. The evaluation of the heat transfer and pressure drop of the dielectric liquid (HFE) are compared to calculations made with the conventional correlations carried out by Gnielinski's and shown by Eq. (4.13) and the existing correlation of fully developed turbulent flow shown by Eq. (4.15); these correlations assume the internal surface of the tube to be smooth [97].

As with previous chapters, the properties of the fluids are obtained at the average bulk temperature (Eq. 4.4). The thermophysical properties of the dielectric liquid (HFE) are provided by the supplier [103, 104] and described in Table 4.2. It should be emphasized here also that the thermophysical properties of the dielectric liquid (HFE) are assumed to be constant and taken at 25°C; with the exception of the density and viscosity which are calculated as a function of the fluid temperature.

Table 4.2: Shows material properties of based liquids and nanoparticles.

Property	dielectric liquid (HFE)	comments
ρ (kg/m^3)	$(1.7162 - 0.0024T)\times 1000$	T is temperature in (°C)
ν (m^2/s)	$(2.74465\log(T) - 14.46578)^{-2.1758}$	T is temperature in (K)
C_p(J/kg.K)	1140	-
k (W/m.K)	0.063	-
β (1/K)	1.51×10^{-3}	-

Measurements were carried out for one specimen of dielectric liquid (HFE) and were repeated three times and averaged. The inlet bulk temperature of the test section was maintained at a constant, the uniform heat generation at about 5000W and the flow rate

was changed from 1.00 to 2.25 GPM (gallon per minute) (i.e. 5×10^{-5} to 0.00013 m^3/s) for each sample.

The results show that the conventional correlations predicts the heat transfer coefficient and pressure drop of the dielectric liquid (HFE) very well with a difference of less than 10%; see Figures 4.29 and 4.30 for local and average Nusselt number respectively, the pressure drop correlation is given by Figures 4.31. This difference could be due to the thermal conductivity and specific heat which is assumed to be constant, see Table 4.2. In addition, the uncertainty is calculated in section 4.6. It is 5% for average Nusselt number and 3.5 - 8.0% for fraction factor and pressure drop; see Appendix C.

The comparison of average heat transfer coefficient of the dielectric liquid (HFE) and water is presented in Figure 4.32. The results show that the heat transfer coefficient of water is significantly higher than dielectric liquid (HFE), this is because the thermal conductivity and specific heat of water is higher by 10 and 4 times respectively. For example at Reynolds number 13000, the heat transfer coefficient is 6500 and 850 $W/m^2.K$ for water and dielectric liquid (HFE), respectively. Also it can be noticed that the heat transfer coefficient of water increases sharply with increasing Reynolds number compared to the dielectric liquid (HFE).

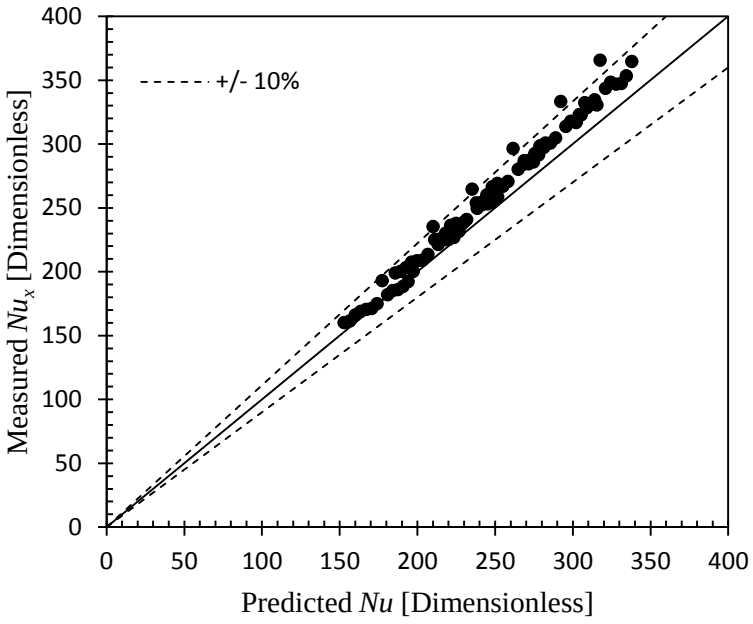

Figure 4.29: Comparison between the measured and the predicted (using Gnielinski's correlation) local Nusselt number of dielectric liquid (HFE)

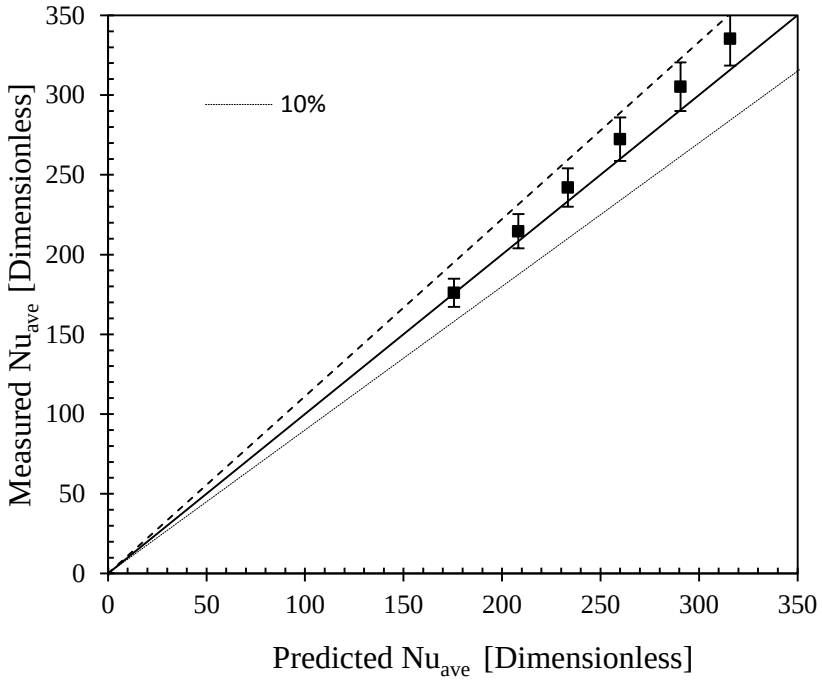

Figure 4.30: Comparison between the measured and the predicted (by Gnielinski's correlation) average Nusselt number of dielectric liquid (HFE)

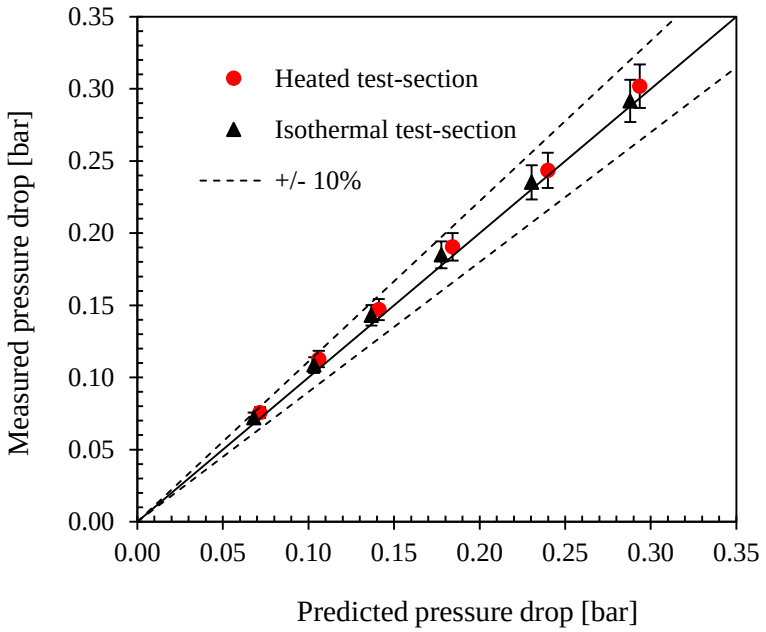

Figure 4.31: Dielectric liquid (HFE) pressure drop comparison-test the heated and isothermal test sections.

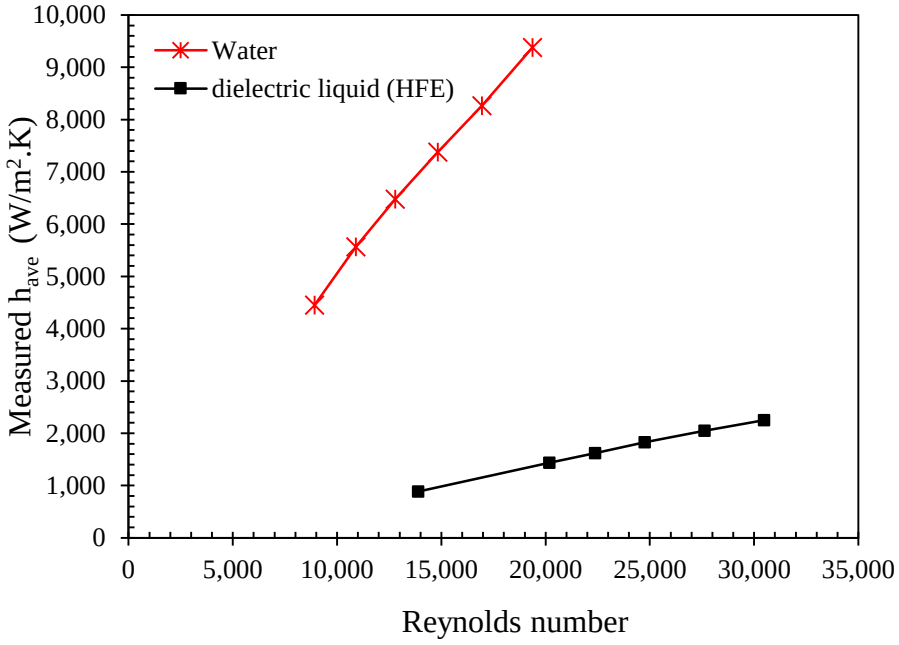

Figure 4.32: Comparison between the measured and average heat transfer coefficient of water and dielectric liquid (HFE)

4.6: Uncertainty of Experiment Results

In experimental work, in order to give a best estimate of the measured variables it is necessary to predict a percentage of error of the variables, which called the uncertainty. The experimental uncertainty inherent in the results occur due to the base errors, which come from the measuring devices accuracy, and random errors, which come from the variation of reading in the experimental results. The uncertainty of the variables in the measurement is calculated by the following equation [105].

$$u=\sqrt{B^2+R^2}$$

Where u is uncertainty, B is the base error and R is the random error.

The Nusselt number was calculated from the equation; $Nu=\frac{hD}{k}$, therefore the uncertainty of Nusselt number should be function of h , D and k uncertainties

$$\delta Nu=\sqrt{\left(\frac{\partial Nu}{\partial h}\delta h\right)^2+\left(\frac{\partial Nu}{\partial D}\delta D\right)^2+\left(\frac{\partial Nu}{\partial k}\delta k\right)^2}$$

Whereas the heat transfer coefficient is obtained by equation; $h=\frac{q}{A(T_{s,in}-T_{b,m})}$, the uncertainty should be :

$$\delta h=\sqrt{\left(\frac{\partial h}{\partial q}\delta q\right)^2+\left(\frac{\partial h}{\partial T_{s,in}}\delta T_{s,in}\right)^2+\left(\frac{\partial h}{\partial T_{b,m}}\delta T_{b,m}\right)^2}$$

Where q is heat source, A inside surface area of the test section, $T_{s,in}$ is inside surface test section temperature and $T_{b,m}$ is average bulk temperature along the test section. Whereas q is heat source and obtained from $q=IV$ or $q=\dot{m}C_p(T_{b,out}-T_{b,in})$, where I is test section pass current, V is test section different voltage both is (measured by digital clamp

meter). $\dot{m}$ is mass flow rate, C_p specific heat of fluid, $T_{b,in}$ and $T_{b,out}$ are inlet and outlet bulk temperature of the test section respectively (measured by thermocouples).

The uncertainty of heat source is calculated from $q=\dot{m}C_p(T_{b,out}-T_{b,in})$

$$\delta q=\sqrt{\left(\frac{\partial q}{\partial \dot{m}}\delta \dot{m}\right)^2+\left(\frac{\partial q}{\partial C_p}\delta C_p\right)^2+\left(\frac{\partial q}{\partial T_{b,out}}\delta T_{b,out}\right)^2+\left(\frac{\partial q}{\partial T_{b,in}}\delta T_{b,in}\right)^2}$$

The uncertainty of the inside surface area of the test section is calculated from: $A=\pi D_{in}L$ where D_{in} (m) test section diameter and L (m) test section length

$$\delta A=\sqrt{\left(\frac{\partial A}{\partial D_{in}}\delta D_{in}\right)^2+\left(\frac{\partial h}{\partial L}\delta L\right)^2}$$

The uncertainty of the mass flow rate is calculated from the equation $\dot{m}=\rho Q$; where ρ(kg/m^3) is fluid density and Q is flow rate (m^3/s) (measured by flow meter)

$$\delta \dot{m}=\sqrt{\left(\frac{\partial \dot{m}}{\partial \rho}\delta \rho\right)^2+\left(\frac{\partial \dot{m}}{\partial Q}\delta Q\right)^2}$$

With regard to the inside surface tube temperature could be obtained from the flowing equation [97].

$$T_{s,in}=T_{s,out}+\frac{q}{16k_{tube}V}(D_{out}^2-D_{in}^2)-\frac{q}{8k_{tube}V}D_{out}^2\ln\frac{D_{out}}{D_{in}}$$

then the uncertainty is :

$$\delta T_{s,in}=\sqrt{\begin{array}{l}\left(\frac{\partial T_{s,in}}{\partial T_{s,out}}\delta T_{s,out}\right)^2+\left(\frac{\partial T_{s,in}}{\partial q}\delta q\right)^2+\left(\frac{\partial T_{s,in}}{\partial k_{tube}}\delta k_{tube}\right)^2+\left(\frac{\partial T_{s,in}}{\partial V}\delta V\right)^2\\ +\left(\frac{\partial T_{s,in}}{\partial D_{out}}\delta T_{out}\right)^2+\left(\frac{\partial T_{s,in}}{\partial D_{in}}\delta D_{in}\right)^2\end{array}}$$

$T_{s,out}$ is outside surface test section temperature (measured by thermocouples) and k_{tube} is thermal conductivity of test section tube (which made of stainless steel)

$k_{tube}=0.0127T_{s,out}+13.23188$ where $T_{s,out}$ is in ˚C

The properties of water and nanofluid are taken at average bulk temperature $T_{b,m}$:

$$T_{b,m}=\frac{T_{b,in}+T_{b,out}}{2}$$

In order to calculate the uncertainty of pressure drop and friction factor a similar procedure are flow by using Eq. (4.15): $\Delta P=f\frac{L}{D}\left(\frac{\rho V^2}{2}\right)$

From the above, it was found that the uncertainties of Nusselt number, pressure drop and friction factor were ranging from 3 - 5%, 4 - 8%, and 3.5 - 8%, respectively, for the base fluid (water) and dielectric liquid (HFE); and for nanofluid was 3 – 8%, 3 - 11% and 4 – 11%, respectively (for more details see Appendix C, Tables A22 - A26). It should be mentioned that the uncertainty of the variables which were used in the calculation of the experiment results, i.e. Nusselt number, pressure drop and friction factor, were taken into account with the exception of the uncertainties of density and specific heat of the nanoparticles as well as nanofluid concentration were neglected.

4.7: Concluding Remarks

The aim of this study was to evaluate the heat transfer performance of common nanofluids: Al_2O_3-water, TiO_2-water and CuO-water nanofluids. The experiment was set up for forced convection to measure and evaluate the heat transfer performance and pressure drop of nanofluids within the turbulent regime. The results show that:

- The heat transfer rate increases with increasing flow rate of the base fluid and nanofluids. However, the heat transfer of the base fluid was better than all nanofluids considered at a specific flow rate under the experimental conditions. This means that using nanofluids at constant flow rate deteriorated the heat transfer rate compared to the base fluid and this deterioration increased with increasing nanoparticles load.
- Assessing the thermal performance of nanofluids by considering the Nusselt number and its variation with Reynolds number is misleading because both Nusselt number and Reynolds number depend on the nanofluid properties (i.e. thermal conductivity, density and viscosity that are function of the volume fraction). This can lead to a false impression that some nanofluids produce an improvement in heat transfer performance. In addition, using nanofluid will require additional pumping power to achieve the corresponding base fluid's Reynolds number.
- The pressure drop of nanofluids increased significantly with increasing flow rate and nanofluid concentration due to the nanofluid viscosity, which increased with increasing nanoparticle load.
- Nanofluids heat transfer performance is mostly dependent on the nanoparticles thermal conductivity.
- The heat transfer coefficient and pressure drop of nanofluids can be predicted very accurately using the existing conventional correlation of single phase correlations, if the properties of the nanofluid are used. This was also noted by [25, 26, 58].

From the above, There are no benefits to using nanofluids to increase the heat transfer performance, however if nanofluids are used as they also increase the fluid's viscosity their use will increase pumping losses and their practical application must be subject to economic evaluation to balance this trade off, this is discussed in Chapter 6.

CHAPTER 5: CFD ANALYSIS OF IMMERSED SERVER COOLING

5.1: Introduction

In a data centre it is important to remove the heat, which is generated mainly within the server by its processors and memory, and finding new ways to cool the servers efficiently to ensure the protection of its components and increase the performance and reliability of the entire data centre. This is one of the most important energy conservation measures that can be applied to a data centre. From the literature, there are several techniques for cooling data centre servers such as forced air cooling, liquid cooling and direct contact cooling (immersion cooling) [3, 78, 79]. In this study, the direct contact liquid cooling strategy is simulated based on Iceotope's design, and the possibility of enhancing the thermal performance using nanofluids is explored.

The direct contact liquid cooling technology is offered by a manufacturer of liquid cooling equipment, Iceotope [3]. The server is sealed in a bath of dielectric liquid (HFE) that submerges the server motherboard and the generated heat is removed by natural convection to a cooled wall of the server bath. This cooled wall maintains its temperature by circulated coolant water see Figure 1.9. In this study, it is attempted to analyse the thermal performance and the flow characteristics of the immersed server based on the Iceotope design but using nanofluids as a coolant.

It was found in the literature that using nanofluids instead of traditional cooling fluids boosts the heat transfer by increasing the thermal conductivity of the nanofluid compared to the base fluid. However, adding nanoparticles to the base fluid will also increase the viscosity, therefore, increasing the pressure drop, which will require higher pumping power. The heat transfer experiments performed in chapter 4 observed that at a given flow rate, the base fluid has a higher heat transfer coefficient than the nanofluids. However, at given Reynolds number, the nanofluids have higher Nusselt numbers. Therefore, by achieving a corresponding Reynolds number when using a nanofluid the

thermal performance may increase but it requires more pumping power than the base fluid. Therefore, the optimisation of the efficient heat transfer versus pumping power is important for the evaluation of the limitations of using nanofluids. An economic analysis is required to evaluate the use of nanofluids in real world applications and optimise the recommended nanoparticles concentration required.

The present problem is solved by using a CFD model based on the finite-element method. The details of the numerical solution procedure are given later in section 5.2. The numerical solution gives the temperature distribution through the server and the pressure drop of nanofluids circulated to cool the dielectric liquid. The temperature and pressure drop are predicted by the model and used as parameters when calculating the power consumption of the server, cooling system and pumping power with various nanofluid types and concentrations. This feeds into an economic analysis in order to determine the optimum concentration of nanoparticles for each type of nanofluid. The details of the economic analysis are described later in chapter 6.

The procedures of numerical analysis and economic analysis may be summarised in the diagram shown in Figure 5.1. The CFD model needs a geometric representation, reliably measured materials properties, accurate boundary conditions to estimate the flow and thermal characteristics accurately. The thermal and flow characteristics of the nanofluids with varying concentrations are fed into an economic analysis based on the present worth method in order to determine the most efficient nanofluid concentration.

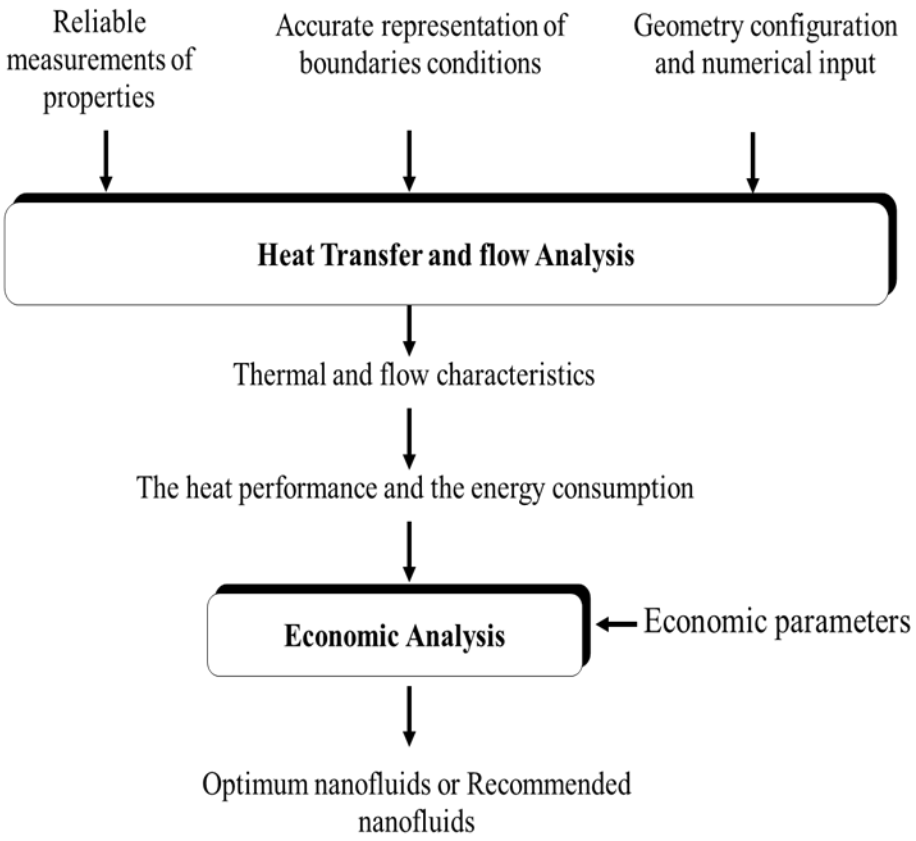

Figure 5.1: Diagram showing a procedure of numerical and economic analysis

5.2: Mathematical Model

This section describes the model used to calculate the thermal and flow characteristics of the data centre server using different nanofluids concentrations. Section 5.2.1 describes the server configuration properties investigated and summarizes the thermal properties of base fluid and nanofluids. The governing equations of the mathematical formulation are explained in Section 5.2.2.

5.2.1: Geometry and boundary conditions

The geometry of the server is based upon the Iecotope server design with dimensions 25 cm wide, 40 cm long, 3 cm high and includes two CPUs, in order to save computational time and memory, only half of the server with one CPU is investigated with a symmetrical condition imposed. Also in order to investigate the effect of the cooled plate configuration on the optimum nanofluid concentration, two configurations are investigated; one uses a half server with cooled plate comprising of two parallel tubes and the second models half server with cooled plate consisting of a serpentine tube. A schematic representation of two half servers based on the Iecotope server model with two different cooled plate configurations is presented in Figure 5.2 (a) and (b).

Figure 5.2 (a) presents the half server with cooled plate comprising two parallel tubes and Figure 5.2 (b) presents the half server with cooled plate having a serpentine tube. Both of them have one CPU (Since the CPU consumes the most power when the server is active [106]) and the same boundary conditions and model geometry. The two servers are composed of two parts; the first part is sealed enclosure filled with dielectric liquid (HFE) and containing the CPU (chip) which dissipates heat (q) via natural convection throughout the fluid region. The second part is a cooled plate, which cools the sealed enclosure by passing a chilled fluid (i.e. water or a nanofluid) at low inlet temperature (T_c). The server models are in vertical position and assumed to be insulated from the outside.

With regard to the fluids (nanofluid in the cooled plates and dielectric liquid (HFE) in the server enclosure), it is important to classify the fluid flows Reynolds number to determine whether the fluid within the tubes is laminar or turbulent for advection or Rayleigh number for natural convection at a certain critical value.

In the cooled plates it is assumed the flow is laminar because when the Reynolds number is determined the fluid velocity required to maintain the chip (CPU) at a safe operational temperature gives a Reynolds number less than 2300[97]; as calculated :

$$\mathrm{Re} = \frac{\rho VD}{\mu}$$

Where ρ and μ are density and dynamic viscosity of the fluid (water or nanofluids) respectively, V average fluid velocity and D is the diameter of the cooled plate tube.

Using the above equation and assuming that all of the chips (CPU) power consumption is dissipated as heat and the safe operational temperature of the chip (CPU) is limited to be less than 85 °C [107]. Therefore, in this study, the power consumption of the CPU should be 80W and the corresponding Reynolds number values to maintain the chip (CPU) at the safe operation temperature are calculated as 50 - 225 for cooled plate with two parallel tubes and 200 - 700 for cooled plate with serpentine tube.

With regards to the heat dissipation of the CPU, the dielectric liquid (HFE) in the enclosure should be turbulent flow as within the enclosure the corresponding Rayleigh number; $Ra = \frac{gL^3\beta\Delta T}{\alpha\nu}$ was calculated to be about 10^8 (the flow is turbulent flow if the $\mathrm{Ra} \geq 10^6$ [108]). Here is β, α and ν are thermal expansion coefficient, thermal diffusivity, kinematic viscosity of dielectric liquid (HFE) and g, L are gravity acceleration and characteristic length, respectively. ΔT is the difference between the cooled and high temperature of the enclosure.

The inlet temperature Tc is taken to be 15 °C, because this is the highest chilled water value that the chiller unit produces at 8 - 15 °C [109]. Since the nanofluids have lower Reynolds number compare to base fluid due to they have a relatively higher

viscosity, the mass flow rate ($\dot{m}$) in the cooled plate is changed to achieve a corresponding particular Reynolds number (Re) of the base fluid; based on the equation of Reynolds number $\dot{m} = \frac{\mathrm{Re}\,\mu A}{D}$ where A is the cross sectional area of the inlet tube.

The chip is assumed to be made of aluminium with thermal conductivity 160 W/m.K, and dimensions of 5.0 cm wide, 5.0 cm long, 0.5 cm high and it is located in the middle of the wall of the server opposite the cooling plate (see Figure 5.2). The heat sink fins of the chip are chosen as copper with thermal conductivity 400 W/m.K and its geometry, the base heat sink fins is 9.0 cm in width, 10 cm length and 0.6 cm in height. The fin is 0.2 cm in width, 10 cm length, 0.6 cm in height and the number of fins is 23. The server is assumed to be half of a server with one CPU with dimension is 12.5 cm in width, 40 cm length and 3 cm in height.

Both of the cooled plates are assumed to be aluminium rectangular plates in the top surface of server, with the same thermal characteristics as the chip, with dimensions 12.5 cm wide, 40 cm long and 1.5 cm high. It has circular tubes along the plate with diameter 1.0 cm that divides the cooled plate into equal parts to remove the heat from the server.

Thermal interfaces between the chip and heat sink fins, and the server and cooled plate are assumed to be in perfect contact and therefore, the interface thermal resistances are assumed negligible. This is of course an idealization and in practical applications, this assumption is often violated unless special measures are used.

With regards to the thermophysical properties of the fluids (i.e. the base fluid (water), nanofluids and dielectric liquid (HFE)), the properties of water and nanofluids used are explained in chapter 4, whereas the properties of dielectric liquid (HFE) is taken from the supplier [103, 104] and described in chapter 4, Table 4.2.

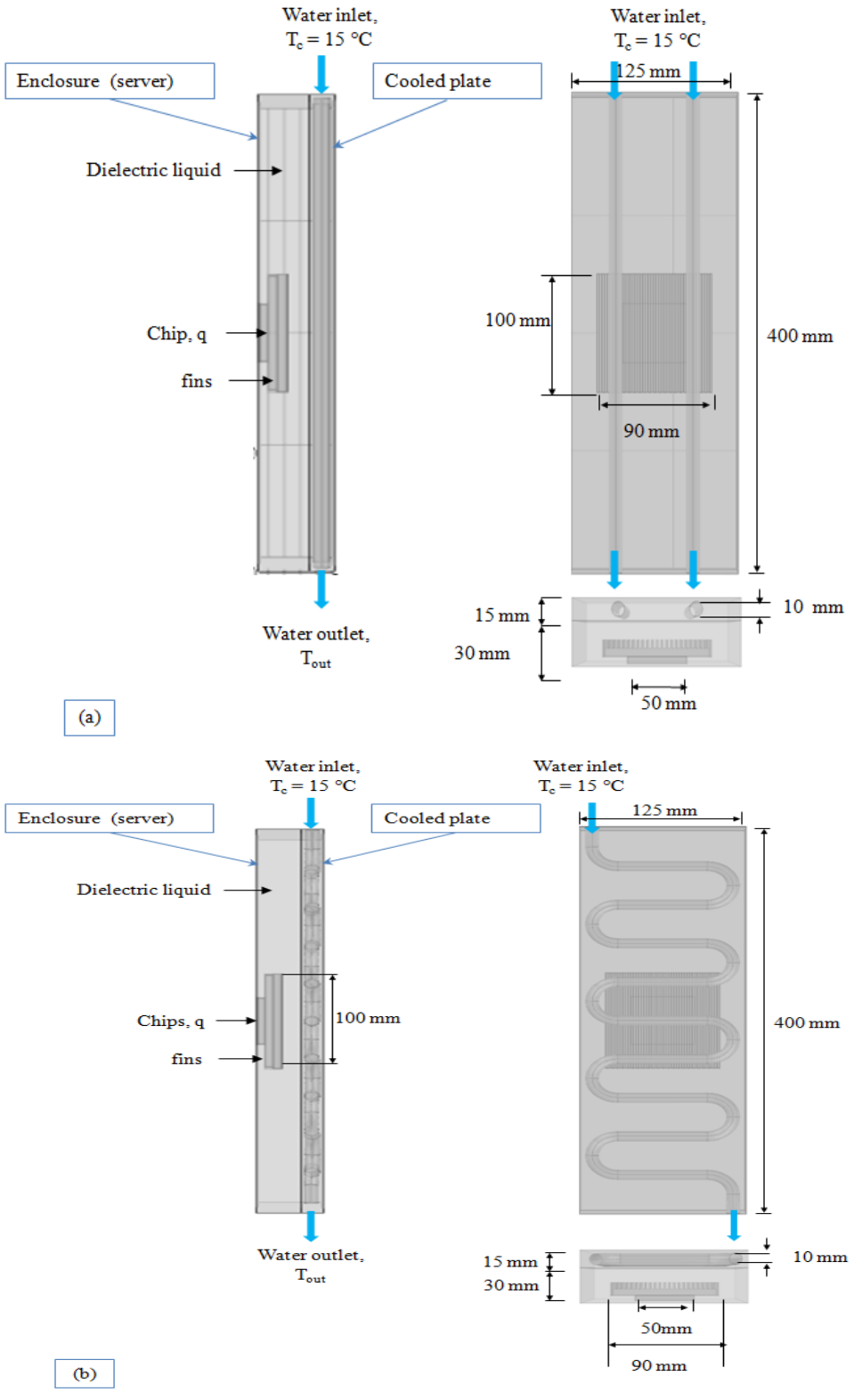

Figure 5.2: Schematic showing the physical model (server) geometry and boundary conditions (a) with cooled plate having two parallel tubes, (b) with cooled plate having serpentine tube benders

5.2.2: Mathematical formulation

The heat transfer process through a server involves both forced convection, from the cooled plates tube, and natural convection within the server enclosure model, which is filled with dielectric liquid (HFE). The flow and heat transfer are governed by solving the appropriate form of the conservation of mass, momentum (Navier –Stokes equation) and energy equations. These equations will be solved subject to initial and boundary conditions appropriate to the physical situation under consideration.

The mass conservation equation: $$\frac{\partial \rho}{\partial t} + \nabla \cdot (\rho V) = 0 \quad (5.1)$$

Momentum equation: $$\rho \frac{DV}{Dt} = -\nabla P + \nabla.(\mu \nabla V) + F \quad (5.2)$$

Energy equation : $$(\rho C_p)\left[\frac{\partial T}{\partial t} + V.\nabla T\right] = \nabla.(k \nabla T) + Q \quad (5.3)$$

Where ρ, μ, k, C_p are density, dynamic viscosity, thermal conductivity and specific heat of fluid (water or nanofluids); V and T are fluid velocity vector and temperature. Q and F are energy source and body force respectively.

5.2.2.1: Laminar flow

Laminar flow is when a fluid flows with smooth layers [110]. The fluid in the cooled plate tubes is laminar as the previous calculations regarding Reynolds number suggest. With regard to the nanofluids, it is assumed that there is no slip between the base fluid and nanoparticles and therefore, it is possible to consider the base fluid and nanoparticles as a homogenous nanofluid with new thermofluid characteristics. This indicates that the above equations can be used.

The flow and heat transfer equations in the cooled plate are formulated using the following basic assumptions:

i. Steady state conditions
ii. Incompressible flow

iii. no chemical reaction

iv. dilute mixture

v. negligible viscous dissipation

vi. negligible radiative heat transfer

vii. nanoparticles and base fluid are locally in thermal equilibrium

Based on the above assumptions, the general governing equation is reduced to the following form:

The mass conservation equation: $\nabla \cdot V = 0$ (5.4)

Momentum equation: $\rho(V.\nabla)V = \rho g - \nabla P + \nabla.(\mu \nabla V)$ (5.5)

Energy equation : $(\rho C_p)V.\nabla T = \nabla.(k \nabla T)$ (5.6)

5.2.2.2: Turbulent flow

In turbulent flow, the flow becomes random and fluctuating with eddies of varying length scales [110]. The fluid in the enclosure is moved due to buoyancy forces (natural convection) in turbulent regime regarding the Rayleigh number, as mentioned previously. The flow and heat transfer are governed by solving the governing equations and applying the Boussinesq approximation in the direction of gravity force. In order to estimate the turbulent flow, there are multiple potential models. This study uses the Reynolds Averaged Navier Stokes (RANS) equation which is the most common method used to solve turbulent flow in the CFD models [110]. This method considers the fluctuation of turbulence by the summation of average the variable of Navier –Stokes equation and its variation.

The mass conservation equation:

$$\nabla \cdot V = 0 \quad (5.7)$$

Momentum equation:

$$\rho(V.\nabla)V = -\nabla P + \nabla.(\mu \nabla V) + \nabla.\tau_{turbulent} + F \quad (5.8)$$

Energy equation :

$$V.\nabla T = \nabla\left(\frac{\nu}{\mathrm{Pr}} + \frac{\nu_t}{\mathrm{Pr}_t}\right)\nabla T + \frac{Q}{\rho C_p} \tag{5.9}$$

where Pr and ν are the Prandtl number and kinematic viscosity of the fluid respectively and the subscript t indicates their turbulent counterparts (i.e. the eddy viscosity). The additional term on the right side of Eq.(5.8) accounts for the turbulence fluctuations (the eddy viscosity). $\tau_{\text{turbulent}}$ is a tensor known as the specific Reynolds stress tensor.

In order to calculate the turbulent term, there are many turbulence models; the common used are the *k*-ε model, the *k*-ω model [110]. In this study, the K-ε turbulence model is used which was established by Launder and Spalding [111], to calculate the eddy viscosity. The k-ε model needs two extra equations to be solved simultaneously with equations of conservation of mass, momentum and energy; these are: turbulent kinetic energy, k and the turbulent dissipation rate, ε; as shown below:

Transport equation for the turbulent kinetic energy, k:

$$\rho\frac{\partial k}{\partial t} + \rho u.\nabla k = \nabla.\left[\left(\mu + \frac{\mu_T}{\sigma_k}\right)\nabla k\right] + p_k - \rho\varepsilon \tag{5.10}$$

Transport equation for the turbulent dissipation rate, ε:

$$\rho\frac{\partial \varepsilon}{\partial t} + \rho V.\nabla\varepsilon = \nabla.\left[\left(\mu + \frac{\mu_T}{\sigma_\varepsilon}\right)\nabla\varepsilon\right] + C_{e1}\frac{\varepsilon}{k}P_k - C_{e2}\rho\frac{\varepsilon^2}{k} \tag{5.11}$$

The production term can be obtained from

$$p_k = \mu_T\left[\nabla V : (\nabla V + (\nabla V)^T) - \frac{2}{3}(\nabla.V)^2\right] - \frac{2}{3}\rho k\nabla.V \tag{5.12}$$

The turbulent dynamic viscosity can be defined as

$$\mu_T = \rho C_\mu \frac{k^2}{\varepsilon}$$

Where, V is average velocity, V^T is average velocity transport, μ_T is turbulent viscosity, ρ density, σ_ε is Prandtl number of ε and σ_k is Prandtl number of k. The empirical turbulent model constant parameters:

$\sigma_k = 1$, $\sigma_e = 1.3$, $C_{e1} = 1.44$, $C_\mu = 0.09$ and $C_{e2} = 1.92$

5.2.2.3: Conjugate heat transfer

In the server model, there are heat transfers through the solids of the heat sink and through the cooled plate by conduction and from these solids to the surrounding fluids (dielectric liquid and nanofluid) by convection; this process is called conjugate heat transfer.

The heat transfer in a solid is dominated by conduction heat transfer :

$$\nabla . k_s \nabla T_s = 0 \tag{5.13}$$

The heat transfer in a fluid is dominated by convection heat transfer, represented by :

$$(\rho C_p) V . \nabla T_f = 0 \tag{5.14}$$

where T_s is the solid temperature and T_f is the fluid temperature on the wall between the solid and fluid and these temperature are the same at the wall. Therefore, the heat flux between the solid and fluid is given by Fourier's law:

$$k_s \nabla T_s = k_f \nabla T_f \tag{5.15}$$

5.3: Validation of CFD Model

Firstly, the validation of the CFD model COMSOL is presented by considering natural convection in an enclosure and forced convection in a channel. The flow and heat transfer are governed by solving the appropriate form of the conservation of mass, momentum (Navier –Stokes equation) and energy equations.

Dimensionless approach

For a given a simplicity with studying flow and heat transfer characteristics a dimensionless parameter should be investigated. There are two considerations of dimensionless approach related to the absence and presence of a reference velocity [112].

In the absence of a reference velocity, as with natural convection, the non-dimensional variables will be [112]:

$$X = \frac{x}{L}, \quad Y = \frac{y}{L}, \quad \tau = \frac{t\alpha_{bf}}{L^2}, \quad U = \frac{uL}{\alpha_{bf}}, \quad V = \frac{\mathrm{v}L}{\alpha_{bf}}, \quad P = \frac{pL^2}{\rho_{nf}\alpha_{bf}{}^2}, \quad \theta = \frac{T - T_c}{T_h - T_c}$$

Where α is thermal diffusivity and defined as: $k/(\rho C_p)$ where k is thermal conductivity, ρ is density and C_p is specific heat.

There are some assumptions, which describe the nanoparticles movement within the base fluid from the literature. All these assumptions consider the density to vary according to the Boussinesq approximation $\rho = \rho_0(1 - \beta\Delta T)$ and this variation appears in the body force term.

Under these scaling, the dimensionless governing equations are:

Continuity equation:
$$\frac{\partial U}{\partial X} + \frac{\partial V}{\partial Y} = 0 \tag{5.16}$$

Momentum equation x-direction

$$\left(\frac{\partial U}{\partial \tau}+U\frac{\partial U}{\partial X}+V\frac{\partial U}{\partial Y}\right)=-\frac{\partial P}{\partial X}+\frac{\mu_{nf}}{\rho_{nf}\alpha_{bf}}\left(\frac{\partial^2 U}{\partial X^2}+\frac{\partial^2 U}{\partial Y^2}\right) \tag{5.17}$$

Momentum equation y-direction

$$\left(\frac{\partial V}{\partial \tau}+U\frac{\partial V}{\partial X}+V\frac{\partial V}{\partial Y}\right)=-\frac{\partial P}{\partial Y}+\frac{\mu_{nf}}{\rho_{nf}\alpha_{bf}}\left(\frac{\partial^2 V}{\partial X^2}+\frac{\partial^2 V}{\partial Y^2}\right)^2+\frac{\rho_{nf}\beta_{nf}}{\rho_{nf}\beta_{bf}}Ra\,\mathrm{Pr}\,\theta \tag{5.18}$$

Energy equation

$$\frac{\partial \theta}{\partial \tau}+U\frac{\partial \theta}{\partial X}+V\frac{\partial \theta}{\partial Y}=\frac{\alpha_{nf}}{\alpha_{bf}}\left(\frac{\partial^2 \theta}{\partial X^2}+\frac{\partial^2 \theta}{\partial Y^2}\right) \tag{5.19}$$

Where Rayleigh number (Ra) and Prandtl number (Pr) are defined:

$$Ra=\frac{L^3 g\beta_{bf}(T_h-T_c)}{\alpha_{bf}\nu_{bf}} \text{ and } \quad \mathrm{Pr}=\frac{\nu_{bf}}{\alpha_{bf}}$$

In the presence of a reference of velocity (u_{in}), as in forced convection, the non-dimensional variable will be [112]:

$$X=\frac{x}{L},\ Y=\frac{y}{L},\ \tau=\frac{tu_{in}}{L},U=\frac{u}{u_{in}},\ V=\frac{\mathrm{v}}{u_{in}},P=\frac{p}{\rho_{nf}u_{in}^2},\theta=\frac{T-T_c}{\Delta T} \text{ where } \Delta T=T_h-T_c$$

Under these scaling, the dimensionless governing equations are:

Continuity equation: $$\frac{\partial U}{\partial X}+\frac{\partial V}{\partial Y}=0 \tag{5.20}$$

Momentum equation x-direction:

$$\left(\frac{\partial U}{\partial \tau}+U\frac{\partial U}{\partial X}+V\frac{\partial U}{\partial Y}\right)=-\frac{\partial P}{\partial X}+\frac{\mu_{nf}}{\rho_{nf}\nu_{bf}}\frac{1}{\mathrm{Re}}\left(\frac{\partial^2 U}{\partial X^2}+\frac{\partial^2 V}{\partial Y^2}\right) \tag{5.21}$$

Momentum equation y-direction:

$$\left(\frac{\partial V}{\partial \tau}+U\frac{\partial V}{\partial X}+V\frac{\partial V}{\partial Y}\right)=-\frac{\partial P}{\partial X}+\frac{\mu_{nf}}{\rho_{nf}\nu_{bf}}\frac{1}{\mathrm{Re}}\left(\frac{\partial^2 V}{\partial X^2}+\frac{\partial^2 V}{\partial Y^2}\right) \tag{5.22}$$

Energy equation:

$$\frac{\partial \theta}{\partial \tau}+U\frac{\partial \theta}{\partial X}+V\frac{\partial \theta}{\partial Y}=\frac{\alpha_{nf}}{\alpha_{bf}}\frac{1}{\mathrm{Re}\,\mathrm{Pr}}\left(\frac{\partial^2 \theta}{\partial X^2}+\frac{\partial^2 \theta}{\partial Y^2}\right) \tag{5.23}$$

Where Re is Reynolds number $\mathrm{Re}=\frac{u_{in}L}{\nu_{bf}}$ and Pr is Prandtl number $\mathrm{Pr}=\frac{\nu_{bf}}{\alpha_{bf}}$

where u_{in} is the reference of velocity of the flow, ν is kinematic viscosity $\nu_{bf}=\frac{\mu_{bf}}{\rho_{bf}}$ and

α is thermal diffusivity $\alpha=\frac{k}{\rho C_p}$

The Nusselt number

The expression of local Nusselt number is $Nu=\frac{hL}{k}$. If the fluid is between two walls one is heated at constant temperature T_h and another is cooled at temperature T_c, therefore:

$$q''=h(T_h-T_c)=-k\left(\frac{\partial T}{\partial y}\right)_{y=0}\Rightarrow h=\frac{-k(\partial T/\partial y)_{y=0}}{T_h-T_c}$$

The Nusselt number become $Nu=\frac{q''L}{k(T_h-T_c)}$ or $Nu=\frac{-(\partial T/\partial y)_{y=0}L}{T_h-T_c}$

From dimensionless definition of $\theta=\frac{T-T_c}{T_h-T_c}$ then $\frac{\partial \theta}{\partial Y}=\frac{-(\partial T/\partial y)L}{T_h-T_c}$

Then the local Nusselt number $Nu=\frac{-(\partial T/\partial y)_{y=0}L}{T_h-T_c}=\left(\frac{\partial \theta}{\partial Y}\right)_{Y=0}$

The average Nusselt number for characteristic length (L) will be: $Nu_{ave} = \frac{1}{L}\int_0^L \left(\frac{\partial \theta}{\partial Y}\right)_{Y=0} dx$

Case Study 1:

In the present case study, the accuracy of the COMSOL programme is validated by comparisons with previous literature. The validation is carried out by using the natural convection for air (Davis's results [113]) and water (Lai and Yang [114]) with Prandtl number 0.71 and 7.02, respectively; in two dimensional square enclosure heated and cooled from the sidewalls and the top and the bottom walls are insulated (as shown on Figure 5.3).

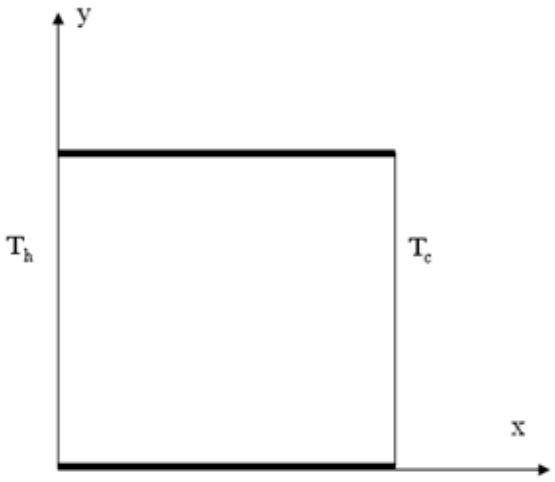

Figure 5.3: Schematic representation of the physical model of square enclosure and coordinates [113].

The effect of the number of elements on results is investigated by comparison the average Nusselt number with Davis's results [113] ,and the results are shown in Table 5.2. It is clearly seen that the results of average Nusselt number are grid independent for all element number.

The comparison observes that the CFD program (COMSOL) gives a good agreement results. Table 5.3 and Table 5.4 summarize the results of the average Nusselt

number showing comparisons between the present study and literatures for air and water and respectively.

Table 5.1: the effect of element numbers on average Nusselt number for different Rayleigh number

	Average Nusselt number					
	(Davis) [113]	Number of elements				
Ra		2554	2800	3908	8240	24912
1×10^3	1.118	1.114	1.115	1.117	1.117	1.118
1×10^4	2.243	2.231	2.232	2.239	2.2413	2.244
1×10^5	4.519	4.471	4.478	4.499	4.50661	4.519
1×10^6	8.799	8.653	8.681	8.743	8.7663	8.807

Table 5.2: comparison with average Nusselt number of Air for validation

Ra	Nu_{ave} present	Nu_{ave} (Davis [113])
1×10^3	1.1171	1.118
1×10^4	2.241	2.243
1×10^5	4.507	4.519
1×10^6	8.766	8.799

Table 5.3: comparison with average Nusselt number of water for validation

Ra	Nu_{ave} present	Nu_{ave} Lai and Yang[114]
1×10^3	1.117	1.128
1×10^4	2.270	2.286
1×10^5	4.703	4.729
1×10^6	9.160	9.173

Case study 2

This case presents and validates the results obtained for forced convection within a horizontal channel completely heated and partially heated at a constant temperature (see Figure 5.4 and Figure 5.5) by using a Cu-water nanofluid (see Table 5.5 for nanoparticle properties) at inlet temperature T_c. It demonstrates the effects of different volume fractions of nanoparticles with various Reynolds number on thermal characteristics. The comparison of average Nusselt number with the literature is given in Table 5.6 and Table 5.7 for completely heated channel and partially heated channel, respectively. The thermophysical properties of the nanofluid are assumed to be constant. The results of COMSOL model also show a good agreement with the literature. In addition, the detail of isotherm contours for the both channels with various Reynolds number and concentrations are shown the same behaviour, as shown in Figure 5.6 and Figure 5.7,

Table 5.4: showing materials thermal properties used.

Nanoparticle type	Density (ρ_p) (kg/m^3)	Thermal conductivity (k_p) (W/m.K)	Specific heat capacity ($C_{p,p}$) (J/kg.K)	Nanoparticle size (nm)
Water	1000	0.6	4182	-
Al_2O_3[26]	3900	42	880	50
CuO [99]	6310	18	549	30
TiO_2[55]	4170	11.8	711	45
Cu[71]	8954	386	383	100

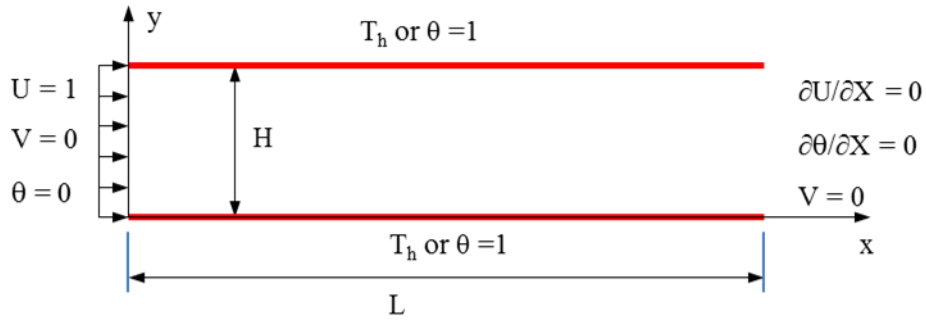

Figure 5.4: Schematic representation of the physical model for heated channel and coordinates [71].

.

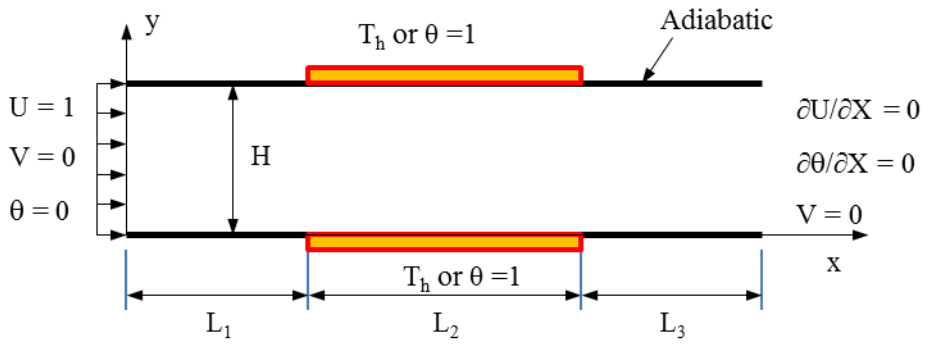

Figure 5.5: Schematic representation of the physical model for partially heated channel and coordinates [72].

Table 5.5: average Nusselt number for various Reynolds number (Re) and volume fraction; showing comparison with Santra et al. [71].

Volume friction	Nu_{ave} of present work		Nu_{ave} of Santra et al.[71]	
	R=500	R=1500	Re =500	Re =1500
0%	4.59	7.09	4.7	7.0
1%	4.88	7.54	4.9	7.5
2%	5.17	7.98	5.2	8.0
3%	5.45	8.42	5.5	8.3
4%	5.73	8.85	5.7	8.8
5%	6.00	9.28	6.1	9.2

Table 5.6: average Nusselt number at various Re and volume fraction; showing comparison with Raisi et al. [72].

Volume friction	Nu_{ave} Present work			Nu_{ave} Raisi et al.[72]		
	R =10	Re =100	Re =500	Re =10	Re =100	Re =500
0%	0.7547	3.4118	6.2309	0.769	3.410	6.055
1%	0.7548	3.6274	6.6303	0.770	3.627	6.465
2%	0.7541	3.8351	7.0227	0.770	3.836	6.868
3%	0.7528	4.0351	7.4097	0.770	4.038	7.267
4%	0.7513	4.2276	7.7923	0.769	4.233	7.661
5%	0.7495	4.4125	8.1715	0.768	4.419	8.051

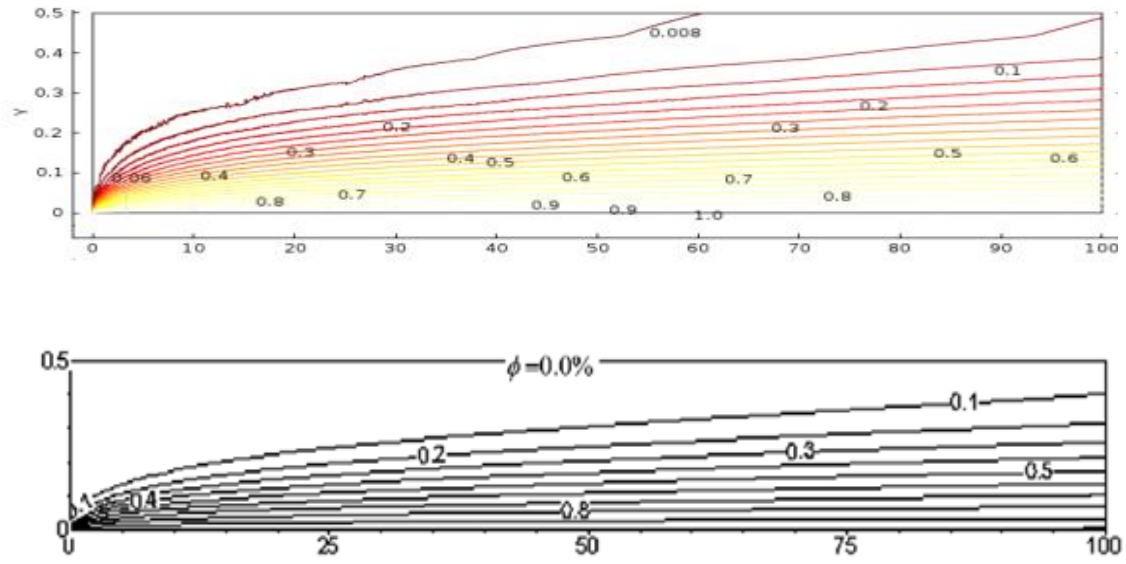

(a)

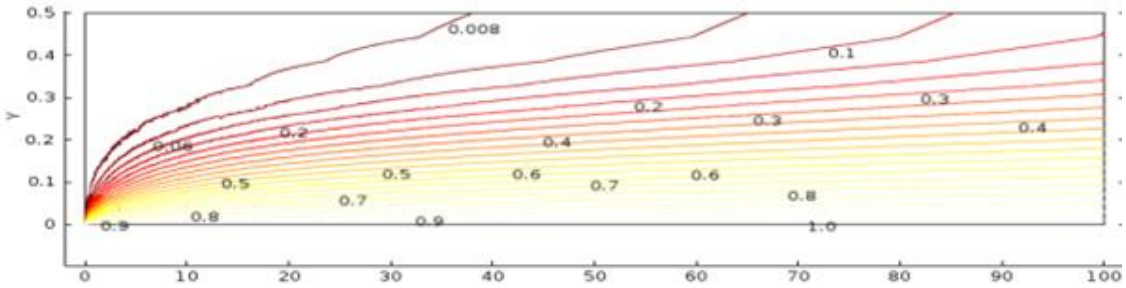

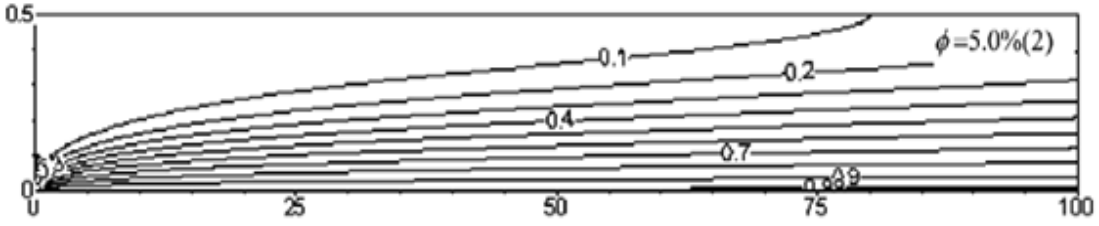

(b)

Figure 5.6: Isotherm contour for Re = 500 comparing with (Santra et al.[71]) ; (a) ϕ = 0% and, (b) ϕ = 5%

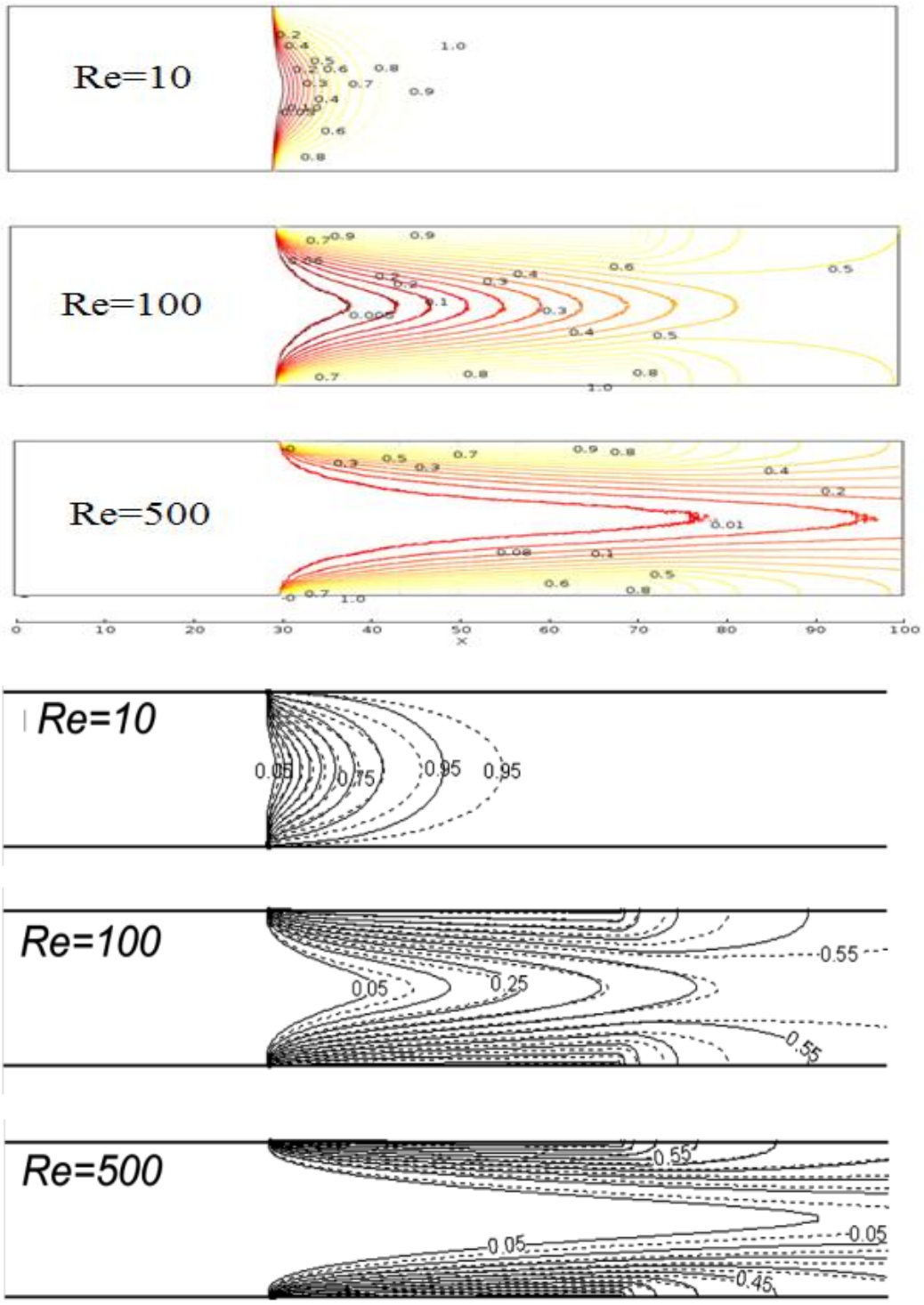

Figure 5.7: Isotherm contour for Re = 10, 100 and 500 comparing with (Raisi et al.[72]) soled line; for ϕ = 3%.

5.4: The Effect of Considering the nanofluid as homogeneous material model and dispersion model on Heat Transfer

Nanofluids consist of a base fluid and nanoparticles; therefore, there are two considerations when modelling nanofluids to describe the nanoparticles in the base fluid. One is the homogeneous model, which considers the nanofluid as a pure material; thus, the base fluid and nanoparticles are dispersed very well and maintained in thermal equilibrium. The second is the dispersion model, which considers the nanofluid as a dilute liquid and allows nanoparticles to move within the base fluid. Therefore, the modelling of heat convection of nanofluid might be considered into two methods; the homogeneous model and the dispersion model [115].

This section attempts to analyse the thermal and flow characteristics of a nanofluid under laminar flow for constant wall temperature (T_h) as shown in Figure 5.4, by considering nanofluids as a homogeneous material model or a dispersion model.

- **Homogeneous model**

This approach treats the nanofluids as pure fluid with new thermal properties and applies the conservation equations (5.1), (5.2), and (5.3).

- **Dispersion model**

This approach treats the nanofluid as mixture or dilute liquid and the enhancement of heat transfer comes from the higher thermal conductivity of the nanoparticles and the dispersion of nanoparticles inside fluid. It is worth mentioning that the heat transfer coefficient is proportional to thermal conductivity. However, the enhancement in the heat transfer is much higher than the enhancement of thermal conductivity by adding nanoparticles [116]. This enhancement might be attributed to movement of nanoparticles in the base fluid. The dispersion of nanoparticles into base fluid due to particle-particle interaction and particle surface interaction which depend on particle size, particle movement, particle concentration, fluid velocity and fluid temperature [11]. Buongiorno [115] summarized the possibility of nanoparticles dispersion in fluid during convection

in the absence of turbulent flow: Inertia, Brownian diffusion, thermophoresis, diffusionphoresis, Magnus effect, fluid drainage, and gravity. It was also observed that only Brownian and thermophoresis diffusion attribute to dispersion of nanoparticles in fluid.

In general, the expression of mass conservation in system is [117]:

$$\frac{\partial}{\partial t}\int_{CV}\rho d\,\forall + \int_{CS}(\rho V + j_p).d\mathrm{A} = 0$$

where $\forall$ and A are control volume and surface respectively. But nanofluid consists of liquid and nanoparticles, therefore:

Mass conservation of liquid:

Mass conservation of liquid is $$\frac{\partial}{\partial t}\int_{CV}(1-\phi)\rho_{bf} d\,\forall + \int_{CS}\rho V.d\mathrm{A} = 0$$

But the volume fraction of nanoparticles is so small compared to the liquid and therefore can be neglected, so the equation becomes:

$$\frac{\partial \rho}{\partial t} + \nabla\cdot(\rho V) = 0$$

Mass conservation of nanoparticles:

The continuity equation for each type of nanoparticles present in the fluid is given by following [117].

$$\frac{\partial}{\partial t}\int_{CV}\phi\rho_p d\,\forall + \int_{CS}(\phi\rho V + j_p).d\mathrm{A} = 0$$

$$\frac{\partial \phi\rho_p}{\partial t} + \nabla\cdot(\phi\rho_p V) + \nabla.j_p = 0$$

But Brownian diffusion and thermophoresis are responsible for the diffusion, therefore:

$$j_p = j_B + j_T$$

Where j_B and j_T are the mass flux of nanoparticles due to Brownian and thermophresis diffusion respectively.

$$\frac{\partial \phi}{\partial t} + \nabla \cdot (\phi V) = -\frac{1}{\rho_p} \nabla .(j_{\mathbf{B}} + j_T)$$

Brownian diffusion (j_B)

It is defined as the movement of nanoparticles within the liquid due to collision between the nanoparticles and the molecules of the base fluid [115]. It could be evaluated by:

$$j_{\mathbf{B}} = -\rho_p D_B \nabla \phi \text{ where } \quad D_{\mathbf{B}} = \frac{\kappa_B}{3\pi \mu d_p} T$$

Where D_B, ρ_p, μ, are Brownian diffusion coefficient, nanoparticle density, dynamic viscosity of fluid; κ_B Boltzmann constant and T is temperature reference.

Thermophoresis (j_T)

It is defined as the migration of a colloidal particle in a solution due to a temperature gradient [118]. It could be calculated from:

$$j_T = -\rho_p D_T \frac{\nabla T}{T} \text{ where } D_T = \beta \frac{\mu}{\rho} \phi \text{ and } \quad \beta = 0.26 \frac{k_f}{2k_f + k_p}$$

Where D_T is thermal diffusion coefficient; ρ_p and k_p are nanoparticle density and thermal conductivity; μ and k_f are fluid dynamic viscosity and thermal conductivity; β thermophoretic coefficient and T is temperature reference.

Mass diffusions due to Brownian diffusion (j_B) and thermophresis (j_T) will be:

$$j_p = j_B + j_T = -\rho_p D_B \nabla \phi - \rho_p D_T \frac{\nabla T}{T}$$

and the mass diffusion of nanoparticles in nanofluid will be:

$$\frac{\partial \phi}{\partial t} + \nabla \cdot (\phi V) = \frac{1}{\rho_p} \nabla . \left(\rho_p D_B \nabla \phi + \rho_p D_T \frac{\nabla T}{T} \right)$$

$$\frac{\partial \phi}{\partial t} + \nabla \cdot (\phi V) = \nabla . \left(D_B \nabla \phi + D_T \frac{\nabla T}{T} \right) \tag{5.24}$$

Therefore, the expression of energy equation and mass diffusion for nanofluid will be:

$$(\rho C_p)_{nf}\left[\frac{\partial T}{\partial t}+V.\nabla T\right]=\nabla.(k_{nf}\nabla T)-j_p C_p \nabla T$$

$$(\rho C_p)_{nf}\left[\frac{\partial T}{\partial t}+V.\nabla T\right]=\nabla.(k_{nf}\nabla T)+(\rho_p C_p)_p\left[D_B \nabla\phi.\nabla T+D_T\frac{\nabla T.\nabla T}{T}\right] \qquad (5.25)$$

The dimensionless approach of the energy equation and the mass diffusion will be:

In the absence of a reference velocity, as in natural convection, the Non-dimensional equation using same scales as before will be [112]:

- Energy equation

$$\frac{\partial\theta}{\partial\tau}+U\frac{\partial\theta}{\partial X}+V\frac{\partial\theta}{\partial Y}=\frac{\alpha_{nf}}{\alpha_{bf}}\left(\frac{\partial^2\theta}{\partial X^2}+\frac{\partial^2\theta}{\partial Y^2}\right)+\frac{(\rho C_p)_p}{(\rho C_p)_{nf}\alpha_{bf}}\left[D_B\left(\frac{\partial\phi}{\partial X}\frac{\partial\theta}{\partial X}+\frac{\partial\phi}{\partial Y}\frac{\partial\theta}{\partial Y}\right)+D_T\frac{\left(\frac{\partial\phi}{\partial X}+\frac{\partial\theta}{\partial Y}\right)^2}{\theta_c}\right] \qquad (5.26)$$

Where $\theta_c=\dfrac{T_c}{T_h-T_c}$

- Mass diffusion equation of nanoparticles:

$$\frac{\partial\phi}{\partial\tau}+U\frac{\partial\phi}{\partial X}+V\frac{\partial\phi}{\partial Y}=\frac{D_B}{\alpha_{bf}}\left(\frac{\partial^2\phi}{\partial X^2}+\frac{\partial^2\phi}{\partial Y^2}\right)+\frac{D_T(T_h-T_c)}{\alpha_{bf}T_c}\left(\frac{\partial^2\theta}{\partial X^2}+\frac{\partial^2\theta}{\partial Y^2}\right) \qquad (5.27)$$

In the presence of a reference of velocity, like force convection, the Non-dimensional equations using same scales as before will be [112]:

Energy equation:

$$\frac{\partial\theta}{\partial\tau}+U\frac{\partial\theta}{\partial X}+V\frac{\partial\theta}{\partial Y}=\frac{\alpha_{nf}}{\alpha_{bf}}\frac{1}{\mathrm{Re}\,\mathrm{Pr}}\left(\frac{\partial^2\theta}{\partial X^2}+\frac{\partial^2\theta}{\partial Y^2}\right)+\frac{(\rho C_p)_p}{\mathrm{Re}\,\nu_{bf}(\rho C_p)_{nf}}\left[D_B\left(\frac{\partial\phi}{\partial X}\frac{d\theta}{\partial X}+\frac{\partial\phi}{\partial Y}\frac{\partial\theta}{\partial Y}\right)+D_T\frac{\left(\frac{\partial\phi}{\partial X}+\frac{\partial\theta}{\partial Y}\right)^2}{\theta_c}\right] \qquad (5.28)$$

Mass diffusion of nanoparticles:

$$\frac{\partial \phi}{\partial \tau} + U\frac{\partial \phi}{\partial X} + V\frac{\partial \phi}{\partial Y} = \frac{D_B}{\mathrm{Re}\,\nu_{bf}}\left(\frac{\partial^2 \phi}{\partial X^2} + \frac{\partial^2 \phi}{\partial Y^2}\right) + \frac{D_T(\Delta T)}{\mathrm{Re}\,\nu_{bf} T_c}\left(\frac{\partial^2 \theta}{\partial X^2} + \frac{\partial^2 \theta}{\partial Y^2}\right) \tag{5.29}$$

Case study 3

This case presents the results obtained for forced convection in a horizontal channel heated completely at constant temperature T_h (see Figure 5.4) and cooled by flow Al_2O_3-water nanofluids (see Table 5.5 for nanoparticle properties) at inlet temperature (T_c = 20 °C) showing the effects of nanoparticles using homogeneous model and dispersion model on thermal characteristic at different volume fraction of nanoparticles with various Reynolds number on thermal characteristics. The thermophysical properties of the nanofluid are assumed to be constant.

Figures 5.6 and 5.7 illustrate the average Nusselt number using a homogenous model and a dispersion model for Al_2O_3-water nanofluids at various temperature differences (T_h - T_c) 10 and 70 °C respectively, for varying Reynolds number with different volume fraction. In general, it is clearly seen that the average Nusselt number increase monotonically with increasing Reynolds numbers and volume fractions. From Figures 5.8 and 5.9, it is observed that the average Nusselt number of dispersion model and homogeneous model is similar. Specifically, there is an enhancement in heat transfer for dispersion model but it is a very small because of the Brownian and thermophresis coefficient having very small values about (1×10^{-10}). For example, under the study considerations the maximum enhancement of dispersion model Nusselt number to homogeneous model are 0.1% and 0.25% for Al_2O_3-water nanofluids at temperature differences 10 and 70 respectively, at Re = 2000 and volume fraction 5.0%. It is also mentioned by MacDevette at el. [96] that the effects of Brownian motion and thermophoresis are negligible. Therefore, in this thesis it is considered that the nanofluid behaves as a homogenous liquid.

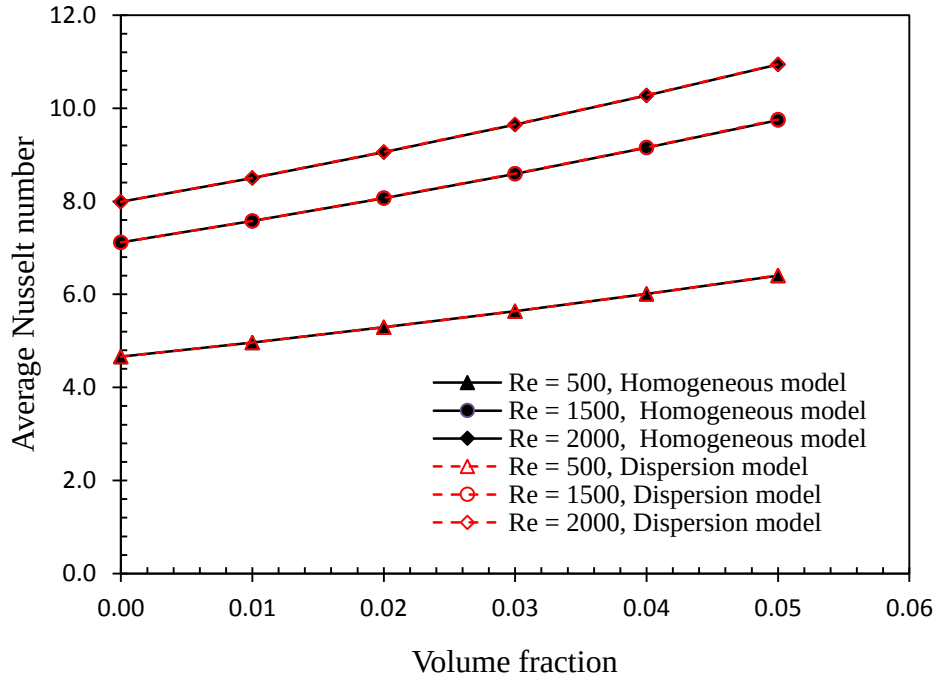

Figure 5.8: Average Nusselt number for various Reynolds number (Re) and volume fraction for Al_2O_3-water nanofluid; showing comparison the homogeneous model and dispersion model results at temperature difference (T_h - T_c = 10)

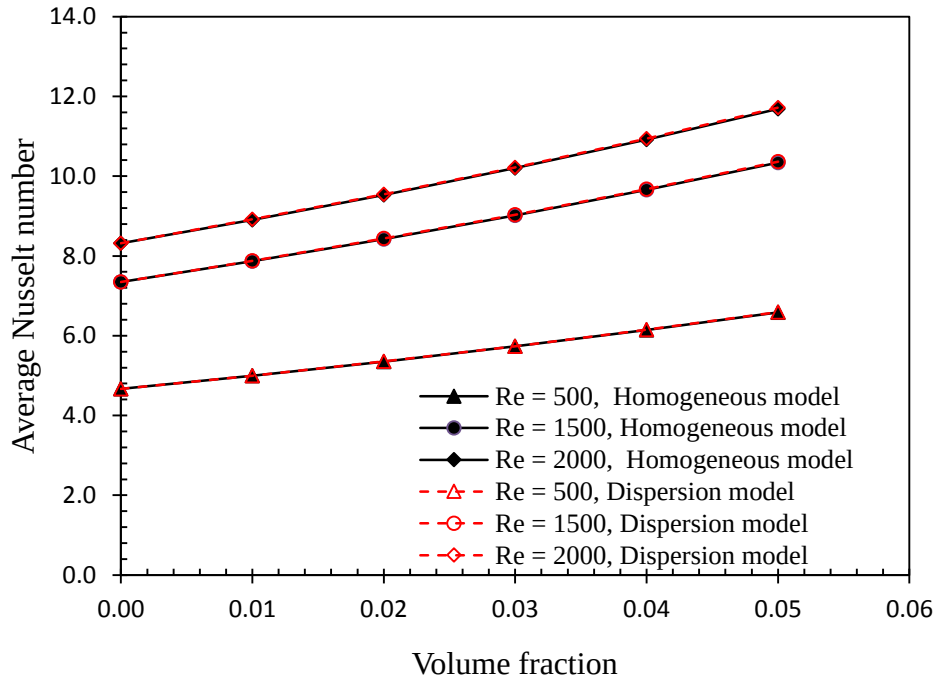

Figure 5.9: Average Nusselt number for various Reynolds number (Re) and volume fraction of Al_2O_3-water nanofluid; showing comparison the homogeneous model and dispersion model results at temperature difference (T_h - T_c = 70)

5.5: The Immersion Server Result and Discussion

This section presents and discusses the thermal and flow characteristics of the server models under consideration by using different nanofluid types and concentrations at varying Reynolds number. The characteristics such as the average top surface temperature of the chip and the cooled plate pressure drop of the half server with cooled plate having two parallel tubes and the half server with cooled plate having serpentine tube are calculated and presented in sections 5.5.1 and section 5.5.2 respectively. These results will be used in an economic analysis in chapter 6.

According to calculation of the Reynolds numbers of the flow through the cooled plate having two parallel tubes and serpentine tube, the Reynolds number for the cooled plate with two parallel tubes is between 50 and 300; whereas the cooled plate having a serpentine tube requires a higher pressure drop when compared to the cooled plate having two parallel tubes. Therefore, the Reynolds number should be higher and it is calculated that Reynolds number should be between 200 and 700. It is interesting to mention that the parallel flow when the inlet flow is from the top to the bottom of the server's cooled plate gives better thermal performance than the counter flow when the inlet flow is opposite direction under the consideration of this study. Therefore, the server with parallel flow rate is considered in this study.

The effect of the number of elements on results is investigated by comparing the average chip surface temperature and cooled plate pressure drop for water at Reynolds number (Re = 100). The results are shown in Table 5.7 and it can clearly be seen that the results are grid independent for all element numbers.

Table 5.7: The effect of element numbers on average chip temperature and cooled plate pressure drop for water at Re = 200.

Numbers of element	Temperature (°C)	Pressure drop (Pa)
692207	83.7	1.96
1677338	82.5	1.83
1952951	81.9	1.89
2553442	81.80	1.88

5.5.1: Half server with cooled plate having two parallel tubes

After validation and mesh sensitivity tests, the average temperature of the top chip surface and pressure drop of the cooled plate of the half server with cooled plate having two parallel tubes are summarised in Figure 5.10 – 5.12 for all nanofluids. Each figure gives the results for Reynolds numbers (Re = 50 – 300) and various volume fractions for a given type of nanofluid. Figure 5.10 summarises the results for Al_2O_3-water nanofluids using a cooled plate with two parallel tubes configuration. The results of temperature are presented in terms of (°C). It is clearly seen that the chip temperature decreases monotonically with increasing Reynolds number and volume fractions. In general, the decrease in the temperature is linear with increasing volume fraction for a particular Reynolds number and it is relatively large and then becomes smaller with a further increase in Reynolds number. Therefore, the temperature difference for a low concentration and a high concentration of a particular Reynolds number decreases with increasing Reynolds number for example the temperature difference are about 3°C and 1.5 °C for Re = 50 and 300 respectively. The same behaviour repeats itself for all others nanofluids studied, as presented in Figure 5.11 and Figure 5.12 for TiO_2-water and CuO-water nanofluids respectively. This feature of reducing the chip temperature is favourable with regard to reliability and reducing the energy consumption of the chip [7, 119-121].

In contrast to the chip temperature, the pressure drop of the cooled plate with two parallel tubes gives an opposite overall behaviour as presented in Figure 5.13- 5.15 for Al_2O_3-water, TiO_2-water and CuO-water nanofluids, respectively. It can be seen that the pressure drop increases monotonically with increasing Reynolds number and volume fraction. In general, the increase in pressure drop is relatively large with increasing nanofluid volume fraction for particular Reynolds number. For example, for Reynolds numbers the pressure drop of Al_2O_3-water nanofluid increases about 25% and 700% with respect to the base fluid for the volume fractions 0.5 and 4 vol.%, respectively. It is also noted that the pressure drop of Al_2O_3-water nanofluids are higher than TiO_2-water and CuO-water nanofluids; this is due to the Al_2O_3-water nanofluids having a higher viscosity (see chapter 3). The consequence of having relatively higher pressure drop with increasing

the volume fraction is unfavourable with regard to increasing the pump energy consumption.

It is interesting to note that Al_2O_3-water nanofluids give lower average chip temperature when compared to the other nanofluids due to their higher thermal conductivity. However, Al_2O_3-water nanofluids have higher pressure drop at cooled plate resulted from having higher viscosity compared to others nanofluids.

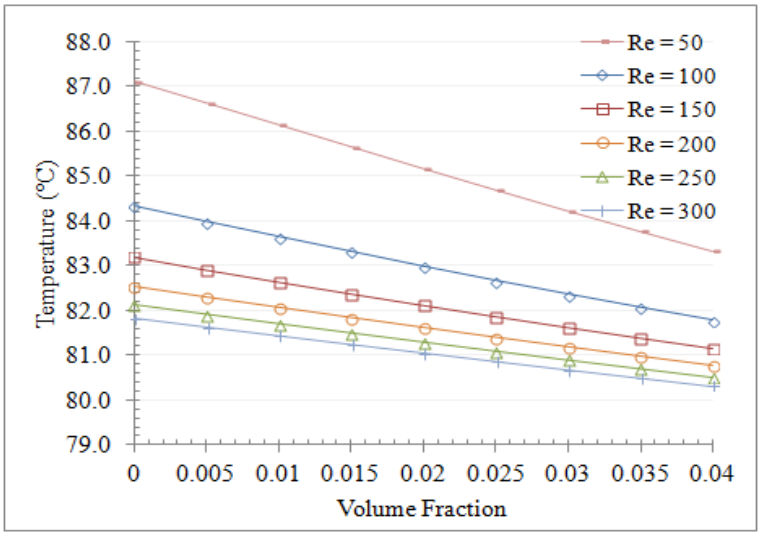

Figure 5.10: Chip temperature of server with cooled plate having two parallel tubes; using Al_2O_3-water nanofluids with various volume fractions and Reynolds numbers

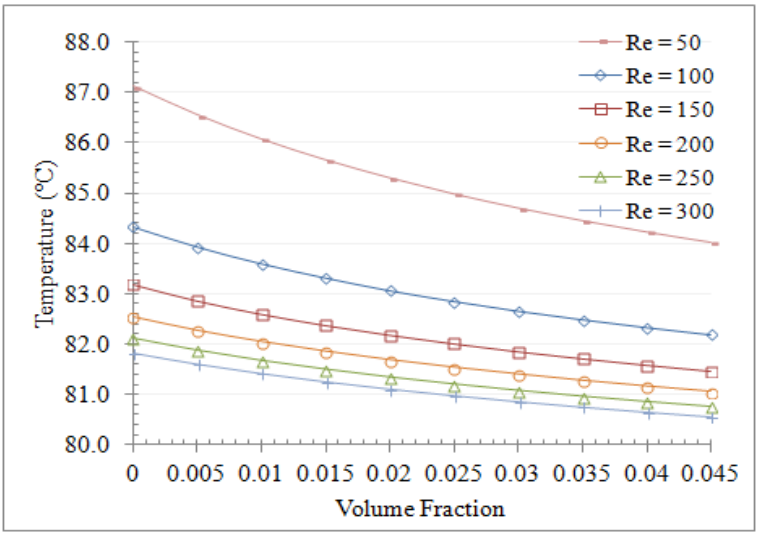

Figure 5.11: Chip temperature of server with cooled plate having two parallel tubes; using TiO_2-water nanofluids with various volume fractions and Reynolds numbers.

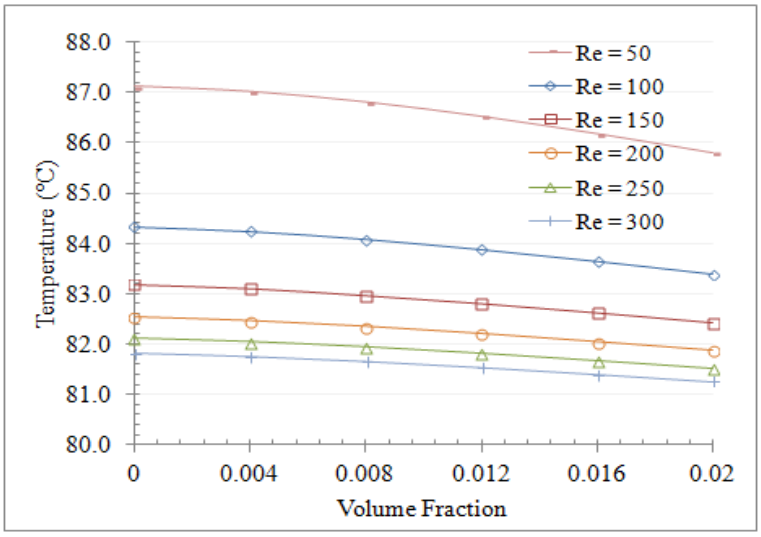

Figure 5.12: Chip temperature of server with cooled plate having two parallel tubes; using CuO-water nanofluids with various volume fractions and Reynolds numbers.

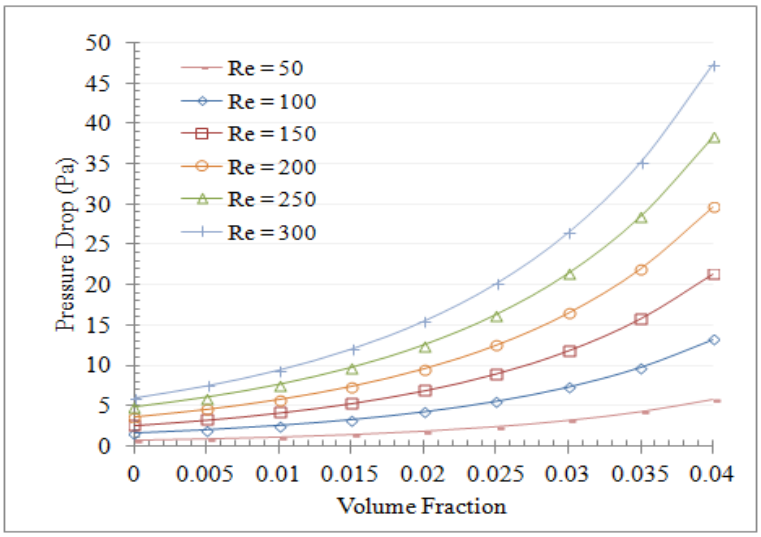

Figure 5.13: Cooled plate with two parallel tubes pressure drop usingAl_2O_3-water nanofluids with various volume fractions and Reynolds numbers.

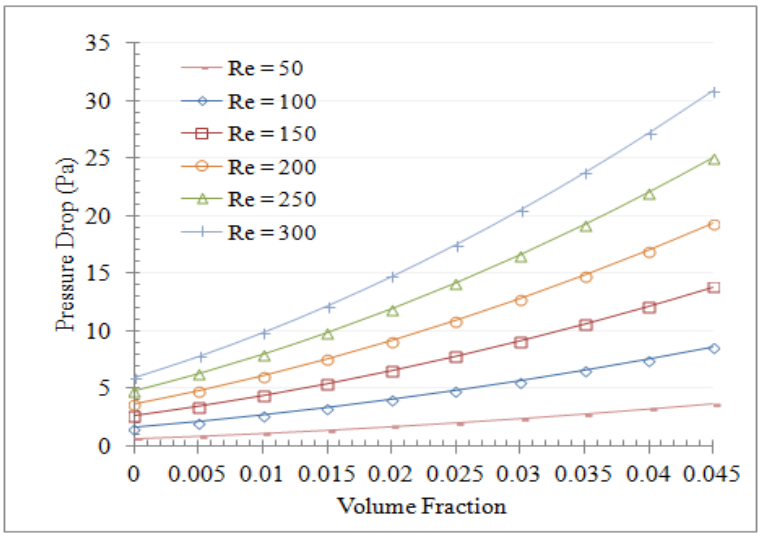

Figure 5.14: Cooled plate with two parallel tubes pressure drop usingTiO_2-water nanofluids with various volume fractions and Reynolds numbers.

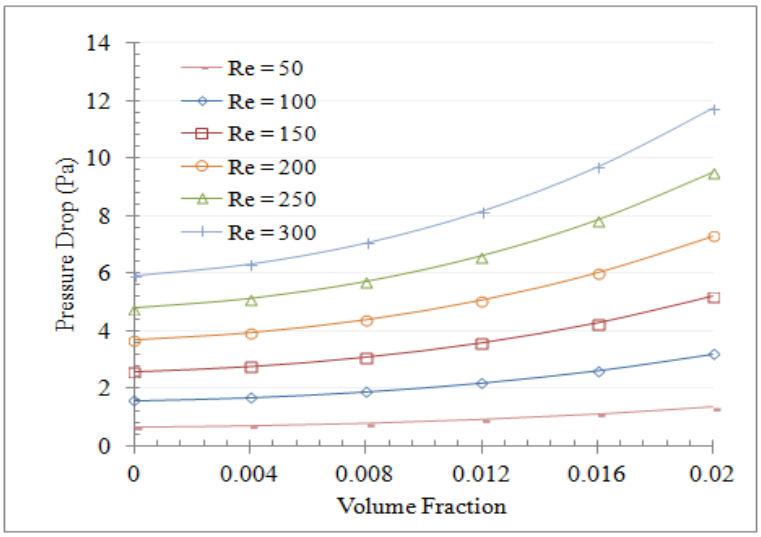

Figure 5.15: Cooled plate with two parallel tubes pressure drop using CuO-water nanofluids with various volume fractions and Reynolds numbers.

The temperature of the cross section in the middle of the server and the temperature contour of the cross section in the middle of the cooled plate having two parallel tubes ; using water and Al_2O_3-water nanofluid with volume fractions (ϕ = 0.04) at Reynolds numbers Re = 50 and 200 is presented in Figures 5.16 and 5.17, respectively.

From Figure 5.16, it can be noticed that the highest temperature is in the CPU and the temperature of the fluid (dielectric liquid) is higher at the top of the server and decrease when go down because of the buoyancy, which dominates the flow of the fluid. Also the temperature of the CPU decreases with increasing Reynolds number and nanofluid concentration as demonstrated by Figure 5.17. It can be seen that the temperature contour has low value and distributes more uniformly along the cross section of the cold plate with high Reynolds number and concentration.

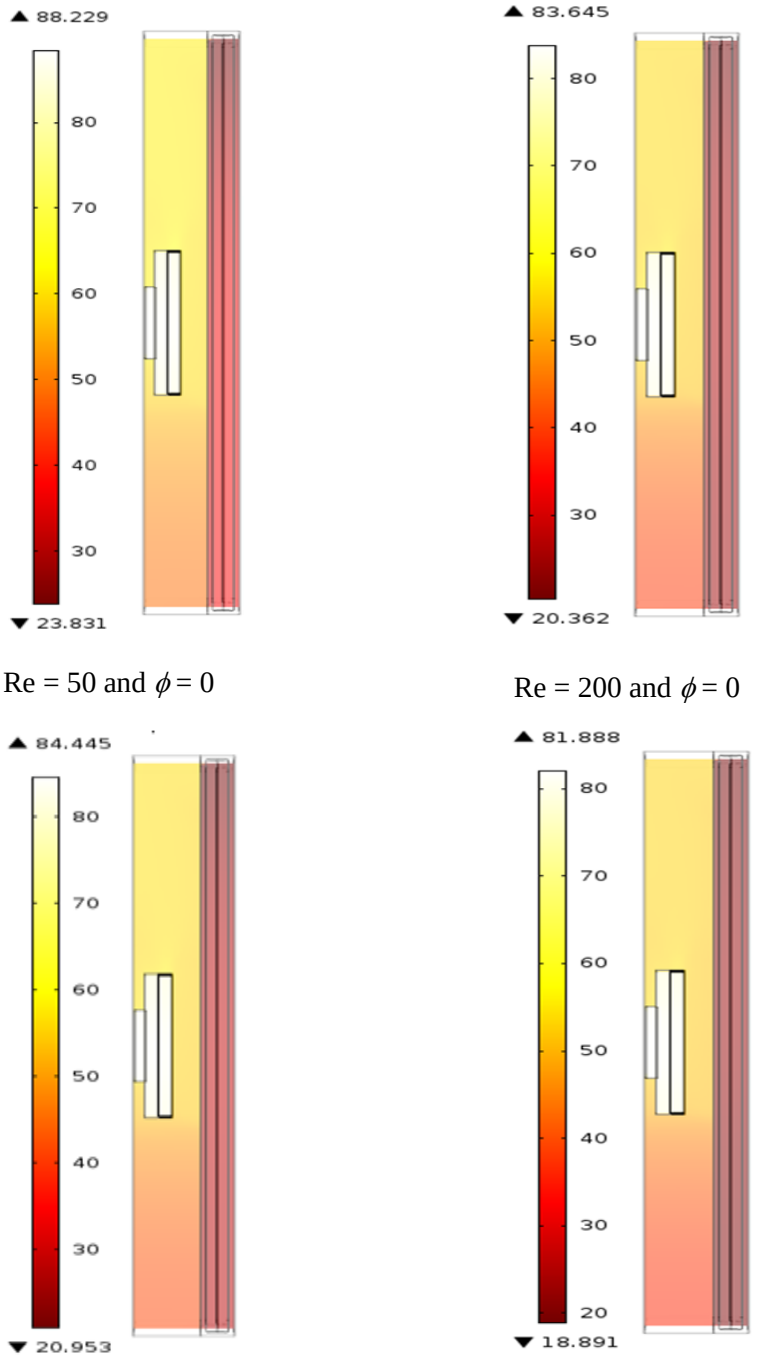

Re = 50 and $\phi = 0$

Re = 200 and $\phi = 0$

Re = 50 and $\phi = 0.04$

Re = 200 and $\phi = 0.04$

Figure 5.16: Temperature of the cross section in the middle of the server with cooled plate having two parallel tubes; using water and Al_2O_3-water nanofluid with volume fractions ($\phi = 0.04$) at Reynolds numbers Re = 50 and 200

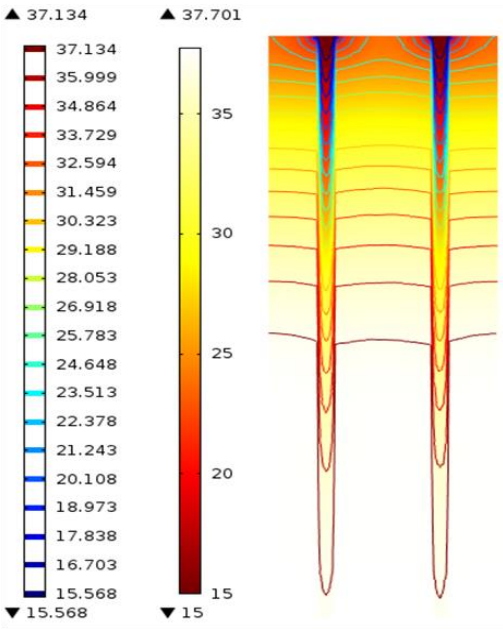

Re = 50 and ϕ =0

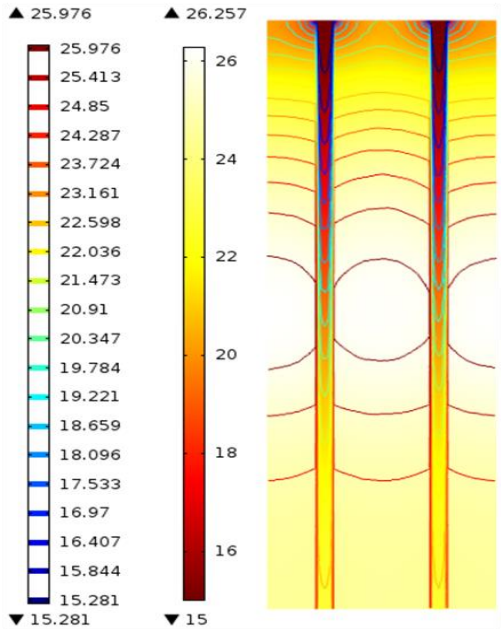

Re = 200 and ϕ =0

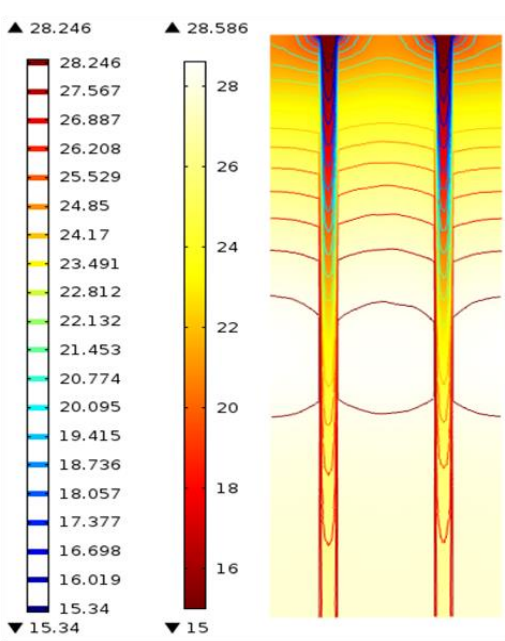

Re = 50 and ϕ =0.04

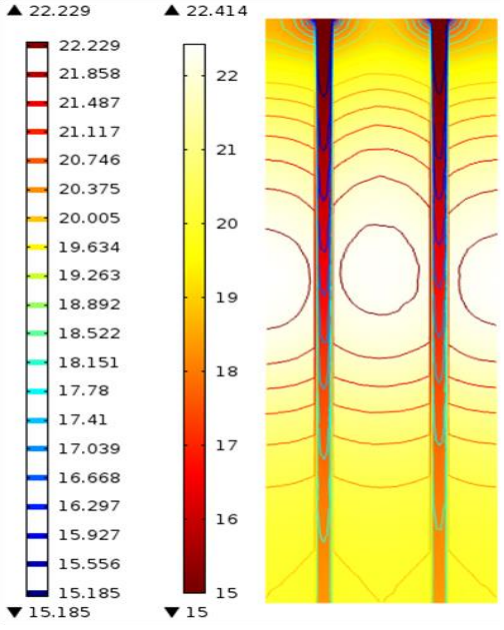

Re = 200 and ϕ =0.04

Figure 5.17: Temperature contour of the cross section in the middle of cooled plate having two parallel tubes; using water and Al_2O_3-water nanofluid with volume fractions (ϕ = 0.04) at Reynolds numbers Re = 50 and 200

5.5.2: Half server with cooled plate having serpentine tube

This section considers the half server with a cooled plate with a serpentine a tube and various nanofluids. The server chip temperature and the cooled plate pressure drop are calculated and summarized in Figures 5.18 – 5.20 and Figures 5.21 – 5.23, respectively. Each figure gives the results for all Reynolds numbers considered (Re = 200 – 700) and various volume fractions for each given type of nanofluid.

Figure 5.18 summarises the results for Al_2O_3-water nanofluids. The results of chip temperatures are presented in terms of (°C). It can clearly be seen that the chip temperature decreases monotonically with increasing Reynolds number and volume fraction. In general, the decrease in the temperature is relatively large and then becomes smaller with further increases in Reynolds number. Similar remarks can be noticed on all others studied nanofluids, as presented in Figure 5.19 and Figure 5.20 for TiO_2 and CuO nanofluids respectively. This feature of reducing the chip temperature is favourable with regards to reliability and reducing the chip energy consumption. It can be observed that using Al_2O_3-water nanofluids result in lower chip temperatures with respect to other nanofluids at the same volume fraction; this is a result of the higher thermal conductivity of Al_2O_3 nanoparticle compared to TiO_2 and CuO nanoparticles.

In contrast the pressure drop of the cooled plate with serpentine tube gives an opposite overall behaviour as presented in Figure 5.21 – 5.23. It can be seen that the pressure drop increases monotonically with increasing Reynolds number and volume fraction. In general, the increase in pressure drop is relatively large with increasing nanofluid concentrations. It is also noteworthy that the pressure drops of Al_2O_3-water nanofluids are higher than TiO_2- water and CuO-water nanofluids; this is due to the Al_2O_3-water nanofluids having a higher viscosity (see chapter 3). The consequence of having relatively higher pressure drop with increasing the volume fraction is unfavourable with regard to increasing the pump energy consumption.

It is interesting to note that using Al_2O_3-water nanofluids give lower average chip temperatures when compared to the other nanofluids due to their higher thermal conductivity. However, it has the highest pressure drop at the cooled plate as a result of

having the highest viscosity of the studied nanofluids. It is also noted that the half server with cooled plates of the serpentine tube design show higher thermal performance and lower chip temperatures with respect to the half server with cooled plate having two parallel tubes. On the other hand, the half server cooled plates with a serpentine tube gives a higher pressure drop when compared to the half server cooled plate with two parallel tubes.

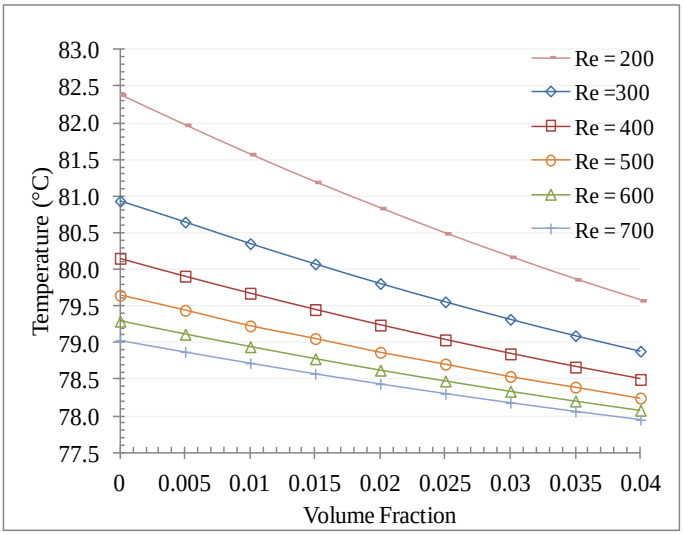

Figure 5.18: Chip temperature of server with cooled plate having serpentine tube; using Al_2O_3-water nanofluids with various volume fractions and Reynolds numbers.

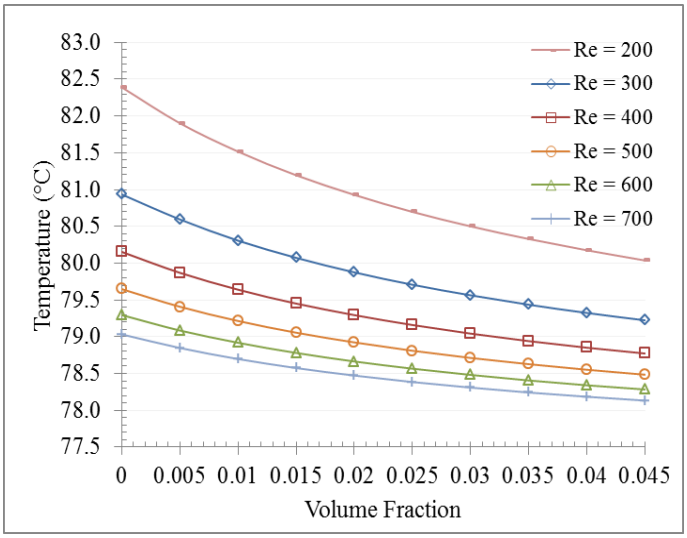

Figure 5.19:Chip temperature of server with cooled plate having serpentine tube; usingTiO_2-water nanofluids with various volume fractions and Reynolds numbers.

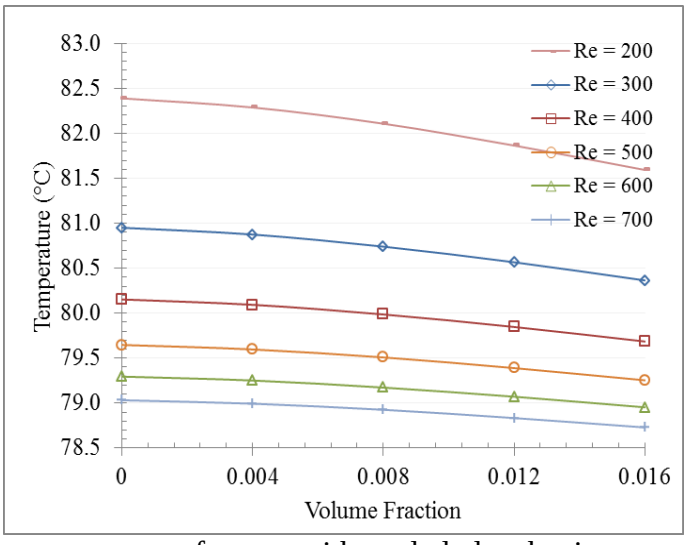

Figure 5.20: Chip temperature of server with cooled plate having serpentine tube; using CuO-water nanofluids with various volume fractions and Reynolds numbers.

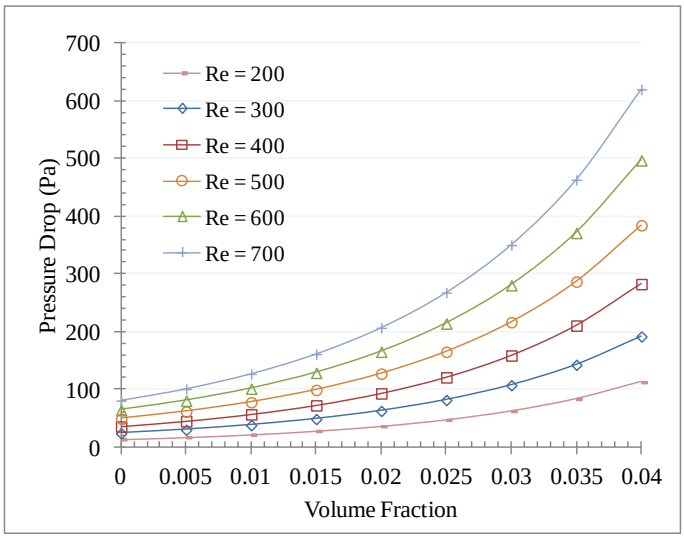

Figure 5.21: Cooled plate with serpentine tube pressure drop for Al_2O_3-water nanofluids with various volume fractions and Reynolds numbers.

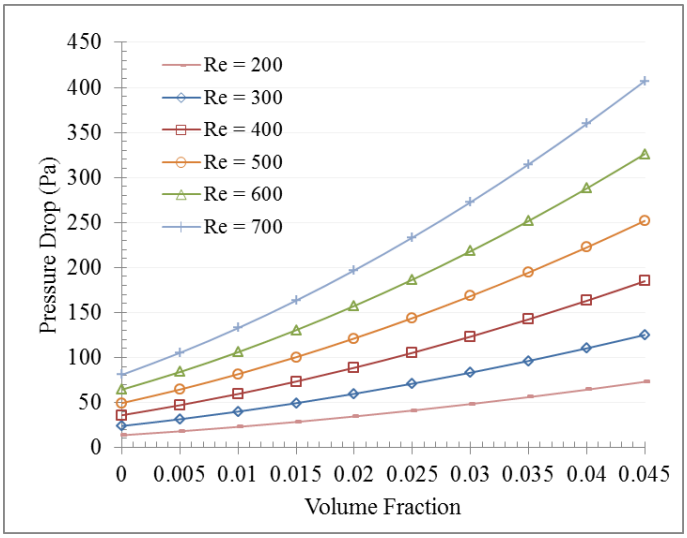

Figure 5.22: Cooled plate with serpentine tube pressure drop for TiO_2-water nanofluids with various volume fractions and Reynolds numbers.

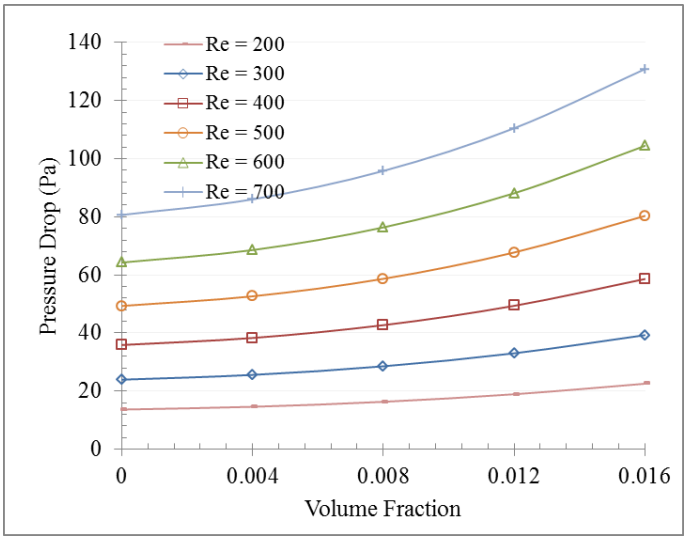

Figure 5.23: Cooled plate with serpentine tube pressure drop for CuO-water nanofluids with various volume fractions and Reynolds numbers.

The temperature of the cross section in the middle of the server and the temperature contour of the cross section in the middle of the cooled plate with serpentine tube ; using water and Al_2O_3-water nanofluid with volume fractions ($\phi = 0.04$) at Reynolds numbers Re = 200 and 600 is presented in Figures 5.24 and 5.25, respectively. It can be seen that the temperature contour in the cross section of cooled plate show low value at high Reynolds number and volume fraction and this contribute to reduce the temperature of the CPU. It is interesting to note that the temperature contour of the cooled plate cross section using water at Re = 600 is almost similar to that using Al_2O_3-water nanofluid with volume fractions $\phi = 0.04$ at Re = 200.

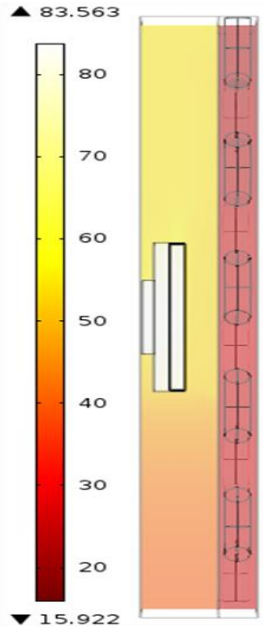

Re = 200 and $\phi = 0$

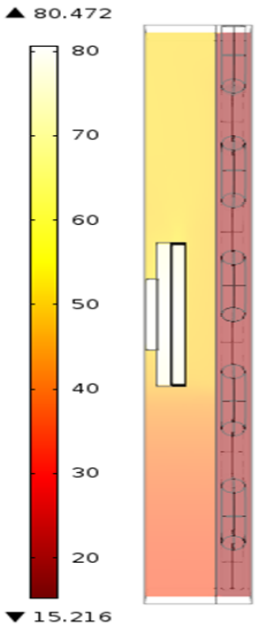

Re = 600 and $\phi = 0$

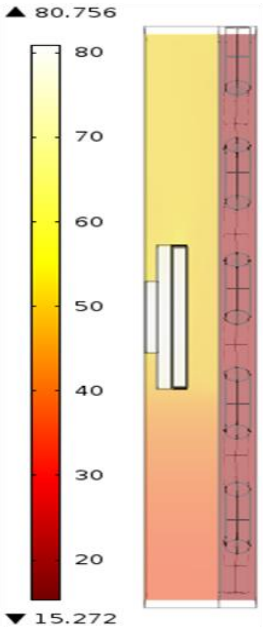

Re = 200 and $\phi = 0.04$

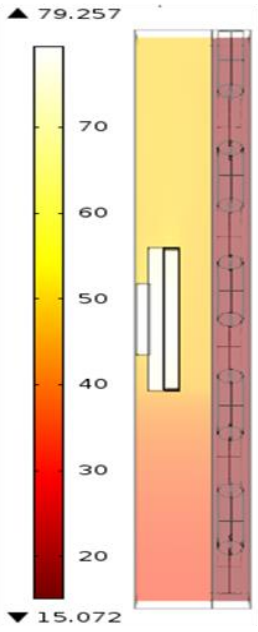

Re = 600 and $\phi = 0.04$

Figure 5.24: Temperature of the cross section in the middle of the server with cooled plate with serpentine tube; using water and Al_2O_3-water nanofluid with volume fractions ($\phi = 0.04$) at Reynolds numbers Re = 50 and 200

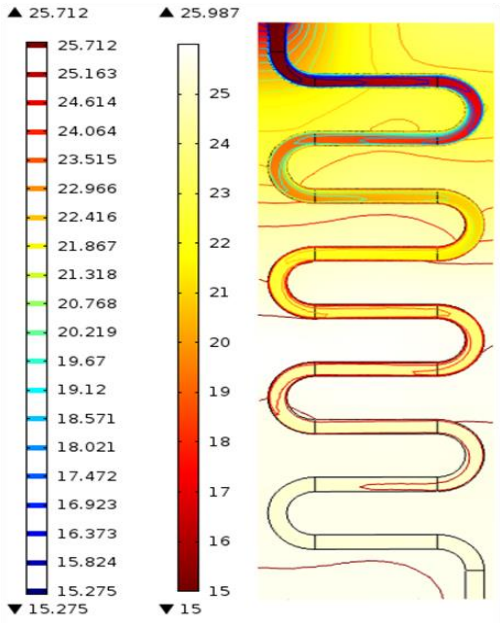

Re = 200 and $\phi = 0$

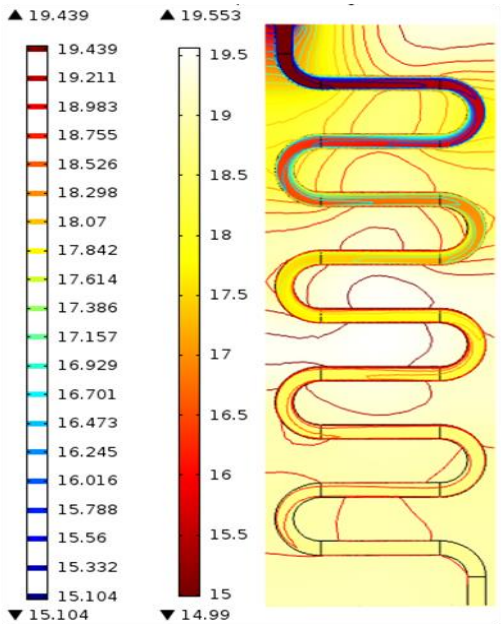

Re = 600 and $\phi = 0$

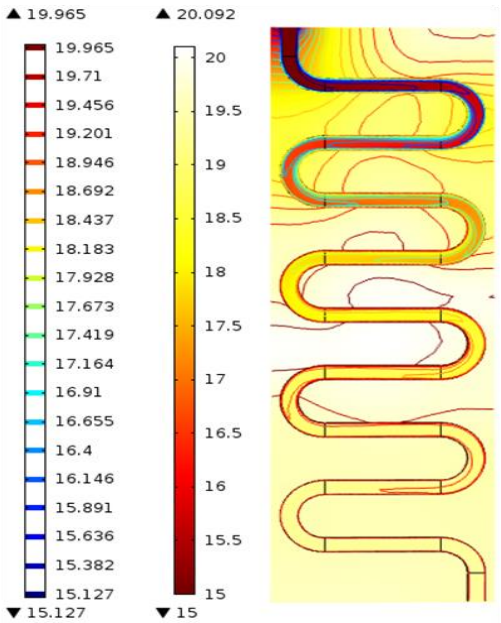

Re = 200 and ϕ =0.04

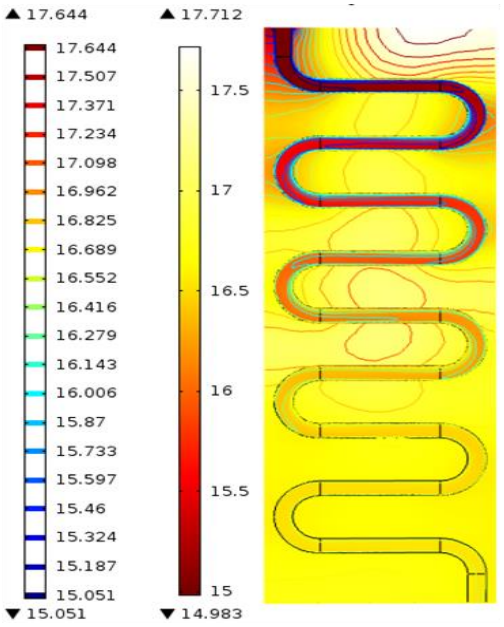

Re = 600 and $\phi = 0.04$

Figure 5.25: Temperature contour of the cross section in the middle of cooled plate with serpentine tube; using water and Al_2O_3-water nanofluid with volume fractions ($\phi = 0.04$) at Reynolds numbers Re = 50 and 200

5.6: Concluding Remarks

The COMSOL CFD package which is based on the finite element method has been used to calculate the temperature of the (CPU) chip surface and the pressure drop of the cooled plate through two different half-server configurations; one with a cooled plate that has two parallel tubes and another with cooled plate that has a serpentine tube. Both half servers are based on the immersion design by Iceotope and use various nanofluids (Al_2O_3-water nanofluids, TiO_2-water nanofluids and CuO-water nanofluids) with varying volume fractions. The variations of the chip temperature and cooled plate pressure drop of typical nanofluid with different volume fractions and Reynolds number were calculated under steady state conditions.

First of all, It is interesting to mention that the parallel flow when the inlet flow is from the top to the bottom of the server's cooled plate is used in this study because it showed better thermal performance than the counter flow when the inlet flow is opposite direction under the consideration of this study. The results of calculation for both servers showed that the average temperature of chip decreased monotonically with increasing Reynolds number of cooled plate and the volume fraction of nanofluid. In contrast, pressure drop of both cooled plate gave the opposite behaviour.

The Al_2O_3-water nanofluids gave better thermal performance (lower chip temperature) compared to TiO_2-water and CuO-water nanofluids for both half servers mainly due to their higher thermal conductivity (see Table 4.1). However, they also gave higher pressure drops than the other fluids due to their higher viscosity (see Figure 3.15). The half server with cooled plate having serpentine tube was thermodynamically better than the half server cooled plate with two parallel tubes and resulted in lower chip temperatures. In contrast, the pressure drop of the cooled plate tubes with a serpentine tube was much higher than the pressure drop of the cooled plate having two parallel tubes.

The results from the analysis in this chapter will be used in the next chapter to formulate an economic assessment of using nanofluids in these cooling systems.

CHAPTER 6: ECONOMIC ANALYSIS OF THE USE OF NANOFLUIDS IN ELECTRONICS COOLING

6.1: Introduction

The purpose of this chapter is to assess the feasibility of using nanofluid coolants from an economic perspective, in the context of the server cooling systems considered in chapter 5.

In this economic analysis, the costs and benefits are evaluated of some alternative engineering projects using the present worth method which applied by converting all the cash flow of the project over its lifetime to single sum equivalent at the present [122]. Therefore the heat transfer efficiency, pressure drop and nanofluids cost versus nanofluid concentration which were calculated by the previous numerical analysis (chapter 5) are fed into an economic analysis model based on the present worth method [123, 124] in order to determine the minimum total projected cost. It is expected that as the concentration of nanoparticles increases the cost of the nanofluid increases while the server power consumption decreases as a consequence of decreasing the components temperature [7, 119-121]; through high heat transfer performance of nanofluid and the cooling system efficiency may increase (run at high load) and consequently the energy cost decrease or remain constant. However, the pump power consumption will increase by adding nanoparticles; due to the viscosity increases [125]. The optimum nanofluid concentration is the concentration at which the total cost of nanofluid and the present value of energy consumption cost due to pump, server and refrigerator system over the estimated lifetime of a system is a minimum. A methodology is proposed by considering only the heat generation through the Central Processing Unit (CPU). The heat generated by the CPU is only considered to simplify the power consumption calculations as the CPU is generally the dominant part of the total heat generation load within a server and its power consumption is dependent on its temperature [6-8]. In some cases within a data centre, reducing the power consumption of the server is more efficient than reducing the power of cooling system by decreasing the environmental temperature [7].

6.2: Details of the Economic Analysis

The total cost (c_{tot}) to be determined is the sum of the initial cost of the nanofluid (c_{nf}) which is paid at the time of construction, plus the present value of the cost of energy consumption over the lifetime of using nanofluid in the system (c_{enr}) taking into account the inflation and interest (discount) rates.

The total cost is given by:

$$c_{tot} = c_{nf} + c_{enr} \quad = c_{nf}(\phi) + C_e PWF \tag{6.1}$$

where c_{nf} is the purchase cost of nanofluid and is presumably a function of nanoparticle concentration, C_e is the current yearly total cost of energy (£/year) and PWF is the present worth factor.

Assuming an inflation rate in energy cost r_i, an interest rate r_d and an expected lifetime of using nanofluid m (years), the present worth factor is calculated as[124]:

In case $r_d \neq r_i$,

$$\text{PWF} = \left(\frac{1+r_i}{r_d - r_i}\right)\left[1-\left(\frac{1+r_i}{1+r_d}\right)^m\right] \tag{6.2}$$

In case $r_d = r_i$,

$$\text{PWF} = \frac{m}{1+r_d} \tag{6.3}$$

The yearly total cost of energy (C_e) is calculated from the yearly total energy consumption (E_{tot}), including the server CPU power (E_s), cooling system power (E_c) and the pump power (E_p). Based on the findings of the earlier chapters, the heat that the CPU produces during its running is predicted to decrease with increasing nanofluid concentration whereas pump power consumption is predicted to increase with increasing nanofluid concentrations. The yearly cost depends on the method and efficiency of the server type, cooling system and pump type. Let the total heat gain from server CPU per

year be Q_g. For vapour-compression cooling the electric energy consumption E_c is given by [126]:

$$E_c = Q_g / p_c \tag{6.4}$$

Where p_c = COP is the average coefficient of performance of the refrigeration system.

The COP is the ratio of the heat removed (Q_g) to the amount of energy (E_c) needed to remove the heat; and the COP is a function of the supply temperature of the refrigeration system and the heat load. The COP of the cooling system ranges from 2 - 12 depend on the supply temperature and the heat load of the chiller as well as the speed of the chiller [127, 128]. In this study it is assumed that COP = 5.0.

The CPU energy consumption (E_s) depends on the workload of the CPU and its resulting temperature [7, 119-121, 129] and this power consumption is an exponential relationship with temperature [130-132]. The CPU power consumption is a combination of dynamic power which is due to the CPU activity power and static power which is due to the CPU leakage current [106, 131, 133].

$$E_s = P_{static} + P_{dynamic} \tag{6.5}$$

The dynamic power ($P_{dynamic}$) can be calculated as [106]:

$$P_{dynamic} = \alpha\omega V^2 \tag{6.6}$$

Where α is the activity factor of the processor, V is the supply voltage and ω is the clockspeed of the CPU (GHz).

The static power (P_{static}) can be calculated as [106]:

$$P_{static} = I_{leak}\, V, \tag{6.7}$$

where I_{leak} is the leakage current, but the leakage current depends on the voltage and temperature; therefore, Frenkel-Poole emission is used to estimate the leakage current [134, 135]:

$$I_{leak} = BV \exp\left(-\frac{E - C\sqrt{V}}{T}\right) \quad . \tag{6.8}$$

Substituting Eq. (6.8) into Eq. (6.7) gives:

$$P_{static} = BV^2 \exp\left(-\frac{E - C\sqrt{V}}{T}\right) \tag{6.9}$$

where B, C, E, are constants related to the CPU and its running and T is the CPU temperature (K).

From Eqs. (6.6) and (6.9), the CPU energy consumption (E_s) is:

$$E_s = BV^2 \exp\left(-\frac{E - C\sqrt{V}}{T}\right) + \alpha\omega V^2 \tag{6.10}$$

In this study, the Intel i7-3770K processor (CPU) is chosen and the corresponding parameter values are [135]:

α = 14.91, B = 4408.2, C = 56.4, E = 2020.9

By substitution in Eq. (6.10), the CPU energy consumption will be:

$$E_s = 4408.2\, V^2 \exp\left(-\frac{2020.9 - 56.4\sqrt{V}}{T}\right) + 14.91\,\omega\, V^2 \tag{6.12}$$

The operating parameters of the CPU such as voltage (V) and frequency (clockspeed) (ω) have been adjusted for each configuration of servers to produce heat (80 W) under operation temperature of using base fluid at lower Reynolds number. Therefore, by applying Eq. (6.12) the half server with cooled plate having two parallel tubes configuration the lower Reynolds was 50 and the voltage 1.124 V, the clockspeed of the CPU to produce 80 W should be is 2.97GHz. Whereas it was 3.06 GHz at the same voltage and Re = 200 for half server with cooled plate having serpentine tube.

As for increasing nanofluid concentrations, the pressure drop across the system will increase. The use of the pump is assumed to be ideal for which the electric energy consumption E_p is given by [125]:

$$E_p = \frac{\dot{m}}{\rho}\frac{\Delta p}{p_p} \tag{6.13}$$

where $\dot{m}$ is mass flow rate, Δp is the pressure drop, ρ is the density of liquid (base fluid and nanofluid) and p_p is the performance factor which is the main part of the pump type and it is taken 0.85 see Table 6.1.

Therefore, the yearly total electric energy consumption is:

$$E_{tot} = E_c + E_p + E_s \tag{6.14}$$

And the yearly total cost of electricity (C_e) is:

$$C_e = E_{tot}\, c_e \tag{6.15}$$

Where c_e is the current local cost of electricity (£/kWh).

In summary the input to the economic analysis model is the yearly values of Q_g and pressure drop versus the volume fractions (ϕ), which are obtained from the numerical analysis in chapter 5, as well as values of the parameters to be specified later (Table 6.1). The output from the economic model is the values of total cost (c_{tot}) versus nanofluid volume fraction (ϕ).

6.3: Economic Parameters

The nominal values of the parameters used in this economic model are summarised in Table 6.1. Where c_{nf} is the cost of nanofluids, c_{bf} is the cost of the base fluid, c_e is an average local charge of business and commercial electricity, P_c is the coefficient of performance of cooling system, P_p is the pump efficiency, m is the lifetime of the system, r_d is the discount rate, and r_i is the inflation rate are taken as the average value over the previous ten years [136, 137]; see Figure 6.1.

Table 6.1 : Nominal values of parameters used in the optimization model.

C_{nf} (£/kg)	c_{bf} (£/kg) water	c_e (£/kWh) [138]	p_c	p_p [139]	m (years) [140, 141]	r_d (%) [136]	r_i (%) [137]
*	0.35	0.108	5	0.85	3	3.4	2.7

*Cost depends on nanofluid type and its concentration used; see Table 6.2.

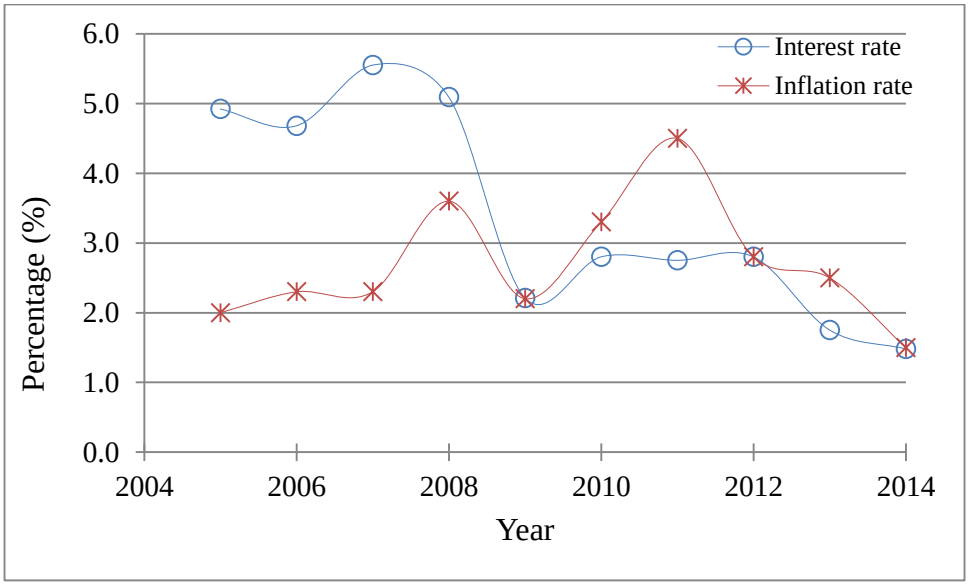

Figure 6.1: Average annual value of interest and inflation rate of the UK over ten years [136, 137].

In this study, the server is assumed to be in operation 24 hours a day over its lifetime and the amount of the fluid (water or nanofluid), which is used in the cooled plate, is calculated from the average capacity of both cooled plate configurations. It is about 0.062 litres and the total capacity of the cooling devise system (i.e. chiller) and cooled plate is 0.124 litters. The study used the three common types of nanofluids Al_2O_3-water, TiO_2-water and CuO-water, considered in the earlier chapters. The nanofluid costs are given in Table 6.2 and reflect the local market values at the time of the investigation, whilst the cost of a nanofluid depends upon the type of base fluid (e.g. water), nanoparticle type, particle size, purity, as well as the nanofluid preparation method. The cost of a nanofluid can be calculated from the commercial cost in pound per kilogram of nanofluid (£/kg) according to its mass fraction. For example the cost of Al_2O_3/water nanofluid is

24.17 £/kg for mass fraction concentration 20 wt% (from Alfa company [142]); and from that it may be assumed that the cost of nanofluid increases linearly with nanoparticle concentration taking into account the cost of the base fluid at no nanoparticle load (for water £ 0.35 per kg at room temperature).

Table 6.2 : cost of nanofluid in commercial companies (Alfa Company)

Nanofluids	c_{nf} (£/kg)**	Comments
Al_2O_3/water[142]	24.17	20wt% or 6.0 vol %
CuO/water[142]	446	50 wt% or 13.6 vol%
TiO_2/water[142]	67.50	35 wt% or 11.0 vol%

**cost of nanofluid at the purchase concentration

It must be noted that special exemptions are not accounted for by the economic model. For example, the temperature of the chip was calculated by assuming that the chip consumes and generates 80 W as in chapter 5, but in the economic model, the CPU power consumption is calculated based on the temperature of the CPU. Therefore the cooling system power consumption is assumed constant with regard to the power consumption of the chip when using base fluid (water). Also, there are generally connection pipes between the system (server) and the pump that would add an extra pressure drop and therefore increasing the pump power consumption related costs; such costs are not included in the present economic analysis. Therefore, the total cost referred to in the study comprises the costs of nanofluids as a function in volume fraction used that are paid for at the time of installation plus the present worth of the cost of electric energy consumption over the lifetime of the system. The optimization of nanofluid concentrations used in the present study is based on the chip power consumption as a function of its temperature, cooling system to remove the assumed 80 W heat generated by the chip, and the pump power consumption due to the pressure drop required to circulate the cooing fluid through the server only.

6.4: Total Cost versus Nanofluids Concentration

6.4.1: Half server with cooled plate having two parallel tubes

Firstly, the base fluid performance for the half server with the two parallel tubes cooled plate configuration at various Reynolds number is presented in Figure 6.2. The results show that the total cost is higher at low Reynolds number because the CPU was not cold enough, when increasing the Reynolds number the temperature of the CPU decreased corresponding the total decrease to reach the optimum total cost at Re = 200. Then when increasing the Reynolds number the total cost increase again because the pumping power costs dominated the savings due to the decreased temperatures and therefore decreased power of the CPU.

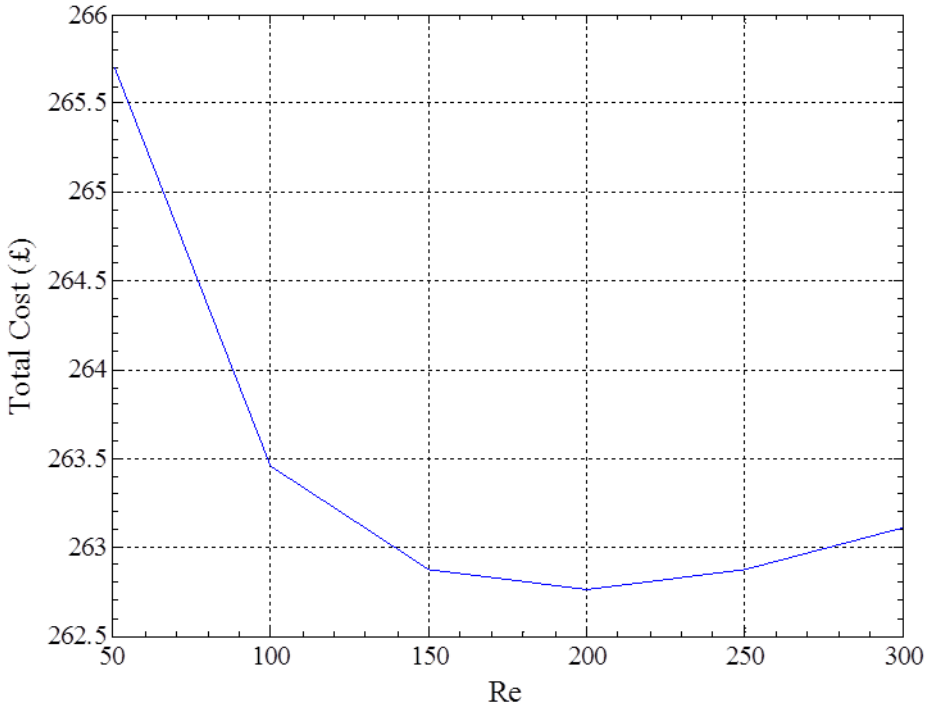

Figure 6.2: Total cost variation with various Reynolds number using the base fluid (water) for half server with cooled plate having two parallel tubes.

On the other hand, Figure 6.3 gives representative results of the variation of the total cost as a function of volume fraction for the half server with cooled plate having two parallel tubes configuration using Al_2O_3-water nanofluid. Each curve on the figure shows a minimum total cost (cost of energy and nanofluid) that gives a corresponding value for the optimum concentration for that particular Reynolds number. It is noted that Reynolds numbers of 200, 250 and 300 give minimum total cost values corresponding when the coolant is pure water (i.e. volume fraction $\phi = 0$). This is because the nanofluid and pumping cost dominates. While Re = 50 and 100 give the minimum total cost at the optimum volume fraction 3.5 and 0.5 vol.% respectively. It is worth mentioning that pure water at Re = 200 gives the lowest minimum total cost. In addition, the total cost curve of Al_2O_3-water nanofluids at Re = 50 changes more gradually with changing volume fraction. Accordingly the exact value for its optimum volume fraction is more flexible in the sense that the optimum volume fraction (ϕ_{opt}) values lies within the range of about 3.0 to 4.0 vol.% which gives practically the same minimum total cost. However, none of the Al_2O_3-water nanofluids offer a saving over using just the base fluid operated at an optimal Reynolds number.

With regards to TiO_2-water nanofluids, Figure 6.4, the optimum volume fraction of TiO_2-water nanofluids for all Reynolds number are pure water (i.e. volume fraction $\phi = 0$), except using nanofluid at Re 50, gives optimum volume fraction 1.0 vol.%. However, the lowest minimum total cost is base fluid (water) is still used at Reynolds number 200. CuO-water nanofluids results are shown in Figure 6.5. It is noted that using base fluid (water) gives the lowest minimum total cost and none of nanofluids gives an optimum volume fraction compared to the base fluid at the same Reynolds number. In addition, the total cost curve changes sharply with a small change in the volume fraction. This is a result of the high purchase cost of CuO-water nanofluids (per unit kilogram) and their lower thermal conductivity compared to Al_2O_3-water nanofluids.

At the other extreme, pure water at Re = 200 gives the lowest minimum total cost (£ 262.76) and therefore they are most cost effective among those investigated under the conditions and factors used in the present study. It is should be mentioned that the optimum volume fraction at Re = 50 for Al_2O_3-water nanofluid and TiO_2-water nanofluid

are 3.5 and 1.0 vol.% respectively; but Al_2O_3-water nanofluid gave lower minimum total cos (£ 264.86 for Al_2O_3-water nanofluid and £ 265.5 for TiO_2-water nanofluid). Although, the viscosity of Al_2O_3-water nanofluid is higher than TiO_2-water nanofluid at these concentration (see chapter3). This is because of Al_2O_3-water nanofluid has lower cost and higher thermal conductivity compared to TiO_2-water nanofluid.

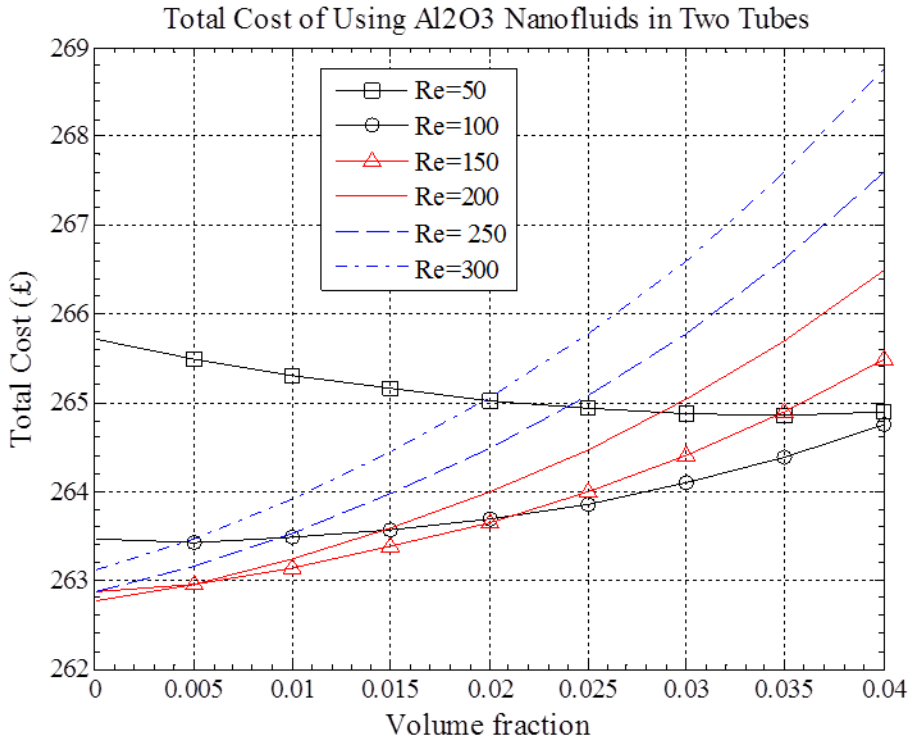

Figure 6.3: Total cost variation with volume fraction using Al_2O_3-water nanofluids for half server with cooled plate having two parallel tubes.

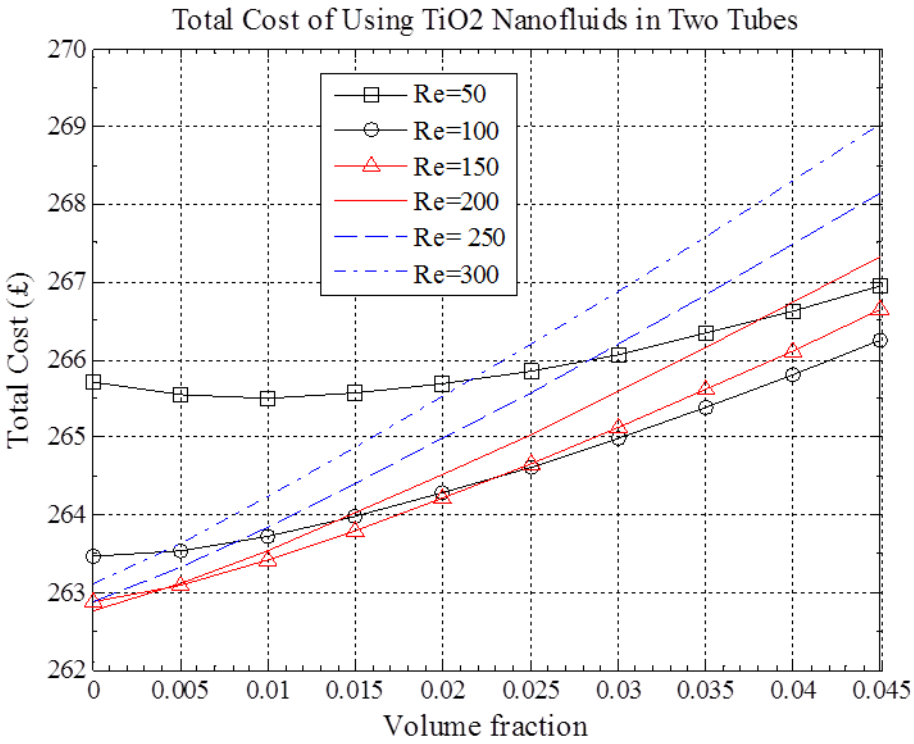

Figure 6.4: Total cost variation with volume fraction usingTiO_2-water nanofluids for half server with cooled plate having two parallel tubes.

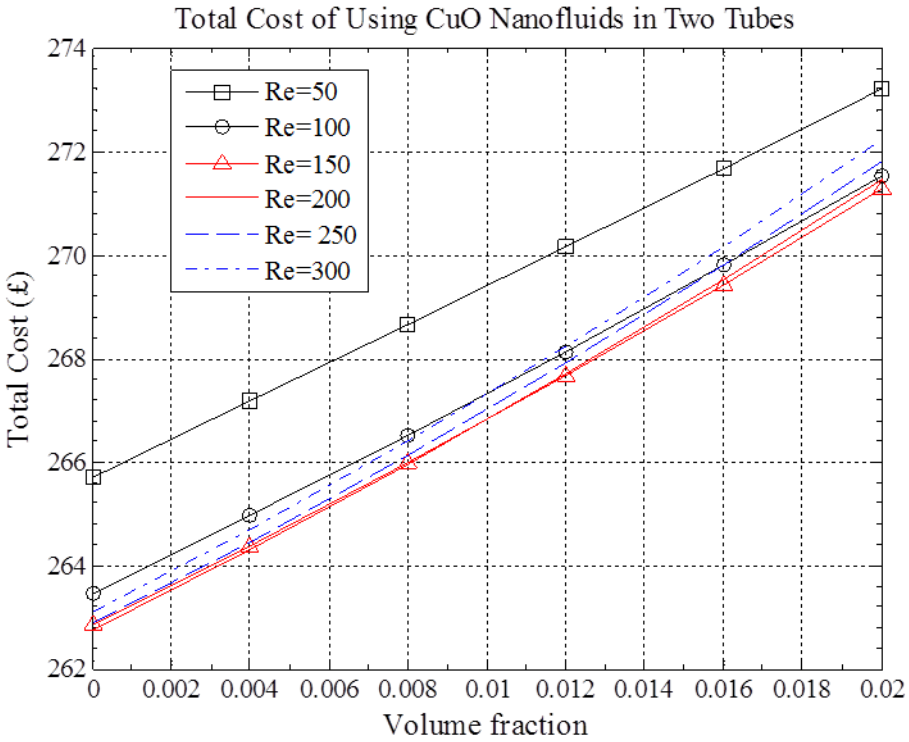

Figure 6.5: Total cost variation with volume fraction using CuO-water nanofluids for half server with cooled plate having two parallel tubes.

Table 6.3 : The cost effectiveness for the tenth lowest minimum total cost in order.

Order	Type of nanofluid	Volume fraction (vol%)	Re	Minimum total cost (£)
1	Water	0.0	200	262.76
2	Water	0.0	150	262.87
3	Water	0.0	250	262.88
4	Al_2O_3	0.5	200	262.95
5	Al_2O_3	0.5	150	262.96
6	TiO_2	0.5	150	263.08
7	TiO_2	0.5	200	263.10
8	Water	0.0	300	263.11
9	Al_2O_3	1.0	150	263.14
10	Al_2O_3	0.5	250	263.16
11	Al_2O_3	1.0	200	263.24
12	TiO_2	0.5	250	263.32
13	Al_2O_3	1.5	150	263.37
14	TiO_2	1.0	150	263.41
15	Al_2O_3	0.5	100	263.43

6.4.2: Half server with cooled plate having serpentine tube

The base fluid performance for the half server with cooled plate having the serpentine tube configuration at various Reynolds number is given in Figure 6.6. It can be seen that the total cost decreases with increasing Reynolds number due to the CPU's decreasing temperature and the minimum total cost at Re = 600. As the Reynolds number is increased past 600 the pumping power becomes more significant and the system less economical.

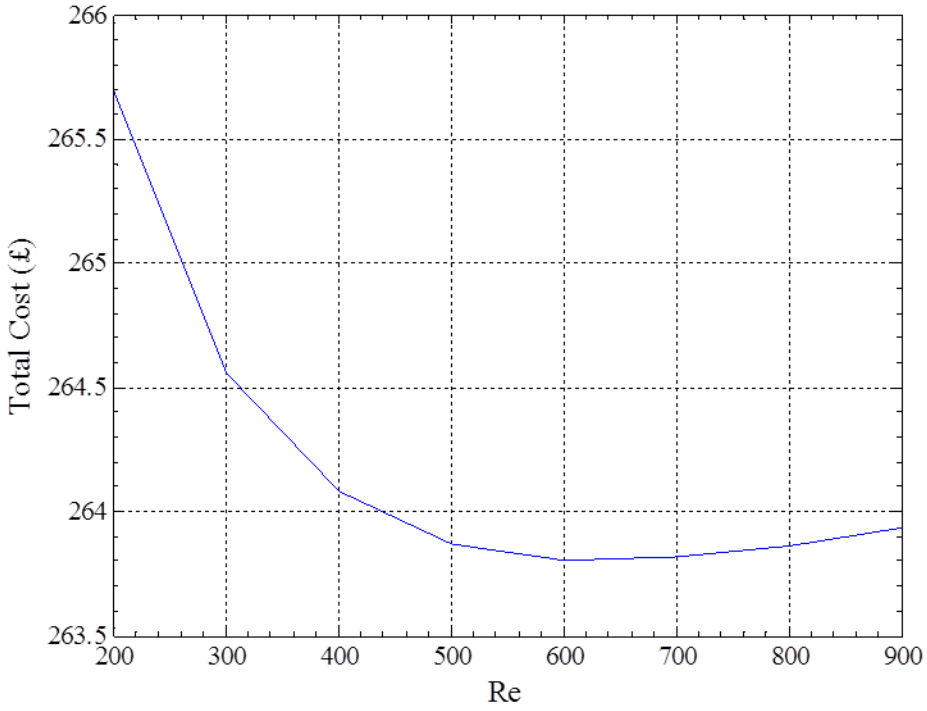

Figure 6.6: Total cost variation with various Reynolds number using the base fluid (water) for the half server with cooled plate having serpentine tube.

Figures 6.7 - 6.9 show representative results of the variation of the total cost with volume fractions for the half server with cooled plate having serpentine tube configuration using Al_2O_3-water, TiO_2-water and CuO-water nanofluids, respectively. Each curve on the figures show a minimum total cost that gives a corresponding value for the recommended concentration for that particular Reynolds number. It is found that using base fluid (water) at Re = 600 gives the lowest minimum total cost and the greatest cost effectiveness at £ 263.80 for the considerations and parameters of this study.

Figure 6.7 shows the total cost variation using Al_2O_3-water nanofluids. It is clearly seen that at Re = 200 the nanofluid gives minimum total cost at 1.5 vol.% and the total cost curve changes more gradually with changing volume fraction between 1.0 and 2.0 vol.%. Other Reynolds numbers show that using the base fluid give the minimum total cost. This is due to the cost of nanofluid and the pumping power.

For TiO_2-water nanofluids, it can be seen that using the base fluid gives minimum total cost compared to all nanofluid concentrations at the same Reynolds number except Reynolds numbers 200 which give an optimum volume fraction with TiO_2-water nanofluids at 0.5 vol.%. It is noted that at this Reynolds number Al2O3-water nanofluids give an optimum volume fraction of 1.5 vol.% which is higher than the optimum volume fraction of TiO_2 nanofluids with lower minimum total cost; this is due to Al_2O_3-water nanofluid having a lower cost and higher thermal conductivity compared to TiO_2-water nanofluids. The results for the CuO-water nanofluids are shown in Figure 6.9. It is clearly seen that all Reynolds numbers show that using the base fluid (water) gives the lowest minimum total cost and none of the nanofluids do give an optimum volume fraction. In addition, it can be seen that the total cost curve changes sharply with a small changes in the volume fraction. This is a result of its highest cost of CuO-water nanofluids (per unit kilogram) and its lowest thermal conductivity compared to Al_2O_3-water nanofluids.

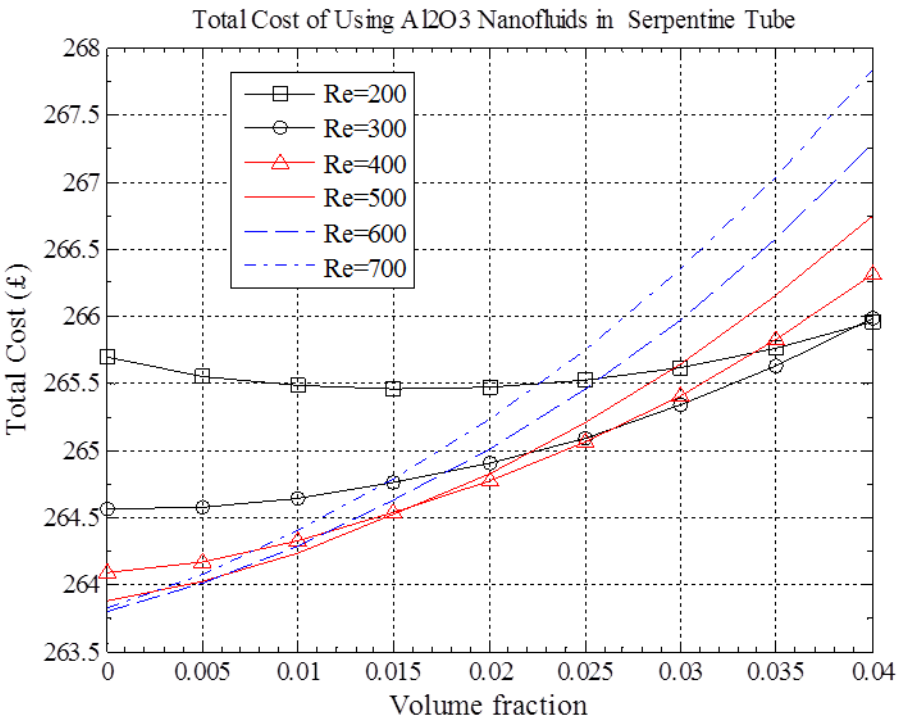

Figure 6.7: Total cost variation with volume fraction using Al_2O_3-water nanofluids for half server with cooled plate having serpentine tube.

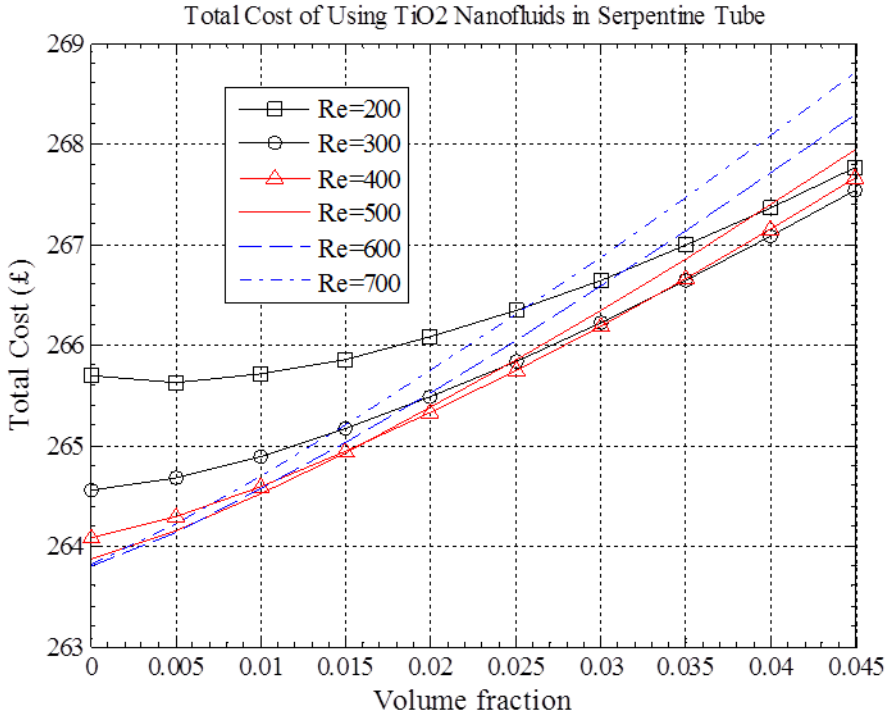

Figure 6.8: Total cost variation with volume fraction using TiO_2-water nanofluids for half server with cooled plate having serpentine tube.

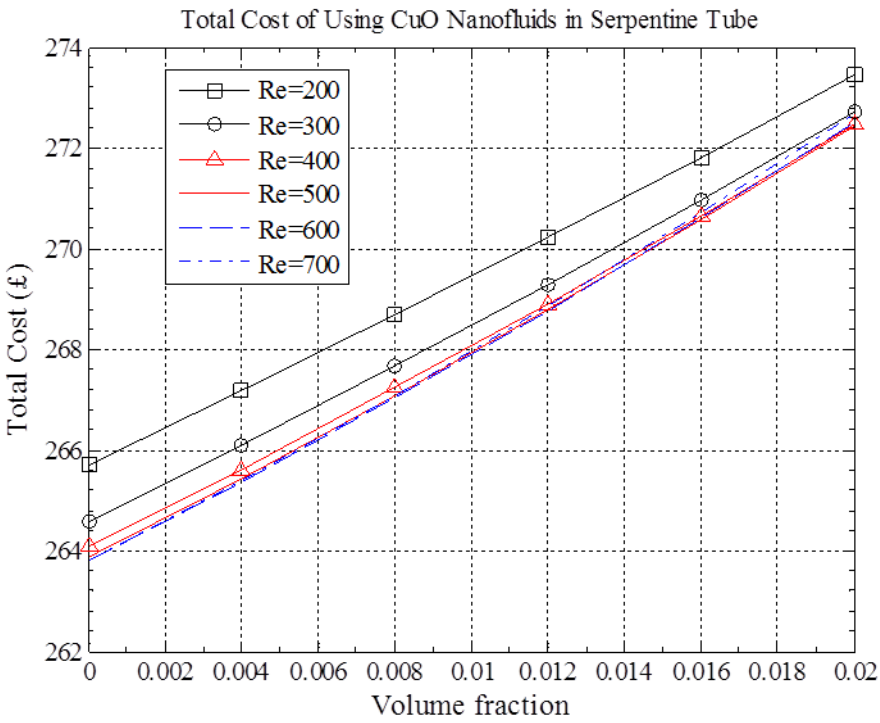

Figure 6.9: Total cost variation with volume fraction using CuO-water nanofluids for half server with cooled plate having serpentine tube.

Table 6.4 : The cost effectiveness for the tenth lowest minimum total cost in order.

Order	Type of nanofluid	Volume fraction (vol%)	Re	Minimum total cost (£)
1	Water	0.0	600	263.80
2	Water	0.0	700	263.82
3	Water	0.0	500	263.87
4	Al_2O_3	0.5	600	264.00
5	Al_2O_3	0.5	500	264.02
6	Al_2O_3	0.5	700	264.07
7	Water	0.0	400	264.08
8	TiO_2	0.5	600	264.14
9	TiO_2	0.5	500	264.16
10	Al_2O_3	0.5	400	264.17
11	TiO_2	0.5	700	264.21
12	Al_2O_3	1.0	500	264.23
13	TiO_2	0.5	400	264.28
14	Al_2O_3	1.0	600	264.29
15	Al_2O_3	1.0	400	264.33

In terms of cost effectiveness, Table 6.3 and Table 6.4 show the order of some lowest minimum total cost using all nanofluids for the half server with cooled plate having two parallel tubes and the half server with cooled plate having serpentine tubes configuration respectively. This order of optimisation is highly affected by the cost and thermophysical properties (i.e. thermal conductivity and viscosity) of the nanofluids. Therefore, it must be emphasised here that if different thermal properties and material costs were used for the different types of nanofluid then the optimisations would be significantly altered. Also of note is that, this optimisation is highly dependent on the type of application. Other properties of nanofluids could be very significant such as erosion and corrosion which were not taken into consideration in the present evaluation [143].

It is interesting to mention that increasing the Reynolds number to use nanofluids instead of base fluid has its limitation, with regard to the type of the practical application configuration and type of nanofluid with its concentration. For example, the half server with cooled plate having two parallel tubes it is worth increasing the Reynolds number up to 100 for Al_2O_3-water and TiO_2-water nanofluids up to 50; however, it is not worth to increase the Reynolds number for CuO-water nanofluids. Whereas for the serpentine cooling plate it is worth to increase the Reynolds number up to 200 for Al_2O_3-water and TiO_2-water nanofluids, but it is not worth to use CuO-water nanofluids under the conditions and parameters used in the present study.

It is worth mentioning that any extra installation costs arising from such as the configuration of the two cooled plates (used to cool the half server) or adding another symmetric half server to become one whole server will not affect the optimum nanofluids concentrations as it will only shift the total cost versus the volume fraction curve in the vertical direction. Also if the study were expanded to include a number of servers as is normally found in a rack in data centre will not affect the optimum nanofluids concentration. Therefore, extra cost not accounted for in the present analysis, for comparison as required, may be added to the total cost value (including the minimum total cost). Of course, the rest of the economic factors, as mentioned in Table 6.1, affect the

values of the optimum nanofluid volume fraction as well as the total cost. Section 6.5 investigates the effect of the economic factors.

6.5: Parametric Study of Economic Factors

A parametric study is carried out in order to investigate the effects of changing economic factors on the optimum nanofluids concentration and minimum total cost. This study is done by employing the half server with cooled plate having serpentine tube and by using Al_2O_3-water nanofluids as coolant.

Tables 6.5 to 6.10 summarise the results of the investigation. In general, the nominal values of the economic parameters are used as a datum for comparison with the results obtained by halving and doubling their values. For example, Table 6.5 compares the values calculated for optimum volume fraction (ϕ_{opt}) and minimum total cost by halving the cost of nanofluids from 24.2 £/kg to 12.1 £/kg, and by doubling the cost to 48.4 £/kg; this is done while keeping the rest of the economic parameters at their nominal values (see Table 6.1). After this is performed, the cost of the nanofluid is changed back to its nominal value and the effect of changing others parameters is investigated as shown in the next tables. This is repeated for the rest of the economic parameters noting that the middle row each table gives the results with the parameters set at their nominal values. It is also noted that the volume fraction would be the recommended optimum volume fraction (ϕ_{opt}) for the particular values of Reynolds numbers used, based on the minimal total cost; and the lowest minimum total cost would be the recommended value of all Reynolds numbers. For example, at the nominal economic parameter values, the optimum volume fraction of all considered Reynolds numbers 200, 300, 400, 500, 600 and 700 are 1.5, 0.0, 0.0, 0.0, 0.0 and 0.0 vol.% respectively; but, the lowest minimum total cost was £ 263.80; at Re = 600 and ϕ_{opt} = 0.0 vol.% (nanofluid is the base fluid, water).

It may be argued that by halving and doubling the nominal values of the economic parameters would give a wide range of values that may not be very realistic at the present time. However, it is believed that this would be quite useful to understand the effect of these economic parameters on optimum nanofluids volume fraction and minimum total cost. Also it is acceptable over a long span of time. Besides, the energy charge was

expected to increase from 2011 to 2021 by 88% from 7.8 to 14.7 p/kWh [144]; and with regard to the inflation rate and interest rate, the average value was taken because they were fluctuated over the previous ten years [136, 137]; see Figure 6.1.

The striking feature of the results summarized in Tables 6.5 to 6.10 are that the optimum volume fraction (ϕ_{opt}) and the corresponding minimum total cost substantially with the change in the economic parameters. While decreasing the cost of a nanofluid forces the optimum volume fraction (ϕ_{opt}) to increase, decreasing the cost of electricity has quite the opposite effect; see Tables 6.5 and 6.6. It is interesting to note that halving the cost of nanofluid, for example, and doubling the cost of electricity have the same effect on the optimum volume fraction (ϕ_{opt}). It is also interesting to note that by doubling nanofluid price and halving the cost of electricity, it is expected that using base fluid for all Reynolds number give the lowest minimum total cost. However, using the base fluid at Re 600 gives the greatest cost effectiveness.

With regard to the effect of changing the efficiency of pump, Table 6.7 shows that decreasing this value decreases the optimum volume fraction (ϕ_{opt}) with increasing the minimum total cost. It is interesting to note that increasing and decreasing the pump efficiency gives the minimum total cost with using base fluid (water) at Re = 700 and Re =500, respectively. From Table 6.8, it is clear that as the system lifetime decreases, the optimum volume fraction (ϕ_{opt}) decreases with similar effect on the minimum total cost and by doubling the system lifetime suggests that the optimum volume fraction increase but still using the base fluid at Re = 600 gives the same minimum total cost. It is also interesting to note that halving and doubling the cost of electricity, for example, and halving and doubling the system lifetime have the same effect on the optimum volume fraction (ϕ_{opt}) and the minimum total cost by halving and doubling the system lifetime is nearly the same that obtained by halving and doubling the cost of electricity.

It is noted that the effect of the inflation rate (r_i) on optimum volume fraction ϕ_{opt} is quite the opposite to that of the discount rate (r_d) as shown in Table 6.9 and Table 6.10. For example, if the inflation rate is expected to increase in the future, it is therefore wise to invest more money now on nanofluid.

It is clear that the changes can be affected by halving and doubling the values of the economic factors. Accordingly, the recommended application of nanofluids in practical applications should be looked upon with extreme care.

Table 6.5: Effect of change in the cost of nanofluid value on the optimum nanofluids volume fraction and minimum total cost for Al_2O_3-water nanofluids using the half server with cooled plate having serpentine tube.

C_{nf} (£/kg)	Re	ϕ_{opt} (vol%)	Minimum total cost (£)
12.1	200	3.5	264.83
	300	1.5	264.38
	400	0.5	264.04
	500	0.0	263.87
	600	0.0	263.80*
	700	0.0	263.82
24.2	200	1.5	265.45
	300	0.0	264.56
	400	0.0	264.08
	500	0.0	263.87
	600	0.0	263.80*
	700	0.0	263.82
48.4	200	0.0	265.69
	300	0.0	264.56
	400	0.0	264.08
	500	0.0	263.87
	600	0.0	263.80*
	700	0.0	263.82

* The lowest minimum total cost

Table 6.6: Effect of change in the cost of electricity value on the optimum nanofluids volume fraction and minimum total cost for Al_2O_3-water nanofluids using two tubes heat sink configuration

c_e (£/kWh)	Re	ϕ_{opt} (vol%)	Minimum total cost (£)
0.055	200	0.0	132.86
	300	0.0	132.30
	400	0.0	132.06
	500	0.0	131.96
	600	0.0	131.92*
	700	0.0	131.93
0.11	200	1.5	265.45
	300	0.0	264.56
	400	0.0	264.08
	500	0.0	263.87
	600	0.0	263.80*
	700	0.0	263.82
0.22	200	3.5	529.66
	300	1.5	528.75
	400	0.5	528.09
	500	0.0	527.70
	600	0.0	527.56*
	700	0.0	527.59

* The lowest minimum total cost

Table 6.7: Effect of change in the pump efficiency values on the optimum nanofluids volume fraction and minimum total cost for Al_2O_3-water nanofluids using two tubes heat sink configuration

P_p (%)	Re	ϕ_{opt} (vol%)	Minimum total cost (£)
50	200	1.0	265.93
	300	0.0	265.10
	400	0.0	264.81
	500	0.0	264.78*
	600	0.0	264.89
	700	0.0	265.09
85	200	1.5	265.45
	300	0.0	264.56
	400	0.0	264.08
	500	0.0	263.87
	600	0.0	263.80*
	700	0.0	263.82
100	200	1.5	265.34
	300	0.0	264.44
	400	0.0	263.93
	500	0.0	263.67
	600	0.0	263.57
	700	0.0	263.54*

* The lowest minimum total cost

Table 6.8: Effect of change in the system lifetime value on the optimum nanofluids volume fraction and minimum total cost for Al_2O_3-water nanofluids using two tubes heat sink configuration

m (year)	Re	ϕ_{opt} (vol%)	Minimum total cost (£)
1.5	200	0.0	133.54
	300	0.0	132.97
	400	0.0	132.73
	500	0.0	132.63
	600	0.0	132.59*
	700	0.0	132.60
3	200	1.5	265.45
	300	0.0	264.56
	400	0.0	264.08
	500	0.0	263.87
	600	0.0	263.80*
	700	0.0	263.82
6	200	3.0	524.34
	300	1.5	523.43
	400	0.5	522.77
	500	0.0	522.37
	600	0.0	522.24*
	700	0.0	522.27

* The lowest minimum total cost

Table 6.9: Effect of change in inflation rate value on the optimum nanofluids volume fraction and minimum total cost for Al_2O_3-water nanofluids using two tubes heat sink configuration

r_i(%)	Re	ϕ_{opt} (vol%)	Minimum total cost (£)
1.35	200	1.5	279.58
	300	0.0	278.68
	400	0.0	278.18
	500	0.0	277.95
	600	0.0	277.88*
	700	0.0	277.90
2.7	200	1.5	265.45
	300	0.0	264.56
	400	0.0	264.08
	500	0.0	263.87
	600	0.0	263.80*
	700	0.0	263.82
5.4	200	1.5	258.57
	300	0.0	257.68
	400	0.0	257.22
	500	0.0	257.01
	600	0.0	256.94*
	700	0.0	256.96

* The lowest minimum total cost

Table 6.10: Effect of change in the discount rate value on the optimum nanofluids volume fraction and minimum total cost for Al_2O_3-water nanofluids using two tubes heat sink configuration

r_d(%)	Re	ϕ_{opt} (vol%)	Minimum total cost (£)
1.7	200	1.5	274.38
	300	0.0	273.48
	400	0.0	272.99
	500	0.0	272.77
	600	0.0	272.70*
	700	0.0	272.71
3.4	200	1.5	265.45
	300	0.0	264.56
	400	0.0	264.08
	500	0.0	263.87
	600	0.0	263.80*
	700	0.0	263.82
6.8	200	1.5	248.99
	300	0.0	248.11
	400	0.0	247.66
	500	0.0	247.46
	600	0.0	247.40*
	700	0.0	247.41

* The lowest minimum total cost

6.6: Concluding Remarks

The variations of temperature and pressure drop with a nanofluid concentration (volume fraction) and Reynolds number under steady state conditions were calculated using the finite element solver program (COMSOL). These characteristics were then used in an economic analysis model in order to calculate and optimise the total cost versus the volume fraction of the nanofluids. The optimum volume fraction was determined for three types of nanofluids (Al_2O_3-water nanofluids, TiO_2-water nanofluids and CuO-water nanofluids) and each was used in two different cooled plate configurations of half of a server, as described in chapter 5 (Figure 5.2). By plotting the sum of the cost of a nanofluid as a function of volume fraction and the present value of energy consumption the chip and pump and cooling system over the lifetime of the system versus the volume fraction of each type nanofluid, the optimum volume fraction was determined at the lowest minimum total cost for a particular Reynolds number.

In terms of cost effectiveness for the values of the economic factors used, pure water at Re = 200 was shown to be the most cost effective for the half server with cooled plate having two parallel tubes at £ 262.76. Whereas, using the base fluid (water) at Re = 600 in the half server with cooled plate having serpentine tube configuration was found to be the most cost effective at £ 263.80. It is interesting to note that the half server with cooled plate having two parallel tubes gives lower cost effectiveness than the half server with cooled plate having serpentine tube, however, the clockspeed for the CPU of the half server with cooled plate having serpentine tube is higher than the CPU of the half server with cooled plate having two parallel tubes. It means that if the CPU of the half server with cooled plate having two parallel tubes is running at the same clockspeed will consume more power. The minimum total cost and optimum volume fraction was a function of the cost and thermophysical properties of the nanofluid, its intended application as well as other economic factors (see Table 6.1).

CHAPTER 7: CONCLUSIONS AND FUTURE WORK

CONCLUSIONS

In this study, an evaluation of the thermal performance and pressure drop of common nanofluids in electronics cooling applications was carried out and the feasibility of using nanofluids to cool a data centre were investigated with the aim of determining the optimum volume fraction of each nanofluid.

The dynamic viscosity of some commonly used nanofluid (Al_2O_3, TiO_2 and CuO water nanofluids) by researchers was measured by using the rotational rheometer called the Malvern Kinexus Pro rheometer. The results of the measurements showed that:

- The viscosity of the nanofluid was strongly dependant on the temperature, volume fraction and type of nanoparticle and that viscosity increased with increasing nanofluid volume fractions but decreased with increasing temperature.

- The relative viscosity of all nanofluids tested is a function of the volume fraction and its type over the volume fraction and temperature range considered in the study and it was observed that the viscosity of Al_2O_3-water nanofluids was highest when compared to other nanofluids with similar volume fractions.

- The new correlation of the viscosity measurement data was developed and used for comparison with literature values. The measured values of dynamic viscosity for Al_2O_3 nanofluids were in good agreement with previous empirical claimed values.

- When comparing the nanofluids tested viscosity with previous experimental studies, the viscosity of the nanofluid with smaller nanoparticle sizes is higher than the nanofluids with large nanoparticle sizes.

- A large difference was found when comparing the theoretical correlations, all of which greatly underestimated the experimental values.

- All tested nanofluids were found to behave as a Newtonian fluid over the volume fractions and temperature range considered in this investigation.

The heat transfer coefficient and pressure drop of the above nanofluids were investigated experimentally. This used a closed loop of circular tube with forced convection heat transfer within the turbulent regime under constant heat flux. It was found that:

- Evaluating heat transfer coefficient by the popular approach of considering the Nusselt number versus Reynolds number is misleading, and creates the impression that, at least for Al_2O_3-water nanofluid, heat transfer is enhanced by using the nanofluid. The problem is that both Nu and Re are dependent on the nanoparticle load.

- The most significant result of this experiment is that using a nanofluid decreased the actual heat transfer rate and this deterioration increased with increasing nanoparticles load.

- The heat transfer coefficient increases with increasing flow rate, however, it decreases with increasing volume fraction. At a constant flow rate, the base fluid (water) gave the highest heat transfer coefficient with respect to the nanofluids. With regard to the pressure drop of nanofluids, it increases significantly with increasing flow rate and nanofluid concentration.

- Nusselt number and pressure drop increased monotonically with increasing Reynolds number and volume fraction, but the pressure drop increased significantly. At constant Reynolds number, the nanofluid showed better Nusselt number, but it cost more energy to pumping the fluid to achieve the same Reynolds number.

- The thermal performance of Al_2O_3-water nanofluids was higher when compared to the other nanofluids and this is attributed to the fact that the Al_2O_3 nanoparticle has highest the thermal conductivity.

- A comparison with the existing nanofluid Nusselt number correlations was made and showed that the Pak and Cho [23] correlation estimated the Nusselt number of Al_2O_3-water nanofluids with an agreement of within 5%.

- It is worth mentioning that by using the properties of nanofluid the existing conventional correlation of single phase could predict the heat transfer coefficient and the pressure drop.

A computer program (COMSOL) which is based on the finite element method was used to calculate the variation of temperature across a CPU chip surface and the pressure drop across the cooled plate with volume fraction of the above nanofluids through two different half servers; one with a cooled plate which has a two parallel tubes and another with a cooled plate which has a serpentine tube. Both half servers use an immersion design created by Iceotope. The variations of the chip temperature and cooled plate pressure drop of typical nanofluid with different volume fractions and Reynolds number of each server was calculated under steady state conditions. The results of the calculations for both servers showed that:

- The server's cooled plates with parallel flow (when the inlet flow is from the top to the bottom) gave better thermal performance than the counter flow.

- The average temperature of chip decreased monotonically with increasing Reynolds number of the cooled plate and the volume fraction of nanofluid.

- The pressure drop of both cooled plates increased monotonically with increasing Reynolds number and volume fraction.

- The thermal performance of nanofluids depends on the nanofluids thermal properties, for example a higher thermal conductivity of Al_2O_3-water nanofluids gave better thermal performance when compared to TiO_2-water and CuO-water nanofluids for both half servers.

The variation of chip temperatures and cooled plate pressure drop with nanofluids volume fraction were used in an economic analysis in order to find the optimum volume fraction,

which corresponded to the minimum total cost. By plotting the sum of the cost of nanofluid as a function of the volume fraction and the present value of power consumption of the chip, pump and cooling system over the lifetime of the system versus the volume fraction of each type nanofluid, the optimum volume fraction was determined at the point of minimum total cost for a particular Reynolds number. Under the economic factors used it was shown that:

- The most cost effective conditions were using a base fluid (water) at Re = 200 for the half server with cooled plate having two parallel tubes. Whereas, it was the base fluid (water) at Re = 600 for the half server with cooled plate having serpentine tube.

- This cost effectiveness was highly affected by the cost and the properties of nanofluid and also other economic parameters such as the cost of energy and lifetime of the application. Therefore, it should be emphasized that had different thermal properties and costs been used for the different types of nanofluids the cost effectiveness would have been significantly affected.

- It is interesting to note that the half server with cooled plate having serpentine tube has higher thermal performance than the half server with cooled plate having two parallel tubes according to the clockspeed of the CPU. Therefore, the cost effectiveness depend upon the type of application the cost as well.

- Properties such as such as erosion and corrosion were not taken into consideration in the present evaluation.

- Based on, the parameters study and the assumption considered in this thesis, using nanofluid in the immersion cooling server is probably not economical.

FUTURE WORK

Following on from this study, future work should include:

- There is a need to perform more systematic and detailed measurements of properties such as the thermal conductivity and viscosity of nanofluids since there is no consistent method in the literature for determining and calculating these values. Future studies should investigate the effects of different nanoparticles, particular type of nanofluid especially on the nanofluid viscosity and thermal conductivity, since adding nanoparticles enhance both the heat transfer and increase the pressure drop.

- Other nanofluid properties and specifically tribological effects such as erosion and corrosion could be very important, depending upon the intended application (i.e. nuclear power); studies should aim to characterise and minimise their adverse effects.

- Further experimental and numerical analyses are needed to investigate the heat transfer performance and the flow characteristics of the pressure drop of nanofluids under laminar and turbulent regimes. The practical application of nanofluids should also be examined further with the objective of minimizing their adverse effects.

- The economic analysis of using nanofluids should be expanded to include other factors such as the cost of nanofluid adverse effects (i.e. erosion and corrosion)

- Further experimental and numerical analysis is needed to investigate the optimum volume fraction of different nanofluids and recommend nanofluid for specific applications.

- There is a need to perform more systematic work on specific applications where the thermal performance of a nanofluid is more significant than the pressure drop.

- Further investigation should be conducted investigating the effect of the geometry of the cooled plate using nanofluids [145]. By changing the flow behaviour of the nanofluid across the cooled plate to achieve a design with optimum heat transfer.

- The cost of a nanofluid is a function of mass fraction or volume fraction, which must be calculated since the suppliers provide the nanofluid at one high concentration. It is suggested that the nanofluid cost (C_{nf}) should consider the cost of a nanofluid as combination of three components; the cost of base fluid (C_{bf}), the cost of nanoparticles (C_p) as a function of mass fraction or volume fraction and the cost of preparing the nanofluid (C_{pre}).

  $$C_{nf} = C_{bf} + \phi C_p + C_{pre}.$$

- Further study should establish the viability of using nanoparticles in a dielectric liquid as it should be investigated at which fraction and particle type causes the fluid to begin to conduct electricity.

- Further investigation is needed to utilise nanofluids within a data centre since there are many cooling techniques, which could use nanofluids instead of traditional cooling liquids such as on-chip liquid cooling or rear door rack liquid cooling systems.

APPENDICES

APPENDIX (A):

RAW DATA OF THE NANOFLUIDS VISCOSITY TESTS

The measuring of the viscosity of all nanofluids (Al_2O_3-water TiO_2-water and CuO-water nanofluid) at atmospheric pressure and different mean temperatures in the range 15 to 40 ^oC was conducted. The measurements were carried out for three specimens of each test sample of the nanofluids. The viscosity was measured for each specimen then the mean values of viscosity were obtained by averaging; see Tables A1 to A3.

Table A 1: Measurement average viscosity of Al_2O_3-water nanofluid for various temperatures and volume fractions

Al_2O_3 nanofluid volume fraction	Temperature (°C)	Averaging viscosity (Pa.s)	Standard deviation	Discrepancy (%)
0.5 vol%	15	0.00130	4.5680×10^{-5}	3.53
	20	0.00116	4.0399×10^{-5}	3.47
	25	0.00106	4.2937×10^{-5}	4.06
	30	0.00095	4.3818×10^{-5}	4.63
	35	0.00084	4.6666×10^{-5}	5.56
	40	0.00075	5.0020×10^{-5}	6.66
0.9 vol%	15	0.00144	5.1571×10^{-5}	3.57
	20	0.00129	4.2604×10^{-5}	3.30
	25	0.00117	4.3243×10^{-5}	3.68
	30	0.00106	4.6421×10^{-5}	4.40
	35	0.00094	4.7816×10^{-5}	5.07
	40	0.00085	4.13675×10^{-5}	4.90
1.8 vol%	15	0.00182	10.1579×10^{-5}	5.59
	20	0.00162	6.60387×10^{-5}	4.08
	25	0.00146	4.50829×10^{-5}	3.09
	30	0.00132	4.74005×10^{-5}	3.58
	35	0.00118	5.68007×10^{-5}	4.83
	40	0.00105	5.42866×10^{-5}	5.16
2.7 vol%	15	0.00219	5.89628×10^{-5}	2.70
	20	0.00195	5.04856×10^{-5}	2.58
	25	0.00177	4.46652×10^{-5}	2.52
	30	0.00160	4.25924×10^{-5}	2.65
	35	0.00145	4.46177×10^{-5}	3.08
	40	0.00131	4.92458×10^{-5}	3.76
3.6 vol%	15	0.00286	6.33813×10^{-5}	2.21
	20	0.00255	5.24546×10^{-5}	2.06
	25	0.00231	4.76655×10^{-5}	2.07
	30	0.00211	4.33474×10^{-5}	2.06
	35	0.00192	4.10906×10^{-5}	2.14
	40	0.00175	4.46296×10^{-5}	2.54
4.7 vol%	15	0.00524	19.1512×10^{-5}	3.65
	20	0.00467	9.45604×10^{-5}	2.02
	25	0.00428	8.23931×10^{-5}	1.92
	30	0.00398	7.24793×10^{-5}	1.82
	35	0.00375	5.7016×10^{-5}	1.52
	40	0.00359	5.06364×10^{-5}	1.41
5.9 vol%	15	0.00625	24.7169×10^{-5}	3.96
	20	0.00550	13.2237×10^{-5}	2.40
	25	0.00497	10.8867×10^{-5}	2.19
	30	0.00456	9.17028×10^{-5}	2.01
	35	0.00427	9.50113×10^{-5}	2.23
	40	0.00408	14.1684×10^{-5}	3.47

Table A 2: Measurement average viscosity of TiO_2-water nanofluid for various temperatures and volume fractions

TiO_2 nanofluid volume fraction	Temperature (°C)	Averaging viscosity (Pa.s)	Standard deviation	Discrepancy (%)
0.5 vol%	15	0.001324	4.3754×10^{-5}	3.30
	20	0.001186	3.7475×10^{-5}	3.16
	25	0.001071	3.9274×10^{-5}	3.67
	30	0.000968	3.7909×10^{-5}	3.92
	35	0.000878	3.4509×10^{-5}	3.93
	40	0.000797	4.0784×10^{-5}	5.12
1.5 vol%	15	0.001666	5.0022×10^{-5}	3.00
	20	0.001479	4.3351×10^{-5}	2.93
	25	0.001317	3.9264×10^{-5}	2.98
	30	0.001185	3.9049×10^{-5}	3.30
	35	0.001071	4.1643×10^{-5}	3.89
	40	0.000966	4.6140×10^{-5}	4.78
2.5 vol%	15	0.00199	6.4614×10^{-5}	3.25
	20	0.001766	6.0530×10^{-5}	3.43
	25	0.001576	6.2641×10^{-5}	3.98
	30	0.00141	5.9982×10^{-5}	4.25
	35	0.001272	5.2440×10^{-5}	4.12
	40	0.001146	5.4301×10^{-5}	4.74
3.5 vol%	15	0.00239	6.5989×10^{-5}	2.76
	20	0.002108	5.7878×10^{-5}	2.75
	25	0.001868	5.2334×10^{-5}	2.80
	30	0.001673	4.4541×10^{-5}	2.66
	35	0.001526	4.1130×10^{-5}	2.70
	40	0.00141	4.1311×10^{-5}	2.93
4.5 vol%	15	0.00278	8.3520×10^{-5}	3.00
	20	0.002437	6.6829×10^{-5}	2.74
	25	0.002155	6.0635×10^{-5}	2.81
	30	0.001926	5.2110×10^{-5}	2.71
	35	0.001746	4.9682×10^{-5}	2.85
	40	0.001591	5.1017×10^{-5}	3.21

Table A 3: Measurement average viscosity of CuO-water nanofluid for various temperatures and volume fractions

CuO nanofluid volume fraction	Temperature (°C)	Averaging viscosity (Pa.s)	Standard deviation	Discrepancy (%)
0.4 vol%	15	0.001192	4.6482×10^{-5}	3.90
	20	0.001069	4.2914×10^{-5}	4.01
	25	0.000959	4.3493×10^{-5}	4.54
	30	0.00086	4.0576×10^{-5}	4.72
	35	0.000775	3.7944×10^{-5}	4.89
	40	0.000693	4.7935×10^{-5}	6.92
0.8 vol%	15	0.001282	4.7129×10^{-5}	3.68
	20	0.001147	4.1226×10^{-5}	3.59
	25	0.00103	4.3828×10^{-5}	4.25
	30	0.000928	4.1125×10^{-5}	4.43
	35	0.000834	3.8395×10^{-5}	4.61
	40	0.000739	4.2342×10^{-5}	5.73
1.2 vol%	15	0.001358	6.0440×10^{-5}	4.45
	20	0.001218	5.4451×10^{-5}	4.47
	25	0.001094	5.8497×10^{-5}	5.35
	30	0.000991	6.0399×10^{-5}	6.10
	35	0.000904	7.6978×10^{-5}	8.51
	40	0.0008	8.0639×10^{-5}	10.08
1.6 vol%	15	0.001511	4.8078×10^{-5}	3.18
	20	0.001349	4.1649×10^{-5}	3.09
	25	0.001214	4.3990×10^{-5}	3.62
	30	0.001097	4.6525×10^{-5}	4.24
	35	0.000981	4.2572×10^{-5}	4.34
	40	0.000874	4.4547×10^{-5}	5.10

APPENDIX (B):

RAW DATA OF THE CONVECTION TESTS

The raw data of the convection test is presented in this section. The measurements were carried out firstly on water for one specimen and repeated the test three times, then, the mean values of the results were obtained by averaging. The inlet bulk temperature of the test section was maintained at around 20 $^{\circ}$C and the uniform heat generation at about 5000W and the flow rate was changed from 0.75 to 2.0 GPM (gallon per minute) (i.e. 5×10^{-5} to 0.00013 m^3/s). The similar conditions of the test conducted for all nanofluids (Al_2O_3-water TiO_2-water and CuO-water nanofluid) and for each concentration of nanofluid for comparison. The data is present below in Tables A4 to A21

Table A 4: Convection test of distilled water test

Measured items	Runs distilled water for flow rate (gpm)					
	0.75	1.0	1.25	1.5	1.75	2.0
Inlet temp. of the heated test-section [° C]	21.00	20.59	20.25	20.16	20.34	20.35
Outlet temp. of the heated test-section [°C]	43.74	38.63	34.90	32.38	30.81	29.42
Inlet temp. of the isothermal test-sect. [°C]	18.94	18.96	18.94	19.11	19.47	19.64
0.203m, Surface thermocouple 1 [°C]	39.07	35.86	33.62	32.15	31.25	30.36
Surface thermocouple 2 [°C]	40.19	36.78	34.40	32.81	31.82	30.85
Surface thermocouple 3 [°C]	41.37	37.77	35.22	33.50	32.42	31.38
Surface thermocouple 4 [°C]	42.58	38.74	35.99	34.14	32.98	31.86
Surface thermocouple 5 [°C]	43.89	39.77	36.85	34.86	33.59	32.40
Surface thermocouple 6 [°C]	45.28	40.90	37.75	35.62	34.24	32.96
Surface thermocouple 7 [°C]	46.60	41.96	38.62	36.35	34.87	33.51
Surface thermocouple 8 [°C]	47.43	42.62	39.15	36.78	35.23	33.82
Surface thermocouple 9 [°C]	49.01	43.90	40.20	37.67	36.00	34.50
Surface thermocouple 10 [°C]	50.52	45.12	41.20	38.50	36.72	35.13
Surface thermocouple 11 [°C]	51.79	46.13	42.02	39.19	37.31	35.64
Surface thermocouple 12 [°C]	53.20	47.27	42.96	39.98	37.99	36.23
Surface thermocouple 13 [°C]	54.42	48.26	43.75	40.64	38.55	36.72
2.842m, Surface thermocouple 14 [°C]	55.79	49.36	44.65	41.39	39.21	37.29
Voltage [V]	14.70	14.70	14.70	14.70	14.70	14.70
Current [Amp]	337.40	337.40	337.40	337.40	337.40	337.40
Vol. flow rate at inlet of the heated test-sect. [gal/min]	0.79	1.03	1.26	1.51	1.75	2.04
DP heated test-section [bar]	0.0338	0.0494	0.0703	0.0948	0.1226	0.1565
DP isothermal test-section [bar]	0.0286	0.0437	0.0641	0.0885	0.1156	0.1488

Table A 5: Convection test of AL_2O_3 (0.5 vol%) nanofluid test

Measured items	Runs Al_2O_3 (0.5 vol%)for flow rate (gpm)					
	0.75	1.0	1.25	1.5	1.75	2.0
Inlet temp. of the heated test-section [° C]	19.82	19.67	19.43	19.96	19.37	19.74
Outlet temp. of the heated test-section [°C]	41.84	37.27	33.88	32.29	29.64	28.77
Inlet temp. of the isothermal test-sect. [°C]	17.79	18.07	18.11	18.87	18.46	18.98
0.203m, Surface thermocouple 1 [°C]	38.47	35.51	33.24	32.32	30.44	29.94
Surface thermocouple 2 [°C]	39.54	36.38	33.98	32.97	30.98	30.42
Surface thermocouple 3 [°C]	40.61	37.31	34.76	33.65	31.56	30.94
Surface thermocouple 4 [°C]	41.68	38.19	35.50	34.28	32.10	31.41
Surface thermocouple 5 [°C]	42.85	39.16	36.32	34.99	32.69	31.94
Surface thermocouple 6 [°C]	44.13	40.21	37.19	35.74	33.31	32.48
Surface thermocouple 7 [°C]	45.36	41.21	38.04	36.48	33.94	33.04
Surface thermocouple 8 [°C]	46.00	41.73	38.46	36.83	34.23	33.29
Surface thermocouple 9 [°C]	47.59	43.05	39.56	37.80	35.05	34.02
Surface thermocouple 10 [°C]	49.02	44.21	40.53	38.63	35.74	34.63
Surface thermocouple 11 [°C]	50.22	45.19	41.34	39.33	36.32	35.15
Surface thermocouple 12 [°C]	51.58	46.27	42.25	40.12	36.99	35.75
Surface thermocouple 13 [°C]	52.73	47.21	43.02	40.78	37.54	36.23
2.842m, Surface thermocouple 14 [°C]	54.05	48.27	43.91	41.53	38.18	36.79
Voltage [V]	14.70	14.70	14.70	14.70	14.70	14.70
Current [Amp]	333.60	333.60	333.60	333.60	333.60	333.60
Vol. flow rate at inlet of the heated test-sect. [gal/min]	0.79	1.03	1.26	1.48	1.77	2.03
DP heated test-section [bar]	0.0334	0.0503	0.0714	0.0937	0.1291	0.1613
DP isothermal test-section [bar]	0.0295	0.0458	0.0664	0.0883	0.1228	0.1542

Table A 6: Convection test of Al_2O_3 (0.9 vol%) nanofluid test

Measured items	Runs Al_2O_3 (0.9 vol%) for flow rate (gpm)					
	0.75	1.0	1.25	1.5	1.75	2.0
Inlet temp. of the heated test-section [° C]	20.91	20.67	20.37	20.27	19.99	20.14
Outlet temp. of the heated test-section [°C]	43.86	38.92	35.13	32.48	30.35	29.33
Inlet temp. of the isothermal test-sect. [°C]	18.74	18.97	18.99	19.13	19.04	19.34
0.203m, Surface thermocouple 1 [°C]	40.43	37.15	34.55	32.76	31.25	30.56
Surface thermocouple 2 [°C]	41.53	38.05	35.31	33.40	31.79	31.05
Surface thermocouple 3 [°C]	42.65	39.00	36.11	34.08	32.38	31.58
Surface thermocouple 4 [°C]	43.76	39.92	36.86	34.71	32.92	32.05
Surface thermocouple 5 [°C]	44.97	40.93	37.70	35.41	33.52	32.60
Surface thermocouple 6 [°C]	46.31	42.01	38.60	36.16	34.15	33.15
Surface thermocouple 7 [°C]	47.59	43.03	39.45	36.87	34.78	33.72
Surface thermocouple 8 [°C]	48.32	43.63	39.92	37.27	35.11	34.00
Surface thermocouple 9 [°C]	49.87	44.91	40.98	38.17	35.89	34.70
Surface thermocouple 10 [°C]	51.36	46.13	41.98	39.00	36.59	35.33
Surface thermocouple 11 [°C]	52.62	47.12	42.80	39.68	37.17	35.85
Surface thermocouple 12 [°C]	54.01	48.26	43.73	40.46	37.85	36.45
Surface thermocouple 13 [°C]	55.22	49.23	44.51	41.11	38.40	36.94
2.842m, Surface thermocouple 14 [°C]	56.57	50.31	45.41	41.86	39.04	37.51
Voltage [V]	14.80	14.80	14.80	14.80	14.80	14.80
Current [Amp]	337.60	337.60	337.60	337.60	337.60	337.60
Vol. flow rate at inlet of the heated test-sect. [gal/min]	0.75	1.01	1.25	1.50	1.76	1.99
DP heated test-section [bar]	0.0354	0.0522	0.0745	0.1022	0.1347	0.1654
DP isothermal test-section [bar]	0.0302	0.0465	0.0682	0.0951	0.1266	0.1560

Table A 7: Convection test of Al_2O_3 (1.8 vol%) nanofluid test

Measured items	Runs Al_2O_3 (1.8 vol%) for flow rate (gpm)					
	0.75	1.0	1.25	1.5	1.75	2.0
Inlet temp. of the heated test-section [° C]	20.28	20.33	20.16	20.10	20.08	20.02
Outlet temp. of the heated test-section [°C]	43.66	39.42	35.11	32.34	30.64	29.30
Inlet temp. of the isothermal test-sect. [°C]	17.99	18.49	18.71	18.89	19.07	19.15
0.203m, Surface thermocouple 1 [°C]	41.56	38.57	35.41	33.41	32.14	31.13
Surface thermocouple 2 [°C]	42.63	39.47	36.18	34.04	32.68	31.60
Surface thermocouple 3 [°C]	43.64	40.40	36.95	34.70	33.27	32.13
Surface thermocouple 4 [°C]	44.71	41.31	37.69	35.31	33.81	32.61
Surface thermocouple 5 [°C]	45.88	42.31	38.50	36.01	34.41	33.15
Surface thermocouple 6 [°C]	47.16	43.41	39.40	36.75	35.05	33.71
Surface thermocouple 7 [°C]	48.42	44.45	40.25	37.46	35.68	34.27
Surface thermocouple 8 [°C]	49.11	45.02	40.70	37.83	36.00	34.54
Surface thermocouple 9 [°C]	50.64	46.32	41.76	38.73	36.78	35.24
Surface thermocouple 10 [°C]	52.13	47.58	42.76	39.56	37.50	35.88
Surface thermocouple 11 [°C]	53.35	48.59	43.56	40.21	38.08	36.39
Surface thermocouple 12 [°C]	54.72	49.72	44.48	40.98	38.75	36.99
Surface thermocouple 13 [°C]	55.90	50.71	45.26	41.63	39.31	37.48
2.842m, Surface thermocouple 14 [°C]	57.23	51.82	46.15	42.37	39.95	38.05
Voltage [V]	14.80	14.80	14.80	14.80	14.80	14.80
Current [Amp]	337.50	337.50	337.50	337.50	337.50	337.50
Vol. flow rate at inlet of the heated test-sect. [gal/min]	0.74	0.98	1.25	1.51	1.75	2.00
DP heated test-section [bar]	0.0372	0.0524	0.0789	0.1102	0.1413	0.1756
DP isothermal test-section [bar]	0.0332	0.0482	0.0739	0.1039	0.1341	0.1671

Table A 8: Convection test of Al_2O_3 (2.7 vol%) nanofluid test

Measured items	Runs Al_2O_3 (2.7 vol%) for flow rate (gpm)					
	0.75	1.0	1.25	1.5	1.75	2.0
Inlet temp. of the heated test-section [° C]	20.06	19.99	19.99	20.44	20.00	20.14
Outlet temp. of the heated test-section [°C]	43.43	38.93	35.21	32.97	30.75	29.55
Inlet temp. of the isothermal test-sect. [°C]	17.72	18.09	18.41	19.21	18.95	19.25
0.203m, Surface thermocouple 1 [°C]	43.62	39.64	36.55	34.67	32.82	31.83
Surface thermocouple 2 [°C]	44.67	40.57	37.27	35.30	33.36	32.31
Surface thermocouple 3 [°C]	45.51	41.36	38.01	35.96	33.94	32.83
Surface thermocouple 4 [°C]	46.51	42.27	38.75	36.56	34.48	33.30
Surface thermocouple 5 [°C]	47.61	43.18	39.53	37.24	35.08	33.84
Surface thermocouple 6 [°C]	48.76	44.22	40.43	38.01	35.73	34.41
Surface thermocouple 7 [°C]	49.92	45.25	41.28	38.73	36.35	34.97
Surface thermocouple 8 [°C]	50.50	45.70	41.65	39.03	36.62	35.20
Surface thermocouple 9 [°C]	51.99	46.99	42.74	39.97	37.43	35.93
Surface thermocouple 10 [°C]	53.48	48.22	43.76	40.82	38.17	36.59
Surface thermocouple 11 [°C]	54.66	49.21	44.55	41.48	38.75	37.09
Surface thermocouple 12 [°C]	55.95	50.29	45.46	42.26	39.43	37.70
Surface thermocouple 13 [°C]	57.08	51.25	46.23	42.90	39.99	38.19
2.842m, Surface thermocouple 14 [°C]	58.40	52.33	47.14	43.66	40.64	38.76
Voltage [V]	14.80	14.80	14.80	14.80	14.80	14.80
Current [Amp]	337.20	337.20	337.20	337.20	337.20	337.20
Vol. flow rate at inlet of the heated test-sect. [gal/min]	0.76	1.00	1.25	1.51	1.75	2.01
DP heated test-section [bar]	0.0379	0.0550	0.0805	0.1121	0.1463	0.1837
DP isothermal test-section [bar]	0.0343	0.0513	0.0762	0.1069	0.1395	0.1752

Table A 9: Convection test of Al_2O_3 (3.6 vol%) nanofluid test

Measured items	Runs Al_2O_3 (3.6 vol%) for flow rate (gpm)					
	0.75	1.0	1.25	1.5	1.75	2.0
Inlet temp. of the heated test-section [° C]	20.60	20.73	20.77	20.70	20.59	20.32
Outlet temp. of the heated test-section [°C]	44.20	39.76	35.96	32.95	31.24	29.34
Inlet temp. of the isothermal test-sect. [°C]	18.20	18.79	19.20	19.45	19.49	19.34
0.203m, Surface thermocouple 1 [°C]	46.11	41.65	38.12	35.50	33.94	32.25
Surface thermocouple 2 [°C]	47.03	42.52	38.82	36.06	34.45	32.67
Surface thermocouple 3 [°C]	47.71	43.26	39.54	36.65	34.99	33.14
Surface thermocouple 4 [°C]	48.65	44.11	40.25	37.26	35.53	33.60
Surface thermocouple 5 [°C]	49.65	45.00	41.02	37.91	36.13	34.10
Surface thermocouple 6 [°C]	50.80	46.00	41.88	38.62	36.76	34.64
Surface thermocouple 7 [°C]	51.89	46.98	42.72	39.30	37.36	35.17
Surface thermocouple 8 [°C]	52.43	47.41	43.07	39.58	37.59	35.36
Surface thermocouple 9 [°C]	53.87	48.66	44.12	40.48	38.40	36.06
Surface thermocouple 10 [°C]	55.27	49.85	45.14	41.31	39.13	36.68
Surface thermocouple 11 [°C]	56.43	50.82	45.91	41.94	39.67	37.14
Surface thermocouple 12 [°C]	57.68	51.90	46.80	42.69	40.33	37.72
Surface thermocouple 13 [°C]	58.79	52.83	47.56	43.32	40.89	38.20
2.842m, Surface thermocouple 14 [°C]	60.11	53.94	48.48	44.09	41.56	38.79
Voltage [V]	14.80	14.80	14.80	14.80	14.80	14.80
Current [Amp]	337.40	337.40	337.40	337.40	337.40	337.40
Vol. flow rate at inlet of the heated test-sect. [gal/min]	0.73	1.00	1.25	1.53	1.76	2.06
DP heated test-section [bar]	0.0399	0.0593	0.0867	0.1232	0.1560	0.2034
DP isothermal test-section [bar]	0.0359	0.0540	0.0806	0.1160	0.1472	0.1924

Table A 10: Convection test of Al_2O_3 (4.7 vol%) nanofluid test

Measured items	Runs Al_2O_3 (4.7 vol%) for flow rate (gpm)					
	0.75	1.0	1.25	1.5	1.75	2.0
Inlet temp. of the heated test-section [° C]	20.00	19.88	19.91	19.97	19.91	20.03
Outlet temp. of the heated test-section [°C]	43.78	39.27	35.42	32.72	30.75	29.60
Inlet temp. of the isothermal test-sect. [°C]	17.52	17.86	18.32	18.67	18.83	19.09
0.203m, Surface thermocouple 1 [°C]	51.13	45.49	40.39	37.18	34.99	33.75
Surface thermocouple 2 [°C]	54.54	46.20	41.12	37.82	35.52	34.21
Surface thermocouple 3 [°C]	54.49	46.64	41.62	38.32	36.04	34.68
Surface thermocouple 4 [°C]	54.16	47.32	42.29	38.92	36.56	35.14
Surface thermocouple 5 [°C]	54.59	48.10	43.02	39.53	37.10	35.63
Surface thermocouple 6 [°C]	55.09	48.95	43.75	40.22	37.70	36.19
Surface thermocouple 7 [°C]	55.80	49.73	44.55	40.92	38.33	36.76
Surface thermocouple 8 [°C]	56.11	50.02	44.81	41.15	38.54	36.93
Surface thermocouple 9 [°C]	57.21	51.12	45.80	42.02	39.30	37.63
Surface thermocouple 10 [°C]	58.41	52.20	46.77	42.88	40.05	38.32
Surface thermocouple 11 [°C]	59.48	53.15	47.54	43.51	40.59	38.80
Surface thermocouple 12 [°C]	60.61	54.13	48.37	44.25	41.24	39.38
Surface thermocouple 13 [°C]	61.42	54.92	49.07	44.84	41.76	39.85
2.842m, Surface thermocouple 14 [°C]	62.68	55.95	49.94	45.59	42.40	40.42
Voltage [V]	14.80	14.80	14.80	14.80	14.80	14.80
Current [Amp]	337.20	337.20	337.20	337.20	337.20	337.20
Vol. flow rate at inlet of the heated test-sect. [gal/min]	0.74	0.99	1.24	1.50	1.76	2.01
DP heated test-section [bar]	0.0398	0.0587	0.0877	0.1280	0.1705	0.2110
DP isothermal test-section [bar]	0.0405	0.0614	0.0906	0.1261	0.1661	0.2042

Table A 11: Convection test of Al_2O_3 (5.9 vol%) nanofluid test

Measured items	Runs Al_2O_3 (5.9 vol%) for flow rate (gpm)					
	0.75	1.0	1.25	1.5	1.75	2.0
Inlet temp. of the heated test-section [° C]	-	20.49	20.03	20.13	20.34	20.44
Outlet temp. of the heated test-section [°C]	-	44.01	35.54	32.98	31.42	30.20
Inlet temp. of the isothermal test-sect. [°C]	--	18.28	18.33	18.72	19.17	19.45
0.203m, Surface thermocouple 1 [°C]	-	67.01	46.90	43.15	39.61	37.55
Surface thermocouple 2 [°C]	-	76.54	49.45	43.28	40.11	38.07
Surface thermocouple 3 [°C]	-	84.67	50.36	43.51	40.40	38.34
Surface thermocouple 4 [°C]	-	87.66	50.30	43.98	40.88	38.82
Surface thermocouple 5 [°C]	-	92.10	50.32	44.55	41.40	39.27
Surface thermocouple 6 [°C]	-	80.51	50.22	45.03	41.92	39.73
Surface thermocouple 7 [°C]	-	75.98	50.44	45.47	42.42	40.25
Surface thermocouple 8 [°C]	-	74.14	50.52	45.72	42.60	40.38
Surface thermocouple 9 [°C]	-	73.31	51.42	46.44	43.28	41.02
Surface thermocouple 10 [°C]	-	72.32	51.99	47.07	43.94	41.68
Surface thermocouple 11 [°C]	-	71.20	52.54	47.65	44.46	42.15
Surface thermocouple 12 [°C]	-	70.70	53.25	48.30	45.03	42.65
Surface thermocouple 13 [°C]	-	70.02	53.64	48.70	45.48	43.08
2.842m, Surface thermocouple 14 [°C]	-	70.06	54.37	49.38	46.10	43.65
Voltage [V]	-	14.80	14.80	14.80	14.80	14.80
Current [Amp]	-	337.60	337.60	337.60	337.60	337.60
Vol. flow rate at inlet of the heated test-sect. [gal/min]	-	0.99	1.25	1.51	1.75	1.99
DP heated test-section [bar]	-	0.0454	0.0935	0.1420	0.1855	0.2313
DP isothermal test-section [bar]	-	0.0504	0.0943	0.1381	0.1792	0.2220

Table A 12: Convection test of TiO_2 (0.5 vol%) nanofluid test

Measured items	Runs TiO_2 (0.5 vol%) for flow rate (gpm)						
	0.75	1.0	1.25	1.5	1.75	2.0	2.25
Inlet temp. of the heated test-section [° C]	19.69	19.88	19.74	19.83	19.41	19.62	19.49
Outlet temp. of the heated test-section [°C]	41.98	38.22	34.47	32.01	29.80	28.68	27.73
Inlet temp. of the isothermal test-sect. [°C]	17.68	18.22	18.45	18.78	18.51	18.87	18.82
0.203m, Surface thermocouple 1 [°C]	39.89	36.92	34.18	32.48	30.85	30.09	29.41
Surface thermocouple 2 [°C]	40.85	37.76	34.88	33.06	31.35	30.53	29.80
Surface thermocouple 3 [°C]	41.83	38.67	35.66	33.74	31.94	31.04	30.28
Surface thermocouple 4 [°C]	42.97	39.72	36.57	34.54	32.67	31.71	30.91
Surface thermocouple 5 [°C]	44.11	40.70	37.41	35.24	33.27	32.24	31.39
Surface thermocouple 6 [°C]	45.35	41.77	38.28	35.97	33.88	32.77	31.86
Surface thermocouple 7 [°C]	46.50	42.77	39.11	36.68	34.50	33.32	32.37
Surface thermocouple 8 [°C]	46.48	42.75	39.09	36.65	34.48	33.30	32.34
Surface thermocouple 9 [°C]	48.70	44.65	40.68	37.99	35.64	34.32	33.28
Surface thermocouple 10 [°C]	49.84	45.59	41.45	38.64	36.18	34.80	33.71
Surface thermocouple 11 [°C]	51.29	46.84	42.47	39.51	36.94	35.48	34.34
Surface thermocouple 12 [°C]	52.60	47.96	43.40	40.29	37.62	36.07	34.88
Surface thermocouple 13 [°C]	53.72	48.88	44.15	40.91	38.15	36.52	35.29
2.842m, Surface thermocouple 14 [°C]	54.61	49.65	44.76	41.42	38.60	36.92	35.66
Voltage [V]	14.70	14.70	14.70	14.70	14.70	14.70	14.70
Current [Amp]	330.70	332.00	333.00	333.10	334.40	333.90	333.90
Vol. flow rate at inlet of the heated test-sect. [gal/min]	0.77	1.00	1.24	1.49	1.74	2.02	2.21
DP heated test-section [bar]	0.0369	0.0522	0.0755	0.1038	0.1358	0.1721	0.2016
DP isothermal test-section [bar]	0.0328	0.0476	0.0704	0.0981	0.1300	0.1661	0.1959

Table A 13: Convection test of TiO_2 (1.5 vol%) nanofluid test

Measured items	Runs TiO_2 (1.5 vol%) for flow rate (gpm)						
	0.75	1.0	1.25	1.5	1.75	2.0	2.25
Inlet temp. of the heated test-section [° C]	19.61	19.74	19.66	19.94	19.69	19.84	19.59
Outlet temp. of the heated test-section [°C]	41.60	37.65	33.98	32.09	30.00	28.88	27.60
Inlet temp. of the isothermal test-sect. [°C]	17.47	18.03	18.30	18.79	18.74	19.03	18.91
0.203m, Surface thermocouple 1 [°C]	42.35	38.60	35.47	34.00	32.31	31.38	30.31
Surface thermocouple 2 [°C]	43.24	39.41	36.13	34.56	32.79	31.81	30.68
Surface thermocouple 3 [°C]	44.02	40.20	36.84	35.20	33.35	32.30	31.13
Surface thermocouple 4 [°C]	45.08	41.13	37.67	35.95	34.02	32.92	31.71
Surface thermocouple 5 [°C]	46.08	42.05	38.46	36.64	34.62	33.46	32.18
Surface thermocouple 6 [°C]	47.15	43.01	39.28	37.35	35.23	33.99	32.65
Surface thermocouple 7 [°C]	48.26	43.98	40.08	38.07	35.85	34.54	33.15
Surface thermocouple 8 [°C]	47.82	43.64	39.81	37.81	35.62	34.33	32.96
Surface thermocouple 9 [°C]	50.23	45.69	41.52	39.32	36.92	35.51	34.01
Surface thermocouple 10 [°C]	51.19	46.51	42.18	39.90	37.43	35.94	34.39
Surface thermocouple 11 [°C]	52.69	47.78	43.24	40.83	38.23	36.66	35.04
Surface thermocouple 12 [°C]	53.94	48.85	44.12	41.60	38.89	37.26	35.57
Surface thermocouple 13 [°C]	54.96	49.71	44.82	42.19	39.40	37.70	35.96
2.842m, Surface thermocouple 14 [°C]	55.77	50.37	45.37	42.68	39.82	38.07	36.30
Voltage [V]	14.70	14.70	14.70	14.70	14.70	14.70	14.70
Current [Amp]	330.00	331.80	333.00	333.20	334.60	334.60	334.30
Vol. flow rate at inlet of the heated test-sect. [gal/min]	0.73	1.00	1.26	1.49	1.76	2.01	2.28
DP heated test-section [bar]	0.0389	0.0556	0.0818	0.1069	0.1417	0.1776	0.2194
DP isothermal test-section [bar]	0.0346	0.0514	0.0772	0.1014	0.1345	0.1689	0.2084

Table A 14: Convection test of TiO_2 (2.5 vol%) nanofluid test

Measured items	Runs TiO_2 (2.5 vol%) for flow rate (gpm)						
	0.75	1.0	1.25	1.5	1.75	2.0	2.25
Inlet temp. of the heated test-section [° C]	19.80	19.84	19.84	19.73	19.56	19.96	19.68
Outlet temp. of the heated test-section [°C]	41.94	37.77	34.26	31.85	29.86	29.17	27.91
Inlet temp. of the isothermal test-sect. [°C]	17.48	18.01	18.35	18.51	18.54	19.09	18.94
0.203m, Surface thermocouple 1 [°C]	46.83	41.51	37.72	35.28	33.32	32.61	31.41
Surface thermocouple 2 [°C]	47.58	42.32	38.35	35.82	33.79	33.03	31.79
Surface thermocouple 3 [°C]	48.11	42.93	38.97	36.40	34.32	33.52	32.23
Surface thermocouple 4 [°C]	48.85	43.79	39.78	37.12	34.97	34.12	32.79
Surface thermocouple 5 [°C]	49.87	44.64	40.51	37.77	35.53	34.65	33.27
Surface thermocouple 6 [°C]	50.75	45.53	41.30	38.46	36.13	35.19	33.75
Surface thermocouple 7 [°C]	51.65	46.41	42.09	39.14	36.74	35.73	34.25
Surface thermocouple 8 [°C]	51.03	45.91	41.66	38.81	36.44	35.44	33.99
Surface thermocouple 9 [°C]	53.40	47.98	43.41	40.31	37.77	36.68	35.09
Surface thermocouple 10 [°C]	54.22	48.70	44.06	40.87	38.25	37.11	35.49
Surface thermocouple 11 [°C]	55.76	49.99	45.12	41.79	39.04	37.83	36.15
Surface thermocouple 12 [°C]	56.85	50.97	45.98	42.53	39.69	38.43	36.69
Surface thermocouple 13 [°C]	57.79	51.79	46.63	43.10	40.18	38.86	37.07
2.842m, Surface thermocouple 14 [°C]	58.56	52.42	47.18	43.55	40.58	39.22	37.40
Voltage [V]	14.70	14.70	14.70	14.70	14.70	14.70	14.70
Current [Amp]	331.40	335.10	333.60	334.00	336.60	333.60	334.90
Vol. flow rate at inlet of the heated test-sect. [gal/min]	0.75	1.01	1.27	1.51	1.78	1.99	2.25
DP heated test-section [bar]	0.0380	0.0567	0.0844	0.1152	0.1534	0.1856	0.2272
DP isothermal test-section [bar]	0.0352	0.0537	0.0807	0.1105	0.1471	0.1775	0.2167

Table A 15: Convection test of TiO_2 (3.5 vol%) nanofluid test

Measured items	Runs TiO_2 (3.5 vol%) for flow rate (gpm)						
	0.75	1.0	1.25	1.5	1.75	2.0	2.25
Inlet temp. of the heated test-section [° C]	19.67	19.72	19.72	19.64	19.87	19.70	19.98
Outlet temp. of the heated test-section [°C]	42.04	37.81	34.19	32.07	30.48	28.96	28.43
Inlet temp. of the isothermal test-sect. [°C]	17.28	17.81	18.20	18.35	18.80	18.77	19.20
0.203m, Surface thermocouple 1 [°C]	51.62	45.47	40.03	37.32	35.26	33.53	32.87
Surface thermocouple 2 [°C]	55.37	46.04	40.66	37.87	35.72	33.94	33.24
Surface thermocouple 3 [°C]	56.08	46.44	41.12	38.36	36.22	34.40	33.67
Surface thermocouple 4 [°C]	55.41	46.98	41.81	39.05	36.85	34.98	34.22
Surface thermocouple 5 [°C]	55.35	47.87	42.53	39.67	37.39	35.47	34.68
Surface thermocouple 6 [°C]	55.49	48.54	43.25	40.31	37.98	36.00	35.16
Surface thermocouple 7 [°C]	55.66	49.32	43.97	40.99	38.59	36.56	35.68
Surface thermocouple 8 [°C]	54.79	48.60	43.43	40.51	38.16	36.17	35.31
Surface thermocouple 9 [°C]	57.17	50.67	45.19	42.11	39.58	37.44	36.50
Surface thermocouple 10 [°C]	57.62	51.21	45.76	42.63	40.06	37.87	36.90
Surface thermocouple 11 [°C]	59.08	52.49	46.84	43.56	40.86	38.58	37.56
Surface thermocouple 12 [°C]	60.03	53.37	47.62	44.26	41.51	39.16	38.10
Surface thermocouple 13 [°C]	60.77	54.07	48.21	44.82	41.99	39.58	38.48
2.842m, Surface thermocouple 14 [°C]	61.34	54.62	48.70	45.25	42.36	39.91	38.78
Voltage [V]	14.70	14.70	14.70	14.70	14.70	14.70	14.70
Current [Amp]	326.00	326.00	330.60	331.00	332.30	332.30	333.30
Vol. flow rate at inlet of the heated test-sect. [gal/min]	0.71	1.00	1.27	1.49	1.75	2.02	2.21
DP heated test-section [bar]	0.0355	0.0571	0.0879	0.1167	0.1561	0.2004	0.2350
DP isothermal test-section [bar]	0.0334	0.0564	0.0865	0.1143	0.1518	0.1940	0.2262

Table A 16: Convection test of TiO_2 (4.5 vol%) nanofluid test

Measured items	Runs TiO_2 (4.5 vol%) for flow rate (gpm)						
	0.75	1.0	1.25	1.5	1.75	2.0	2.25
Inlet temp. of the heated test-section [° C]	-	20.08	20.15	20.03	19.90	19.71	19.55
Outlet temp. of the heated test-section [°C]	-	38.38	35.00	32.53	30.49	29.16	28.21
Inlet temp. of the isothermal test-sect. [°C]	-	18.07	18.55	18.72	18.82	18.78	18.72
0.203m, Surface thermocouple 1 [°C]	-	50.44	44.39	40.09	37.16	35.44	34.29
Surface thermocouple 2 [°C]	-	53.75	44.88	40.73	37.70	35.92	34.72
Surface thermocouple 3 [°C]	-	54.85	45.18	41.08	38.09	36.33	35.11
Surface thermocouple 4 [°C]	-	54.33	45.71	41.60	38.56	36.74	35.51
Surface thermocouple 5 [°C]	-	54.19	46.32	42.16	39.06	37.20	35.95
Surface thermocouple 6 [°C]	-	53.86	46.90	42.77	39.64	37.75	36.45
Surface thermocouple 7 [°C]	-	53.72	47.53	43.39	40.22	38.28	36.95
Surface thermocouple 8 [°C]	-	52.62	46.65	42.72	39.61	37.75	36.45
Surface thermocouple 9 [°C]	-	54.80	48.57	44.41	41.12	39.11	37.72
Surface thermocouple 10 [°C]	-	55.15	49.00	44.88	41.55	39.53	38.11
Surface thermocouple 11 [°C]	-	56.27	50.08	45.81	42.38	40.26	38.79
Surface thermocouple 12 [°C]	-	57.07	50.78	46.47	42.97	40.80	39.31
Surface thermocouple 13 [°C]	-	57.52	51.31	46.97	43.43	41.22	39.68
2.842m, Surface thermocouple 14 [°C]	-	57.92	51.68	47.32	43.73	41.50	39.96
Voltage [V]	-	14.70	14.70	14.70	14.70	14.70	14.70
Current [Amp]	-	327.60	328.40	329.20	330.00	332.20	333.30
Vol. flow rate at inlet of the heated test-sect. [gal/min]	-	1.00	1.25	1.50	1.77	2.00	2.19
DP heated test-section [bar]	-	0.0545	0.0880	0.1227	0.1673	0.2059	0.2414
DP isothermal test-section [bar]	-	0.0549	0.0882	0.1220	0.1648	0.2017	0.2353

Table A 17: Convection test of CuO (0.4 vol%) nanofluid test

Measured items	Runs CuO (0.4 vol%) for flow rate (gpm)						
	0.75	1.0	1.25	1.5	1.75	2.0	2.25
Inlet temp. of the heated test-section [° C]	19.89	20.23	20.01	19.60	20.11	19.56	19.81
Outlet temp. of the heated test-section [°C]	42.36	37.86	34.42	31.66	30.32	28.67	27.88
Inlet temp. of the isothermal test-sect. [°C]	17.63	18.53	18.63	18.46	19.17	18.74	19.13
0.203m, Surface thermocouple 1 [°C]	38.99	36.12	33.85	31.97	31.23	29.99	29.52
Surface thermocouple 2 [°C]	40.14	37.06	34.65	32.66	31.82	30.52	30.00
Surface thermocouple 3 [°C]	41.25	38.00	35.44	33.32	32.40	31.04	30.46
Surface thermocouple 4 [°C]	42.33	38.88	36.19	33.97	32.95	31.54	30.91
Surface thermocouple 5 [°C]	43.52	39.87	37.03	34.69	33.58	32.11	31.42
Surface thermocouple 6 [°C]	44.92	41.01	37.99	35.49	34.24	32.70	31.94
Surface thermocouple 7 [°C]	46.15	42.02	38.82	36.21	34.89	33.29	32.48
Surface thermocouple 8 [°C]	45.66	41.56	38.39	35.83	34.51	32.94	32.13
Surface thermocouple 9 [°C]	48.40	43.81	40.29	37.45	35.94	34.21	33.29
Surface thermocouple 10 [°C]	49.50	44.69	41.01	38.06	36.45	34.68	33.70
Surface thermocouple 11 [°C]	51.03	45.91	42.02	38.90	37.18	35.32	34.28
Surface thermocouple 12 [°C]	52.38	47.01	42.93	39.67	37.86	35.94	34.83
Surface thermocouple 13 [°C]	53.58	47.96	43.72	40.33	38.40	36.41	35.25
2.842m, Surface thermocouple 14 [°C]	54.47	48.65	44.29	40.82	38.81	36.78	35.56
Voltage [V]	14.70	14.70	14.70	14.70	14.70	14.70	14.70
Current [Amp]	335.60	335.60	335.60	335.60	335.60	335.60	335.60
Vol. flow rate at inlet of the heated test-sect. [gal/min]	0.77	1.03	1.26	1.51	1.77	2.00	2.27
DP heated test-section [bar]	0.0337	0.0515	0.0731	0.0992	0.1310	0.1605	0.1983
DP isothermal test-section [bar]	0.0276	0.0447	0.0657	0.0911	0.1219	0.1506	0.1863

Table A 18: Convection test of CuO (0.9 vol%) nanofluid test

Measured items	Runs CuO (0.8 vol%) for flow rate (gpm)						
	0.75	1.0	1.25	1.5	1.75	2.0	2.25
Inlet temp. of the heated test-section [° C]	19.55	19.45	19.51	19.75	20.53	20.20	19.41
Outlet temp. of the heated test-section [°C]	42.23	37.63	34.06	31.80	30.82	29.34	27.50
Inlet temp. of the isothermal test-sect. [°C]	17.44	17.78	18.14	18.60	19.57	19.38	18.68
0.203m, Surface thermocouple 1 [°C]	38.97	35.83	33.56	32.24	31.84	30.78	29.34
Surface thermocouple 2 [°C]	40.07	36.79	34.36	32.93	32.45	31.32	29.82
Surface thermocouple 3 [°C]	41.13	37.71	35.13	33.59	33.01	31.82	30.28
Surface thermocouple 4 [°C]	42.18	38.60	35.88	34.22	33.56	32.32	30.72
Surface thermocouple 5 [°C]	43.36	39.61	36.72	34.94	34.20	32.89	31.23
Surface thermocouple 6 [°C]	44.74	40.77	37.67	35.75	34.91	33.53	31.80
Surface thermocouple 7 [°C]	45.93	41.75	38.48	36.45	35.51	34.07	32.28
Surface thermocouple 8 [°C]	45.43	41.29	38.06	36.02	35.05	33.64	31.91
Surface thermocouple 9 [°C]	48.16	43.59	39.97	37.69	36.56	35.00	33.10
Surface thermocouple 10 [°C]	49.26	44.48	40.69	38.29	37.08	35.46	33.52
Surface thermocouple 11 [°C]	50.73	45.68	41.67	39.11	37.79	36.09	34.07
Surface thermocouple 12 [°C]	52.08	46.79	42.57	39.87	38.46	36.68	34.59
Surface thermocouple 13 [°C]	53.27	47.74	43.35	40.53	39.02	37.19	35.04
2.842m, Surface thermocouple 14 [°C]	54.10	48.39	43.85	40.92	39.34	37.46	35.29
Voltage [V]	14.70	14.70	14.70	14.70	14.70	14.70	14.70
Current [Amp]	333.40	333.40	333.40	333.40	333.40	333.40	333.40
Vol. flow rate at inlet of the heated test-sect. [gal/min]	0.76	1.01	1.25	1.50	1.75	1.99	2.25
DP heated test-section [bar]	0.0368	0.0540	0.0781	0.1051	0.1357	0.1666	0.2070
DP isothermal test-section [bar]	0.0306	0.0474	0.0710	0.0979	0.1265	0.1564	0.1948

Table A 19: Convection test of CuO (1.2 vol%) nanofluid test

Measured items	Runs CuO (1.2 vol%) for flow rate (gpm)						
	0.75	1.0	1.25	1.5	1.75	2.0	2.25
Inlet temp. of the heated test-section [° C]	19.95	19.95	19.79	19.51	19.75	19.43	19.49
Outlet temp. of the heated test-section [°C]	42.34	38.00	34.30	31.64	30.07	28.45	27.55
Inlet temp. of the isothermal test-sect. [°C]	17.58	18.08	18.28	18.24	18.71	18.56	18.78
0.203m, Surface thermocouple 1 [°C]	39.13	36.18	33.71	31.89	30.89	29.71	29.11
Surface thermocouple 2 [°C]	40.21	37.10	34.45	32.52	31.44	30.20	29.55
Surface thermocouple 3 [°C]	41.27	38.03	35.23	33.19	32.02	30.70	30.01
Surface thermocouple 4 [°C]	42.34	38.92	35.96	33.81	32.55	31.18	30.43
Surface thermocouple 5 [°C]	43.54	39.92	36.79	34.51	33.16	31.70	30.91
Surface thermocouple 6 [°C]	44.80	40.99	37.67	35.25	33.79	32.25	31.40
Surface thermocouple 7 [°C]	46.05	42.02	38.52	35.98	34.42	32.81	31.90
Surface thermocouple 8 [°C]	46.69	42.54	38.93	36.32	34.70	33.05	32.10
Surface thermocouple 9 [°C]	48.32	43.89	40.06	37.28	35.54	33.79	32.78
Surface thermocouple 10 [°C]	49.75	45.07	41.01	38.08	36.24	34.40	33.33
Surface thermocouple 11 [°C]	50.95	46.07	41.82	38.76	36.82	34.91	33.79
Surface thermocouple 12 [°C]	52.30	47.18	42.74	39.54	37.49	35.50	34.32
Surface thermocouple 13 [°C]	53.47	48.13	43.51	40.19	38.04	35.99	34.76
2.842m, Surface thermocouple 14 [°C]	54.80	49.21	44.39	40.94	38.68	36.54	35.26
Voltage [V]	14.60	14.60	14.60	14.60	14.60	14.60	14.60
Current [Amp]	337.10	337.10	337.10	337.10	337.10	337.10	337.10
Vol. flow rate at inlet of the heated test-sect. [gal/min]	0.76	1.01	1.25	1.50	1.75	2.03	2.26
DP heated test-section [bar]	0.0342	0.0506	0.0746	0.1017	0.1339	0.1708	0.2071
DP isothermal test-section [bar]	0.0301	0.0460	0.0693	0.0958	0.1271	0.1626	0.1970

Table A 20: Convection test of CuO (1.6 vol%) nanofluid test

Measured items	Runs CuO (1.6 vol%) for flow rate (gpm)						
	0.75	1.0	1.25	1.5	1.75	2.0	2.25
Inlet temp. of the heated test-section [° C]	20.15	20.02	20.06	19.96	19.79	20.04	20.14
Outlet temp. of the heated test-section [°C]	42.76	37.88	34.59	31.96	30.09	29.12	28.48
Inlet temp. of the isothermal test-sect. [°C]	17.64	18.06	18.46	18.68	18.71	19.13	19.13
0.203m, Surface thermocouple 1 [°C]	39.51	36.19	34.04	32.29	30.99	30.37	29.92
Surface thermocouple 2 [°C]	40.59	37.09	34.78	32.92	31.54	30.85	30.37
Surface thermocouple 3 [°C]	41.67	38.00	35.56	33.58	32.11	31.35	30.84
Surface thermocouple 4 [°C]	42.73	38.88	36.30	34.19	32.65	31.82	31.27
Surface thermocouple 5 [°C]	43.89	39.86	37.12	34.89	33.24	32.36	31.76
Surface thermocouple 6 [°C]	45.17	40.92	38.00	35.62	33.87	32.92	32.27
Surface thermocouple 7 [°C]	46.40	41.92	38.84	36.33	34.49	33.47	32.79
Surface thermocouple 8 [°C]	46.97	42.36	39.20	36.61	34.73	33.67	32.96
Surface thermocouple 9 [°C]	48.64	43.75	40.36	37.60	35.60	34.45	33.69
Surface thermocouple 10 [°C]	50.08	44.91	41.33	38.40	36.29	35.06	34.25
Surface thermocouple 11 [°C]	51.28	45.88	42.14	39.08	36.87	35.58	34.73
Surface thermocouple 12 [°C]	52.65	46.99	43.06	39.86	37.55	36.18	35.29
Surface thermocouple 13 [°C]	53.81	47.93	43.82	40.49	38.09	36.66	35.73
2.842m, Surface thermocouple 14 [°C]	55.11	48.99	44.69	41.23	38.73	37.23	36.25
Voltage [V]	14.60	14.60	14.60	14.60	14.60	14.60	14.60
Current [Amp]	337.60	337.60	337.60	337.60	337.60	337.60	337.60
Vol. flow rate at inlet of the heated test-sect. [gal/min]	0.77	1.01	1.25	1.51	1.76	2.02	2.22
DP heated test-section [bar]	0.0340	0.0527	0.0762	0.1062	0.1392	0.1741	0.2031
DP isothermal test-section [bar]	0.0314	0.0495	0.0721	0.1015	0.1331	0.1669	0.1947

Table A 21: Convection test of dielectric liquid (HFE)

Measured items	Runs distilled water for flow rate (gpm)					
	1.0	1.25	1.5	1.75	2.0	2.25
Inlet temp. of the heated test-section [° C]	28.227	26.317	24.816	23.576	22.651	22.036
Outlet temp. of the heated test-section [°C]	63.350	54.934	49.698	45.320	41.785	39.158
Inlet temp. of the isothermal test-sect. [°C]	24.086	22.709	21.640	20.785	20.164	19.779
0.203m, Surface thermocouple 1 [°C]	77.418	67.704	62.368	57.576	53.640	50.754
Surface thermocouple 2 [°C]	79.410	69.375	63.948	58.985	54.901	51.889
Surface thermocouple 3 [°C]	80.538	70.733	64.939	59.780	55.687	52.638
Surface thermocouple 4 [°C]	82.180	71.919	65.764	60.538	56.425	53.361
Surface thermocouple 5 [°C]	84.140	73.633	67.210	61.689	57.507	54.309
Surface thermocouple 6 [°C]	86.287	75.469	68.980	63.350	58.781	55.485
Surface thermocouple 7 [°C]	87.765	76.635	70.130	64.439	59.732	56.331
Surface thermocouple 8 [°C]	86.322	75.365	69.013	63.460	58.843	55.496
Surface thermocouple 9 [°C]	90.854	79.240	72.370	66.376	61.557	58.015
Surface thermocouple 10 [°C]	92.503	80.631	73.669	67.449	62.512	58.831
Surface thermocouple 11 [°C]	94.730	82.458	75.278	68.878	63.861	60.069
Surface thermocouple 12 [°C]	96.565	84.162	76.774	70.188	65.083	61.179
Surface thermocouple 13 [°C]	98.150	85.422	77.970	71.150	65.951	61.936
2.842m, Surface thermocouple 14 [°C]	99.017	86.359	78.718	72.091	66.563	62.396
Voltage [V]	14.7	14.7	14.7	14.7	14.7	14.7
Current [Amp]	325	325	325	325	325	325
Vol. flow rate at inlet of the heated test-sect. [gal/min]	1.016	1.283	1.500	1.736	2.009	2.278
DP heated test-section [bar]	0.080	0.115	0.148	0.189	0.240	0.295
DP isothermal test-section [bar]	0.077	0.111	0.144	0.184	0.231	0.284

APPENDIX(C):

THE UNCERTAINTY OF CONVECTION TESTS

The uncertainty of Nusselt number, friction factor and pressure drop for the convection test of the water, nanofluids and dielectric liquid (HFE) are calculated as shown in chapter 4 (section 4.6).

Table A 22: the uncertainty of Nusselt number and pressure drop of water at different flow rate

	Flow rate (gpm)	Uncertainty of Nu_{ave} (%)	Uncertainty of friction factor (%)	Uncertainty of drop pressure (%)
water	0.75	3.05	8.36	8.30
	1.0	3.23	6.70	6.58
	1.25	3.54	6.04	5.85
	1.5	3.82	6.16	5.90
	1.75	4.20	5.40	5.01
	2.0	4.85	4.22	3.52

Table A 23: the uncertainty of Nusselt number and pressure drop of dielectric liquid (HFE) at different flow rate

	Flow rate (gpm)	Uncertainty of Nu_{ave} (%)	Uncertainty of friction factor (%)	Uncertainty of drop pressure (%)
water	1.0	4.83	8. 70	8.66
	1.25	4.74	4.79	4.72
	1.5	4.75	6.09	6.04
	1.75	4.76	4.13	4.05
	2.0	4.78	3.75	3.67
	2.25	4.80	3.61	3.52

Table A 24: the uncertainty of Nusselt number and pressure drop of Al_2O_3-water nanofluids at different flow rate

Nanofluid	Flow rate (gpm)	Uncertainty of Nu_{ave} (%)	Uncertainty of friction factor (%)	Uncertainty of drop pressure (%)
AL_2O_3 (0.5 vol%)	0.75	3.29	7.27	7.20
	1.0	3.20	5.91	5.77
	1.25	3.49	5.30	5.08
	1.5	3.74	4.61	4.27
	1.75	4.09	4.56	4.08
	2.0	4.54	4.35	3.69
AL_2O_3 (0.9 vol%)	0.75	3.20	6.19	6.11
	1.0	3.11	7.62	7.51
	1.25	3.51	3.57	3.24
	1.5	3.73	3.88	3.46
	1.75	4.10	4.19	3.67
	2.0	4.52	3.49	2.65
AL_2O_3 (1.8 vol%)	0.75	3.60	8.01	7.94
	1.0	3.13	5.30	5.15
	1.25	3.37	6.04	5.85
	1.5	3.66	4.82	4.48
	1.75	3.96	3.79	3.21
	2.0	4.38	3.73	2.95
AL_2O_3 (2.7 vol%)	0.75	3.77	15.68	9.56
	1.0	3.11	7.82	7.72
	1.25	3.41	4.54	4.28
	1.5	3.59	3.91	3.50
	1.75	3.85	3.73	3.15
	2.0	4.27	3.93	3.20
AL_2O_3 (3.6 vol%)	0.75	4.02	13.85	9.51
	1.0	3.17	7.01	6.89
	1.25	3.31	3.16	2.78
	1.5	3.57	2.96	2.36
	1.75	3.84	3.23	2.52
	2.0	4.42	3.43	2.50
AL_2O_3 (4.7 vol%)	0.75	5.42	9.76	9.71
	1.0	3.62	4.80	4.64
	1.25	3.39	3.62	3.30
	1.5	3.55	3.19	2.66
	1.75	4.25	3.49	2.84
	2.0	4.06	3.10	2.09
AL_2O_3 (5.9 vol%)	1.0	49.43	29.65	29.63
	1.25	5.95	5.81	5.61
	1.5	3.83	2.72	2.07
	1.75	3.82	2.45	1.39
	2.0	4.11	5.73	5.26

Table A 25: the uncertainty of Nusselt number and pressure drop of TiO_2-water nanofluids at different flow rate

Nanofluid	Flow rate (gpm)	Uncertainty of Nu_{ave} (%)	Uncertainty of friction factor (%)	Uncertainty of drop pressure (%)
TiO_2 (0.5 vol%)	0.75	2.76	9.46	9.40
	1.0	3.73	7.50	7.40
	1.25	3.52	5.13	4.91
	1.5	3.81	4.53	4.18
	1.75	4.07	4.48	4.01
	2.0	4.49	4.12	3.42
	2.25	4.79	4.11	3.26
TiO_2 (1.5 vol%)	0.75	2.61	9.60	9.54
	1.0	3.64	6.99	6.88
	1.25	3.49	5.40	5.18
	1.5	3.69	4.75	4.42
	1.75	3.94	3.61	3.00
	2.0	4.27	3.66	2.85
	2.25	4.64	3.43	2.26
TiO_2 (2.5 vol%)	0.75	2.52	7.18	7.10
	1.0	3.81	4.77	4.60
	1.25	3.61	3.97	3.67
	1.5	3.67	3.42	2.93
	1.75	3.87	3.26	2.54
	2.0	4.12	3.36	2.48
	2.25	4.43	3.29	2.09
TiO_2 (3.5 vol%)	0.75	2.70	8.90	8.85
	1.0	8.03	4.75	4.58
	1.25	4.11	4.00	3.70
	1.5	3.74	3.36	2.87
	1.75	3.89	3.20	2.49
	2.0	4.07	3.23	2.26
	2.25	4.33	3.21	2.02
TiO_2 (4.5 vol%)	0.75	-	-	-
	1.0	3.78	8.12	8.02
	1.25	8.55	4.02	3.73
	1.5	4.11	3.47	3.00
	1.75	3.93	3.24	2.52
	2.0	4.01	3.36	2.48
	2.25	4.10	3.25	2.10

Table A 26: the uncertainty of Nusselt number and pressure drop of CuO-water nanofluids at different flow rate.

Nanofluid	Flow rate (gpm)	Uncertainty of Nu_{ave} (%)	Uncertainty of friction factor (%)	Uncertainty of drop pressure (%)
CuO (0.4 vol%)	0.75	3.00	7.55	7.48
	1.0	3.25	5.54	5.39
	1.25	3.48	5.63	5.42
	1.5	3.75	4.55	4.20
	1.75	4.16	4.61	4.13
	2.0	4.49	3.84	3.08
	2.25	4.91	4.01	3.08
CuO (0.8 vol%)	0.75	2.97	6.99	6.92
	1.0	3.19	5.90	5.76
	1.25	3.41	3.45	3.10
	1.5	3.73	4.98	4.66
	1.75	4.12	4.32	3.82
	2.0	4.44	4.38	3.75
	2.25	4.77	3.86	2.91
CuO (1.2 vol%)	0.75	3.04	11.60	11.56
	1.0	3.23	4.69	4.52
	1.25	3.48	4.32	4.05
	1.5	3.82	4.91	4.59
	1.75	4.12	4.10	3.57
	2.0	4.51	3.71	2.91
	2.25	5.06	3.76	2.76
CuO (1.6 vol%)	0.75	3.13	7.38	7.30
	1.0	3.33	5.55	5.40
	1.25	3.95	5.48	5.27
	1.5	3.80	4.39	4.02
	1.75	4.23	4.62	4.15
	2.0	4.97	4.24	3.57
	2.25	4.89	4.08	3.22

APPENDIX (D):

TEST SECTION SURFACE TEMPERATURE

In order to show more details of the test section surface temperature variations as affected by nanofluids concentration, the temperature variation along the test section at the outside surface ($T_{s,out}$) for Al_2O_3-water nanofluid, TiO_2-water nanofluid and CuO-water nanofluid are presented in Figures A.1 to A. 6, Figures A. 7 to A.13 and A. 14 to A. 20, respectively. These data are given for different volume fractions and various flow rate (Gallon per min). It should be emphasized here again that at the low flow rate i.e. less than 1.5 GPM and high volume fraction of Al_2O_3-water nanofluid i.e. 4.7 vol.% and 5.9 vol.%. The flow was laminar or transitional flow and the maximum flow rate of Al_2O_3-water nanofluid was 2.0 GPM at maximum volume fraction. In addition, at the lowest flow rate (0.75 GPM) and the highest concentration of Al_2O_3-water nanofluid (5.9 vol.%) and TiO_2-water nanofluid (4.5 vol.%.), it could not be measured because the measured test section surface temperature reached the boiling temperature of water.

From the figures, it is clearly seen that the temperature of the test section increases and varies in a linear trend along the test section. This indicates that the test has reached a steady state. The effect of the nanoparticles load is clearly seen from these figures that at constant flow rate, the surface temperature increases with increasing nanoparticle load. This is due to the higher viscosity, which increases with increasing nanoparticle load. It is also noted that the surface temperature decreases as the flow rate increases, as expected.

It also should be mentioned that for Al_2O_3-water nanofluid at highest nanoparticle loads (4.7 vol.% and 5.9 vol.%) and low flow rate 1.25, 1.0 and 0.75 GPM, the temperature distribution at the entrance was nonlinear and beyond a critical point becomes linear. As mentioned above, this due to that at low flow rate for Al_2O_3-water nanofluid, the flow was laminar or transition. Therefore, the hydrodynamical and thermal entry length to achieve fully developed conditions is $x = 0.05Re\ D_{in}$ and $x = 0.05Re\ Pr\ D_{in}$ for laminar flow, respectively, but it is $10 \leq x/D_{in} \leq 60$ and $x = 10D_{in}$ for turbulent flow [97]. It seems that laminar flow takes a long distance to achieve fully developed. Besides, the effect of nanoparticle on fluid flow is due to increase the viscosity. Regarding TiO_2-water

nanofluid at the highest nanoparticles loads and the low flow rate (1.0 and 0.75 GPM) also there is a nonlinear in the temperature distribution at entrance of test section; this could be due to the acidity of the liquid.

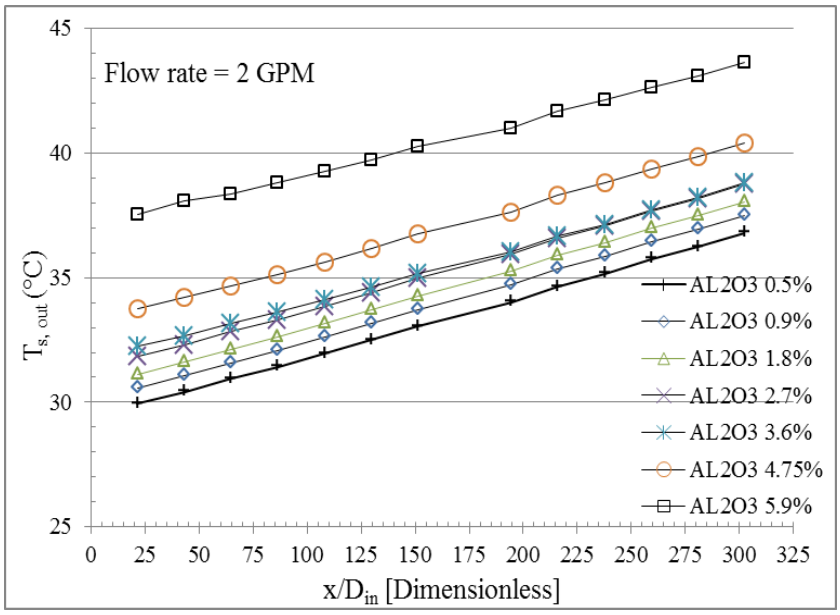

Figure A 1: Show temperature distribution along the test-section for Al_2O_3-water nanofluids with difference volume fraction, at flow rate (2.0 GPM).

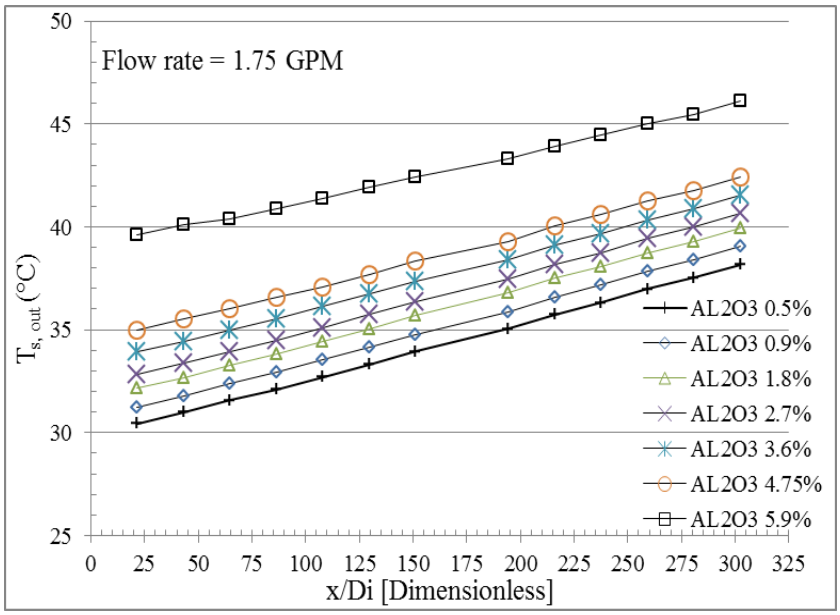

Figure A 2: Show temperature distribution along the test-section for Al_2O_3-water nanofluids with difference volume fraction, at flow rate (1.75 GPM).

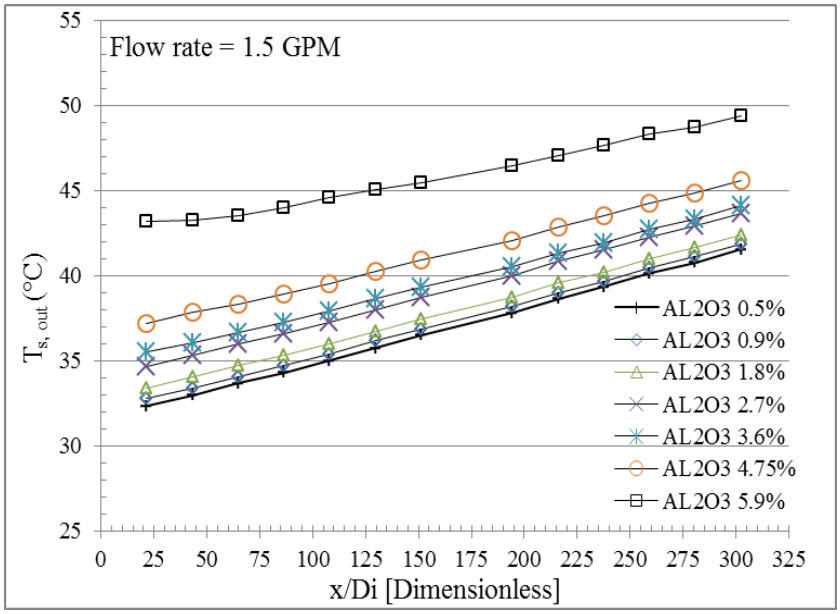

Figure A 3: Show temperature distribution along the test-section for Al_2O_3-water nanofluids with difference volume fraction, at flow rate (1.5 GPM).

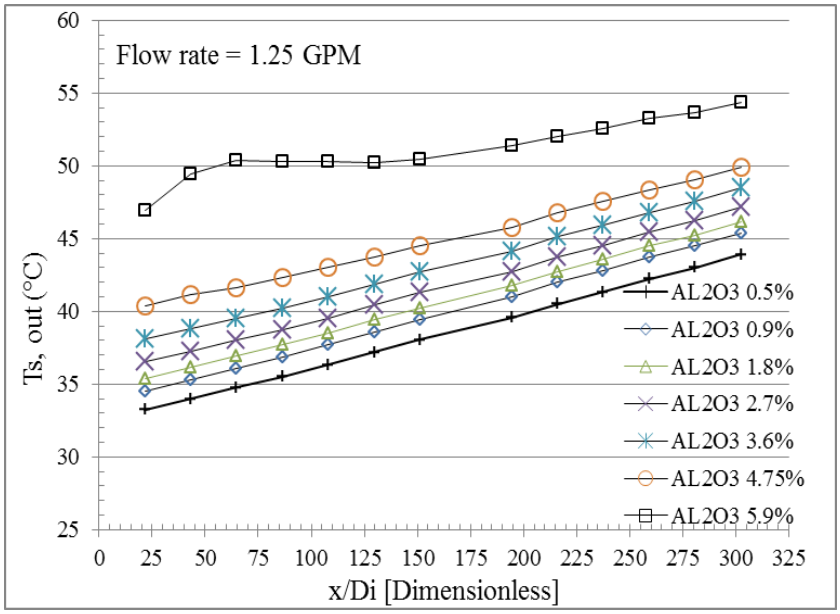

Figure A 4: Show temperature distribution along the test-section for Al_2O_3-water nanofluids with difference volume fraction, at flow rate (1.25 GPM).

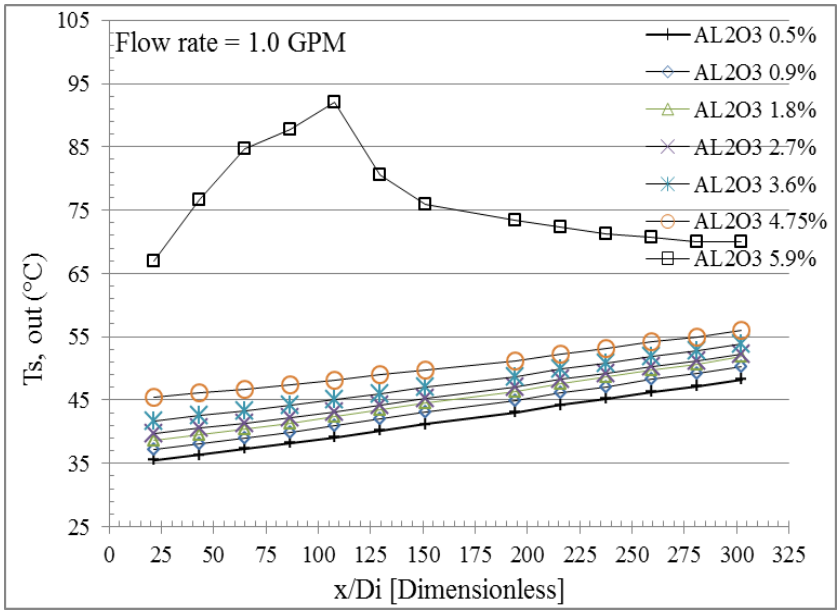

Figure A 5: Show temperature distribution along the test-section for Al_2O_3-water nanofluids with difference volume fraction, at flow rate (1.0 GPM).

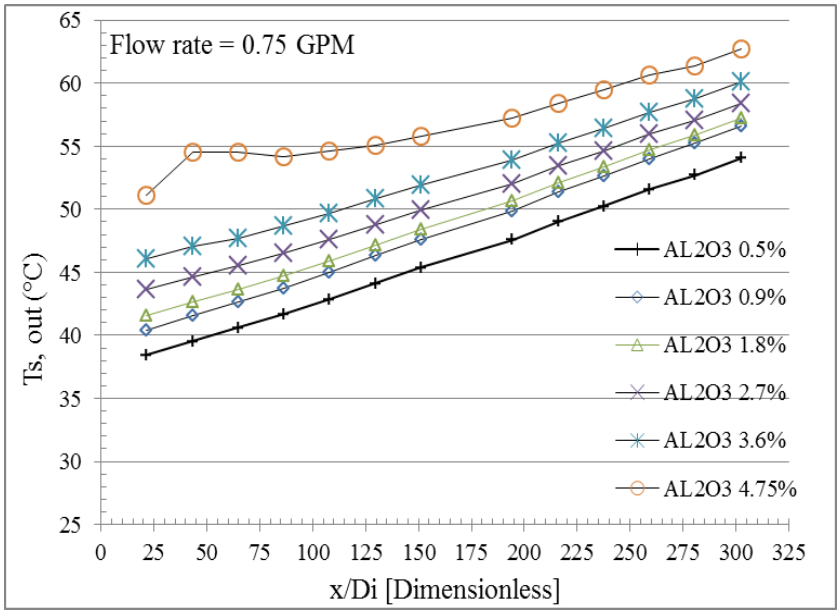

Figure A 6: Show temperature distribution along the test-section for Al_2O_3-water nanofluids with difference volume fraction, at flow rate (0.75 GPM).

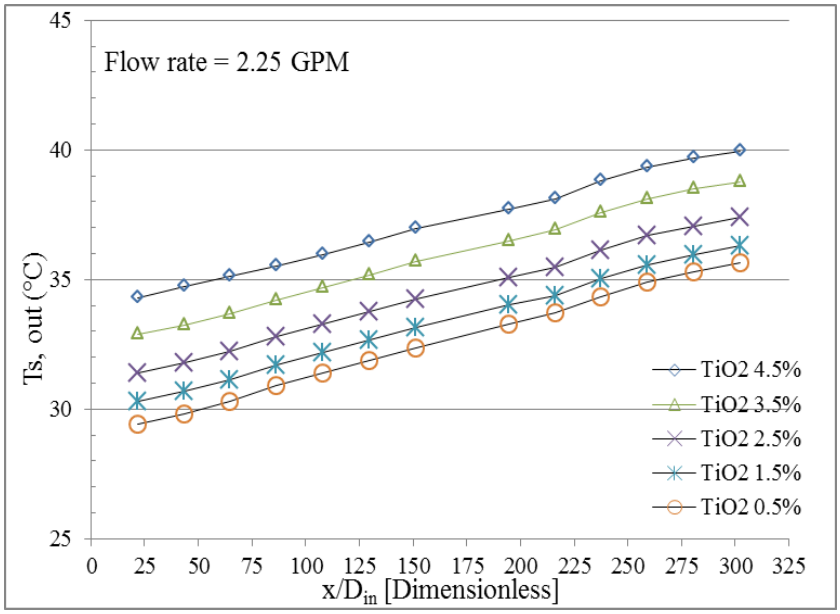

Figure A 7: Show temperature distribution along the test-section for TiO_2-water nanofluids with difference volume fraction, at flow rate (2.25 GPM).

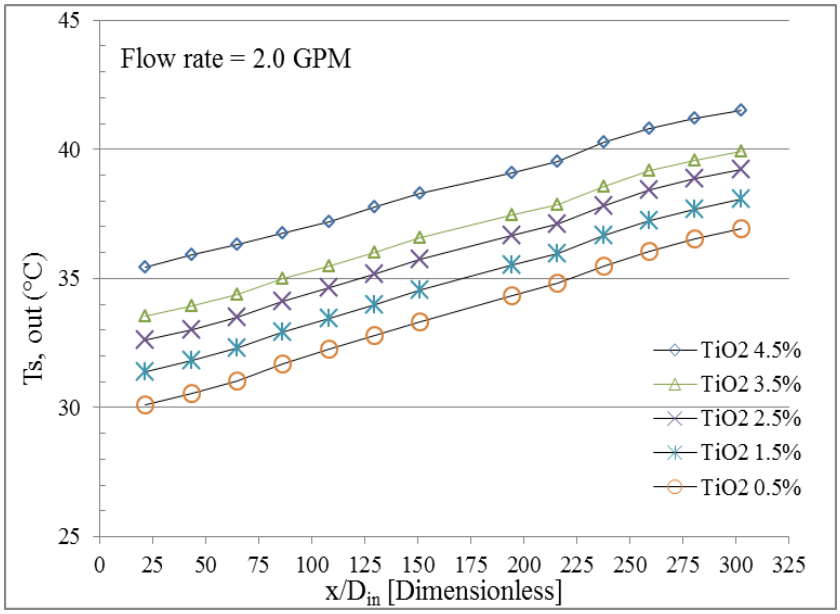

Figure A 8: Show temperature distribution along the test-section for TiO_2-water nanofluids with difference volume fraction, at flow rate (2.0 GPM).

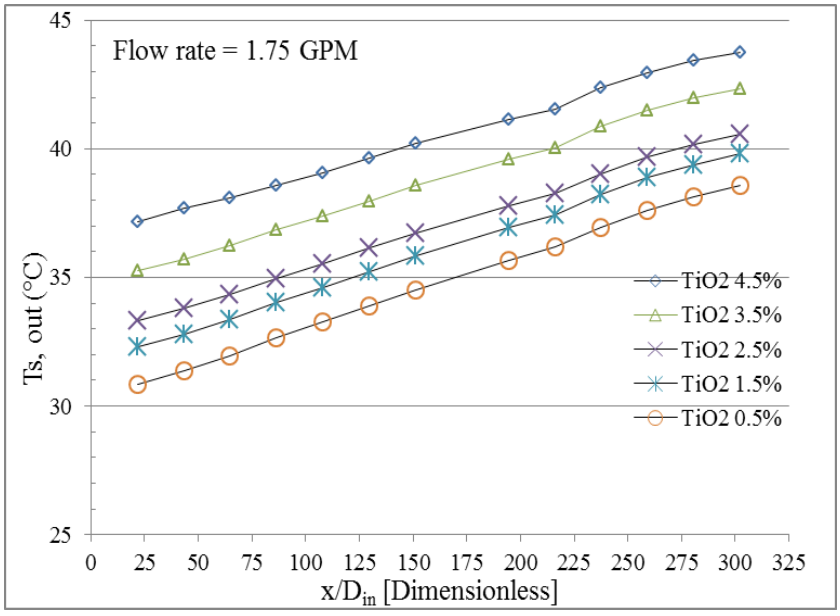

Figure A 9: Show temperature distribution along the test-section for TiO_2-water nanofluids with difference volume fraction, at flow rate (1.75 GPM).

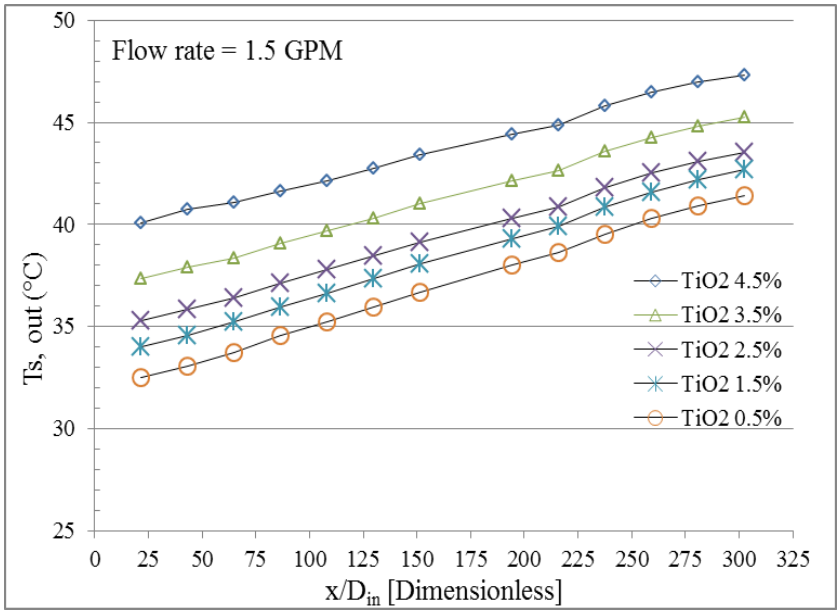

Figure A 10: Show temperature distribution along the test-section for TiO_2-water nanofluids with difference volume fraction, at flow rate (1.5 GPM).

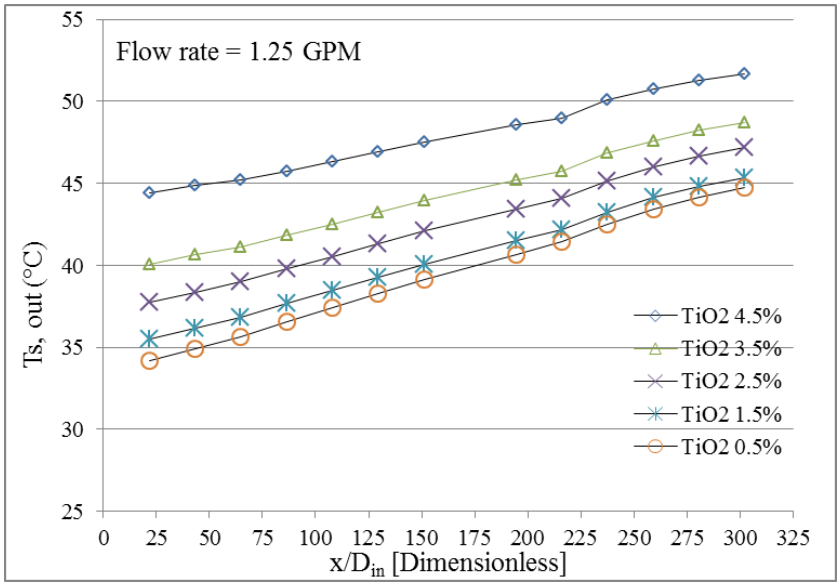

Figure A 11: Show temperature distribution along the test-section for TiO_2-water nanofluids with difference volume fraction, at flow rate (1.25 GPM).

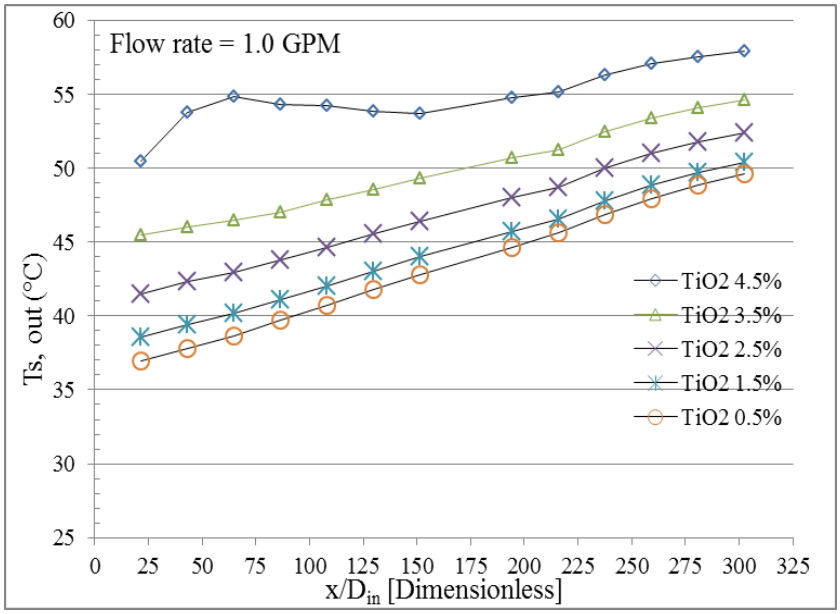

Figure A 12: Show temperature distribution along the test-section for TiO_2-water nanofluids with difference volume fraction, at flow rate (1.0 GPM).

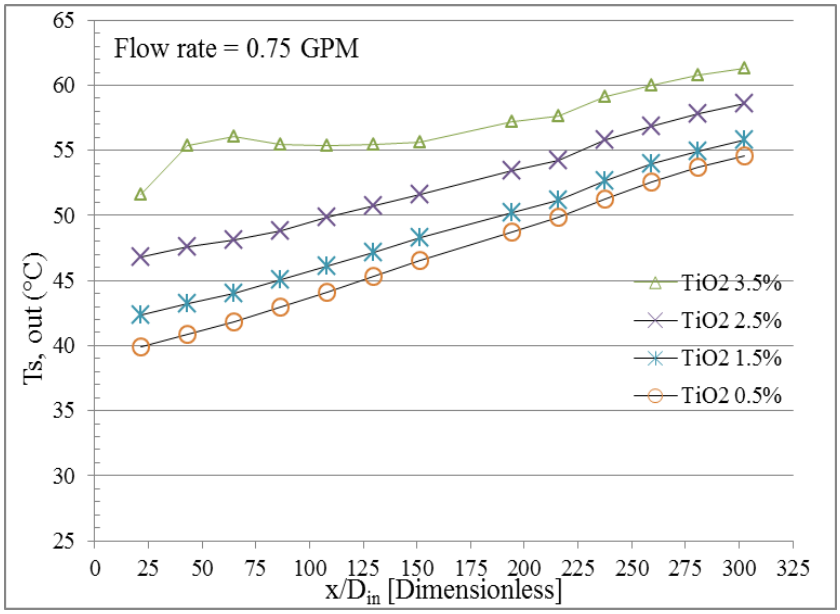

Figure A 13: Show temperature distribution along the test-section for TiO_2-water nanofluids with difference volume fraction, at flow rate (0.75 GPM).

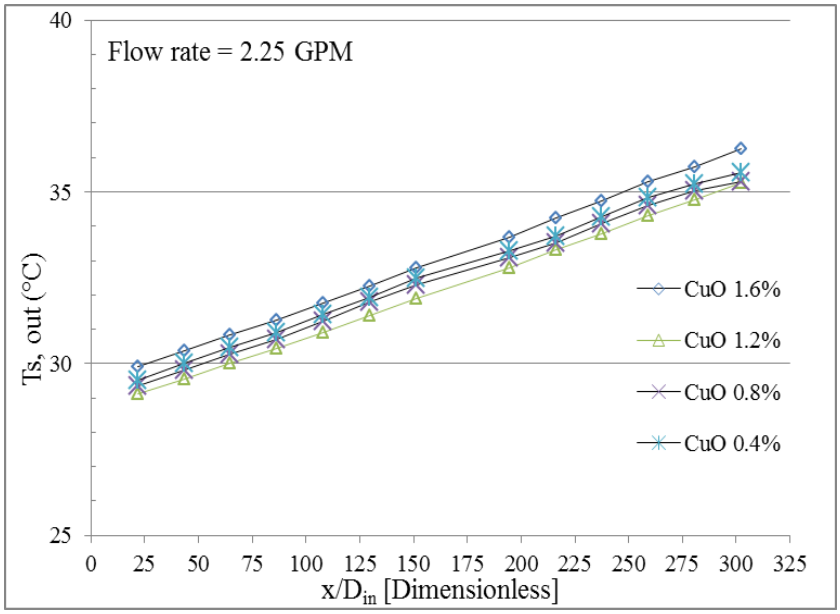

Figure A 14: Show temperature distribution along the test-section for CuO-water nanofluids with difference volume fraction, at flow rate (2.25 GPM).

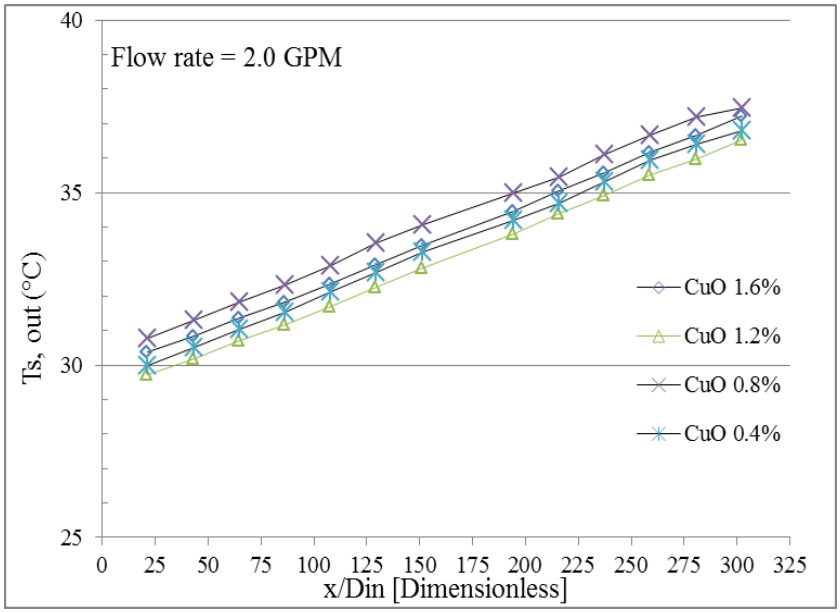

Figure A 15: Show temperature distribution along the test-section for CuO-water nanofluids with difference volume fraction, at flow rate (2.0 GPM).

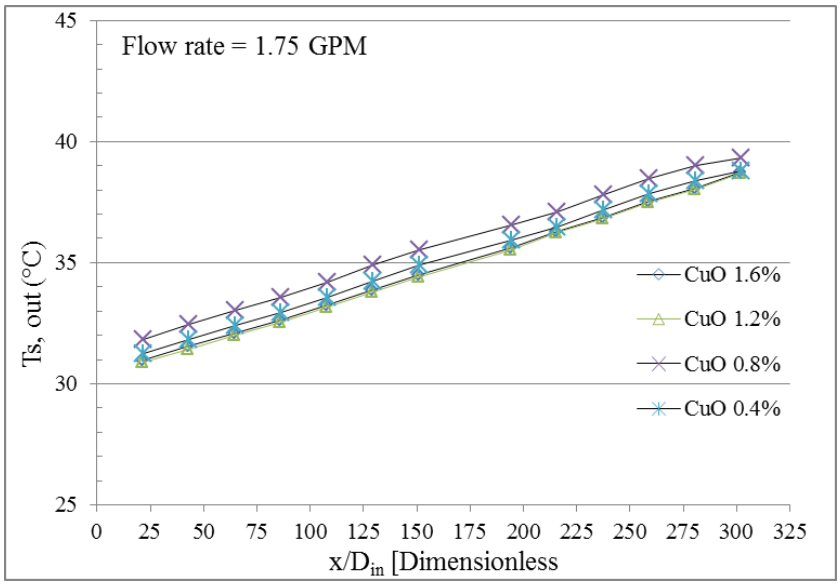

Figure A 16: Show temperature distribution along the test-section for CuO-water nanofluids with difference volume fraction, at flow rate (1.75 GPM).

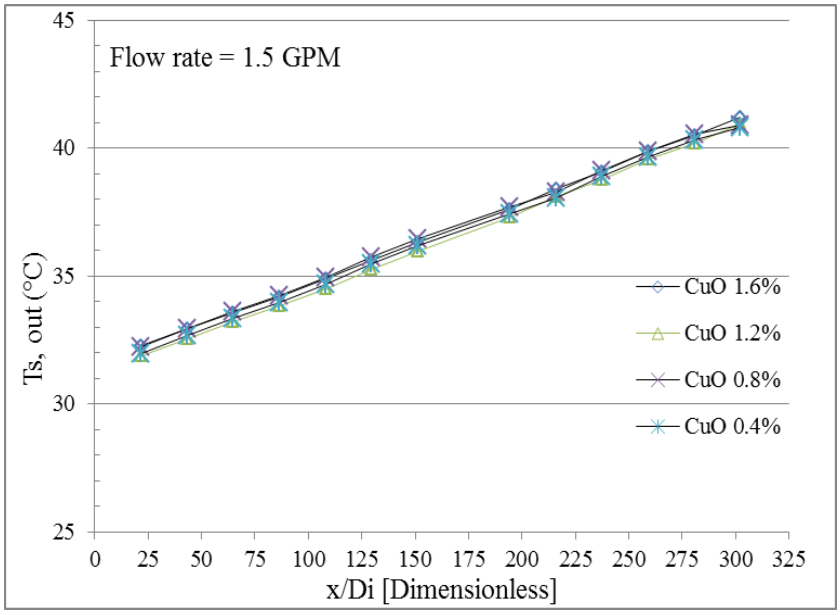

Figure A 17: Show temperature distribution along the test-section for CuO-water nanofluids with difference volume fraction, at flow rate (1.5 GPM).

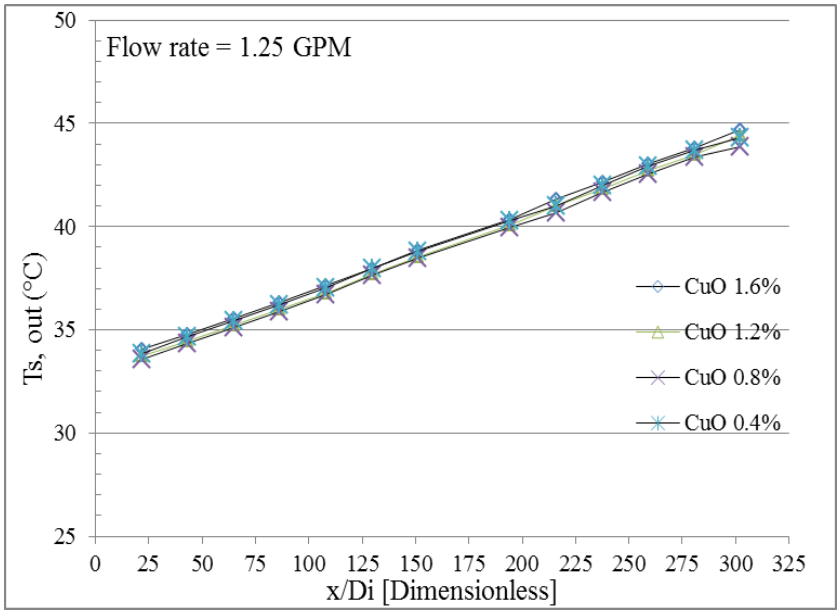

Figure A 18: Show temperature distribution along the test-section for CuO-water nanofluids with difference volume fraction, at flow rate (1.25 GPM).

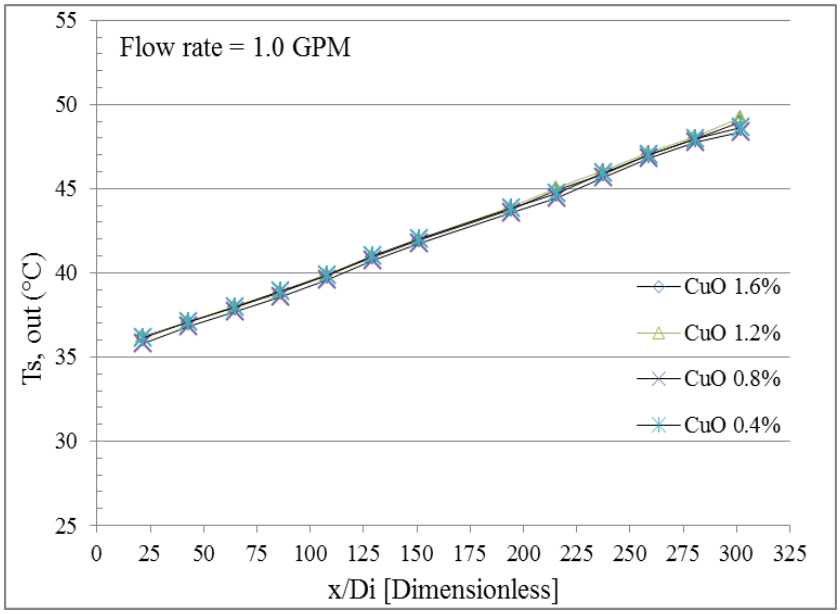

Figure A 19: Show temperature distribution along the test-section for CuO-water nanofluids with difference volume fraction, at flow rate (1.0 GPM).

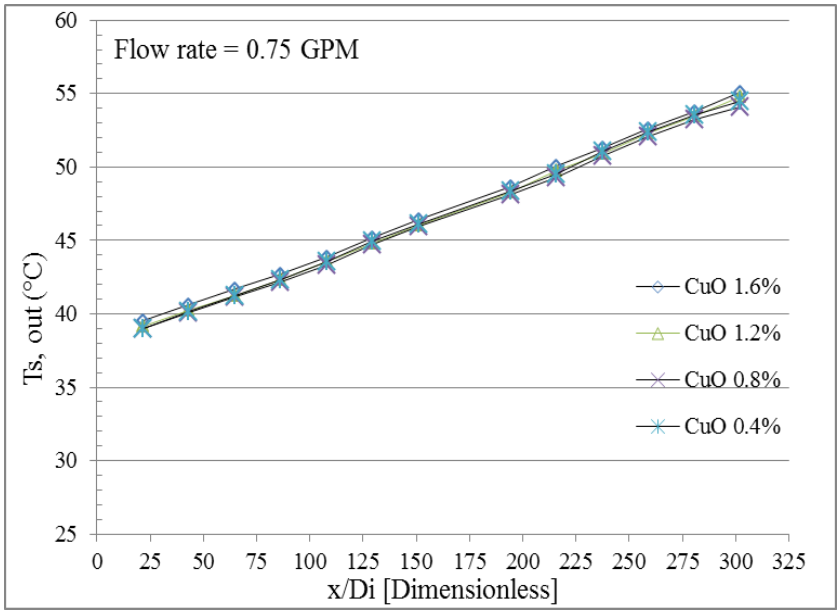

Figure A 20: Show temperature distribution along the test-section for CuO-water nanofluids with difference volume fraction, at flow rate (0.75 GPM).

REFERANCES

1. Zeadally, S., S. Khan, and N. Chilamkurti, Energy-efficient networking: past, present, and future. The Journal of Supercomputing: p. 1-26.
2. Pan, Y., R. Yin, and Z. Huang, Energy modeling of two office buildings with data center for green building design. Energy and Buildings, 2008. 40(7): p. 1145-1152.
3. Dai, J., et al., Optimum Cooling of Data Centers. 2014: Springer.
4. Koomey, J.G., Growth in data center electricity use 2005 to 2010. August 2011, Analytics Press.
5. John Pflueger , A.E., The energy smart data centre, in Greening the data centre. February 2008, Dell Power Solution.
6. Ouchi, M., et al. Thermal management systems for data centers with liquid cooling technique of CPU. in Thermal and Thermomechanical Phenomena in Electronic Systems (ITherm), 2012 13th IEEE Intersociety Conference on. 2012.
7. Patterson, M.K. The effect of data center temperature on energy efficiency. in Thermal and Thermomechanical Phenomena in Electronic Systems, 2008. ITHERM 2008. 11th Intersociety Conference on. 2008.
8. Bircher, W.L. and L.K. John, Complete System Power Estimation Using Processor Performance Events. Computers, IEEE Transactions on, 2012. 61(4): p. 563-577.
9. Ralph, L., Webb, , Principles of enhanced heat transfer. 1994, New York: John Wiley & Sons.
10. Wang, X.-Q. and A.S. Mujumdar, A review on nanofluids - part I: theoretical and numerical investigations. Brazilian Journal of Chemical Engineering, 2008. 25: p. 613-630.
11. Sarit K. Das, et al., Nanofluids: Science and Technology. 2007: Wiley-Interscience.
12. Buongiorno, J., et al., A benchmark study on the thermal conductivity of nanofluids. Journal of Applied Physics, 2009. 106(9): p. 094312-094312-14.
13. Wu, J.M. and J. Zhao, A review of nanofluid heat transfer and critical heat flux enhancement—Research gap to engineering application. Progress in Nuclear Energy, 2013. 66(0): p. 13-24.
14. Saidur, R., K.Y. Leong, and H.A. Mohammad, A review on applications and challenges of nanofluids. Renewable and Sustainable Energy Reviews, 2011. 15(3): p. 1646-1668.
15. Sivashanmugam, P., Application of Nanofluids in Heat Transfer. An Overview of Heat Transfer Phenomena. 2012.
16. Mishra, P.C., et al., Application and Future of Nanofluids in Automobiles: An Overview on Current Research.
17. Bhogare, R.A. and B. Kothawale, A Review on applications and challenges of Nano-fluids as coolant in Automobile Radiator.
18. Sundar, L.S., et al., Empirical and theoretical correlations on viscosity of nanofluids: A review. Renewable and Sustainable Energy Reviews, 2013. 25(0): p. 670-686.

19. Kleinstreuer, C. and Y. Feng, Experimental and theoretical studies of nanofluid thermal conductivity enhancement: a review. Nanoscale Research Letters, 2011. 6(1): p. 1-13.
20. Duangthongsuk, W. and S. Wongwises, Measurement of temperature-dependent thermal conductivity and viscosity of TiO2-water nanofluids. Experimental Thermal and Fluid Science, 2009. 33(4): p. 706-714.
21. Lee, J.-H., et al., Effective viscosities and thermal conductivities of aqueous nanofluids containing low volume concentrations of Al2O3 nanoparticles. International Journal of Heat and Mass Transfer, 2008. 51(11–12): p. 2651-2656.
22. Fedele, L., L. Colla, and S. Bobbo, Viscosity and thermal conductivity measurements of water-based nanofluids containing titanium oxide nanoparticles. International Journal of Refrigeration, 2012. 35(5): p. 1359-1366.
23. Pak, B.C. and Y.I. Cho, Hydrodynamic and heat transfer study of dispersed fluids with submicron metallic oxide particles. Experimental Heat Transfer, 1998. 11(2): p. 151-170.
24. Chandrasekar, M., S. Suresh, and A. Chandra Bose, Experimental investigations and theoretical determination of thermal conductivity and viscosity of Al2O3/water nanofluid. Experimental Thermal and Fluid Science, 2010. 34(2): p. 210-216.
25. Williams, W., L.-W. Hu, and J. Buongiorno, Experimental Investigation of Turbulent Convective Heat Transfer and Pressure Loss of Alumina/Water and Zirconia/Water Nanoparticle Colloids (Nanofluids) in Horizontal Tubes. Journal of Heat Transfer, 2008. 130(4): p. 042412-042412.
26. Heyhat, M.M., et al., Experimental investigation of turbulent flow and convective heat transfer characteristics of alumina water nanofluids in fully developed flow regime. International Communications in Heat and Mass Transfer, 2012. 39(8): p. 1272-1278.
27. Mondragón, R., et al., Experimental characterization and modeling of thermophysical properties of nanofluids at high temperature conditions for heat transfer applications. Powder Technology, 2013. 249(0): p. 516-529.
28. Turgut, A., et al., Thermal Conductivity and Viscosity Measurements of Water-Based TiO2 Nanofluids. International Journal of Thermophysics, 2009. 30(4): p. 1213-1226.
29. Nguyen, C.T., et al., Temperature and particle-size dependent viscosity data for water-based nanofluids – Hysteresis phenomenon. International Journal of Heat and Fluid Flow, 2007. 28(6): p. 1492-1506.
30. Pastoriza-Gallego, M.J., et al., CuO in water nanofluid: Influence of particle size and polydispersity on volumetric behaviour and viscosity. Fluid Phase Equilibria, 2011. 300(1–2): p. 188-196.
31. Duan, F., D. Kwek, and A. Crivoi, Viscosity affected by nanoparticle aggregation in Al2O3-water nanofluids. Nanoscale Research Letters, 2011. 6(1): p. 1-5.
32. Bobbo, S., et al., Viscosity of water based SWCNH and TiO2 nanofluids. Experimental Thermal and Fluid Science, 2012. 36(0): p. 65-71.
33. Rohini Priya, K., K.S. Suganthi, and K.S. Rajan, Transport properties of ultra-low concentration CuO–water nanofluids containing non-spherical nanoparticles. International Journal of Heat and Mass Transfer, 2012. 55(17–18): p. 4734-4743.

34. Mahbubul, I.M., R. Saidur, and M.A. Amalina, Latest developments on the viscosity of nanofluids. International Journal of Heat and Mass Transfer, 2012. 55(4): p. 874-885.
35. Khanafer, K. and K. Vafai, A critical synthesis of thermophysical characteristics of nanofluids. International Journal of Heat and Mass Transfer, 2011. 54(19–20): p. 4410-4428.
36. Mena, J.B., et al., Extrapolation of Al2O3–water nanofluid viscosity for temperatures and volume concentrations beyond the range of validity of existing correlations. Applied Thermal Engineering, 2013. 51(1–2): p. 1092-1097.
37. Corcione, M., Empirical correlating equations for predicting the effective thermal conductivity and dynamic viscosity of nanofluids. Energy Conversion and Management, 2011. 52(1): p. 789-793.
38. Nwosu, P.N., J. Meyer, and M. Sharifpur, Nanofluid Viscosity: A Simple Model Selection Algorithm and Parametric Evaluation. Computers & Fluids, (0).
39. Roberts, N.A. and D. Walker, Convective performance of nanofluids in commercial electronics cooling systems. Applied Thermal Engineering, 2010. 30(16): p. 2499-2504.
40. Rafati, M., A.A. Hamidi, and M. Shariati Niaser, Application of nanofluids in computer cooling systems (heat transfer performance of nanofluids). Applied Thermal Engineering, 2012. 45–46(0): p. 9-14.
41. Liu, M., M. Lin, and C. Wang, Enhancements of thermal conductivities with Cu, CuO, and carbon nanotube nanofluids and application of MWNT/water nanofluid on a water chiller system. Nanoscale Research Letters, 2011. 6(1): p. 297.
42. Bi, S., et al., Performance of a domestic refrigerator using TiO2-R600a nano-refrigerant as working fluid. Energy Conversion and Management. 52(1): p. 733-737.
43. Peyghambarzadeh, S.M., et al., Experimental study of heat transfer enhancement using water/ethylene glycol based nanofluids as a new coolant for car radiators. International Communications in Heat and Mass Transfer. 38(9): p. 1283-1290.
44. Peyghambarzadeh, S.M., et al., Improving the cooling performance of automobile radiator with Al2O3/water nanofluid. Applied Thermal Engineering. 31(10): p. 1833-1838.
45. Naraki, M., et al., Parametric study of overall heat transfer coefficient of CuO/water nanofluids in a car radiator. International Journal of Thermal Sciences, 2013. 66(0): p. 82-90.
46. Teng, T.-P., et al., Performance evaluation on an air-cooled heat exchanger for alumina nanofluid under laminar flow. Nanoscale Research Letters, 2011. 6(1): p. 1-11.
47. Yousefi, T., et al., An experimental investigation on the effect of Al2O3–H2O nanofluid on the efficiency of flat-plate solar collectors. Renewable Energy, 2012. 39(1): p. 293-298.
48. Lu, L., Z.-H. Liu, and H.-S. Xiao, Thermal performance of an open thermosyphon using nanofluids for high-temperature evacuated tubular solar collectors: Part 1: Indoor experiment. Solar Energy, 2011. 85(2): p. 379-387.

49. Zhu, Q., et al., Characterization of Thermal Radiative Properties of Nanofluids for Selective Absorption of Solar Radiation. International Journal of Thermophysics, 2013. 34(12): p. 2307-2321.
50. Chaji, H., et al., Experimental Study on Thermal Efficiency of Flat Plate Solar Collector Using TiO2/Water Nanofluid. Modern Applied Science, 2013. 7(10): p. p60.
51. Fotukian, S.M. and M. Nasr Esfahany, Experimental investigation of turbulent convective heat transfer of dilute γ-Al2O3/water nanofluid inside a circular tube. International Journal of Heat and Fluid Flow, 2010. 31(4): p. 606-612.
52. Sahin, B., et al., Experimental investigation of heat transfer and pressure drop characteristics of Al2O3–water nanofluid. Experimental Thermal and Fluid Science, 2013. 50(0): p. 21-28.
53. Li, Q., Y. Xuan, and J. Wang, Investigation on convective heat transfer and flow features of nanofluids. Journal of Heat transfer, 2003. 125: p. 151-155.
54. Abbasian Arani, A.A. and J. Amani, Experimental investigation of diameter effect on heat transfer performance and pressure drop of TiO2–water nanofluid. Experimental Thermal and Fluid Science, 2013. 44(0): p. 520-533.
55. Sajadi, A.R. and M.H. Kazemi, Investigation of turbulent convective heat transfer and pressure drop of TiO2/water nanofluid in circular tube. International Communications in Heat and Mass Transfer. 38(10): p. 1474-1478.
56. Chen, H., et al., Heat transfer and flow behaviour of aqueous suspensions of titanate nanotubes (nanofluids). Powder Technology, 2008. 183(1): p. 63-72.
57. He, Y., et al., Heat transfer and flow behaviour of aqueous suspensions of TiO_2 nanoparticles (nanofluids) flowing upward through a vertical pipe. International Journal of Heat and Mass Transfer, 2007. 50(11-12): p. 2272-2281.
58. Kayhani, M.H., et al., Experimental study of convective heat transfer and pressure drop of TiO2/water nanofluid. International Communications in Heat and Mass Transfer, 2012. 39(3): p. 456-462.
59. Sajadi, A.R. and M.H. Kazemi, Investigation of turbulent convective heat transfer and pressure drop of TiO2/water nanofluid in circular tube. International Communications in Heat and Mass Transfer, 2011. 38(10): p. 1474-1478.
60. Fotukian, S.M. and M. Nasr Esfahany, Experimental study of turbulent convective heat transfer and pressure drop of dilute CuO/water nanofluid inside a circular tube. International Communications in Heat and Mass Transfer, 2010. 37(2): p. 214-219.
61. Lai, W.Y., et al., Convective Heat Transfer for Water-Based Alumina Nanofluids in a Single 1.02-mm Tube. Journal of Heat Transfer, 2009. 131(11): p. 112401-112401.
62. Wen, D. and Y. Ding, Experimental investigation into convective heat transfer of nanofluids at the entrance region under laminar flow conditions. International Journal of Heat and Mass Transfer, 2004. 47(24): p. 5181-5188.
63. Rayatzadeh, H.R., et al., Effects of continuous sonication on laminar convective heat transfer inside a tube using water–TiO2 nanofluid. Experimental Thermal and Fluid Science, 2013. 48(0): p. 8-14.

64. Rea, U., et al., Laminar convective heat transfer and viscous pressure loss of alumina–water and zirconia–water nanofluids. International Journal of Heat and Mass Transfer, 2009. 52(7): p. 2042-2048.
65. Anoop, K.B., T. Sundararajan, and S.K. Das, Effect of particle size on the convective heat transfer in nanofluid in the developing region. International Journal of Heat and Mass Transfer, 2009. 52(9â€“10): p. 2189-2195.
66. Zeinali Heris, S., S.G. Etemad, and M. Nasr Esfahany, Experimental investigation of oxide nanofluids laminar flow convective heat transfer. International Communications in Heat and Mass Transfer, 2006. 33(4): p. 529-535.
67. Heris, S.Z., et al., Laminar convective heat transfer of Al 2 O 3/water nanofluid through square cross-sectional duct. International Journal of Heat and Fluid Flow, 2013. 44: p. 375-382.
68. Gupta, M., et al., A comprehensive review of experimental investigations of forced convective heat transfer characteristics for various nanofluids. International Journal of Mechanical and Materials Engineering, 2014. 9(1): p. 1-21.
69. Demir, H., et al., Numerical investigation on the single phase forced convection heat transfer characteristics of TiO2 nanofluids in a double-tube counter flow heat exchanger. International Communications in Heat and Mass Transfer, 2011. 38(2): p. 218-228.
70. Lotfi, R., Y. Saboohi, and A.M. Rashidi, Numerical study of forced convective heat transfer of Nanofluids: Comparison of different approaches. International Communications in Heat and Mass Transfer. 37(1): p. 74-78.
71. Santra, A.K., S. Sen, and N. Chakraborty, Study of heat transfer due to laminar flow of copperâ€“water nanofluid through two isothermally heated parallel plates. International Journal of Thermal Sciences, 2009. 48(2): p. 391-400.
72. Raisi, A., B. Ghasemi, and S.M. Aminossadati, A Numerical Study on the Forced Convection of Laminar Nanofluid in a Microchannel with Both Slip and No-Slip Conditions. Numerical Heat Transfer, Part A: Applications. 59(2): p. 114-129.
73. He, Y., et al., Numerical investigation into the convective heat transfer of TiO2 nanofluids flowing through a straight tube under the laminar flow conditions. Applied Thermal Engineering, 2009. 29(10): p. 1965-1972.
74. Fard, M.H., M.N. Esfahany, and M. Talaie, Numerical study of convective heat transfer of nanofluids in a circular tube two-phase model versus single-phase model. International Communications in Heat and Mass Transfer, 2010. 37(1): p. 91-97.
75. Keshavarz Moraveji, M. and E. Esmaeili, Comparison between single-phase and two-phases CFD modeling of laminar forced convection flow of nanofluids in a circular tube under constant heat flux. International Communications in Heat and Mass Transfer, 2012. 39(8): p. 1297-1302.
76. Otanicar, T.P. and J.S. Golden, Comparative environmental and economic analysis of conventional and nanofluid solar hot water technologies. Environmental science & technology, 2009. 43(15): p. 6082-6087.
77. Faizal, M., et al., Energy, economic and environmental analysis of metal oxides nanofluid for flat-plate solar collector. Energy Conversion and Management, 2013. 76(0): p. 162-168.

78. Patterson, M. and a.D. Fenwick, The State of Data Center Cooling. A review of current air and liquid cooling solutions. March 2008, Intel Corporation, White Paper.
79. Cengel, Y.A., Heat and mass transfer: a practical approach. 2007: McGraw-Hill.
80. Tuma, P., Open Bath Immersion Cooling In Data Centers: A New Twist On An Old Idea. December 2010, 3M Company, St. Paul, Minnesota.
81. Kennedy, D., Understanding Data Center Cooling Energy Usage & Reduction Methods. 2009, Data center energy, Rittal White Paper 507.
82. Turner IV, W.P., Changing Cooling Requirements Leave Many Data Centers At Risk.
83. ASHRAE, ASHRAE environment guidelines for datacom equipment: Expanding therecommended environmental envelope. Technicalreport, American Society of Heating, Regrigeratingand Air-Conditioning Engineers, Inc. 2008.
84. Villa, H., Rittal liquid cooling series. 2006.
85. Ten Steps to Increasing Data Center Efficiency Availability through Infrastructure Monitoring. Emerson Network Power White Paper, 2010.
86. Warrier, P., et al., Novel heat transfer fluids for direct immersion phase change cooling of electronic systems. International Journal of Heat and Mass Transfer, 2012. 55(13): p. 3379-3385.
87. Mohapatra, S.C., An overview of liquid coolants for electronics cooling.
88. http://asetek.com.
89. http://www.iceotope.com/.
90. Yu, W., et al., Review and Comparison of Nanofluid Thermal Conductivity and Heat Transfer Enhancements. Heat Transfer Engineering, 2008. 29(5): p. 432-460.
91. Wang, X.-Q. and A.S. Mujumdar, Heat transfer characteristics of nanofluids: a review. International Journal of Thermal Sciences, 2007. 46(1): p. 1-19.
92. Choi, S.U.-S., Nanofluid technology : current status and future research. 1998. Medium: P; Size: 26 pages.
93. Fox, R.W., A.T. McDonald, and P.J. Pritchard, Introduction to Fluid Mechanics. 2005: Wiley.
94. Secco, R.A., M. Kostic, and J.R. deBruyn, Fluid Viscosity Measurement, in Measurement, Instrumentation, and Sensors Handbook, Second Edition. 2014, CRC Press. p. 46-1-46-31.
95. Enviromental Controllers User Manual. 2009, Malvern Instruments Ltd.
96. MacDevette, M.M., T.G. Myers, and B. Wetton, Boundary layer analysis and heat transfer of a nanofluid. Microfluidics and Nanofluidics, 2014. 17(2): p. 401-412.
97. Incropera, F.P., Fundamentals of heat and mass transfer. 6th ed. 2007, Hoboken, NJ: John Wiley. xxv, 997 p.
98. Williams, W.C., Experimental and Theoretical Investigation of Transport Phenomena in Nanoparticle Colloids (Nanofluids),. Massachusetts Institute of Technology, 2007(Cambridge, Massachusetts).
99. Patel, H., T. Sundararajan, and S. Das, An experimental investigation into the thermal conductivity enhancement in oxide and metallic nanofluids. Journal of Nanoparticle Research, 2010. 12(3): p. 1015-1031.

100. Utomo, A.T., et al., Experimental and theoretical studies of thermal conductivity, viscosity and heat transfer coefficient of titania and alumina nanofluids. International Journal of Heat and Mass Transfer, 2012. 55(25–26): p. 7772-7781.
101. Yu, W. and S.U.S. Choi, The Role of Interfacial Layers in the Enhanced Thermal Conductivity of Nanofluids: A Renovated Maxwell Model. Journal of Nanoparticle Research, 2003. 5(1-2): p. 167-171.
102. Duangthongsuk, W. and S. Wongwises, An experimental study on the heat transfer performance and pressure drop of TiO2-water nanofluids flowing under a turbulent flow regime. International Journal of Heat and Mass Transfer, 2010. 53(1–3): p. 334-344.
103. Electronics, M., 3M™ Novec™ 7300 Engineered Fluid. 2005.
104. Division, M.E.M.M., 3M™ Thermal Management Fluids. 2009.
105. Figliola, R.S. and D.E. Beasley, Theory and Design for Mechanical Measurements. 5th edition ed. 2010: Wiley. pp. 161-198.
106. Minjoong Kim, M.K., et al., A Simple Model for Estimating Power Consumption of a Multicore Server System. International Journal of Multimedia and Ubiquitous Engineering, 2014. 9(2): p. 153-160.
107. Gurrum, S.P., et al., Thermal issues in next-generation integrated circuits. Device and Materials Reliability, IEEE Transactions on, 2004. 4(4): p. 709-714.
108. Holman, J., Heat Transfer. 2009: McGraw-Hill Education. p. 347-351.
109. Evans, T., The Different Technologies for Cooling Data Centers. APC white paper, 2012. 59.
110. Cengel, Y. and J. Cimbala, Fluid Mechanics Fundamentals and Applications: Third Edition. 2013: McGraw-Hill Higher Education.
111. Launder, B.E. and D.B. Spalding, The numerical computation of turbulent flows. Computer Methods in Applied Mechanics and Engineering, 1974. 3(2): p. 269-289.
112. Lewis, R.W., P. Nithiarasu, and K. Seetharamu, Fundamentals of the Finite Element Method for Heat and Fluid Flow. 2004: Wiley.
113. De Vahl Davis, G., Natural convection of air in a square cavity: A bench mark numerical solution. International Journal for Numerical Methods in Fluids, 1983. 3(3): p. 249-264.
114. Lai, F.-H. and Y.-T. Yang, Lattice Boltzmann simulation of natural convection heat transfer of Al2O3/water nanofluids in a square enclosure. International Journal of Thermal Sciences, 2011. 50(10): p. 1930-1941.
115. Buongiorno, J., Convective transport in nanofluids. Journal of Heat Transfer-Transactions of the Asme, 2006. 128(3): p. 240-250.
116. Hwang, K.S., S.P. Jang, and S.U.S. Choi, Flow and convective heat transfer characteristics of water-based Al2O3 nanofluids in fully developed laminar flow regime. International Journal of Heat and Mass Transfer, 2009. 52(1-2): p. 193-199.
117. Bird, R.B., Transport phenomena. 1960, New York,: Wiley. 780 p.
118. Geelhoed, P., J. Westerweel, and D. Bedeaux, Thermophoresis. 2001: p. 2061-2064.
119. El-Sayed, N., et al., Temperature management in data centers: why some (might) like it hot. SIGMETRICS Perform. Eval. Rev., 2012. 40(1): p. 163-174.

120. Iyengar, M., et al. Server liquid cooling with chiller-less data center design to enable significant energy savings. in Semiconductor Thermal Measurement and Management Symposium (SEMI-THERM), 2012 28th Annual IEEE. 2012.
121. Mesa-Martinez, F.J., et al. Measuring power and temperature from real processors. in Parallel and Distributed Processing, 2008. IPDPS 2008. IEEE International Symposium on. 2008.
122. Remer, D.S., et al., The state of the art of present worth analysis of cash flow distributions. Engineering Costs and Production Economics, 1984. 7(4): p. 257-278.
123. White, J.A., K. Case, and D.B. Pratt, Principles of engineering economic analysis. 2009, Hoboken, N.J: Wiley.
124. Ohunakin, O., O. Oyewola, and M. Adaramola, Economic analysis of wind energy conversion systems using levelized cost of electricity and present value cost methods in Nigeria. International Journal of Energy and Environmental Engineering, 2013. 4(1): p. 1-8.
125. Routbort, J., et al., Pumping power of nanofluids in a flowing system. Journal of Nanoparticle Research, 2011. 13(3): p. 931-937.
126. Dai, Y.J., et al., Use of liquid desiccant cooling to improve the performance of vapor compression air conditioning. Applied Thermal Engineering, 2001. 21(12): p. 1185-1202.
127. Moore, J.D., et al. Making Scheduling" Cool": Temperature-Aware Workload Placement in Data Centers. in USENIX annual technical conference, General Track. 2005.
128. Beitelmal, M.H. and C.D. Patel, Model-based approach for optimizing a data center centralized cooling system. Hewlett-Packard (HP) Lab Technical Report, 2006.
129. Da Costa, G., et al., Minimization of Costs and Energy Consumption in a Data Center by a Workload-Based Capacity Management, in Energy Efficient Data Centers, S. Klingert, M. Chinnici, and M. Rey Porto, Editors. 2015, Springer International Publishing. p. 102-119.
130. DeVogeleer, K., et al. Modeling the temperature bias of power consumption for nanometer-scale CPUs in application processors. in Embedded Computer Systems: Architectures, Modeling, and Simulation (SAMOS XIV), 2014 International Conference on. 2014.
131. Won Ho, P. and C.H.K. Yang, Effects of Using Advanced Cooling Systems on the Overall Power Consumption of Processors. Very Large Scale Integration (VLSI) Systems, IEEE Transactions on, 2013. 21(9): p. 1644-1654.
132. Seongmoo, H., K. Barr, and K. Asanovic. Reducing power density through activity migration. in Low Power Electronics and Design, 2003. ISLPED '03. Proceedings of the 2003 International Symposium on. 2003.
133. Mesa-Martinez, F.J., E.K. Ardestani, and J. Renau. Characterizing processor thermal behavior. in ACM SIGARCH Computer Architecture News. 2010: ACM.
134. Sze, S.M. and K.K. Ng, Physics of semiconductor devices. 2006: John Wiley & Sons.
135. Anandtech. i7-3770K vs. i7-2600K: Temperature, Voltage, GHz and Power-Consumption Analysis

136. Interest Rates on Savings Accounts since 1960. http://swanlowpark.co.uk/savingsinterestannual.jsp 28/12/2014
137. Historical Inflation Rates for United Kingdom (2005 to 2015). http://www.rateinflation.com/inflation-rate/uk-historical-inflation-rate 13/01/2015.
138. Business and Commercial Electricity Prices. 2014, Business Electricity Prices: http://www.businesselectricityprices.org.uk/.
139. Casey, B. Hydraulic Pumps and Motors: Considering Efficiency 2011.
140. Zhipeng, W. and G. Aiping. Qualitative and Quantitative Analysis the Value of Cloud Computing. in Information Management, Innovation Management and Industrial Engineering (ICIII), 2011 International Conference on. 2011.
141. Garnier, C., Data centre life cycle assessment guidelines. The Green Grid, white paper, 2012. 45: p. v2.
142. https://www.alfa.com/.
143. Celata, G.P., et al., Experimental results of nanofluids flow effects on metal surfaces. Chemical Engineering Research and Design, 2013.
144. Callaway, M., The energy price challenge 2011: A Power Efficiency p. White Paper.
145. Khoshvaght-Aliabadi, M. and A. Alizadeh, An experimental study of Cu–water nanofluid flow inside serpentine tubes with variable straight-section lengths. Experimental Thermal and Fluid Science, 2015. 61: p. 1-11.